

**CHARACTERISATION OF BISMUTH-BASED
ERBIUM-DOPED FIBRE AND ITS APPLICATION
IN WIDE-BAND OPTICAL AMPLIFIERS**

NIZAM TAMCHEK

**FACULTY OF SCIENCE
UNIVERSITY OF MALAYA**

2009

NIZAM TAMCHEK

**CHARACTERISATION OF BISMUTH-BASED ERBIUM-DOPED FIBRE
AND ITS APPLICATION IN WIDE-BAND OPTICAL AMPLIFIERS**

Ph. D

2009

**CHARACTERISATION OF BISMUTH-BASED
ERBIUM-DOPED FIBRE AND ITS APPLICATION
IN WIDE-BAND OPTICAL AMPLIFIERS**

NIZAM TAMCHEK

**THESIS SUBMITTED IN FULFILMENT OF THE
REQUIREMENT FOR THE DEGREE OF
DOCTOR OF PHILOSOPHY**

**FACULTY OF SCIENCE
UNIVERSITY OF MALAYA**

2009

UNIVERSITI MALAYA

ORIGINAL LITERARY WORK DECLARATION

Name of Candidate: NIZAM TAMCHEK (I.C/Passport No: 770306-04-5369)

Registration/Matric No: SHC 050018

Name of Degree: Degree Of Doctor Of Philosophy

Title of Project Paper/Research Report/Dissertation/Thesis ("this Work"):

CHARACTERISATION OF BISMUTH-BASED ERBIUM-DOPED FIBRE AND ITS
APPLICATION IN WIDE-BAND OPTICAL AMPLIFIERS

Field of Study: Photonic

I do solemnly and sincerely declare that:

- (1) I am the sole author/writer of this Work;
- (2) This Work is original;
- (3) Any use of any work in which copyright exists was done by way of fair dealing and for permitted purposes and any excerpt or extract from, or reference to or reproduction of any copyright work has been disclosed expressly and sufficiently and the title of the Work and its authorship have been acknowledged in this Work;
- (4) I do not have any actual knowledge nor do I ought reasonably to know that the making of this work constitutes an infringement of any copyright work;
- (5) I hereby assign all and every rights in the copyright to this Work to the University of Malaya ("UM"), who henceforth shall be owner of the copyright in this Work and that any reproduction or use in any form or by any means whatsoever is prohibited without the written consent of UM having been first had and obtained;
- (6) I am fully aware that if in the course of making this Work I have infringed any copyright whether intentionally or otherwise, I may be subject to legal action or any other action as may be determined by UM.

Candidate's Signature



Date 15 NOV 2009

Subscribed and solemnly declared before,

Witness's Signature



Date 19 NOV 2009

Name:

Designation: Pegawai Penyelidik

MOHD. ZAMANI ZULKIFLI

PHOTONICS RESEARCH CENTRE
UNIVERSITY OF MALAYA

ABSTRACT

In this thesis, the characterisation of Bismuth based Erbium-doped Fibre Amplifier (Bi-EDFA) for Conventional- and Long- (C+L) Wide-band optical amplifier in Wavelength Division Multiplexing (WDM) optical network was presented and performed. Bismuth based Erbium-doped Fibre is a novel optical gain material that was specifically developed for current and future optical amplifiers.

The work focuses on the optical amplifier's characteristic and performance of Bi-EDFA using bi-directional pumping configuration as a potential optical amplifier for 1.55 μm optical communication. The material, physical and optical characteristics of Bi-EDF are calculated, measured and successfully demonstrated the necessary properties for efficient optical amplifier but also highlight the problem associated with higher Erbium ions dopant concentration and Bismuth host glasses. In addition, the effect of self-saturation was investigated and found to influence the gain, noise and efficiencies of the output signal. These important knowledge then discussed for development and prospect of Bi-EDFA as potential optical amplifier in future optical communication system.

ABSTRAK

Dalam tesis ini, ciri-ciri penguat gentian berdopan erbium berasas Bismuth (Bi-EDFA) untuk gelombang konvensional (lajur C) dan gelombang panjang (lajur L) lajur-lebar di dalam sistem multiplek pembahagian panjang gelombang telah dilakukan and di bentangkan. Penguat gentian berdopan erbium berasas Bismuth adalah penguat cahaya yang nobel yang telah dibangunkan khas untuk penguat gentian kegunaan sekarang dan masa hadapan.

Kerja-kerja penyelidikan menumpukan ciri-ciri dan prestasi Bi-EDFA menggunakan konfigurasi dwi-arah pam sebagai peguat gentian yang berpotensi untuk komunikasi cahaya di 1.55 μm . Ciri-ciri bahan, fizikal dan cahaya Bi-EDF telah dikira, diukur dan telah berjaya menunjukkan sifat-sifat yang diperlukan sebagai penguat gentian yang cekap tetapi juga telah mengemukakan masalah-masalah yang berkaitan dengan kandungan erbium ion yang tinggi and gelas berasas bismuth. Tambahan itu, kesan-kesan tepu-sendiri telah disiasat dan di dapati telah mempengaruhi keluaran penguat, kebisingan dan kecekapan isyarat keluaran. Pengetahuan yang penting ini telah dibincangkan untuk pembangunan dan prospek penguat gentian berdopan erbium berasas Bismuth sebagai penguat gentian yang berpotensi di dalam sistem komunikasi cahaya masa hadapan.

ACKNOWLEDGEMENT

My sincere thanks to my supervisor Professor Harith Ahmad for his interesting insight and his invaluable guidance, criticisms and encouragement and also the opportunity that he gave to conduct this research project.

Also, I would like to thanks to my co-supervisor Dr. Sulaiman Wadi Harun for his support, advice and cooperation. Special thanks for Dr. Prabakaran Poopalan for his helpful co-operation and advice as well as to Dr. Thirumeni Subramanian, Chong Wu Yi, research members at Photonics Research Laboratory and others for their support during the course of my research.

Finally, I would like to thank my family and friends for their endless mental support. This thesis is dedicated to them as a token of my gratitude and heartfelt respect.

LIST OF CONTENTS

	Page
ABSTRACT	i
ABSTRAK	ii
ACKNOWLEDGEMENT	iii
LIST OF CONTENTS	iv
LIST OF FIGURES	viii
LIST OF TABLES	xiv

CHAPTER 1

INTRODUCTION

1.1	Optical Fibre History and Technology	1
1.2	Erbium-Doped Fibre Amplifier (EDFA)	7
1.3	Limitation of Silica-based EDFA	9
1.3.1	Concentration Quenching	9
1.3.2	Amplification Bandwidths	12
1.3.3	Saturation Output Power	13
1.4	Motivation of the study	14
1.5	Thesis Overview	15
	REFERENCES	18

CHAPTER 2

THEORETICAL BACKGROUND

2.1	Introduction	23
2.2	Erbium ions in glass host	
2.2.1	Brief of Glass host and Erbium ion	24
2.2.2	The requirements for EDFs as optical amplifier	30
2.2.3	Energy level system of Er^{3+} :glass	42
2.3	Light amplification principles of EDFA	
2.3.1	General Theory	48
2.3.2	Rate Equations	48
2.3.3	Light propagation and amplification	49
2.3.4	Er^{3+} ion Absorption and Emission Cross Section	55
	I. Judd-Ofelt Theory	55
	II. McCumber Theory	57
	REFERENCES	59

CHAPTER 3

CHARACTERISATION OF ERBIUM-DOPED BISMUTH FIBRE

3.1	Introduction	70
3.2	Physical Properties of Bismuth glass host	71
3.3	Characteristics of Bi-EDF	83
3.3.1	Judd-Ofelt Intensity Analysis	89
3.4	McCumber Cross Section Analysis	94

3.5	1550 nm Transition Lifetime	99
3.6	Upconversion Fluorescence	103
3.7	Optical Amplifier Figure-of-merit (FOM)	108
	REFERENCES	110

CHAPTER 4

CHARACTERISATION OF ERBIUM-DOPED BISMUTH FIBRE AMPLIFIER

4.1	Introduction	121
4.2	EDFA Pumping Configurations	122
4.3	EDFA Simulation	124
4.4	The Experimental Result	128
	I. Gain and Noise Figure (NF)	129
	II. Quantum and power conversion efficiency (QCE, PCE)	144
	III. Self-Saturation	150
	IV. Amplification bandwidth	153
	V. Temperature effect in Bi-EDF optical amplifier	159
	REFERENCES	166

CHAPTER 5

BISMUTH-BASED EDFA IN WDM OPTICAL NETWORK

5.1	Introduction	171
5.2	Gain Equalisation in WDM Optical Systems	171

I.	Gain Saturation	180
II.	Gain Compression	183
III.	Gain Flatness	185
IV.	Gain Spectral Hole Burning	189
REFERENCES		193

CHAPTER 6

DISCUSSION and CONCLUSION		
6.1	Introduction	197
6.2	Erbium-doped Bismuth Optical Fibre Spectroscopic Properties	198
6.3	C+L band Bismuth-based EDFA	201
6.4	Bi-EDFA in WDM optical network system	203
6.5	Issues and Suggestion for Future Work	205
REFERENCES		207

APPENDIX

Reprint of Selected Paper	209
---------------------------	-----

LIST OF FIGURES

CHAPTER 1.	INTRODUCTION	Page
1.1	Growth of global traffic by client segments (voice, transaction data and Internet), as viewed from year 2000. The figures in parenthesis indicate the projected yearly growth rates for each segment.	6
1.2	Basic EDFA configuration	8
CHAPTER 2.	THEORETICAL BACKGROUND	
2.1	Alkali silicate glass structure based on (Si^{4+} , O^{2-}) network formers and alkali ion network modifier. The fourth bridging oxygen of the silicon tetrahedron is outside the plane of the figure	24
2.2	Pyramidal polyhedron structure of Bi_2O_3 glass	26
2.3	The splitting of the 4f electronic energy of Er^{3+} ions, illustrating the effect of electrostatic-electron interactions and spin-orbit splitting	28
2.4	Transmission loss spectrum of silica glass fibre from visible to near-infrared region	30
2.5	Comparison of optical amplifiers bandwidth using EDF with silica, fluoride and telluride host glasses, Raman amplifiers and semiconductor optical amplifiers (SOA).	33
2.6	Schematic representation of concentration quenching effect in Er^{3+} ions using two-level approximation (donor (D) and acceptor (A)). The horizontal lines represent Stark manifolds of the 4f levels of Er^{3+} . (a) resonant energy migration, (b) cross relaxation, (c) Cooperative frequency upconversion	35
2.7	Possible upconversion transitions from cooperative frequency upconversion process. $\text{Er}^{3+}(1)$ is a donor and $\text{Er}^{3+}(2)$ is a acceptor.	37
2.8	Examples of cladding-pumped structures for optical amplifier profile: (a) eccentric core, (b) rectangular, (c) D-shape, (d) star, (e) polygon, (f) holey (air)	40
2.9	Bismuth-based erbium doped fibre amplifier with 4x4 cm in dimension (courtesy of Asahi Glass Co.)	42

2.10	Energy levels of erbium-ion showing possible absorption spectrum (pump band) at 980 nm and 1480 nm and radiative transition (gain spectrum at 1520-1610nm) and the multiple lines representing the Stark levels.	43
2.11	Representation of absorption, stimulated emission and spontaneous decay	44
2.12	Illustration of ligand field of Er^{3+} ions and host	46
2.13	(a) Effect of Stark splitting in the energy level, (b) effect of inhomogeneous broadening, where random field variations from site to site cause changes in the Stark splitting and centre wavelengths of laser transitions	47
2.14	Light amplification after propagation in length L of gain medium	50

CHAPTER 3. CHARACTERISATION OF ERBIUM-DOPED BISMUTH FIBRE

3.1	Sequence of measurement in Bi-EDF for basic parameters characterisation	71
3.2	(a) Cross section of the sample using SEM. (b) Closed-up area for EDX measurement	72
3.3	The energy spectra of the sample from EDX measurement.	73
3.4	Refractive index of (a) bismuth borate glasses and (b) silica glasses with different dopant and oxide addition taken from Refs. [16] and [17]	76
3.5	Lanthana cubical (a) and phosphorus pentavalent link with three singly-bonded and one doubly-bonded oxygen (b).	79
3.6	Variations of T_g (glass transition temperature) with (a) Al_2O_3 [17] (b) Bi_2O_3 [17,18] and (c) La_2O_3 [19]	81
3.7	Element distribution on Bi-EDF sample from EDAX measurement	82
3.8	Mixed angle fusion splicing between Bi-EDF and Silica fibre.	83
3.9	Transmission spectra measurement set-up, OSA: Optical Spectrum Analyser	85
3.10	Absorption spectra of T1L Bismuth fibre (Solid line indicate the data	86

extrapolation).

3.11	Normalised absorption intensity of Bi-EDF and Si-EDF (courtesy of Asahi Glass and Fibercore Ltd.)	87
3.12	Fluorescence intensity of Bi-EDF and Si-EDF under 1480 nm pumping.	88
3.13	Normalised fluorescence spectra of Er^{3+} in various type of glasses under 979 nm pumping taken from Ref. [13]	89
3.14	Experimental and calculated absorption and emission cross sections of Er^{3+} ions $^4\text{I}_{13/2}$ transition Bi-EDF.	96
3.15	The difference between measured and calculated emission cross-section in Bi-EDF as a function of wavelength	96
3.16	Measured and calculated McCumber cross-section ratio η of Bi-EDF	98
3.17	Determination of lifetime using a pulsed laser and time resolved measurements. (a) A narrow excitation pulse and (b) the time decay of the resulting fluorescence.	100
3.18	Experimental set-up for lifetime measurement. The Wavelength Selective Coupler (WSC) and the thin-film filter (TFF) is used to filter out the 1530 nm emission from the 1480 nm laser diode (LD).	101
3.19	Measured 1550 nm lifetime of Bi-EDF. (Solid lines indicate fitting to the data)	102
3.20	Measured upconversion fluorescence spectra of Bi-EDF under 1480 nm LD excitation	105
3.21	(a) The upconversion fluorescence at 975 nm versus 1480 nm pump power and (b) fluorescence power at 980 nm versus power at 1550 nm. The number in figure (a) and (b) denote the slope values at low and high pump power, respectively.	107

CHAPTER 4. CHARACTERISATION OF ERBIUM-DOPED BISMUTH FIBRE AMPLIFIER

4.1	Basic single-pass bi-directional configuration set-up of Bi-EDF amplifier, TLS:Tunable Laser Source, VOA:Variable Optical Attenuator, CIR: Circulator, LD:Laser Diode, ISO:Isolator,	123
-----	--	-----

OSA:Optical Spectrum Analyser

4.2	The excited state N_2 population density for Bi-EDF for different pumping configuration.	125
4.3	The simulation results of (a) forward ASE and signal power (b) for Bi-EDF for different pumping configuration.	127
4.4	The Bi-EDF forward ASE spectrum for different pumping configuration	128
4.5	Determination of the ASE level using linear interpolation	131
4.6	The gain of Bi-EDF for different forward (a) and backward (b) pump power ratio. The broken line correspond to gain coefficient of the Bi-EDFA. (A) = uni-directional backward pumping, (B,C,D) = bi-directional pumping with forward pump was fixed at 50, 100, 150 mW, (E) = uni-directional forward pumping, (F,G,H) = bi-directional pumping with backward pump power was fixed at 50, 100, 150 mW	134
4.7	The NF of Bi-EDF for different forward (a) and backward (b) pump power increment. F: forward, B: backward (bi-directional), For/Back Only: Uni-directional forward/backward pump	141
4.8	The gain and NF with bi-directional pumping with equal ratio (balanced)	143
4.9	The (a) QCE and (b) PCE of Bi-EDF for different forward and backward pump ratio. F: forward, B: backward pumping (bi-directional); For/Back: Uni-directional forward/backward pump	146
4.10	Forward and backward ASE spectrum power and power ratio P_{for}/P_{back} as a function of total pump power with 0 dBm input signal (under bi-directional configuration with equal power ratio)	149
4.11	The gain (a) and NF (b) as a functions of input signal power at signal wavelength of 1560nm with bi-directional pump configuration. F### - B\$\$\$: Forward pump = %%% and backward pump = *** mW for a total pump power of %%% + *** mW (bi-directional)	151
4.12	The gain (a) and NF (b) at 0dBm input signal power as a functions of input signal wavelength at different bi-directional pump power configuration. FOR: forward, BACK: backward pumping (uni-directional), F### - B\$\$\$: Forward pump = %%% and backward pump = *** mW for a total pump power of ### + *** mW (bi-directional)	154
4.13	The QCE at 0dBm input signal power as a functions of input signal wavelength at different bi-directional pump configuration. FOR: forward, BACK: backward pumping (uni-directional), F### - B\$\$\$:	157

Forward pump = %%% and backward pump = *** mW for a total pump power of %%% + *** mW (bi-directional)

- 4.14 The QCE different as the function of input wavelength in bi-directional pump configuration at 200 and 250 mW pump power with different forward and backward pump power. 158
- 4.15 The experimental set-up to measure the effect of fibre temperature, TLS:Tunable Laser Source, VOA:Variable Optical Attenuator, CIR:Circulator, LD:Laser Diode, ISO:Isolator, OSA:Optical Spectrum Analyser 161
- 4.16 The gain (a) and the NF (b) at 0dBm input signal power as a functions of input signal wavelength at different temperature. 162
- 4.17 The gain and NF different at 0 °C and 63 °C as a functions of input signal wavelength. 163
- 4.18 The QCE / temperature (slope coefficient) as a functions of input signal wavelength. 164

CHAPTER 5. BISMUTH-BASED EDFA IN WDM OPTICAL NETWORK

- 5.1 Schematic for 4 channel WDM optical system, LD: Laser diode, OSA: Optical Spectrum Analyser 172
- 5.2 The signal gain and NF for the 4 channel WDM system testing 174
- 5.3 The signal SNR and noise level for the 4 channel WDM testing system 175
- 5.4 Wavelength Add/Drop Multiplexer (WADM) (a) and 4x4 Active Cross-connects Switch (b) 177
- 5.5 Gain and NF at 1560 nm when another signal is dropped and added into the Bi-EDFA 178
- 5.6 Gain slope between all 4 signal channel when input power at 1560 nm is varied from -5 to -30 dBm 179
- 5.7 The signal gain (a) and NF (b) at 1560 nm when a other signal channel is dropped and added into the Bi-EDFA 182
- 5.8 The signal gain at 1560 nm with different saturating signal wavelength 183
- 5.9 The signal gain (a) and NF (b) at 1560 nm with different saturating 184

signal power

- | | | |
|------|---|-----|
| 5.10 | Gain flatness of Bi-EDFA. Gains for input signal power of 0 and -20 dBm are given for comparison, Sat: saturating laser power | 186 |
| 5.11 | NF of the signal input for gain flatness measurement of Bi-EDFA. The NF for input signal power of 0 and -20 dBm is shown for comparison | 187 |
| 5.12 | Peak power of Bi-EDFA in gain flatness measurement. The peak power for input signal power of 0 and -20 dBm is shown for comparison | 188 |
| 5.13 | The spectral hole-burning effect with different saturating signal power at 1560 nm | 191 |

LIST OF TABLES

CHAPTER 2.	THEORETICAL BACKGROUND	Page
2.1	Electron configuration with their corresponding electronics configurations and ground states of selected lanthanide elements in the +3 ionisation state (trivalent).	6
CHAPTER 3.	CHARACTERISATION OF ERBIUM-DOPED BISMUTH FIBRE	
3.1	Bi-EDF glass composition analysis from EDAX	74
3.2	Bi-EDF optical specification	83
3.3	Doubly reduced matrix element of $U^{(0)}$ for Er^{3+} taken from Ref. [47] and used in the Judd-Ofelt coefficient calculations	90
3.4	Judd-Ofelt coefficient for various glasses. (I):LKBBG: $5Li_2O \cdot 5K_2O \cdot 10BaO \cdot 50Bi_2O_3 \cdot 30Ga_2O_3 \cdot 0.406Er_2O_3$; [54] (II):Bismuth-Borate: $(Er_2O_3)_{0.0025}((Bi_2O_3)_{0.25}(B_2O_3)_{0.75})_{0.9975}$; [55] (III):S25AlN: $25SiO_2 \cdot 25AlO_{3/2} \cdot 25NaO_{1/2} \cdot 0.5ErO_{3/2}$ [56]	91
3.5	Cooperative upconversion coefficients for bismuth host glass with comparison with other works	104
3.6	FOM of various glass host for optical amplifiers	109
CHAPTER 4.	CHARACTERISATION OF ERBIUM-DOPED BISMUTH FIBRE AMPLIFIER	
4.1	Bi-EDF parameters used for the theoretical calculation	125
4.2	Gain variation in bi-directional pumping configuration with different pump power addition with total pump power was fixed 180mW.	136
4.3	Input and output signal dynamic range	150
4.4	The depths of the NF dip with total pump power	152
4.5	3dB bandwidth of Bi-EDF bi-directional pumping	155

CHAPTER 1

INTRODUCTION

1.1 Optical Fibre History and Technology

The idea of using light as a method of communications is not new. Since the advent of man, light has been extensively used convey signal and information over long distances, especially when quick messaging is required (i.e. Warnings and cues used in ancient war, lighthouses, beacons etc.). In modern telecommunications however, the boom of the internet and mass communications networks, requires for rapid transfer of large amounts of information over even larger distances across the globe. As the bounds of wired communications become strained, man has again turned to light signals as a conduit to meet up to the demands of the ever increasing information bandwidth. These light signals traverse the globe through bundles of fine glass strings known as optical fibre glass.

Works on the optical fibre glass began with the research team headed by Antoni E. Karbowiak who worked under Reeves at the Standard Telecommunication Laboratories to study optical waveguides for communication. It was they who first begin to work on glass fibres that could be used in communications. However, the revolutionary breakthrough came when a young engineer named Charles K. Kao joined the team and speculated that silica-based optical fibres may exhibit losses as low as 20 dB/km [1]. At the same time, researchers at Corning Glass Works (now Corning Inc.), Robert Maurer, Donald Keck and Peter Schultz began work on fused

silica; a material that could be made extremely pure, but has a high melting point and low refractive index, which was then made into a cylindrical preform and drawn to silica fibre using a process known as 'Inside Soot Deposition' [2].

In 1974, a group from Bell Laboratories made a significant breakthrough. By developing a Modified Chemical Vapour Deposition (MCVD) method, they managed to produce fibres with a loss of 1.1 dB/km at a wavelength of 1.06 μm [3,4,5]. Over the next several years, fibre losses saw a dramatic drop, due to improved fabrication methods and the lesser impurity in the the raw materials used. The communication window was then shifted to the longer wavelength region where silica fibres exhibited lower attenuation.

While the losses in optical fibres had been significantly reduced, transmission signals were still subjected to the inherent losses within the optical fibre. As a result, the signal power degrades over distance, making optical communications is only suitable for short distances. Overcoming this problem required the use of an amplifying mechanism, and early systems employed electronic regeneration to accomplish this task. However, electronics regeneration devices are expensive and bulky; its components are bit-rate sensitive and required reprimand for higher bit rates and so a more viable alternative was sought after.

C. J. Koester *et.al* first reported an 'optical amplifier' using a Neodymium ion doped into a silica fibre [6, 7]. Subsequently, further work has been done by some groups to develop semiconductor laser diodes as a pump source. Progress was slow, until 20 years later when a group from University of Southampton reported high-gain fibre amplifiers operating in the 1550 nm region using Erbium-Doped Fibre (EDF) [8] as gain medium. These research efforts, in conjunction with the development of

semiconductor laser diodes at 980 nm [9] and 1480 nm [10] as pump sources, accelerated the deployment of optical amplifiers and revolutionized the optical telecommunications industry. The main reason for the strong impact optical communication has on today's telecommunication systems is that optical fibres have many advantages as compared to traditional copper or coaxial cables. Optical fibres has the ability to carry much more information and deliver it with greater fidelity than either copper wire or coaxial cable. By that, fibre optic cables can support much higher data rate, and at greater distance, than coaxial cables, making it ideal for transmission of serial digital data. In addition, a fibre optic cable is totally immune to virtually all kinds of interference, including lightning and additionally it will not conduct electricity. It can therefore come in direct contact with high voltage electrical equipment and power lines. It will also not create ground loops of any kind. As the basic fibre material is made of glass, it will not corrode and is unaffected by most chemicals, means it also can be buried directly in most kinds of soil or exposed to most corrosive atmospheres in chemical plants without significant concern. Since the only carrier in the fibre is light, there is no possibility of a spark from a broken fibre. Even in the most explosive of environment, there is no fire hazard, and no danger of electrical shock to personnel repairing broken fibres.

Fibre optic cables are also virtually unaffected by outdoor atmospheric conditions, allowing them to be lashed directly to telephone poles or existing electrical cables without concern for extraneous signal pickup. Its usually much smaller and lighter in weight than a wire or coaxial cable with similar information carrying capacity. It is also easier to handle and install, and uses less duct space (frequently it can be installed without ducts). Because the data is transmitted in light

form, fibre optic cables are ideal for secure communications systems because it is very difficult to tap the information but very easy to monitor. In addition, there is absolutely no electrical radiation from a fibre.

With these advantages, the research activities surged forward to increase the capacity of the optical system by utilising all low loss optical signal region of silica fibres. There are two common techniques to increase network capacity in optical networks, namely Time-Division Multiplexing (TDM) and Wavelength-Division Multiplexing (WDM) .

TDM uses the time slice method to share information between different channels onto a single data carrier. In the time slot, the signal is modulated with the first information channel; for the next time slot, the signal is modulated with the second information channel, and so forth [11]. The duration of a time slot demands upon a number of different designs and the transmission speed needed for each link. Each communication path is assigned into a specific time slot and no other source is permitted to transmit at the same time. The multiplexer at the source end takes in data from the source connected to it, and inserts packets of data from each other into the fibre during the appropriate TDM time slot. The de-multiplexer at the end then must recognize the time slots, unload the data from each slot, and send it as a continuous stream to the corresponding user.

Wavelength-Division Multiplexing (WDM) on the other hand is much simpler and was introduced to optical communications links to overcome the restrictions of TDM systems. The WDM system uses specific signal carriers at different carrier wavelengths to carry data. These signal carriers have individual data-rates and can be combined or divided depending on data usage [11]. Optical

networks with WDM systems can avoid many of the constraints and implementation difficulties that limit the performance and at the same time making do without the need for expensive re-cabling therefore, reduce the cost of upgrading the network significantly . It also opens up a new era of optical fibre communications where a single fibre can carry many different channels of data and can be re-routed to different destinations [12]. The ability to increase bandwidth capacity and reconfiguration of the network will enable network providers to keep costs down.

WDM technologies are important in long-haul applications where greater bandwidth capacity is needed. Wide Area Networks (WAN), such as Cable Television (CATV) systems which represent a large market, though there are economical concerns due to expensive base of installed cables. The dramatic increase in the number of wavelengths carried on single fibre links has resulted in a more narrow channel spacing that has created a new class in the WDM domain, namely Dense Wavelength-Division Multiplexing (DWDM) systems. The DWDM system can have more than 40 channels in a single fibre mostly in the communication frequency centred at 193 THz (1550 nm). With 40 Gbit/s per channels and 128 channels, a single fibre can transmit data at almost 5.12 Tbit/s [13]. Figure 1.1 shows the projected global-traffic from year 2000 for voice, data and Internet. The yearly growth is dominated by Internet with growth rates of 157% with expected data capacity of 120 Tb/s at year 2010. Therefore from this growth rates, currently deployed WDM optical networks will need higher number of channels with higher data rate to bear the demands.

The deployment of the DWDM in long-haul systems requires a broadband optical amplifier in order to amplify multiple signal wavelengths [14,15]. Therefore,

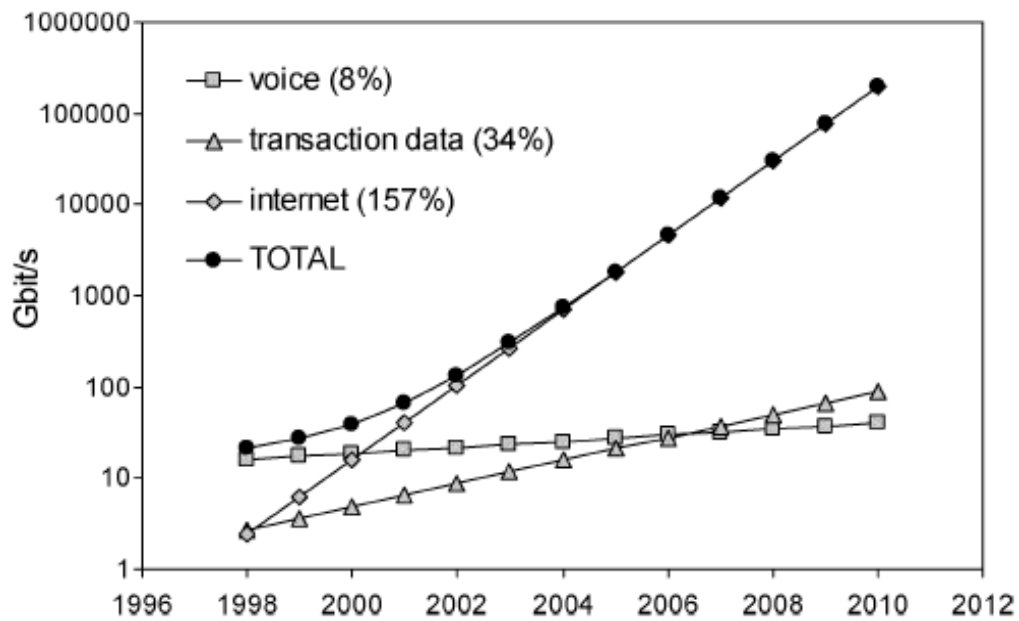


Figure 1.1 Growth of global traffic by client segments (voice, data and Internet), as viewed from year 2000. The figures in parenthesis indicate the projected yearly growth rates for each segment. [16]

until the development of broadband optical amplifiers, the DWDM system is unfortunately only limited to short-range links where the power budget is low. Compared to conventional optical-electrical-optical (O-E-O) converters as in a repeater that have narrow and fixed amplification bandwidths, optical amplifiers are immune and transparent to input signals of different bit rates or formats and can be used to achieve simultaneous amplification of multiple optical signals over silica fibre. Combined losses [15] due to Rayleigh scattering, hydroxyl absorption and absorption due to the vibration of silicon-oxygen bonds are minimum, which is most suitable for DWDM optical networks. This flexibility enables optical amplifiers to be fully utilised in the long-haul DWDM network with lower cost and complexity [16].

1.2 Erbium-Doped Fibre Amplifier (EDFA)

The EDFA is the crucial element in optical fibre communications today [16,17]. It has several advantages such as :

1. High signal gain
2. Wideband amplification
3. High saturation power
4. Low signal noise
5. Low crosstalk between different signals
6. Data bit-rate independent
7. Polarization insensitive
8. Low non-linear effect such as four wave mixing (FWM), cross-phase modulation (XPM).

These are characteristics, which cannot be achieved by ordinary electronics based amplifiers thus, making the optical amplifier very important in DWDM networks. Furthermore the ready available of laser diodes as a pump source makes it even more viable [17]; hence, making the optical amplifier devices compact and suitable for low spatial and cost effective applications. In addition to these advantages, the EDFA is compatible with current WDM optical networks that utilise silica-based optical fibre, thereby making the device integration process seamless.

In general, an EDFA consists of a length of fibre made from silica that has been specially doped with a Rare-Earth (RE) element (Erbium) that can transfer photon energy from separate pump laser diode to the signal wavelength, thus, in

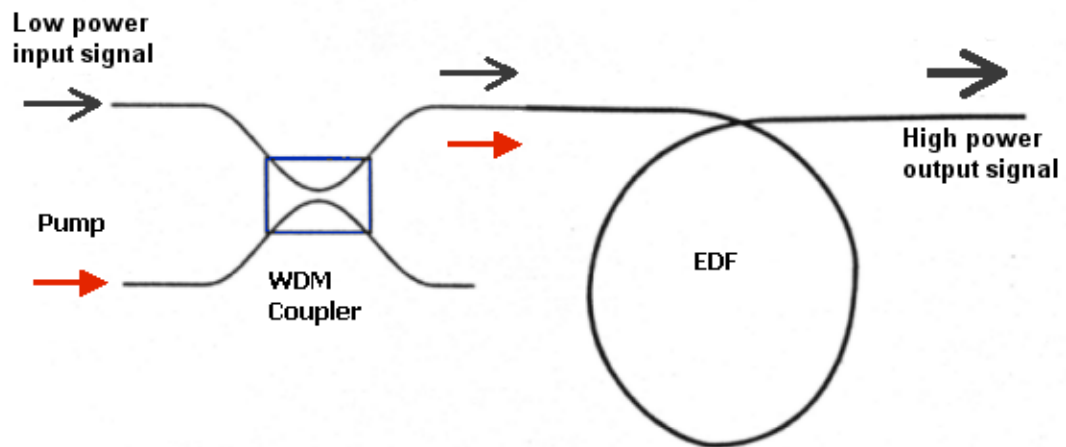


Figure 1.2 Basic EDFA configuration

effect amplifying it. The basic EDFA configuration is shown in Figure 1.2. The laser diode output and the incoming signal are combined through a Wavelength Division Coupler (WDC) coupler and are launched into an erbium-doped fibre. Pump photons excite the erbium ions which in turn gives signal amplification in the 1.55 μm wavelength region.

The RE doping process into silica glass produces a degeneracy of the RE energy level from the perturbation of the glass ligand (electric) field that is known as Stark splitting [17-19]. These degeneracy are in Boltzmann thermal equilibrium [19] that arises numerous complicated effects and must be assessed carefully to determine the spectroscopic properties of the glass host when excited by external radiation. Several approximation calculation have been developed based on Judd-Ofelt [20, 21] and McCumber [22] theories to perceive the implication of the Er^{3+} ions 4f energy level degeneracy by the glass ligand field. Since development of these theories, researcher finally can track-down the effect of ligand field and lead to development of multicomponent glass host [23-25] such as Zirconium Barium Lanthanide

Natrium Fluoride (ZBLAN) [24] and antimony silicate (AS) [25, 26] for optical amplifier and laser application.

The energy conversion process also depends on many other parameters from pump radiation wavelength, fibre geometry and profile, doping concentrations, optical amplifier design, etc [17-19]. For wide-band amplification applications, these parameters became critical as minor changes in these parameters can reduce/limit the signal performance significantly. Therefore, it is necessary to understand in detail the nature of these parameters and how it affects the amplifier operation.

1.3 Limitation of Silica-based EDFA

The deployment of silica-based EDFA in today's optical networks has accounted for the expansion of optical telecommunication system utilising both the DWDM and TDM system in tandem. However, the ever-increasing demand for higher data capacity and longer transmission distance in current optical telecommunication system has accelerated the silica-based EDFA to its limit. The most common drawback of silica-based EDFA is limited RE doping concentration, amplification bandwidth and saturation output power.

1.3.1 Concentration Quenching

During EDF fabrication process, the RE is doped into the fibre core to activate the 1550 nm luminescence. The doping process occurs at random and may form the ions cluster if the cohesive force of the glass atoms is strong. Glass with

strong cohesive force requires higher cohesive energy density to break all its intermolecular physical link [27]. Therefore this kind of glass material is known to have low solubility constants.

Silica glass has been recognised to have low RE solubility that cause high concentration RE silica glass easier to form ion clustering [17, 19]; which results in effect of *concentration quenching*. Despite this, the RE solubility can be improved by adding other glass network modifiers such as Al_2O_3 to the EDF. However, the maximum number of Er^{3+} ions concentration is still limited to a few thousand ppm. In the case of Al/Ge-doped silica-based glass EDFA, the Er^{3+} ions is limited to only 1000 wt ppm before concentration quenching occurs [23, 28].

Under the effect of concentration quenching, due to the fact that excited Er^{3+} ions are packed within a short fibre length, it triggers an interionic energy processes such as energy migration, cross-relaxation and upconversion [19]. The details of these processes are discussed in chapter 2. These energy processes cause the gain coefficient per unit length of silica-based EDFA to be lower compared with other glass host. Consequently, causing an increases of the silica-based EDFA length and also the pump power for high output power applications. Therefore, this will increase the cost of EDFA device and more importantly the total optical nonlinearity of the EDF.

The optical nonlinearity in optical fibre can be divided into two categories. The first type arise due to the interaction of light waves (photon) with glass phonons while the second type are related to dependency of light intensity with refractive index of the optical fibre [29]. These effects are characterised and influenced by the optical dispersion, effective area of the optical fibre, overall fibre length, signal

wavelength spacing in multi-channel systems, the degree of longitudinal uniformity of the fibre characteristics, signal source linewidth and the intensity of the signal. The example of the nonlinear effects in optical fibre are Self-Phase Modulation (SPM), Cross-Phase Modulation (XPM), Four-Wave Mixing (FWM), Stimulated Raman Scattering (SRS) and Stimulated Brillouin Scattering (SBS) [29, 30].

The optical nonlinearity in an EDF have a significant impact on the performance of WDM optical networks system. They may lead to signal attenuation, distortion and cross-channel interference. In a WDM system, these effects restrict the wavelength spacing between different signal channel, signal power per channel, signal data rate and transmission distances [29].

Due to numerous limitation of silica-based EDFA for WDM optical network, other host glass such as bismuth, ZBLAN, and phosphate glass have been developed to compensate of low RE silica glass solubility. These host glasses have been successfully doped with RE up to 12.2×10^{20} ion/cm³ [31] without ion clustering and as a result, produce lower/less concentration quenching effect. With high RE solubility, the total EDF length for signal amplification is reduced significantly for ultra-compact application, thus, lead to a new research for ultrafast generation and soliton amplification using optical fibre [32]. Glasses such as bismuth and phosphate have also shown better thermal stability and chemical durability compared to fluoride-based glass such as ZBLAN. Beside their high RE solubility, glasses such as phosphate and ZBLAN glasses are difficult to fabricate due to their hygroscopic and devitrification properties that may result in many difficulties in fabrication process and during optical amplifier's deployment [23, 31].

1.3.2 Amplification bandwidths

Silica-based EDFAs have a limited amplification bandwidth that ranges from wavelength of 1530 to 1565 nm, which known as the C-band region. By exploiting signal and ASE re-absorption properties in longer EDF length, the amplification bandwidth is expanded to longer wavelengths (i.e. from 1570 to 1600 nm), which are known as L-band region. However this technique is unfavorable because its also increases the optical nonlinearity that worsens the signal quality at the transmitter ends [30]. Besides that, the efficiency of the optical amplifier becomes lower due to the effects of Excited-State Absorption (ESA) [19, 22, 23], where, excited Er^{3+} ions at metastable state may experience re-absorption to a higher energy level rather than undergoing stimulated emission to ground state.

With growing demand for increased data bandwidths in DWDM optical network systems, subsequent research activity has given rise to a new technique to harvest the L-band region. New glass hosts doped with Er^{3+} ions such as bismuth [31] and telluride [34] glass and optical amplifiers based on Raman effect [30, 35] have shown to be promising technologies for attaining increased transmission capacity for current and future DWDM networks.

Raman optical amplifiers use the principles of stimulated emission process associated with Raman scattering in an optical fibre for the amplification of signals. Raman scattering generates a Stokes shift [36] corresponding to the glass optical phonon (molecular vibrational state), which is approximately 13.2 THz [35, 36] for silica-based optical fibre that amplifies longer signal wavelengths by the equivalent amount of the frequency shift. Because the amplification region is dependent on the

pump wavelength, wider amplification bandwidth of more than 100 nm [36] can be achieved by using multiple pump wavelengths across the target gain window.

However, there are several disadvantages inherent to the Raman amplification process such as shorter process lifetime, higher signal cross-talk and noise due to cross-gain saturation, pump noise, interference of Double-Rayleigh Backscattered (DRBS) noise, Four-Wave Mixing (FWM) and cost-efficiency due to the multiple pump source requirement for broadband amplification. For these reason, Raman optical amplifier is unfavourable for high data rate, low-cost and long-haul WDM optical networks.

1.3.3 Saturation output power

The maximum optical output power generated from an optical amplifier can be assessed by the saturation output power parameter. This parameter is defined as the ratio of output power at which there is a 50% reduction under its unsaturated condition [19]. This general definition shows the range of input signal power required for constant signal gain at a given LD pump power. In WDM optical networks where input signals can vary significantly, fixed signal gain value is preferred to maintain small output power fluctuations as well as low signal cross-talk and noise in a multiple-signal amplification system.

As the signal gain in EDFA is dependent on the signal wavelength, different wavelengths have different saturation output power values [19]. This leads to nonuniform output power across the amplification region, which increases the error rate of the system. However, other glass hosts such as Fluoride-based glasses [37, 38]

are known to have flatter signal gain that is capable of improving the flatness of the EDFA gain profile. Other techniques using active and passive optical filter such as acousto-optic filter, strain-tuned Bragg grating and planar integrated optics filters have successfully controlled the signal flatness by regulating the saturating effect in EDFAs [39, 40, 41].

From the brief discussion, the requirement of an optical amplifier device for current and future WDM optical networks is has still not been met due to the specific problems of the various amplifiers. While the Raman optical amplifier is certainly a promising device, it is held back by a number of intrinsic problems. New glass host EDFs have yet to make a breakthrough for commercial applications, mainly because of lack of details in terms of their characterisation and performance in WDM optical networks. In this thesis, a Bismuth-based EDFA (Bi-EDFA) is proposed as a solution to improve existing optical amplifier performance. The Bi-EDF is characterised and its capability in WDM network environment is investigated.

1.4 Motivation of the Study

In this thesis, the motivation of the research was to develop and improve the understanding of a different glass host for EDFAs, specifically bismuth-based EDFAs from the point of view of their physical, spectroscopic and optical properties for an application as wide-band optical amplifiers. Hopefully this new found information would help the development of EDFAs for current and future WDM optical networks.

Preliminary studies by other researchers [28-34] shows that the bismuth-

based EDFA has a significant advantages in which other host glass EDFAs cannot compete. The Bi-EDF has a lower melting temperature compared to a silica EDF, which makes it easier to be fabricated. The Bi-EDF also has good thermal stability and chemical durability, and is capable of supporting high Er^{3+} ion concentrations of up to 13,000 wt-ppm (more than 10 to 100 times compared to conventional silica based EDF). The Bi-EDFA has a high signal saturation power and flatness as well a wider amplification bandwidths (i.e. from 1530 nm to 1620 nm). It only uses a short length of active medium for C- and L- band region amplification, which increases the compactness of the device and reduces the potential optical nonlinearity effect in the amplifier.

In summary, Bi-EDFAs have demonstrated a lot of significant advantages as compared to normal silica based EDFAs. However, in order for these advantages to be fully utilized in inherent DWDM optical networks and in order for these amplifiers to be commercially viable replacements to currently deployed silica based EDFAs, further investigation is required.

1.5 Thesis Overview

This thesis is divided to four chapters that covers the theoretical background, bismuth glass spectroscopic properties, basic bismuth-based EDFA characterisation and performance investigation of bismuth-based EDFA in a WDM system.

In chapter 2, in order to explain the effect of glass host for optical amplifiers, a brief theoretical background of the fluorescence of Er^{3+} ion in glass host is discussed. Here also, the detailed description of optical glass host property,

requirement and its influence [20-31] on the optical amplifier application is presented. Also, the importance of current optical fibres and amplifiers for future optical telecommunications are also discussed in detail.

In the following chapter, Chapter 3, the characterisation of erbium-doped bismuth fibre is presented. The bismuth glass as a host, whose physical and optical properties and composition effect using the Judd-Ofelt and McCumber theories are discussed extensively. The distribution of the stimulated and upconversion emissions have been carried out to evaluate the performance of bismuth host glass. Using this information, the Figure of Merit (FOM) of optical amplifier is calculated and compared with other glass host.

In Chapter 4, in the first sections, using the result of erbium-doped bismuth fibre discussed earlier in chapter 3, the performance of bismuth-based EDFA is simulated. Later in the next section, all the basic measurements that are needed to be done for the determination of the optical amplifier properties and performance evaluation are proposed, discussed and compared with simulation data and result from other researchers. This section reveals the effect of the optical amplifiers pump configuration on the optical performance and the same is discussed.

In Chapter 5, the details of bismuth-based EDFA measurement for WDM optical networks are discussed. The gain saturation, flatness, output signal Signal-to-Noise Ratio (SNR) and channel spacing using gain hole burning technique is proposed and evaluated for a 4 channel system. Later, to determine the performance of bismuth-based EDFA in multiple channel optical system, saturating tone techniques is suggested and discussed.

In the final chapter, the summary on Bi-EDFA as an optical amplifier is made

and compared with conventional silica EDF. Future work is proposed to improve the capability and functionality of Bi-EDFA and bismuth host glass and to exploit it in later optical telecommunication systems.

REFERENCES

- [1] K. C. Kao and G. A. Hockham, "*Dielectric fibre surface waveguide for optical frequencies*" Proc. IEE, Volume 113, pp. 1151-1158, 1966
- [2] Midwinter, J.E., " *The future development of optical communication systems,*" All-Optical Networking: Existing and Emerging Architecture and Applications/Dynamic Enablers of Next-Generation Optical Communications Systems/Fast Optical Processing in Optical Transmission/VCSEL and Microcavity Lasers. 2002 IEEE/LEOS Summer Topi , 15-17 July 2002, pp. MB1-3 -MB1-4, 2002
- [3] J. B. MacChesney, P. B. O' Connor, F. V. DiMarcello, J. R. Simpson and P. D. Lazay, "*Preparation of low loss optical fibres using simultaneous vapor phase deposition and fusion,*" Proc. Int. Congress on Glass, Volume 6, pp. 40-45, 1974
- [4] W. G. French, J. B. MacChesney, P. B. O' Connor and G. W. Taskar, "*Optical waveguides with very low losses,*" Bell System Tech. J., May-June 1974, Volume 3, pp. 951-954, 1974
- [5] J. B. MacChesney and P. B. O' Connor, "*Optical fibre fabrication and resulting production,*" U.S. Patent 4.217.027 (Filed Aug.29, 1977)
- [6] C. J. Koetser and E. Snitzer, "*Fibre laser as a light amplifier,*" J. Opt. Soc. Amer., Volume 53, No. 4, pp. 515, 1963
- [7] C. J. Koetser and E. Snitzer, "*Amplification in a fibre laser,*" Appl. Opt., Volume 3, pp. 1182-1186, 1964
- [8] R. J. Mears, L. Reekie, I. M. Jauncey and D. N. Payne, "*Low-noise erbium-*

- doped fibre amplifier operating at 1.54 μm ,*” Electron. Lett., Volume 23, No. 19, pp. 1026-1028, 1987
- [9] R. S. Vodhanel, R. I. Laming, V. Shah, L. Curtis, D. P. Bour, W. L. Barnes, J. D. Minelly, E. J. Tarbox and F. J. Favire, “*Highly efficient 978 nm dipole pumped erbium-doped fibre amplifier with 24 dB gain*”, Electron. Lett., Volume 25, No. 20, pp. 1386-1388, 1989
- [10] M. Suyama, K. Nakamura, S. Khasiwa and H. Kuwahara, “*14.4 dB gain of erbium-doped fibre amplifier pumped by 1.49 μm laser diode*,” Proc. Optical fibre Communication, OFC' 89, paper PD2., 1989
- [11] Andre Girard, “*Guide to WDM technology and testing: A unique reference for the fiber-optic industry*”, EXFO Electro-optical engineering Inc., Quebec City, Canada, 2000
- [12] K. Sato, “*Advances in transport network technologies*,” Artech House, 1996, Norwood, MA
- [13] Agarwal, A., Banerjee, S., Grosz, D.F., Kung, A.P., Maywar, D.N., Gurevich, A., Wood, T.H., “*Ultra-high-capacity long-haul 40-Gb/s WDM transmission with 0.8-b/s/Hz spectral efficiency by means of strong optical filtering*”, Photonics Technol. Lett., IEEE , Vol. 15 Issue: 3 , pp.470 -472.,2003
- [14] J. Simpson, “*Fiber-based amplifiers: Progress in 1990*,” Optical Fiber Communication (OFC 1991), Proc. Vol. 2, invited paper FA1, pp. 191
- [15] T. Li, “ *The impact of optical amplifiers on long-distance lightwave telecommunications*,” Proc. IEEE, 1993, Volume 18, pp. 1568
- [16] E. Desurvire, “ *Capacity demand and technology challenges for lightwave systems in the next two decades*”, J. Light. Tech., Vol. 24, pp. 4697, 2006.

- [17] A. Bjarklev, “*Optical fiber amplifiers, design and system applications,*” Artech House , 1993, Norwood, MA ,
- [18] S. V. Kartapoulos, “*Introduction to DWDM Technology: Data in A Rainbow*”, Wiley Interscience, Chapter 8, 2000, pp.124
- [19] E. Desurvire, “*Erbium-doped fiber amplifiers: Principle and Application,*” John Wiley & Son Inc., New York, 1994.
- [20] B. R. Judd, “*Optical absorption intensities of rare earth ions*” Phys. Rev., Vol. 127, 1962, pp. 750
- [21] G. S. Ofelt, “*Intensities of crystal spectra of rare earth ions*”, J. Chem. Phys., Vol. 37, 1962, pp. 511
- [22] D. E. McCumber, “*Theory of phonon-terminated optical masers*”, Phys. Rev., Vol. 134, No. 2A, 1964, pp. 299
- [23] Naoki Sugimoto, “*Optical amplifier materials*”, Current Opinion in Solid State & Materials Science, 2001, Vol. 5, pp. 471
- [24] J.D. Minelli, W. L. Barnes, R. I. Laming, P. R. Morkel, J. E. Townsend, S. G. Grubb, D. N. Payne, “*Er³⁺ / Yb³⁺ co-doped power amplifier pumped by a 1W diode array,*” Proc. Topical Meeting of Optical Amplifiers and Applications, 1992, Optical Society of America, pp. Pd2
- [25] John D. Minelly, Adam J. E. Ellison, “*Multi-component silica glasses for broad bandwidth optical amplifiers*”, Conference on Lasers and Electro-optics, CLEO 2001, 2001, pp. 352
- [26] A. J. G. Ellison, D. E. Goforth, B. N. Samson, J. D. Minelly, J. P. Trentelman, D. L. McEnroe, B. P. Tyndell, “*Extending the L-band to 1620 nm using MCS fiber*”, Optical Fiber Communication Conference and Exhibit, 2001, (OFC

- 2001), Vol. 2, pp. TuA2-1
- [27] Jozef Bicerano, *"Prediction of polymer properties"*, CRC Press, 2002
- [28] Laming R. I., *"Saturated erbium-doped fiber amplifiers"*, Optical Amplifiers and their Applications, OAA 1990, pp. MB3
- [29] Biswanath Mukherjee, *"Optical WDM Networks"*, Springer Science+Business Media, 2006
- [30] Govind P. Agrawal, *"Nonlinear Fiber Optics"*, Academic Press, 2001
- [31] Liyan Zhang, Nan-Kuang Chen, Lili Hu, *"High Er^{3+} concentration low refractive index fluorophosphate glass for evanescent wave optical amplifiers"*, Phys. B: Condens. Matter, Vol. 403, Issues 19-20, 2008, pp. 3470
- [32] Kondo Y., Nagashima T., Takenobu S., Sugimoto N., Ito S., *"Fabrication of Bi_2O_3 -based Er-doped waveguide for integrated optical amplifiers"*, Optical Fiber Communication Confe. And Exhibit. 2002 (OFC 2002), 2002, pp. 17
- [33] Gin Jose, Purnananda Nandi, Shoxiang Shen, Jian Zhang, Animesh Jha, *"Novel glass hosts for integrated planar amplifiers in optical communication window (1200-1700 nm)"*, International Conference on Transparent optical Networks, ICTON 2007, 2007, pp. We. A4.2
- [34] H. X. Yang, H. Lin, L. Lin, Y. Y. Zhang, B. Zhai, E. Y. B. Pun, *"Powerful visible upconversion fluorescence of Er^{3+} in novel bismuth gallate glasses compared with in common tellurite glasses"*, Jour. Alloys and Compounds, Vol. 453, Iss. 1-2, 2006, pp. 493
- [35] H. S. Seo, W. J. Chung, J. T. Ahn, *"A novel hybrid silica wide-band amplifier covering S + C + L bands with 105 nm bandwidth"*, IEEE Photon. Technol. Lett., Vol. 17, No. 9, 2005, pp. 1830

- [36] S. Namiki, Y. Emori, “*Ultrabroad-band Raman amplifiers pumped and gain-equalized by wavelength-division-multiplexed high-power laser diodes*”, IEEE Selected Topics in Quantum Electronics, Vol. 7, no. 1, 2001, pp. 3
- [37] M. Yamada, T. Kanamori, Y. Terunuma, K. Oikawa, M. Shimizu, S. Sudo, K. Sagawa, “*Fluoride-based erbium-doped fiber amplifier with inherently flat gain spectrum*”, IEEE Photon. Technol. Lett., Vol. 8, 1996, pp. 882
- [38] D. Bayart, B. Clesca, L. Hamon, J. L. Beylat, “*Experimental investigation of the gain flatness characteristics for 1.55 μ m erbium-doped fluoride fiber amplifier*”, IEEE Photon. Technol. Lett., Vol. 6, 1994, pp. 613
- [39] H. S. Kim S. H. Yun, H. K. Kim, B. Y. Kim, “*Actively gain-flattened erbium-doped fiber amplifier over 35 nm by using all-fiber acousto-optic tunable filters*”, IEEE Photon. Technol. Lett. Vol. 10, 1998, pp. 1278
- [40] M. Rochette, M. Guy, S. Larochelle, J. Lauzon, F. Trepanier, “*Gain equalization of EDFA's with Bragg gratings*”, IEEE Photon. Technol. Lett. Vol 11, 1999, pp. 536
- [41] P. M. Schiffer, C. R. Doerr, L. W. Stulz, M. A. Cappuzzo, E. J. Laskowski, A. Paunescu, L. T. Gomez, J. V. Gates, “*Smart dynamic wavelength equalizer based on an integrated planar optical circuit for use in the 1550 nm region*”, IEEE Photon. Technol. Lett., Vol 11, 1999, pp. 1150

CHAPTER 2

THEORETICAL BACKGROUND

2.1 Introduction

Light amplification by rare-earth (RE) ions in an optical fibre is a process that involves many fundamental principles of physics, ranging from classical to quantum electromagnetic theories to the most crucial principles in LASER (Light Amplification by Stimulated Emission of Radiation) physics. Therefore, a theoretical analysis is essential in understanding and predicting the RE interaction and behaviour so that the design and performance of an optical fibre amplifier can be improved. In this chapter, the description of the fundamental relationship between the host glass and the RE (Erbium) and EDFA will be discussed.

Glass as an amorphous material that plays an undeniably crucial role in telecommunications today. The idea to use glass to guide light dates back to as far as two centuries ago. However, it is only in the 1970s that the idea was finally realised by a team from Corning Glass Works. After intensive research and development by other researchers around the world, silica (SiO_2) glass was identified and recognized as the best transmission medium for optical communications [1]. Subsequently, with the development of solid state lasers and increasing demands for larger information transmission bandwidth, the demand for an all-optical amplifier systems to replace the expensive and complicated optical-electrical-optical (O-E-O) regenerator systems

sky-rocketed. The RE, Erbium was singled out from lanthanide series of elements to perform the amplification task because its emission coincided with the 1550 nm low loss transmission band of silica-based optical fibres. In order to explore its full potential, substantial theoretical and experimental work was carried out and by 1987, a team of researchers from Southampton University had successfully demonstrated the use of the erbium-doped silica host glass as an optical amplifier for optical telecommunication systems in the infrared 1550 nm wavelength region – (also known as the third window of optical fibre communications).

2.2 Erbium ions in glass host

2.2.1 Brief of Glass host and Erbium ion

Glass host

Glass is a uniform solid phase of material, produced when a molten material cools too fast that there is not enough time to form periodically-ordered crystal lattice structures or crystallisation [1]. The lattice structure of SiO_2 glass, the most common type of glass is short in three-dimensional matrix (polyhedra) without any symmetry or uniform/periodic structure (although the valences are balanced), causing it to be hard but at same time brittle and transparent (translucent). The matrix is built from basic structural units made of glass network formers. The most common glass network former is silica tetrahedron $(\text{SiO}_4)^{2-}$ linked with broad bond angle oxygen atom links to form a tetrahedral structure. Other glass formers are germanium oxide (GeO_2), boric oxide (B_2O_3), phosphorus pentoxide (P_2O_5), arsenic oxide (As_2O_3), phosphorus trioxide (P_2O_3), antimony oxide (Sb_2O_3) etc. These materials are capable of forming glass structure due to their low crystallisation rate and form three-

dimensional matrices with oxygen atoms [1, 2, 3]. Other compounds, such as the oxides of alkali-metals or alkali-earth metals, (e.g. sodium (Na), lithium (Li), aluminium (Al), titanium (Ti), etc) can also be added to the glass as network modifiers. These modifiers cause the former bridging ions to become non-bridging, thus breaking the lattice and results in a less tight network structure. Network modifiers are used to facilitate the incorporation of trivalent rare earth ions such as Er^{3+} ions [1, 2] and also reduces the glass fusion temperature and viscosity [1, 2, 3]. The structure of a typical alkali silicate glass is illustrated in Figure 2.1.

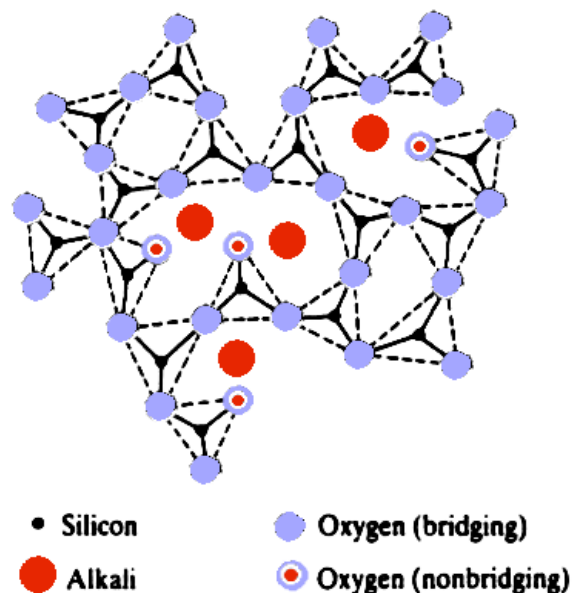


Figure 2.1 Alkali silicate glass structure based on $(\text{Si}^{4+}, \text{O}^{2-})$ network formers and alkali ion network modifier. The fourth bridging oxygen of the silicon tetrahedron is outside the plane of the figure [1].

Silica glass has resistive properties to deformation at high temperatures as well as high melting temperature and low thermal expansion coefficient [3]. Furthermore, silica glass has good chemical durability and highly transparent in both the visible and infrared regions where optical fibre telecommunications systems are being

deployed [2, 3].

However, the continuous demands for wider bandwidth and longer distances in existing optical fibre telecommunication systems has pushed the silica host glass to its limit as a host for optical amplification. Limited RE ion doping concentrations, short gain bandwidths and low output power are all limitations of silica based EDFA. However, these shortcomings have initiated an explosion in the research for a new type of glass host for future optical amplifiers [4, 5]. Glass hosts such as ZBLAN, fluoride, phosphate and bismuth [4, 5] are being studied due to their advantages of high RE doping concentrations, larger stimulated emission cross-sections around the 1.5 μm bands and wide gain bandwidths [5]. From the study, bismuth based glass has shown to be the most promising, as fluoride, phosphate and ZBLAN glass hosts have major drawbacks during the fabrication process such as hygroscopic, having poor glass thermal stability and ease of devitrification. For this reason, these glass hosts were unfavourable to fibre manufacturers [4, 5].

The bismuth host glass on the other hand has received increased interest due to their multiple application potentials in optical fibre telecommunications [5, 6]. Optical amplifiers using bismuth host have been studied and are capable of exhibiting broadband gain bandwidth due to a large emission cross-section [5] and high RE ions concentration without concentration quenching [6] that is preferred in the design of high power and compact optical amplifiers. Furthermore, they have the advantage of lower splice losses when spliced with the normal silica based optical fibre [6] thus raising its potential as a broadband optical amplifier for optical telecommunication systems.

Bismuth is the most metallic material in the periodic table under Group V (pnictogens) block elements that is capable of forming oxide glass with a molecular formula of Bi_2O_3 . bismuth based glass has a low melting point of approximately 817 °C [6], making it less difficult to fabricate as compared to silica glass, (whose melting point exceeds 1700°C [3]). Bismuth glass also has a high refractive index that makes it suitable for high efficiency optical amplifiers.

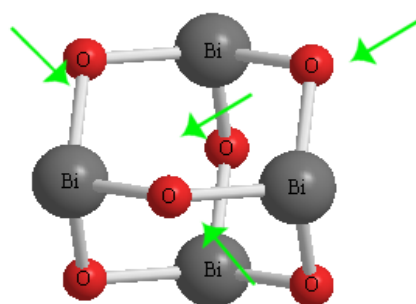


Figure 2.2 Pyramidal polyhedron structure of Bi_2O_3 glass (The arrow is demonstrative of the possible non-bridging oxygen atoms that bond with the RE ions)

Bismuth glass has a pyramidal polyhedron structure whereby the faces and the base of the structure are triangular and converge on the apex as shown in Figure 2.2. above. The apexes of the polyhedron are occupied by three oxygen atoms with strong bonds and short Bi-O distance. However, these distance are not the same in the case of the glass due to distorted oxygen lone pairs [7] inhibiting the crystallisation process. A high oxygen atom ratio in the vicinity of the heavy bismuth atoms makes the bismuth glass host capable of incorporating and bonding with more RE ions via non-bridging oxygen atoms, thus increasing the RE emission cross-section and lowering the RE clustering for a lower concentration quenching effect [4-6].

Erbium ion

Erbium is a trivalent lanthanide that has an electron configuration of $[\text{Xe}]4f^{12}6s^2$, where $[\text{Xe}]$ represents the closed shell electron configuration of Xenon (as given in Table 2.1). It has a sharp absorption and luminescence spectra band from the visible to the near infrared region due to its specific 4f electronic energy level splitting as shown in Figure 2.3. Erbium naturally exists in two oxidation states, namely Er^{2+} and Er^{3+} . However, it is the triple charged ion state that has garnered a lot of interest, especially in the photonics community because of its radiative transitions in the infrared region around $1.55\ \mu\text{m}$ coinciding well with the third window of optical telecommunication system [4-6]. This triple charged ion is formed by losing one 4f electron and both the 6s electrons with the 5s and 5p shielding the

Table 2.1. Electron configuration with their corresponding electronics configurations and ground states of selected lanthanide elements in the +3 ionisation state (trivalent).

Element	Atomic number	Electron configuration	R^{3+}
La	57	$[\text{Xe}] 5d^1 6s^2$	-
Pr	59	$[\text{Xe}] 4f^3 6s^2$	$^3\text{H}_4$
Nd	60	$[\text{Xe}] 4f^4 6s^2$	$^4\text{I}_{9/2}$
Pm	61	$[\text{Xe}] 4f^5 6s^2$	$^5\text{I}_4$
Sm	62	$[\text{Xe}] 4f^6 6s^2$	$^6\text{H}_{5/2}$
Eu	63	$[\text{Xe}] 4f^7 6s^2$	$^7\text{F}_0$
Gd	64	$[\text{Xe}] 4f^8 6s^2$	$^8\text{S}_{7/2}$
Tb	65	$[\text{Xe}] 4f^9 6s^2$	$^7\text{F}_6$
Dy	66	$[\text{Xe}] 4f^{10} 6s^2$	$^3\text{H}_{15/2}$
Ho	67	$[\text{Xe}] 4f^{11} 6s^2$	$^5\text{I}_8$
Er	68	$[\text{Xe}] 4f^{12} 6s^2$	$^4\text{I}_{15/2}$
Tm	69	$[\text{Xe}] 4f^{13} 6s^2$	$^3\text{H}_6$
Yb	70	$[\text{Xe}] 4f^{14} 6s^2$	$^2\text{F}_{7/2}$

remaining 4f orbitals [8,9]. Thus, the shielded Er^{3+} ion's 4f orbitals generate luminescence which is weakly dependent on the host material.

The luminescence transition of trivalent Erbium ions in a glass host is initiated from a parity forbidden f-f electric dipole transitions within the inner-shell 4f when the ions are excited by an external excitation energy [8, 9]. This forbidden electric transitions are allowed in a crystal and glass host because of the interaction of the crystal field creating a mix of odd- and even-parity wavefunctions that relaxes the dipole selection rules. The 4f shell is shielded from external field of the glass host by the outer shells 5s and 5p, thus the luminescence retains its sharp spectral lines. This also causes the luminescence lifetime to be longer since it lacks other non-radiative decay processes.

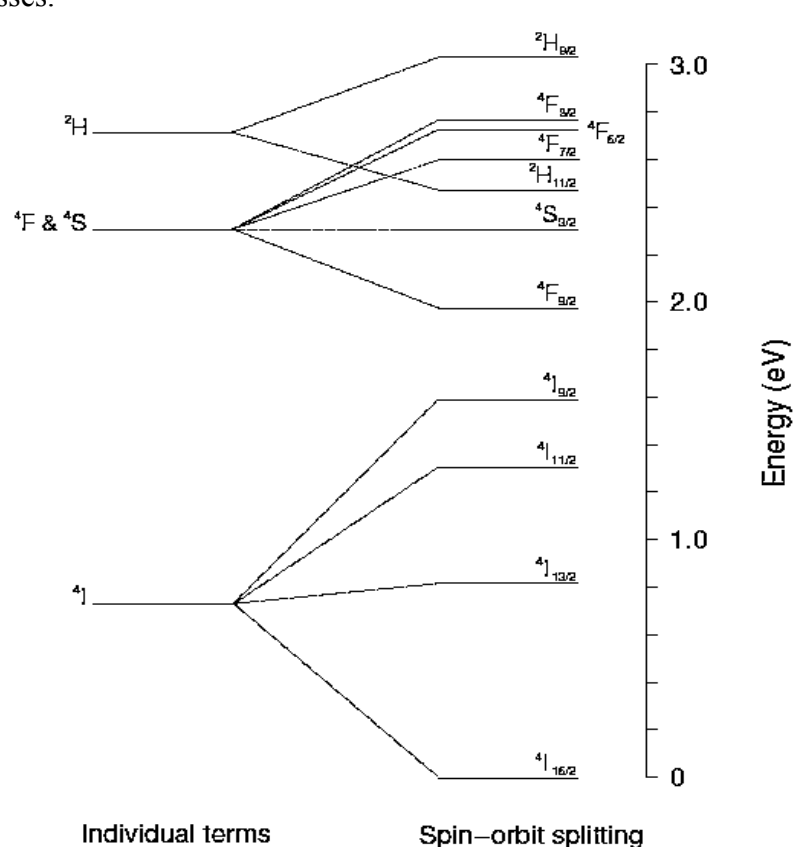


Figure 2.3 The splitting of the 4f electronic energy of Er^{3+} ions, illustrating the effect of electrostatic-electron interactions and spin-orbit splitting.

2.2.2 The Requirements for EDFs as Optical Amplifier

There are many key aspects of an optical amplifier that are required for future telecommunications systems. The following characteristics are the current major requirements of optical amplifiers [2-17]:

- **Glass material and properties and fibre mode profile design:**
low intrinsic and extrinsic loss properties, low absorption and scattering, precise control of fibre mode and refractive-index profile in the radial direction
- **Rare-earth material:**
wider emission spectra, higher doping concentration/solubility, high input saturation power
- **Efficiency:**
high pump photon to signal conversion, low upconversion, low noise figure
- **Cost:** low cost fabrication process, compact, high chemical and physical/mechanical stability and durability

All these factors are major aspects of optical amplification that are necessary and important features for future optical telecommunications systems.

Optical absorption and scattering loss

The key principle of an EDFA is to amplify an optical signal as it travels along an optical fibre over long distances. This is because as a signal travels along the fibre,

it will experience loss, thus losing power. These losses originate from the glass material and its manufacturing parameters and can be categorized into either intrinsic or extrinsic loss [2,3]. Intrinsic losses are inherent to the fibre material arise from the fundamental material properties of the glasses used in fabrication. It is caused by density fluctuations, electronic transitions and lattice vibrational (atoms bonds) absorption. The intrinsic losses can be reduced by careful and appropriate choice of material compositions. Figure 2.4 show the loss spectrum in silica glass fibre such as UV resonance tail or Urbach edge, hydroxyl ion phonon and multiphonon absorption, and Rayleigh scattering. As illustrated in the figure, the Rayleigh scattering loss is the leading losses in modern telecoms grade low O-H phonon absorption silica glass fibre.

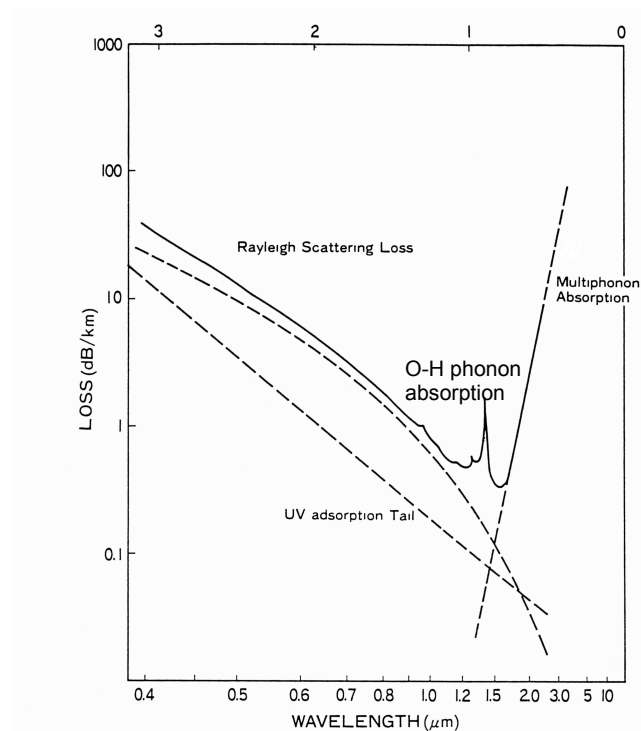


Figure 2.4 Transmission loss spectrum of silica glass fibre from visible to near-infrared region [13].

Extrinsic losses on the other hand arise from outside sources such as imperfections in the fabrication process, material impurities or structural defects.

Most extrinsic loss are contributed by the hydroxyl ion group, which acts as an impurity as shown in Figure 2.4 that attenuates the optical signal at 1.38 μm , 1.24 μm and 0.95 μm [12]. However, in recent ultra low loss silica fibres, these losses have been reduced significantly so that they have very little effect on signal power. The reason behind this success is the advanced fabrication process control used and the high purity starting materials adopted.

The only remaining limitation of recent ultra low loss silica fibres is the intrinsic loss. Because intrinsic loss rises from the strong mutual interaction between signal photon and the material itself [12, 13], it is very much more difficult to remove as compared to extrinsic losses.

There are two known interactions in a glass material that causes these high loss: phonon and multiphonon absorptions. Phonon absorption is caused by bending and stretching vibrations between neighbouring atoms in the glass lattice [12-14].

By using a simple two atoms per cell model, the vibrational frequency ω_T at the cross point in transverse mode can be given as [13]

$$\omega_T^2 = 2C \left(\frac{1}{M_1} + \frac{1}{M_2} \right) \quad , \quad (2.1)$$

where M_1 , M_2 are the mass of the atoms and C is a binding force constant. Here, the frequency, ω_T depends on the mass of the two atoms and is absorbed to the crystal resonantly. As the result, any signal photon that matches this frequency ω_T will have a higher absorption coefficient than others [13].

Multiphonon absorption on the other hand is the result of the combined effect of two interrelated mechanisms: the electric moment associate with the distorted charge density of atoms from photon interactions and non-harmonic inter-ionic

potentials from electronic charge density interaction. The absorption coefficient is given by [13,14]

$$A_{MP} = K \exp\left(-\gamma \frac{\nu}{\nu_0}\right), \quad (2.2)$$

where K and γ , are constants of the material and ν_0 a longitudinal optical phonon absorption frequency. According to T. Izawa *et.al.* and L.L. Boyer *et. al.* [13,14], when the atomic potential in the glass is weak, the non-linear effects of the optical interaction becomes strong and a fine structure of absorption spectra is observable. Consequently, it can be seen that phonon and multiphonon absorptions are dependent on the atom, i.e., mass and also host material's optical phonon frequency.

Scattering loss is another type of loss commonly encountered in glass hosts and is caused by effects such as concentration fluctuations and acoustic and optical phonon interaction [13,15]. The losses occur in such a way that when an incoming photon strikes this structure, it transfers/scatters the photon energy to other directions [15]. These microscopic variations are associated with the glass random molecular structure that causes Rayleigh scattering, Raman scattering and Brillouin scattering [11,13,15-17]. The Rayleigh scattering loss is dependent on wavelength, λ^{-4} and the fibre core composition, e.g. GeO₂-doped SMF [13,15,16]. As the loss of modern telecom grade optical fibre is about ≈ 0.12 to 0.15 dB/km near signal wavelength of $1.55 \mu\text{m}$, the minimum loss level is mainly limited by this fundamental process that dominates at short wavelengths. Raman scattering is a quantum-mechanical process of photon scattering when the signal photon frequency and wave vector matches the optical phonon of the glass material [17]. Brillouin scattering is also similar as Raman scattering processes except that now the signal photon frequency and wave

vector match the acoustic phonon of the glass material instead [17]. Both Raman and Brillouin scattering loss are usually very weak and dependent on wavelength as λ^{-4} [11,13,15,17]; however it is the Rayleigh scattering loss, which is that dominates.

Amplification bandwidth

Silica glass fibre for optical telecommunication systems utilises optical wavelengths ranging from 1300 nm to 1600 nm, where fibre background loss is lowest [9,10,11,13,15]. Long haul transmission systems are possible with silica-based optical amplifiers with rare-earth doping especially erbium ions. EDF with silica host glass is very efficient at generating fluorescence emissions from 1520 nm to 1600 nm (C+L band region) [2]. This breakthrough has expanded the long-haul optical telecommunication system to new distances of 7000 km [11,12,18,19]. Although long-haul optical telecommunication is proven and utilised, currently deployed optical systems only focuses on one-third of the overall wavelength window from the silica fibre low loss region. The main reason of this is the lack of amplification bandwidth and optical sources [2,11,12]. Based on these factors, optical engineers are now looking for alternative solutions to widen the optical bandwidth. Figure 2.5 shows a bandwidth comparison of optical amplifiers including EDF-based amplifier with silica, fluoride and telluride glass host, Raman amplifiers and also quantum-dot semiconductor optical amplifiers (SOA). Furthermore, optical amplifiers should have a uniform or flat gain [2, 6,11,18] in order to ensure the maximum applicable amplification bandwidth. This is the major obstacle to the current silica-based EDF since it has a narrow gain bandwidth due to high emission intensity at Er^{3+} peak emission wavelength [2,6,11].

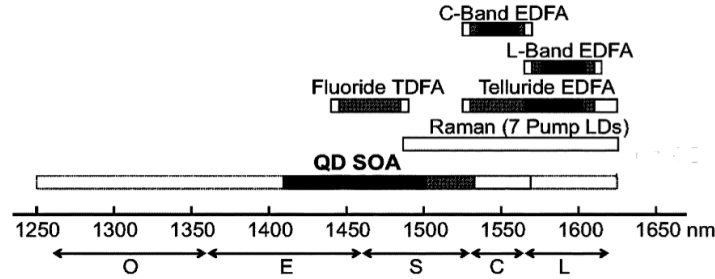


Figure 2.5 Comparison of optical amplifiers bandwidth using EDF with silica, fluoride and telluride host glasses, Raman amplifiers and SOA.

Recent studies have demonstrated that a wide and flat amplification spectra can be realised by substituting the EDF host material from silica with fluoride [13,14,20], tellurite [22] and bismuth [6,23,24]. These new hosts yield a wider emission cross-section over signal wavelength amplification range (1530 – 1550 nm) due to different Stark splitting compared with silica host [2]. Other researcher also tried to incorporate new RE material such as Thulium (Tm^{3+}) in these new type of host glasses [22] to explore new amplification region cries a view to widen the current amplification bandwidths.

Presently, in order to utilise the L-band amplification region, optical engineers have been forced to use longer EDFs. This system has been demonstrated in Japan and South Korea but suffers from a few major limitations. When this system is combined with a high bit-rate signal, non-linear effects such as cross-phase modulation (XPM), self-phase modulation (SPM) [25,26] and four-wave mixing (FWM) [27] become more evident and detrimental. For optical amplifier manufacturers, using longer EDF lengths also signifies extra cost and space, making it commercially less viable. This also increases the amplifier complexity and thus the resources required to manufacture the amplifier. Besides that, due to the low pump

power conversation efficiency and being far from the Er^{3+} ions emission cross-section [28], the gain of the signal is small, requiring a larger number of optical amplifiers to achieve the desired output signal power.

Concentration Quenching

EDF from silica host glass has a limitation on the RE doping concentration [29, 30]. The ability to have high concentration RE doping is crucial in producing higher signal gain per pump power ratio without extending the EDF length. To archived maximum signal gain per launched pump power, the Er^{3+} ion distribution should ideally be uniform in the centre of the fibre core [30, 31]. However, when the rare earth concentration increase, the ion distribution and distance is reduced due to residual interaction such as local charge compensation [31]. This can generate undesirable effects (especially in silica-based optical fibre amplifier) such as the reduction of the fluorescence bandwidth and lifetime as well as concentration quenching [2,29-32]. These effects have led to an increase in the pump power required for optical gain and also higher noise penalties [2]. Figure 2.6 shows the three main concentration quenching processes [2,32-36] that are actually significant in an EDFA, namely

(a) Resonant energy migration [2, 33, 34] where an excited ion (donor) transfers its energy to a nearby ion (acceptor) in the ground state. This process ends with the donor in the ground state and the acceptor in the excited state. The mutual energy is proportional to the inverse of the third power of the inter-ionic distance and results in an energy spatial migration (diffusion) and random excitation energy transfer through the host [34].

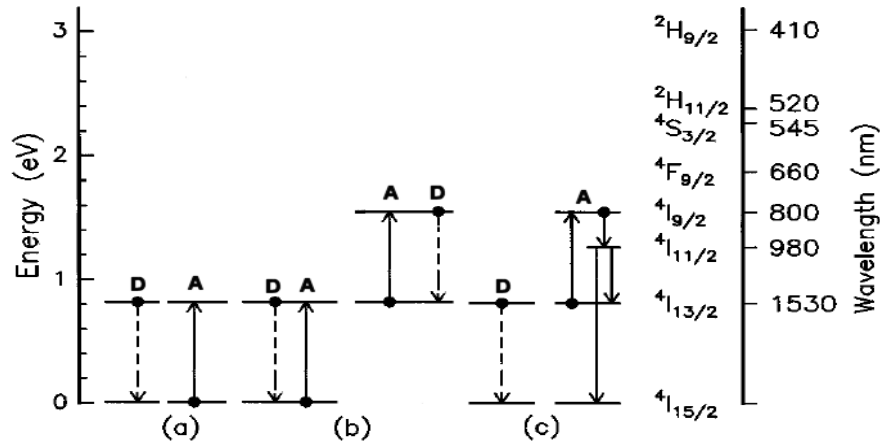


Figure 2.6 Schematic representation of concentration quenching effect in Er^{3+} ions using two-level approximation (donor (D) and acceptor (A)). The horizontal lines represent Stark manifolds of the $4f$ levels of Er^{3+} . (a) resonant energy migration, (b) cross relaxation, (c) Cooperative frequency upconversion

(b) Cross-relaxation [1, 34, 35] whereby energy is transferred between the donor and acceptor, thus promoting the acceptor to a higher energy state. Initially, the acceptor can be either in an excited state or in the ground state, as shown in the Figure 2.6 (b). This process can happen at any energy state and it is said to be resonant if the energy gaps are equally matched or phonon-assisted if the mismatch is compensated by the addition of phonon processes [2, 29]. Phonon-assisted cross-relaxation in RE doped glass is comparable with multiphonon processes [13, 14] that depend on the host phonon frequency as shown in Equation. (2.2). In case of the process occurring when the ions are in the form of a pair or a cluster (separated by less than 0.5 nm [35]), the energy transfer is very efficient and this special cross-relaxation is called Pair-induced Quenching (PIQ) [36, 37]. This clustered ion structure in the glass host is unknown, complicated and can form in many shapes with different host compositions and fabrication processes [36, 37]. As the cluster distance and

distribution becomes closer, the energy transfer process can happen very fast in a sub-microsecond timescale [38] that lowers the population inversion thus reducing the output signal gain and efficiency dramatically [39].

(c) Cooperative frequency upconversion [2, 35, 40] is also a special case of the cross-relaxation process where an acceptor ion that has been promoted to a higher energy state by a donor ion is relaxed non-radiatively (phonon) [40] to a lower level and then relaxes radiatively (photon) to the ground level. In this process, the emitted photon has a higher energy than the incident photon due to higher energy gaps as shown in Figure 2.7. As the process is repeated several times with the same acceptor ion, the emitted photon can have a much higher energy. This upconversion process is dependent on the Er^{3+} ions energy gaps and is capable of converting the infrared photon pump into visible light [2,33].

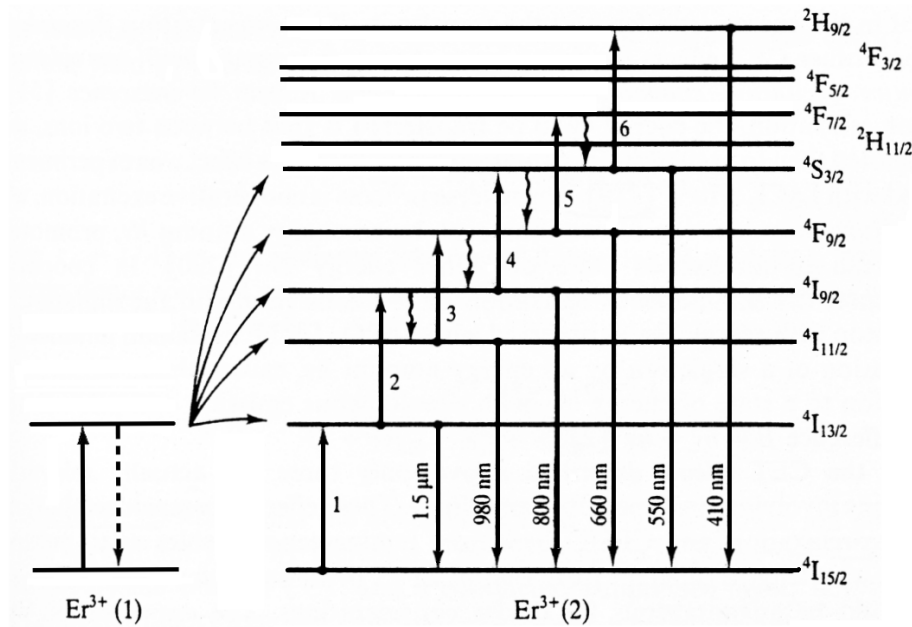


Figure 2.7 Possible upconversion transitions from cooperative frequency upconversion process. $\text{Er}^{3+}(1)$ is a donor and $\text{Er}^{3+}(2)$ is a acceptor.

The degree of energy transfer by concentration quenching processes especially by upconversion mechanisms varies between glass hosts with random (uniform) and clustered ion distributions [41]. For random RE ions distributed in the glass host, the energy transfer is a homogeneous process that depends more on the excitation energy, while for clustered RE ions, the energy transfer is an inhomogeneous process, which is largely dependent on the interionic distance [2]. Since the upconversion processes in a highly-doped glass host is mostly inhomogeneous [2,41], the energy transfer occurs at a high efficiency thus reduces the 1.55 μm emission significantly.

In order to increase the Er^{3+} ion distribution, several techniques have been developed. The common technique is accomplished by adding alkali-metals as glass modifiers [42] such as Aluminium, Phosphorus, Natrium, Lanthanum, Germanium, Magnesium, etc as co-dopants. These co-dopants are capable of increasing the amount of non-bridging oxygens [42, 43] by altering the glass matrix coordination; thus reducing the Er^{3+} ion clustering capability. Other techniques such as altering the glass host network former also affects the ion distribution [44, 45]. Glass hosts such as phosphate and bismuth have high RE solubility [44,45] that are capable of generating very efficient 1.55 μm emissions. Most recent studies have demonstrated that new rare-earth doping techniques known as the direct nanoparticles deposition (DND) [46,47] using nanosize particles of the dopants simultaneously with silica glass deposition. This technique has shown smaller amount Er^{3+} ion clustering and is capable of producing very efficient high gain amplifiers with short EDF lengths [47].

Optical output power

Optical amplifiers are required to have a high signal output power to keep up with today's long-haul optical DWDM transmission systems. In an optical repeater configuration for example, this could provide a greater distance between repeaters, while in a power amplifier configuration it would allow the signal to be split into a greater number of fibre lines for re-networking [2, 48, 49]. From the energy conservation principles, the output signal saturation power P_s^{sat} of optical amplifiers in highly saturated condition is defined as [2]

$$P_s^{\text{sat}}(v_s) = P_s^{\text{in}}(v_s) + P_s^{\text{IS}}(v_s) + P_p(v_s) \left(1 - e^{-P_s^{\text{IS}}(v_s)/P_p^{\text{IS}}(v_p)} \right), \quad (2.3)$$

where $P_{s,p}^{\text{IS}}$ is the 'intrinsic saturation power' at signal/pump $v_{s,p}$ is defined from basic laser system [50] as

$$P_{s,p}^{\text{IS}}(v_{s,p}) = \frac{h v_{s,p} \pi \omega_{s,p}^2}{[\sigma_a(v_{s,p}) + \sigma_e(v_{s,p})] \tau}, \quad (2.4)$$

Here $v_{s,p}$ is the signal/pump frequency, $\omega_{s,p}$ is the fibre mode radius (spot size) [51], τ is the $^4\text{I}_{13/2}$ state fluorescence lifetime and $\sigma_a(v_{s,p})$ and $\sigma_e(v_{s,p})$ are the erbium absorption and emission cross sections constants, respectively. As a result, the output power of optical amplifier are limited by the signal and pump intrinsic saturation power. In order to improve the total output power, the optical amplifier must have a smaller optical mode radius, larger absorption and emission cross section and longer fluorescence lifetime as shown by the equation.

The requirement for single mode propagation in a high power fibre laser had pushed optical fibre manufacturers to fabricate fibre which is small core radius r_{core} with high relative refractive index contrast between the core and the cladding [52]. This is shown by V number expression, given as

$$V = \frac{2\pi r_{\text{core}}}{\lambda} \text{NA} \quad (2.5)$$

with NA being the fibre numerical aperture and λ is the signal wavelength. For single mode propagation, V has to be ≤ 2.405 . With this problem, several attempts to design different index profiles for optical amplifiers have taken place. Snitzer *et. al.* [53] proposed an eccentrically positioned core or a rectangular fibre shape for high power applications. The irregular fibre profiles shown in Figure 2.8 have successfully increased the beam paths for better pump absorption cross sections and generated more than 100 W of optical power at 1.55 μm [54]. These sophisticated fibre profiles also allows the usage of multi-mode fibre laser diodes that give better light coupling efficiency and higher brightness compared with single-mode fibre laser diodes [53].

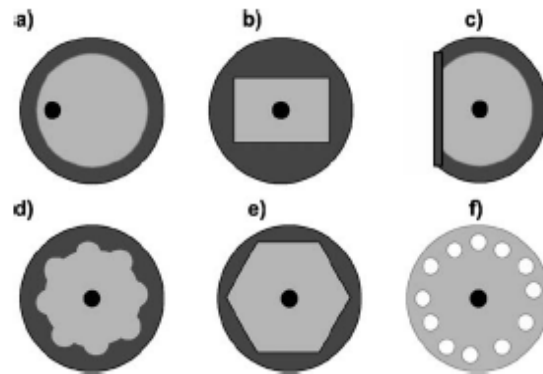


Figure 2.8 Examples of cladding-pumped structures for optical fibre amplifier profile: (a) eccentric core, (b) rectangular, (c) D-shape, (d) star, (e) polygon, (f) holey (air) taken from [54]

The absorption cross sections of an Er^{3+} optical amplifier also can be increased by co-doping Ytterbium (Yb) in the host [55]. Compared to other lanthanide elements, Yb^{3+} has larger absorption cross section at near 910 and 975 nm for laser emissions at about 1040 nm. In addition, the availability of powerful diode pump sources at 975 nm has also contributed towards the interest in this technique.

The amplification process is done by efficient resonant energy transfer between Yb^{3+} emission ($^2\text{F}_{5/2} \rightarrow ^2\text{F}_{7/2}$) and Er^{3+} absorption ($^4\text{I}_{15/2} \rightarrow ^4\text{I}_{11/2}$) energy levels. The non-radiative energy transfer then decays rapidly to the Er^{3+} $^4\text{I}_{13/2}$ upper level and maintains the population inversion of Er^{3+} larger thus generating a higher laser emission at 1.55 μm [55]. Using this method with an irregular fibre core made from phosphosilicate fibre, Y. Jeong *et. al.* [55] has demonstrated a continuous-wave fibre laser with an output power of 297 W at 1567 nm.

Cost and Complexity

In order to boost the optical fibre transmission system, the fundamental element to the optical system providers that has to be kept in mind are the cost and complexity of the system. Utilising matured glass material such as silica glass as the transmission medium reduces the cost of the system, thus increasing coverage and feasibility for long haul application to local areas. Currently deployed Fibre To The Home/Passive Optical Network (FTTH/PON) to serve as an information network (video, voice, data, etc) is limited to a small number of users due to high optical loss budgets and system complexity. As the result, the research of low-cost solutions and small footprint are more attractive from the service provider's point of view rather than simply being a state-of-art discovery. This can be archived by careful evaluation of current requirements and future demands, where a ultra-broadband (or multi-terahertz) optical amplifiers is undoubtedly needed [56]. With current technology limited to complex Raman amplifiers and QD-SOA, new types of EDFA will be considered for low cost and simpler reason. The development of bismuth-based EDFA optical module as shown in Figure 2.9 by Asahi Glass Co. open a possibility

to optical system provider to design and develop broadband optical amplifier that is low cost and easy to implement in complex optical network telecommunication system.

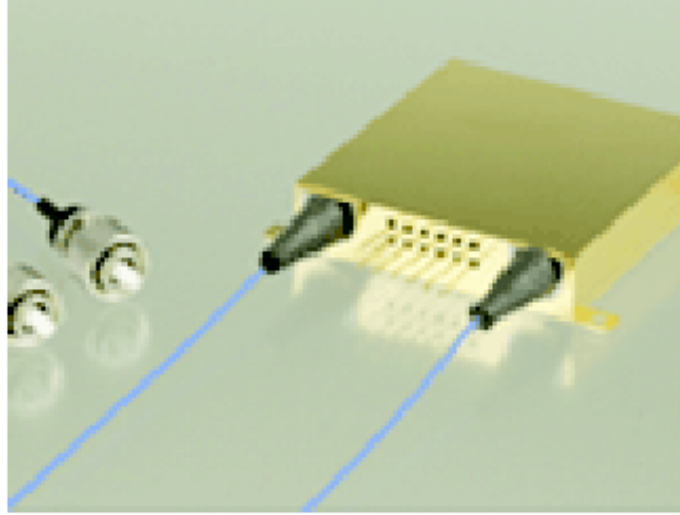


Figure 2.9 Bismuth-based erbium doped fibre amplifier with 4x4 cm in dimension (courtesy of Asahi Glass Co.)

2.2.3 Energy level system of Er^{3+} :glass

Energy levels of the Er^{3+} ions are labelled using Russel-Saunders or the LS coupling scheme according to their orbital momentum, \mathbf{L} , orbital angular momentum \mathbf{J} and spin momentum \mathbf{S} , [57]. In the LS coupling scheme, orbital momentum and spin are the sum of momenta and spins of individual electrons, thus

$$\mathbf{L} = \sum_{i=1}^N \mathbf{l}_i, \quad \mathbf{S} = \sum_{i=1}^N \mathbf{s}_i, \quad (2.6)$$

are the total orbital and total spin momentum operators, respectively, and

$$\mathbf{J} = \mathbf{L} + \mathbf{S} \quad (2.7)$$

is the total angular momentum operator which has $2J+1$ eigenstates depicted by the

magnetic quantum number $M = -J, -J+1, \dots, J$. The electronic states of ions is presented using the vector term symbol $^{2S+1}L_J$ where J and S are specified with numbers $(0, 1/2, 1, \dots)$, L is traditionally specified with letters S, P, D, F, G, H, \dots , according to the Clebsch-Gordan series respectively, which is given in details in Table 2.1.

The energy level structure of Er^{3+} ions in glass host is shown in Figure 2.10. The ground level has a configuration of 4I , which splits into $9/2$, $11/2$, $13/2$ and $15/2$ due to the ligand field interaction between the non-central electrostatic fields, electron spin and its orbital angular momentum [9, 58]. The absorption bands of 1480 nm and 980 nm shown in the figure corresponds to transitions from the ground level $^4I_{15/2}$ to the top of the $^4I_{13/2}$ and $^4I_{11/2}$ manifolds, respectively.

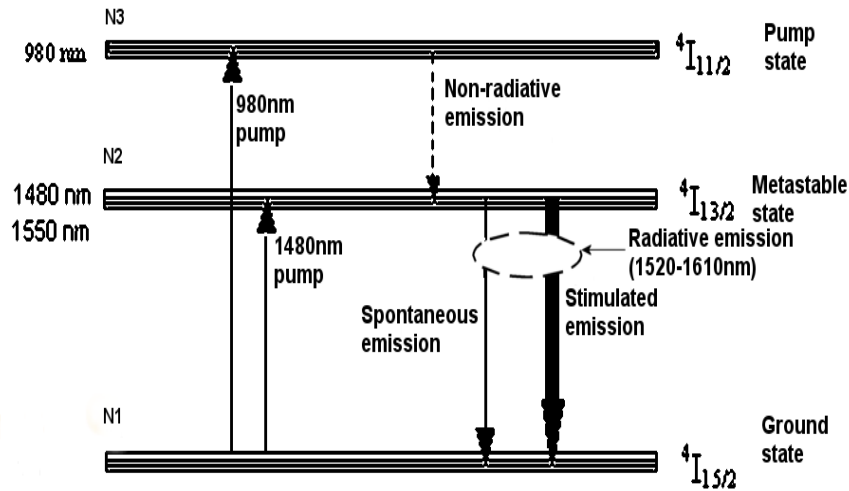


Figure 2.10 Energy levels of erbium-ion showing possible absorption spectrum (pump band) at 980 nm and 1480 nm and radiative transition (gain spectrum at 1520-1610nm) and the multiple lines representing the Stark levels.

The emission of excited Er^{3+} ion is shared between radiative and nonradiative emission. The radiative emissions depend on the energy gap/separation between the energy levels ranging from 10^3 to 10^4 cm^{-1} . Radiative emissions release transition

energy by emitting photons at a transition frequency given by Planck's Law, $E = h\nu$ [58]. The strong emission band around $1.55\ \mu\text{m}$ is a radiative emission from the first excited state $^4\text{I}_{13/2}$, which is also known as the metastable level to the ground level $^4\text{I}_{15/2}$. This emission has a long lifetime (up to 10 ms in silica glass host [2]) and high quantum efficiency ($\approx 80\%$) [2] due to short non-radiative processes [2, 59]. While, the other non-radiative emission is in the form of one or several quantized lattice vibrations or phonons [58] and depend on glass medium. The emission from the $^4\text{I}_{9/2}$ and $^4\text{I}_{11/2}$ levels are mostly nonradiative emissions [2] and are subjected to multiphonon relaxations. The effect of multiphonon relaxation in an optical amplifier results in an emission at a visible wavelength that is also known as the upconversion effect [35, 38]. The visible emission is possible because the Er^{3+} ions at this emitting level populates more easily through this condition than through direct excitation from external photons [58, 60].

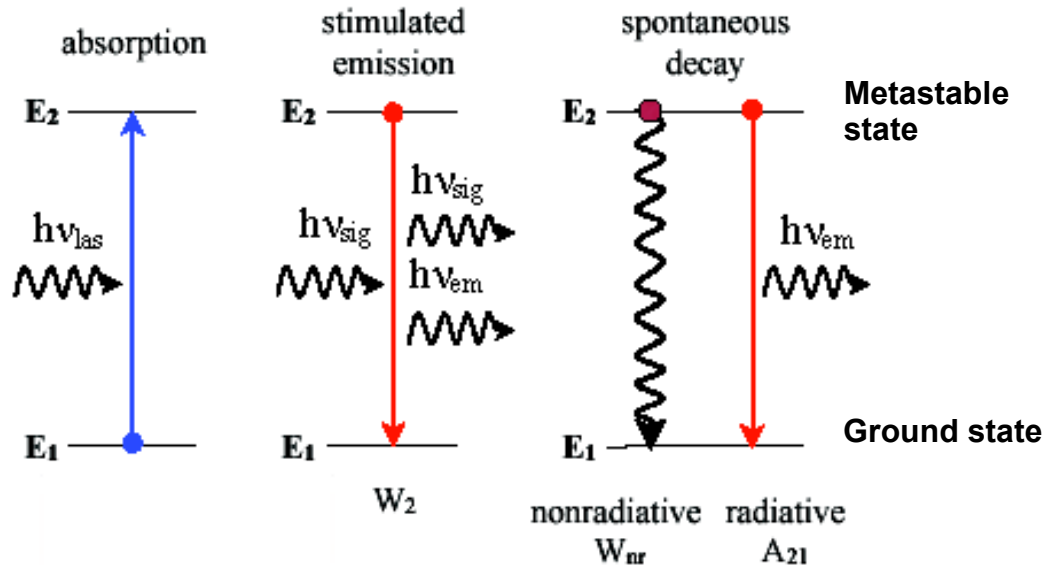


Figure 2.11 Representation of absorption, stimulated emission and spontaneous decay

It is clearly seen, that by exciting the Er^{3+} ions with a photon at 980 nm or 1480 nm produces the non-equilibrium condition, the number of ions in the metastable state can be increased. In order to obtain signal amplification, the number of ions in the metastable state must exceed the number of ions in the ground state. This condition is known as 'population inversion'. For that reason, to produce high population inversion, the energy decay rate by radiative emissions should be slower than the pumping rate with other non-radiative emissions kept at a minimum.

Radiative emission can be further divided into two types as shown in Figure 2.11. The decay can occur spontaneously, which is known as spontaneous emission or stimulated by the signal photon, which is known as stimulated emission. Spontaneous emission occurs when the ions spontaneously drop from an upper level to a lower level by emitting a photon radiation at the transition frequency [58]. Due to each individual ion radiating independently, the emission of the spontaneously emitting ion is noise-like in character, that is with random phase and direction. This emission is usually referred as incoherent emission. Typically, less than 1% of the spontaneous emission is captured by the optical fibre mode and becomes a source of optical noise [2]. When the noise gets amplified, it results in amplified spontaneous emission (ASE), which is actually stimulated by the spontaneous emission.

Stimulated emission occurs when an external signal photon is incident upon the Er^{3+} ions [58]. The signal photon will then cause the ions to release the extra energy by emitting a photon that is identical to the original signal photon. The additional photons increase the number of signal photons of the system and these photons are coherent with the applied signal, thus amplification is achieved.

Stark Splitting

Ligand fields of the host material generates an effect known as Stark splitting [2, 59] that breaks the degeneracy of the individual Er^{3+} ions 4f energy levels and results in multiple sub-levels (see Figure 2.12). The luminescence broadening at room temperature is the consequence of Stark splitting effect. This Stark sub-level is populated according to the Boltzmann's thermal distribution, which depends on separation energy and temperature and makes it possible to consider each of them as a single energy level [2, 9, 61].

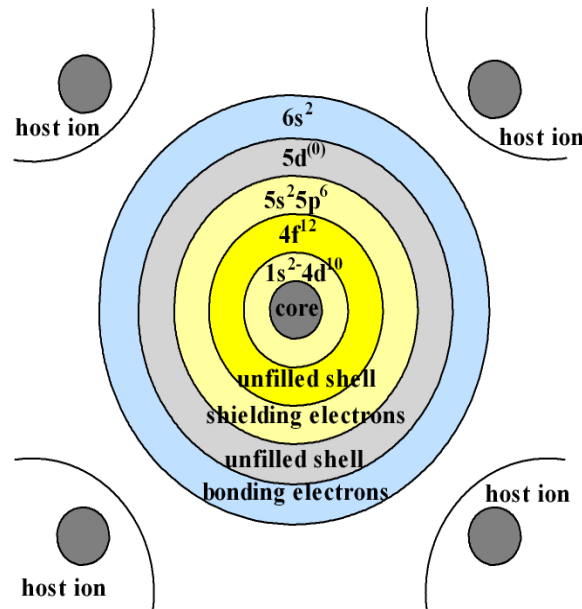


Figure 2.12 Illustration of ligand field of Er^{3+} ions and glass host

The Stark levels in the silica glass host can be split into 7 and 8 sub-levels, yielding a total of 56 transitions. With multiple transitions, the Er^{3+} ion emissions in a silica host has a high possibility to be re-absorbed and re-emitted at longer wavelengths [2, 62]. This phenomenon is known as the quasi-two-level pumping system and increases the advantage of erbium doping in a silica host as an optical

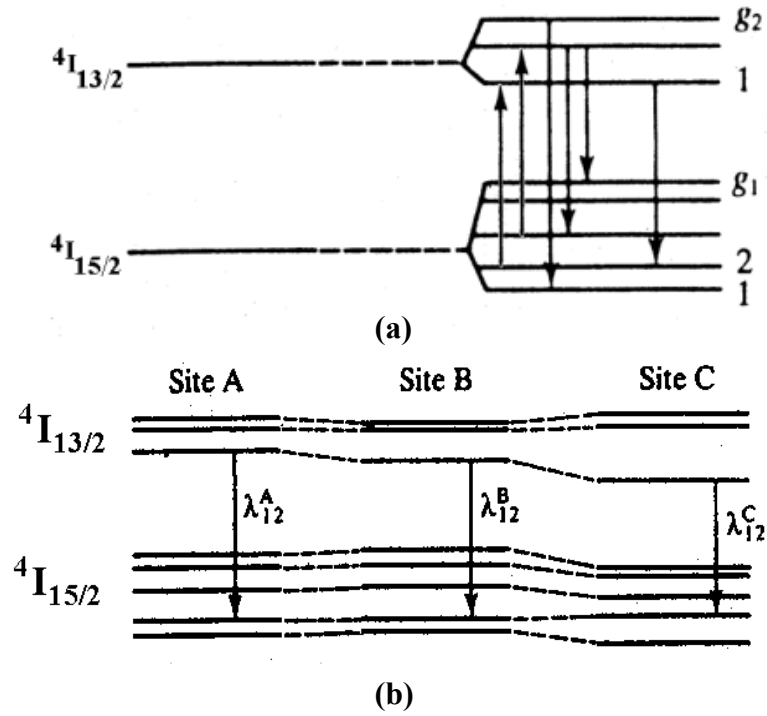


Figure 2.13 (a) Effect of Stark splitting in the energy level, (b) effect of inhomogeneous broadening, where random field variations from site to site cause changes in the Stark splitting and centre wavelengths of laser transitions [2].

amplifier with wider optical bandwidth. In fact, the L-band amplification region was accomplished from this quasi-two-level mechanism [2, 63].

Figure 2.13 (a) shows the lower $^4I_{15/2}$ and upper energy levels $^4I_{13/2}$ split into manifolds g_1 and g_2 , thus creating a $g_1 \times g_2$ superposition of possible laser transitions. As such the Stark splitting broadens the laser transition, the transition manifold is not homogeneous [2, 59], since each laser transition between the two Stark manifolds has different characteristics.

The Fig. 2.13 (b) shows the effect of site to site variations on the Stark levels. Because it occurs randomly, this causes a deviation in transition wavelength and inhomogeneous broadening of the laser line [62]. Inhomogeneous broadening can be

viewed as the qualitative differences in transition line characteristics such as line shape and centre frequency [64]. These differences originate from distinct local atom environments in the host glass material such as missing or misplaced neighbour atom, trapped atom charges, alternative charge states, etc [2]. The inhomogeneous line widths generally depend weakly on temperature, and are characterized by Gaussian and Lorentzian lineshapes [65] for zero-phonon energy by the Voigt function [66].

2.3 Light Amplification Principles of EDFA

2.3.1 General Theory

The general theory of light amplification in optical fibre is based on simple rate equations which describe the fractional light amplification as it travels a certain distance in an active medium [2, 31, 56, 64-67]. This theory uses the energy level ion population density, pump light intensity and rates equation which are fundamental properties of the atom in a particular environment to interpret the interactions of the atom (absorption or emission) when an electromagnetic field is incident on it [43, 58].

2.3.2 Rate Equations

Rate equations are developed from atomic energy levels to describe the effect of absorption, stimulated emission and spontaneous emission. In this dissertation, the rate equations developed by Giles *et.al.* [64-67], for Er^{3+} ions based on a three-level laser system are used to explain the amplification process in the EDF. The three-level

laser system uses three energy levels, which are the ground energy level as level 1, the metastable level as a level 2 and the pump level as level 3 as shown in Figure. 2.10.

N_1 , N_2 and N_3 are denoted as the densities of the ions in the respective energy levels of ground state, metastable state and pump state. R_{13} is the pumping rate from level 1 to level 3 and the R_{31} is the stimulated emission rate from level 3 to level 1. The radiative decay comprises of transitions from level 3 to level 2 and from level 2 to level 1 giving a total rate of ${}^R W_3$ which is the sum of ${}^R W_{32}$ and ${}^R W_{21}$. In level 3, nonradiative decay is predominant over the overall spontaneous decay rate, i.e. ${}^{NR} W_{32} \gg {}^R W_3$. So, the spontaneous decay rate between level 3 and level 2 can be simplified to W_{32} . The Spontaneous Decay rate from level 2 and level 1 is $W_{21} = {}^R W_{21} + {}^{NR} W_{21}$. It is assumed that spontaneous decay is dominated by the Radiative Decay Rate, ${}^R W_{21} \gg {}^{NR} W_{21}$. Thus, the Spontaneous Decay Rate between level 2 and level 1 can be simplified to W_{21} . The Stimulated Absorption Rate between level 1 and level 2 and Emission Rate between level 2 and level 1 are denoted by S_{12} and S_{21} .

Let the total local erbium ion density $\rho_{Er} = N_1 + N_2 + N_3$ and for initial conditions when there is no pump energy, $\rho = N_1$ and $N_2 = N_3 = 0$ where all ions are in the ground state. From here, the atomic rate equations for N_1 , N_2 and N_3 can be written corresponding to their population as

$$\frac{dN_1}{dt} = -R_{13}N_1 + R_{31}N_3 - S_{12}N_1 + S_{21}N_2 + W_{21}N_2 \quad , \quad (2.8)$$

$$\frac{dN_2}{dt} = S_{21}N_1 - S_{21}N_2 - W_{21}N_2 + W_{32}N_3 \quad , \quad (2.9)$$

$$\frac{dN_3}{dt} = R_{13}N_1 - R_{31}N_3 - W_{32}N_3 \quad . \quad (2.10)$$

2.3.3 Light propagation and amplification

Light propagation in the fibre is complicated by the distributed nature of the amplifier [58], and this often requires a complex numerical solution. The amplification in the the EDF can be explained by calculating the optical fields in *slices*, Δz along the propagation direction as shown in Figure 2.14 . Light in the fibre can be assumed to be propagating as a number of optical beams of frequency bandwidth $\Delta\nu_k$ that are centred at the optical wavelength $\lambda_k = c/\nu_k$. This notation describes both narrow line beams such as the pump and signal sources where $\Delta\nu_k \approx 0$, as well as the broadband ASE, where $\Delta\nu_k$ equals to the frequency steps used in the calculation to resolve the ASE spectrum [67]. The integration over the optical frequency is then approximated by a summation over z *slices*.

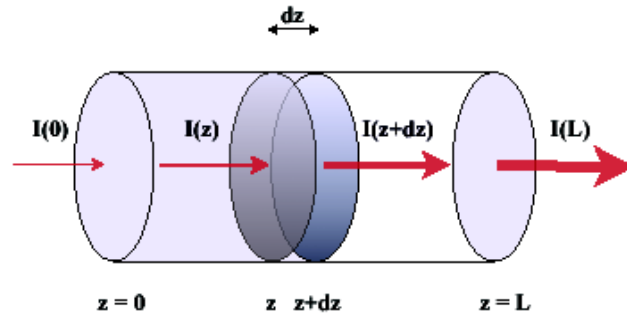


Figure 2.14 Light amplification after propagation in length L of gain medium

For a typical fibre amplifier parameter, treating the 980 nm pumped amplifier as a two-level model is valid for average pump powers less than 1 W [2, 67]. This is satisfied for all reported fibre amplifier experiments [62]. Reducing the EDFA model from a three-level to a two-level gain medium causes the order of the differential equations involved to be reduced. Hence, the complexity of the model is relaxed.

Equation 2.11 represents the particle conservation for a two-level system under fibre radial and azimuthal representation.

$$\begin{aligned} N_i &= n_i(r, \phi, z) \quad \text{for } i = 1, 2 \\ n_t(r, \phi, z) &= n_1(r, \phi, z) + n_2(r, \phi, z) \end{aligned} \quad (2.11)$$

The integration of the light intensity distribution of the k-th beam $I_k(r, \phi, z)$ over the radial and azimuthal co-ordinates gives the beam's total power $P_k(z)$ at position z in the fibre amplifier is given by

$$P_k(z) = \int_0^{2\pi} \int_0^\infty I_k(r, \phi, z) r dr d\phi, \quad (2.12)$$

where the light intensity I_k is normalized by

$$i_k(r, \phi) = \frac{I_k(r, \phi, z)}{P_k(z)}, \quad (2.13)$$

where i_k is the normalized optical density. Here $I_k(r, \phi, z)$ is a separable light intensity variable such that the shape of the k-th optical mode is independent of z .

The propagation equation integrated over the fibre transverse direction including the pump light absorption, signal stimulated emission and spontaneous emission is given by [2, 64-67]

$$\begin{aligned} \frac{dP_k(z)}{dz} &= u_k \sigma_{ek} \int_0^{2\pi} \int_0^\infty i_k(r, \phi, z) n_1(r, \phi, z) r dr d\phi (P_k(z) + \hbar \nu_k \Delta \nu_k) \\ &- u_k \sigma_{ak} \int_0^{2\pi} \int_0^\infty i_k(r, \phi, z) n_1(r, \phi, z) r dr d\phi (P_k(z)) \end{aligned} \quad (2.14)$$

where u_k denotes the propagation direction of the k-th wavelength and takes the value of +1 and -1 for forward and backward directions respectively, and $\sigma_{ak,ek}$ is the wavelength dependent absorption cross section and emission cross section via $\sigma_{ak}\Gamma_k n_t$ and $\sigma_{ek}\Gamma_k n_t$ respectively, assuming uniform doping, with Γ_k representing the overlap

integral between the dopant and the optical mode while n_t is the total population in the fibre. Due to the Er^{3+} ions σ_{ak} and σ_{ak} cross section are very dependence with glass host, these parameters were obtained only by direct measurement on actual EDF.

The term $m h \nu_k \Delta \nu_k$ is the contribution of spontaneous emission from the local n_2 population, and its growth through the amplifier. The number of modes, m is normally 2, as in the case of the LP_{11} optical mode in the fibre that supports the two polarization states of the lowest order (first order transverse electric and magnetic field, TE_{01} TM_{01}).

The light propagation equation above can be solved via several numerical methods to resolve the spectral modelling. The 'Giles model' [64] is the most comprehensive model that provides results in full spectral solution for pump, signal and ASE in both directions. In this model, the equation is integrated both in the backward and forward directions along the fibre until the specified convergence parameters were reached [65].

Although this model includes the ASE in the signal gain and noise calculations when compared with the real EDFA it is was found to be less realistic, because the actual optical amplifier has many detrimental effect such as fibre background loss, Excited State Absorption (ESA), saturation and upconversion that deteriorate the overall performance [2, 64, 65, 67].

For that reason, the propagation equation in Eq. 2.14 needs extra modifications to include all the detrimental effects and thus, making it more practical for real applications. Let us again re-define pump, absorption and emission rates R , S and W in Eqs. 2.8, 2.9 and 2.10 for a two level laser system,

$$R_{12}(z, v_p)\tau = \frac{P_p(z, v_p)}{P_{sat}(v_p)}, \quad (2.15)$$

$$S_{12}(z, r, v_s)\tau = \sum_s \frac{\sigma_a(v_s)}{\sigma_a(v_s) + \sigma_e(v_s)} \frac{P_s(z, v_s)}{P_{sat}(v_s)}, \quad (2.16)$$

$$W_{21}(z, r, v_s)\tau = \sum_s \frac{\sigma_e(v_s)}{\sigma_a(v_s) + \sigma_e(v_s)} \frac{P_s(z, v_s)}{P_{sat}(v_s)}, \quad (2.17)$$

where the saturation power at signal (or pump v_p) frequency v_s is defined from the basic laser system [50] (Eq. 2.4). Eq. 2.14 therefore becomes,

$$\begin{aligned} \frac{dP_k(z)}{dz} = & \overbrace{u_k(\alpha_k + g_k^*) \frac{\bar{n}_2}{\bar{n}_t} P_k(z)}^{\text{amplification}} + \overbrace{u_k g_k^* \frac{\bar{n}_2}{\bar{n}_t} m h v_k \Delta v_k}^{\text{ASE power}} \\ & - \underbrace{u_k(\alpha_k + I_k) P_k(z)}_{\text{attenuation}}. \end{aligned} \quad (2.18)$$

Here the α_k and g_k^* are the fibre absorption and gain spectra, respectively. Expressed in terms of the distributions of the Er^{3+} ions and optical modes, these quantities are,

$$\begin{aligned} \alpha_k &= \sigma_{ak} \int_0^{2\pi} \int_0^\infty i_k(r, \phi) n_t(r, \phi, z) r dr d\phi, \\ g_k^* &= \sigma_{ek} \int_0^{2\pi} \int_0^\infty i_k(r, \phi) n_t(r, \phi, z) r dr d\phi. \end{aligned} \quad (2.19)$$

\bar{n}_2/\bar{n}_t is the average ion density ratio where,

$$\frac{\bar{n}_2}{\bar{n}_t} = \frac{\sum_k \frac{P_k(z) \alpha_k}{P_k^{sat}(\alpha_k + g_k^*)}}{1 + \sum_k \frac{P_k(z)}{P_k^{sat}}}. \quad (2.20)$$

From Eq. 2.18, we can see that the signal output power of the optical amplifier depends on the absorption and emission cross sections of Er^{3+} in the EDF and the saturation output power P_k^{sat} of the EDFA. The output power is also affected by the ASE power that may saturate the output power as demonstrated by E. Desurvire *et al.*

al. [2, 64] and Giles *et.al.* [64, 67] in their experimental studies.

2.3.4 Er³⁺ ion Absorption and Emission Cross Section

The Er³⁺ absorption and emission cross section is an important variable in understanding the intrinsic workings of an EDFA. This cross section determines the distribution of optically induced transition processes [58] for evaluation of light amplification (as shown in the $\sigma_{ak,ek}$ term of Eq. 2.20). The emission cross sections that are directly related to the signal amplification are difficult to measure using standard techniques because of the varying structure of Stark splitting within each energy level manifold and its magnitude or oscillator strength. In practice, it is easier to measure the absorption cross section by standard 'cut-back' techniques [2] and calculate the emission cross section from the absorption results. This technique is referred to as the method of reciprocity using several theories developed by Judd [69], Ofelt [70], and McCumber [71]. In this thesis, these theories are considered for cross section predictions of the Er³⁺ ions in bismuth glass host.

I. Judd-Ofelt Theory

In 1962, Judd [69] and Ofelt [70] both independently developed the theoretical method to calculate the electric dipole matrix element. They used the principle of the intensity of the forbidden f-f electric dipole transition that originated from the opposite parity mixture of the 4fⁿ configurations. They then established a correlation between calculated intensities of electronic transitions from Russel-Saunders coupling scheme with observed intensities under absorption cross section measurement using the atomic oscillator strength principle [70].

In this theory the intensity strength dependency of the host glass can be determined using 3 parameters Ω_2 , Ω_4 and Ω_6 [69, 70], which are due to the mixed opposite parity $4f^n$ and $4f^{n-1}5d$ ligand fields and also by the totally asymmetric vibrations from the lanthanide ion and ligand interactions [72].

The Judd-Ofelt theory defines the electronic dipole oscillator strength P for a transition between a ground level i and an excited level j in isotropic medium as [69]

$$P_{ij} = \frac{8\pi^2 m \nu}{3h(2J+1)n^2} \chi_e \sum_{t=2,4,6} \Omega_t \left| \langle i \| U^{(t)} \| j \rangle \right|^2, \quad (2.21)$$

where m is the mass of an electron, h is Plank's constant, ν is the frequency of the transition and $(2J+1)$ is the degeneracy of the ground level that rises from ligand field Stark splitting. Here, χ_e is the Dexter correction [73] for the local field and n is the refractive index of the medium

$$\chi_e = \frac{n(n^2 + 2)^2}{9}. \quad (2.22)$$

In the last term of Eq. (2.21), the factor $\langle i \| U^{(t)} \| j \rangle$ is the doubly reduced matrix elements of the tensor transition operator and represents the radial contribution of the oscillating dipole operator of the atom, which has been described in more detail by Ofelt [73], Weber [74, 75], Carnal et. al. [76-78] and C. G. Walrand [79]).

The set of coefficients Ω_2 , Ω_4 and Ω_6 can be computed using least-square fitting procedures if the oscillator strength P is known from the measured absorption data; where the area under the absorption intensity data is directly proportional to the oscillator strength [80]. This method is capable of producing good agreement with experiment data [81] under the following assumption of immutable condition

- equal occupancy of the J-th level, and

- spin-orbital splitting is small compared to the energy difference between two electronic configurations.

By using these assumption, the Judd-Ofelt theory is able to define and describe the luminescence spectra mechanism of rare earth materials in glass and crystal [69-79].

II. *McCumber Theory*

The limitation of the Judd-Ofelt theory in predicting the RE material electronic band transitions has driven other researchers to develop a new theory to explain this behaviour. McCumber [81, 83] has developed a theory derived from generalisations of Einstein's relations for broadband transitions in a dielectric medium (dense gas, liquid and solid materials). These generalizations are capable of analysing the unique effect of absorption, spontaneous emission and stimulated emission at any frequency by a simple relation [2, 82, 83]

$$\sigma_a(\nu) = \sigma_e(\nu) \exp\left(\frac{h(\nu - \epsilon)}{k_B T}\right), \quad (2.23)$$

where $\sigma_a(\nu)$ and $\sigma_e(\nu)$ are the absorption and emission cross sections, k_B is Boltzmann's constant and $h\epsilon$ is the energy separation between two manifolds while maintaining the lattice temperature T constant. Since the energy manifold widths exceed $k_B T$, the absorption and emission spectra are offset from each other with the absorption spectra shifting to a higher frequency and the emission spectra shifting to a lower frequency. Calculations performed using Eq. 2.23 required an assumption that the time required to establish a thermal distribution within each manifold is short compared to the lifetime of the manifold. Compared to the Judd-Ofelt theory, the

McCumber theory relates the absorption and stimulated emission at the same frequency and allows cross section predictions, absolute values as well as spectral distributions that are inaccessible experimentally. The calculated emission cross section using the McCumber theory also has good agreement with measured emission cross section [84, 85] with simple assumption and less complexity.

In this chapter, we have discussed the vital theoretical aspect of optical amplification using RE material, notably Er^{3+} ion optical fibre. In the next chapter, the investigation of the effect of Er^{3+} ions in bismuth host glass using the Judd-Ofelt and the McCumber theory will be discussed with comparisons to other types of host glass.

REFERENCES

- [1] W. H. Zachariasen, “*The atomic arrangement in glass*”, J. Am. Chem. Soc., Vol. 54, pp. 3842-3851, 1932
- [2] E. Desurvire, “*Erbium-doped fiber amplifiers: Principle and Application*,” John Wiley & Son Inc., New York, 1994.
- [3] R. H. Doremus, “*Glass Science*”, John Wiley & Son Inc., New York, 1973.
- [4] Shiqing Xu , Zhongmin Yang, Shixun Dai, Jianhu Yang, Lili Hu, Zhonghong Jiang, “*Spectral properties and thermal stability of Er -doped oxyfluoride silicate glasses for broadband optical amplifier*”, Journal of Alloys and Compounds, Vol 361 , pp 313–319, 2003
- [5] Shiqing Xu , Zhongmin Yang, Shixun Dai, Guonian Wang, Lili Hu, Zhonghong Jiang, “*Effect of Bi₂O₃ on spectroscopic properties of Er³⁺-doped lead oxyfluorosilicate glasses for broadband optical amplifiers*”, Jour. Non-Crystalline-Solids, vol. 347, pp. 197, 2004
- [6] Yutaka Kuroiwa, Naoki Sugimoto, Kastuhiro Ochiai, Seiki Ohara, Yasuji Fukasawa, Setsuro Ito, Setsuhisa Tanabe, Teiichi Hanada, “*Bi₂O₃ based erbium doped fiber (Bi-EDF) for candidate of the broadband and compact amplifiers*”, Report of the Research Laboratory, Asahi Glass Co. Ltd., Vol. 51, paper 2, 2001
- [7] N. Jakubowicz, O. Perez, D. Grebille, H. Leligny, “*Bi³⁺ electronic lone pair configuration in the modulated Bi-2212 type oxides*”, J. Solid State Chem, Vol139, pp. 194, 1998
- [8] T. Oestereich, C. Swiatkowski, I. Broser, “*Erbium luminescence in doped*

- amorphous silicon*”, Appl. Phys. Lett. Vol. 56, No. 5, pp. 446, 1990
- [9] A. J. Kenyon, “*Erbium in silicon*”, Semicond. Sci. Technol. , Vol 20, pp. R65-R84, 2005
- [10] D. Gloge, “*The optical fibre as transmission medium*,” Reports. Prog. Phys., Vol. 42, pp. 1777-1824, 1979
- [11] G. Keiser, “*Optical Fiber Communications, International Edition 1991*,” McGraw-Hill Inc., Singapore, 1991.
- [12] B. C. Bagley, C. R. Kurkjian, J. W. Mitchel, G. E. Peterson, and A. R. Tynes, “*Material, properties, and choices*,” Optical Fiber Telecommunication, Academic, New York, 1979
- [13] T. Izawa and S. Sudo, “*Optical Fibers: Materials and fabrication*”, KTK Scientific Publishers, Tokyo, 1986
- [14] L. L. Boyer, J. A. Harrington, M. Hass, and H. B. Rosenstock, “*Multiphonon absorption in ionic crystal*”, Phys. Rev. B., Vol. 11, pp. 1665, 1975.
- [15] John P. Powers, “*An introduction to fiber optic systems*”, Aksen Associates Inc. Publishers, 1993
- [16] R. Olshansky, “*Propagation in glass optical waveguides*”, Rev. Mod. Phys. 51, pp. 341-367, 1979
- [17] Fredrik Jonsson, “*Lectures Notes on nonlinear optics*”, Course given at the Royal Institute of Technology, Dept. of Laser Physics and Quantum Optics, Stockholm, Sweden, Jan 8 – Mac 24, 2003
- [18] Vaa, M.; Bakhshi, B.; Golovchenko, E.A.; Chai, Y.; Heismann, F.; Li, H.; Arend, M.; Patterson, W.W.; Duff, D.G.; Simons, A.L.; Harvey, G.T.;

- Maybach, R.L.; Bergano, N.S., “*Demonstration of 640 Gbit/s x 7000 km submarine transmission system technology ready for field deployment*”, OFC 2001, Vol. 3, pp. :WF5-1 – WF5-3, 2001
- [19] Davidson, C.R.; Chen, C.J.; Nissov, M.; Pilipetskii, A.; Ramanujam, N.; Kidorf, H.D.; Pedersen, B.; Mills, M.A.; Lin, C.; Hayee, M.I.; Cai, J.X.; Puc, A.B.; Corbett, P.C.; Menges, R.; Li, H.; Elyamani, A.; Rivers, C.; Bergano, N.S., “*1800 Gb/s transmission of one hundred and eighty 10 Gb/s WDM channels over 7000 km using the full EDFA C-band*”, OFC 2000, Vol. 4, pp. 242 – 244, 2000
- [20] M. Yamada, T. Kanamori, Y. Terunuma, K. Oikawa, M. Shimizu, S. Sudo, K. Sagawa, “*Fluoride-based erbium-doped fiber amplifier with inherently flat gain spectrum*”, IEEE Photonics. Technol. Lett., Vol 8, No. 7, 1996, pp. 882
- [21] D. Bayart, B. Clesca, L. Hamon, J. L. Beylat, “*1.55 μ m fluoride-based EDFA with gain-flatness control for multiwavelength applications*”, Electron. Lett. Vol. 30. No. 17, 1994, pp. 1407
- [22] Lihui Huang, Shaoxiong Shen, Xiaobo Liu, Animesh Jha, “*Broadband emissions in Er³⁺-Tm³⁺ codoped tellurite glass fibre*”, Conference on Laser and Electro-optics (CLEO 2004), Vol. 1, 2004, pp. 1
- [23] S. Tanabe, N. Sugimoto, S. Ito and T. Hanada, “*Broad-band 1.5 μ m emission of Er³⁺ ions in bismuth-based oxide glasses for potential WDM amplifier*”, Journal of Luminescence, Vol. 87-89, 2000, pp 670-672
- [24] H. Hayashi, N. Sugimoto, S. Tanabe, “*High-performance and wideband amplifier using bismuth-oxide based EDF with cascade configurations*”,
-

- Opt. Fib. Technol., Vol. 12, 2006, pp. 282
- [25] Y. Liu, S. Bursev, S. Tsude, S. P. Hegarty, R. S. Mozdy, M. Hempstead, G. G. Luther, and R. G. Smart, “*Four-wave mixing in EDFAs*,” Electron. Lett., vol. 35, no. 24, pp. 2130-2131, 1999.
- [26] S. Tadic, G. Pendock, A. Srivastava, P. Wysocki, and A. Chraplyvy, “*Signal impairment due to four-wave mixing in L-band EDFAs*,” 25th Eur. Conf. Optical Communication, Nice, France, 1999, Paper PD1–11.
- [27] M. Shtaiif, M. Eiselt, R. W. Tkach, R. H. Stolen, and A. H. Gnauck, “*Crosstalk in WDM systems caused by cross-phase modulation in erbium-doped fiber amplifiers*,” IEEE Photonics. Technol. Lett., vol. 10, pp. 1796–1798, Dec. 1998.
- [28] J. Kaur, K. Thyagarajan, “*A study on the performance of L-band EDFAs under different pumping configurations*”, J. of Opt. Comm., Vol. 194, pp. 131-136, 2001.
- [29] P. Myslinski, D. Nguyen, and J. Chrostowski, “*Effects of concentration on the performance of erbium-doped fiber amplifiers*,” IEEE J. of Lightwave Tech., vol. 15, no. 1, pp. 112-120, 1997.
- [30] P. Myslinski, , C. Szubert, Member, IEEE, Allan J. Bruce, D. J. DiGiovanni, and B. Palsdottir, “*Performance of High-Concentration Erbium-Doped Fiber Amplifiers*”, IEEE Photonics. Technol. Lett, Vol. 11, pp. 973, 1999
- [31] E. Desurvire, J. L. Zyskind, C. R. Giles, “*Design optimization for efficient erbium-doped fiber amplifiers*”, IEEE Journal Light. Tech. Vol. 8, pp. 1730, 1990
- [32] Nikonorov, N.; Przhevuskii, A. “*Concentration dependence of up-*
-

- conversion quenching rate in Er-doped glass fiber*”, Lasers and Electro-Optics Society Annual Meeting, (LEOS '97) Conference Proceedings., IEEE, Vol. 2, 1997, pp. 306 - 307
- [33] F. E. Auzel, “*Materials and devices using double-pumped Phosphors with energy transfer*”, Proceeding of the IEEE, Vol. 61, No. 6, 1973, pp. 758
- [34] Y. Yan, A. J. Faber and H. de Waal, “*Luminescence quenching by OH groups in highly Er-doped phosphate glasses*”, Journal of Non-Crystalline Solids, Vol. 181, 1995, pp. 283-290
- [35] G. N. Van den Hoven, E. Snoeks, and A. Polman, “*Upconversion in Er-implanted Al_2O_3 waveguides*”, Journal of Applied Physics, Vol. 79, No. 3, 1996, pp. 1258-1266
- [36] E. Delevaque, T. Georges, M. Monerie, P. Lamouler, J. F. Bayon, “*Modelling of Pair-Induced Quenching in Erbium-doped Silicate Fibers,*” IEEE Photonics. Technol. Lett. Vol 5, No.1, 1993, pp. 73-75
- [37] J. Nilsson, B. Jaskorzynska, P. Blixt, “*Performance Reduction and design modification of Erbium-doped fiber amplifiers resulting from Pair-Induced Quenching*”, IEEE Photonics. Technol. Lett. Vol 5, No.12, 1993, pp. 1427
- [38] P. Myslinski, J. Fraser, J. Chrostowski, “*Nanosecond kinetics of upconversion process in EDF and its effect on EDFA performance*”, Proc. Opt. Amplifiers and Their Appl., Davos, Switzerland, Vol. ThE3-1, 1995, pp. 100-103
- [39] Ming Ding, Peter K. Cheo, “*Dependence of Ion-Pair Self-pulsing in Er-doped Fiber Lasers on emission to absorption ratio*”, IEEE Trans. Photonics. Technol. Lett. Vol. 8, No. 12, 1996, pp.1627-1629
-

- [40] P. Blixt, J. Nilsson, T. Carlness, and B. Jaskorzynska, “*Concentration-dependent upconversion in Er^{3+} -doped fiber amplifiers: Experiments and Modeling*”, IEEE Trans. Photonics. Technol. Lett. Vol. 3, No. 11, 1991, pp. 996-998
- [41] J. L. Philipsen, J. Broeng, A. Bjarklev, S. Helmfrid, D. Bremberg, B. Jaskorzynska, B. Palsdottir, “*Observation of strongly nonquadratic homogeneous upconversion in Er^{3+} -doped silica fibers and re-evaluation of the degree of clustering*”, IEEE J. Quantum Electron., Vol. 35, No. 11, 1999, pp. 1741
- [42] Yongjun Fu, Kai Zheng, Wei Jian, Shuisheng Jian, “*Performance of optical amplifier employing silica host magnesium-aluminium-germanium co-doped erbium-doped fiber*”, Chinese Optics Letters, Vol. 3, Issue 4, 2005, pp. 187- 189
- [43] B. James Ainslie, “*A review of the fabrication and properties of erbium-doped fibers for optical amplifiers,*” J. of Light. Technol., Vol. 9, No. 2, 1991, pp.220
- [44] Chun Jiang, Weisheng Hu, Qingji Zeng, “*Improved gain characteristics of high concentration erbium-doped phosphate fiber amplifier,*” IEEE Photonics. Tech. Lett., Vol. 16, No. 3, 2004, pp. 774
- [45] Dai S., Xu T.,Nie Q., Shen X., Wang X., “*Concentration quenching in Erbium doped bismuth silicate glasses*”, Chin. Phys. Lett., Vol. 23, No. 7, 2006, pp. 1923
- [46] S. Tammela, P. Kiiveri, S. Sarkilahti, M. Hotoleanu, H. Valkonen, M. Rajala, J. Kurki, K. Janka, “*Direct nanoparticle deposition process for*

- manufacturing very short high gain Er-doped silica glass fibers*”, 28th European Conference on Optical Communication, 2002, Vol. 4, 2002, pp 1-2
- [47] Tammela Simo, Söderlund Mikko, Koponen Joona, Philippov Valery, Stenius Per. , “*The potential of direct nanoparticle deposition for the next generation of optical fibers*”, Proceedings of Optical Components and Material III, Vol. 6116, 2006, pp. 94
- [48] Yung-Kuang Chen, Tsair-Chun Liang, Chia-Hsiung Chang, “*Optimum configuration for high-power low-noise-figure erbium-doped fiber amplifiers for lightwave CATV applications*”, J. Opt. Comm., Vol. 168, 1999, pp. 467-479
- [49] H. Toba, K. Inoue, N. Shibata, K. Nosu, K. Iwatsuki, “*16-Channel optical FDM distribution/transmission experiment utilizing Er^{3+} -doped fibre amplifier*”, Electron Lett. Vol. 25, 1989, pp. 885-887
- [50] A. Yariv, “*Quantum Electronics, Second Edition*”, John Wiley, New York, 1975
- [51] F. F. Ruhl, “*Accurate analytical formulas for gain-optimised EDFAs*”, Electron. Lett., Vol 28, No. 3., 1992, pp. 312
- [52] Nakazawa M., Kimura Y., Suzuki K., “*An ultra-efficient erbium doped fibre amplifier of 102dB/mW at 0.98 μ m pumping and 5.1 dB/mW at 1.48 μ m pumping*”, Proc. of Topical meeting on optical amplifiers and their applications, Optical Society of America, Monterey, California, 1990, pp. PDP-1 .
- [53] E. Snitzer, H. Po. R. P. Tuminelli, F. Hakimi, “*Optical fiber lasers and*
-

- amplifiers*”, US-Patent, US 4,815,079, 1989
- [54] V. Doya, O. Legrand, F. Montessagne, “*Optimized absorption in a chaotic double-clad fiber amplifier*”, Opt. Lett, Vol 23, 2001, pp. 872-874
- [55] Y. Jeong, S. Yoo, C. A. Codemard, J. Nilsson, J. K. Sahu, D. N. Payne, R. Horley, P. W. Turner, L. Hickey, A. Harker, M. Lovelady, A. Piper, “*Erbium:Ytterbium codoped large-core fiber laser with 297-W continuous-wave output power*”, IEEE J. of Selected Topics in Quantum Electronics, Vol. 13, 2007, pp. 573-579
- [56] E. Desurvire, “*Capacity demand and technology challenges for lightwave systems in the next two decades*”, J. Light. Technol., Vol 24, No. 12, 2006, pp. 4697
- [57] H. Haken and H. C. Wolf, “*The physics of atom and quanta*”, Fourth Edition, Springer-Verlag, New York, 1994.
- [58] A. E. Siegman, “*Lasers*”, University Science Books, Mill Valley, CA, 1986
- [59] M. J Yadlowsky, E. M. Deliso and V. L. Da Silva, “*Optical fibers and amplifiers for WDM Systems*”, Proc. Of the IEEE, Vol. 85, No. 11, 1997, pp. 1765-1779
- [60] O. L. Malta, “*Ligand-rare-earth ion energy transfer in coordination compounds. A theoretical approach*”, J. of Lumin., Vol. 71, 1997, pp. 229-236
- [61] H. Przybylinska, W. Jantsch, Yu. Suprun-Belevitch, M. Stepikhova, L. Palmetshofer, G. Hendorfer, A. Kozanecki, R. J. Wilson, B. J. Sealy, “*Optically active erbium centres in silicon*”, Phys. Rev. B, Vol. 54, No. 4, 1996, pp. 2532
-

- [62] M. J. Weber, "*Fluorescence and glass lasers*", J. Non-Cryst. Solids, Vol. 47, No. 1, 1982, pp. 117
 - [63] Y. Sun, J. W. Sulhoff, A. K. Srivastava, J. L. Zyskind, T. A. Strasser, J. R. Pedrazzani, C. Wolf, J. Zhou, J. B. Judkins, R. P. Espindola, A. M. Vengsarkar, "*80 nm ultra-wideband erbium-doped silica fibre amplifier*", Electron. Lett., Vol. 33, Iss. 23, 1997, pp. 1965
 - [64] Desurvire. E, Simpson. J. R., "*Amplification of spontaneous emission in erbium-doped single-mode fibers*", J. Light. Technol., Vol. 7, Iss. 5, 1989, pp. 835-845
 - [65] A. A. Kaminskii, "*Laser crystals, Springer series in optical sciences*", Springer-Verlag, New York, Vol. 14, 1990
 - [66] Guokui Liu, Bernard Jacquier, "*Spectroscopic properties of rare earths in optical materials*", Tsinghua University Press and Springer-Verlag Berlin Heidelberg, 2005
 - [67] P. C. Becker, N. A. Olsson, J. R. Simpson, "*Erbium-doped fiber amplifiers, Fundamentals and Technology*", Academic Press, 1997
 - [68] C. Randy Giles and E. Desurvire, "*Modelling Erbium-doped fiber amplifiers*," J. Lightwave Tech. Volume 9, No. 2, Feb 1991, pp. 271-283
 - [69] M. M. Kozak, R. Caspary, and U. B. Unrau, "*Computer Aided EDFA design, simulation and optimization*," Proc. Of 3rd Int. Conf. Transparent Optical Network, We. P.24, 2001, pp. 308-311.
 - [69] B. R. Judd, "*Optical absorption intensities of rare earth ions*" Phys. Rev., Vol. 127, 1962, pp. 750
 - [70] G. S. Ofelt, "*Intensities of crystal spectra of rare earth ions*", J. Chem.
-

- Phys., Vol. 37, 1962, pp. 511
- [71] D. E. McCumber, “*Theory of phonon-terminated optical masers*”, Phys. Rev., Vol. 134, No. 2A, 1964, pp. 299
- [72] R. Reisfeld, Y. Eckstein, “*Dependence of spontaneous emission and nonradiative relaxations of Tm^{3+} and Er^{3+} on the glass host and temperature*”, J. Chem. Phys., Vol. 63, No. 9, 1975, pp. 4001
- [73] D. L. Dexter, “*Solid State Physics, edited by F. Seitz and D. Turnbull*”, Academic Press Inc. New York, Vol. 6, 1958, pp. 360
- [74] M. J. Weber, “*Spontaneous Emission Probabilities and Quantum efficiencies for Excited States of Pr^{3+} in LaF_3* ”, J. Chem. Phys., Vol. 48, 1964, pp 4774
- [75] M. J. Weber, “*Probabilities for radiative and nonradiative decay of Er^{3+} in LaF_3* ”, Phys. Rev., Vol. 157, No. 2, 1967, pp. 262
- [76] W. T. Carnal, P. R. Fields, and K. Rajnak, “*Electronic Energy Levels in the Trivalent Lanthanide Aquo Ions I. Pr^{3+} , Nd^{3+} , Pm^{3+} , Sm^{3+} , Dy^{3+} , Ho^{3+} , Er^{3+} and Tm^{3+}* ”, J. Chem. Phys., Vol. 49, No. 10, 1968, pp 4424
- [77] W. T. Carnall, Jan. P. Hessler, H. R. Hoekstra, C. W. Williams, “*The absorption spectra and excited state relaxation properties of lanthanide and actinide halide vapor complexes. I. $ErCl_3(AlCl_3)_x$* ”, J. Chem. Phys., Vol. 68, No. 9, 1978, pp. 4304
- [78] W. T. Carnall, G. L. Goodman, K. Rajnak, R. S. Rana, “*A systematic analysis of the spectra of the lanthanides doped into single crystal LaF_3* ”, J. Chem. Phys., Vol 90, No. 7, 1989, pp. 3443
- [79] C. Gorller-Walrand, L. Fluyt, A. Ceulemans, “*Magnetic dipole transitions*

- as standards for Judd-Ofelt parametrization lanthanide spectra*”, J. Chem Phys. Vol. 95, No. 5, 1991, pp. 3099
- [80] W. T. Carnall, P. R. Fields, B. G. Wybourne, “*Spectral intensities of the trivalent lanthanides and actinides in solution. I: Pr^{3+} , Nd^{3+} , Er^{3+} , Tm^{3+} , and Yb^{3+}* ”, J. Chem. Phys., Vol. 42, No. 11, 1965, pp. 3797
- [81] K. Binnesmans, C. Gorller-Walrand, “*Letter to Editor: Are the Judd-Ofelt intensity parameters sensitive enough to reflect small compositional changes in lanthanide-doped glasses?*”, J. Phys.: Condens. Matter, Vol. 10, No. 10, 1998, L167-L170
- [82] D. E. McCumber, “*Theory of phonon-terminated optical masers*”, Phys. Rev., Vol. 134, No. 2A, 1964, pp. A299
- [83] D. E. McCumber, “*Einstein relations connecting broadband emission and absorption spectra*”, Phys. Rev., Vol. 136, No. 4A, 1964, pp. A954
- [84] M. J. Miniscalco, R. S. Quimby, “*General procedure for the analysis of Er^{3+} cross sections*”, Opt. Lett. , Vol. 16, No. 4, 1991, pp. 258
- [85] R. M. Martin, R. S. Quimby, “*Experimental evidence of the validity of the McCumber theory relating emission and absorption for rare-earth glasses*”, J. Opt. Soc. Am. B., Vol. 23, No. 9, 2006, pp.1770

CHAPTER 3

CHARACTERISATION OF ERBIUM-DOPED BISMUTH FIBRE

3.1 Introduction and Methodology

The characteristics and optical transitions of Er^{3+} ions in a glass host are essential parameters to dictate the performance of optical amplifiers for optical telecommunications. To this end, several theories have been developed for the evaluation of these parameters and in particular, two theories stand out, namely the Judd-Ofelt and the McCumber theories. These two theories will be discussed and employed for the purpose of optical amplifier glass host analysis in this chapter. The Judd-Ofelt theory is based on the static, free-ion and single configuration model for optical intensity transition probabilities. In this model, the explanation of mixed odd and even wavefunction interactions due to the ligand fields of the RE dopant (Er^{3+} ions) and host glass at the 4f and 5d shell, which is also known as the oscillator strength. The McCumber theory uses a generalization of the original Einstein A and B coefficients and is applied to the broadband transitions between the Stark manifolds for the RE absorption and emission cross sections spectra with simple reciprocal relationships. From here, the quantum efficiency and the transition lifetime will be characterised and studied in the evaluation of bismuth glass. The details Bi-EDF characterisation parameter and measurement is shown in Figure 3.1.

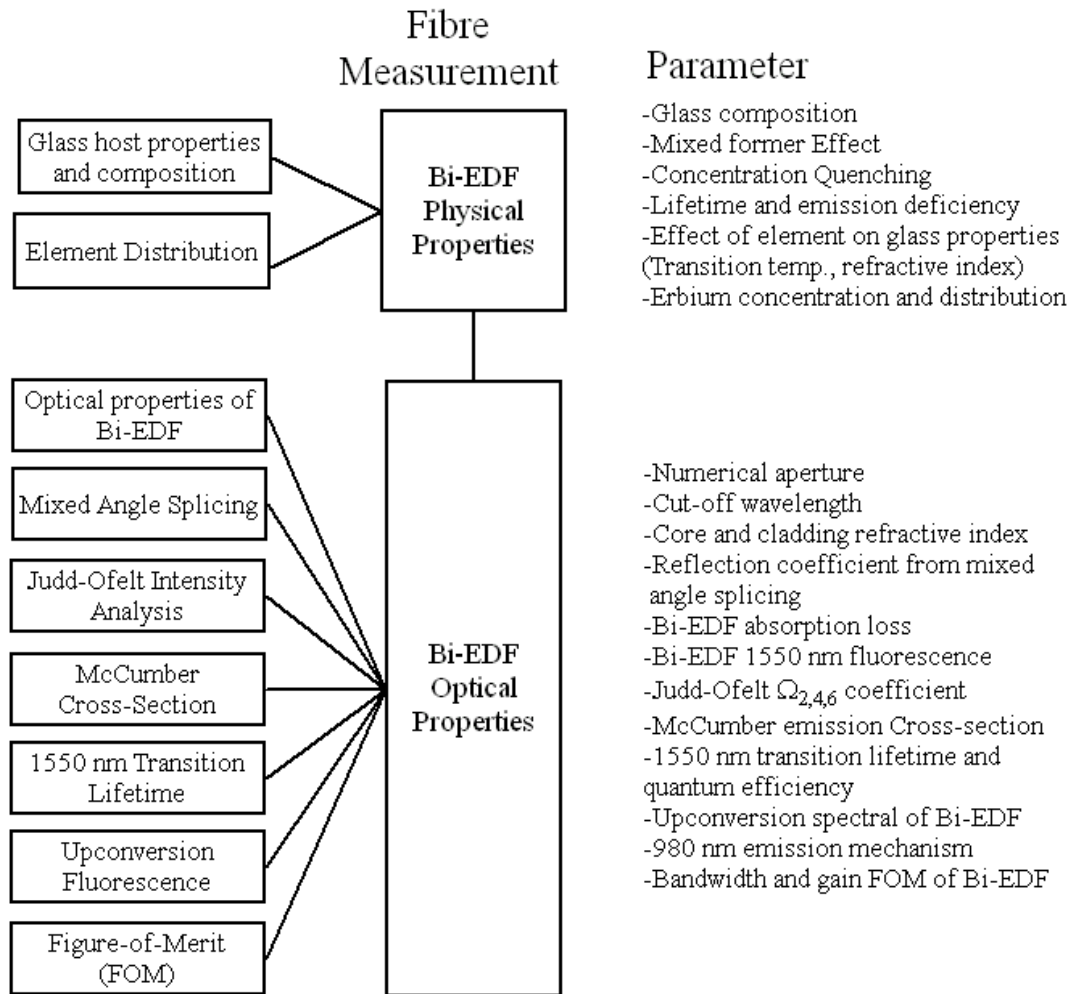


Figure 3.1 Sequence of measurement in Bi-EDF for basic parameters characterisation

3.2 Physical Properties of Bismuth Glass Host

Glass host properties and composition

The host material and composition of an optical amplifier have been observed to affect various optical transition parameters such as spectra width and broadening, flatness, lifetime and efficiency [1-7]. This know-how of the host composition or local structure is an important parameter in optical telecommunication because of the requirement for a wider and flatter spectrum with minimum gain ripples for

wavelength-division-multiplexed (WDM) network systems [3,4], greater gain ratio per launch pump-power and high output power for long haul systems [5] is sought after. Also, a low optical signal-to-noise ratio (OSNR) or Noise Figure (NF) and signal interaction such as Four-wave Mixing (FWM) and Cross-gain modulation (XGM) [4,6] are a concern. Finally, efficiency and user-friendliness allows its use in many parts of the network, compact and cheap devices such as planar Erbium-Doped Waveguide Amplifiers (EDWA) [6,7].

The bismuth glass erbium-doped fibre (Bi-EDF) used in this work is a commercially available T1L type fibre from Asahi Glass Co. Ltd. The bismuth glass is doped with 3250 wt. ppm of Er^{3+} and approximately 4.4 wt% Lanthanum. The actual glass composition is measured using a Scanning Electron Microscopy (SEM) and an Energy Dispersive X-Ray Microanalysis (EDX) with JEOL JSM 6460LA. This machine has a magnification range from 5 to 300,000 times and the capability to detect light elements from Boron up to Uranium (for element composition analysis) and under low vacuum mode, the machine is capable of measuring non-conductive

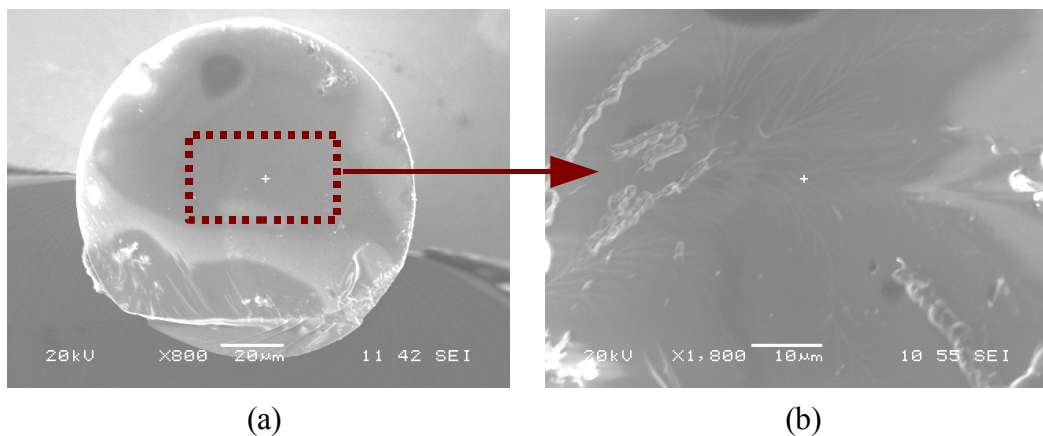


Figure 3.2 (a) Cross section of the sample using SEM. (b) Closed-up area for EDX measurement

and uncoated specimens.

Figures 3.2 (a) and (b) displays the cross-section image of Bi-EDF sample taken using SEM for the EDX measurement. Because the sample is made from glass (that is a non-conductive material) there is a 'negative-charge build-up' effect especially as seen at the top-left of Figure 3.2 (a). This effect can be reduced if the sample is coated with a conductive material such as gold or carbon, but the downside is that it can produce large background emissions that can reduce the accuracy of element quantification. For the EDX measurement, the sample is bombarded with electrons accelerated to 20 kV and the emitted x-ray from the sample is captured and analysed using integrated 'Analysis Station' software.

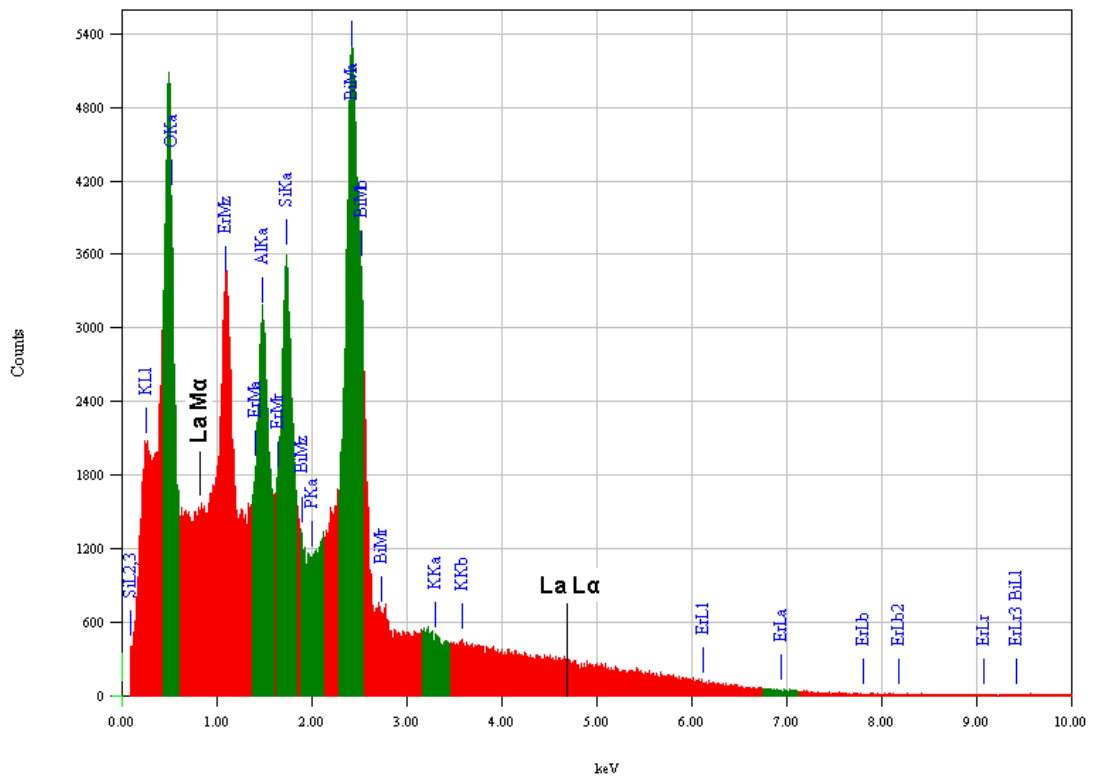


Figure 3.3 The energy spectra of the sample from EDX measurement.

The energy spectra of the sample from the EDX measurement is indicated in Figure 3.3. The elemental analysis was done from this spectra with quantitative setting of 'standard-less' with ZAF for oxide calculations. The result is listed in Table 3.1.

The analysis from the EDAX measurement has disclosed that the Bi-EDF glass network formers are bismuth oxide Bi_2O_3 , silica oxide SiO_2 and alumina/aluminium oxide Al_2O_3 [8]. There is also a small percentage of potassium oxide K_2O and phosphorus oxide P_2O_5 that is added in the glass as network modifiers and Er_2O_3 is also detected as the activator of the 1.55 μm transition in optical transmission systems.

However from this result alone one is unable to form complete Bi-EDF stoichiometric ratios for chemical formula calculations. This is due to the fact that the EDAX is not capable of detecting the element La that should exist in the sample. The low detection ability is expected to be due to the element La having a high X-Ray principal energy [9] and thus, completely diffused in the glass. It is prudent to note that the principle energy lines $\text{La}\alpha$ and $\text{M}\alpha$ of La are 4.6510 and 0.8332 keV

Table 3.1 Bi-EDF glass composition analysis from EDAX

Element	Mass (%)	Error (%)
Bi_2O_3	67.80	1.88
SiO_2	14.24	0.81
Al_2O_3	16.96	0.87
K_2O	0.05	0.29
P_2O_5	0.53	0.64
Er_2O_3	0.42	1.67
Total	100.00	6.17

respectively (the excited electron energy $E_c(L) = 5.483$ keV, $E_c(M) = 0.832$ keV) as displayed in Figure 3.2. The measured spectra have larger background noise levels (>300 counts at 4.6 KeV) that is superimposed atop the real La spectra.

Mixed Former Effect

The effect of the Bi_2O_3 composition in the Erbium-doped bismuth silicate glass has been reported by Tanabe *et. al* [10, 11], Jianhu Yang *et. al* [12, 13] and Zhou. Y. *et. al* [14]. They have observed that glass with bismuth addition causes the emission spectra of Er^{3+} ions in the glass to widen, to be more efficient and produces a longer transition lifetime [10, 11, 12] by affecting the glass ligand field and this is also known as the 'mixed-former' effect [13]. From this effect, the ligand field of the glass can be disturbed by using the glass former element that has high electronegativity (electronegativity is the power of an ion in a atom/molecule to attract electrons to itself and it is represented in the Pauling scale). Because bismuth has a high electronegativity of $\chi = 2.02$ [13] compared to other glass formers, it has a higher effect on the glass ligand field and for that reason, changes the bonding condition between the glass former. This effectively increases the field strength around the Er^{3+} ions lattice and resultantly, increases the site-to-site symmetry [5,15] and covalence bonds between erbium and oxygen atom that are in a triangle structure [8,12]. Besides that, the aluminium addition is also expected to cause a similar behaviours as the electronegativity of the aluminium is about $\chi = 1.1$.

An adjustment with glass former or modifier concentration also affects the glass refractive index and fluorescence lifetime due to disruption of the glass host

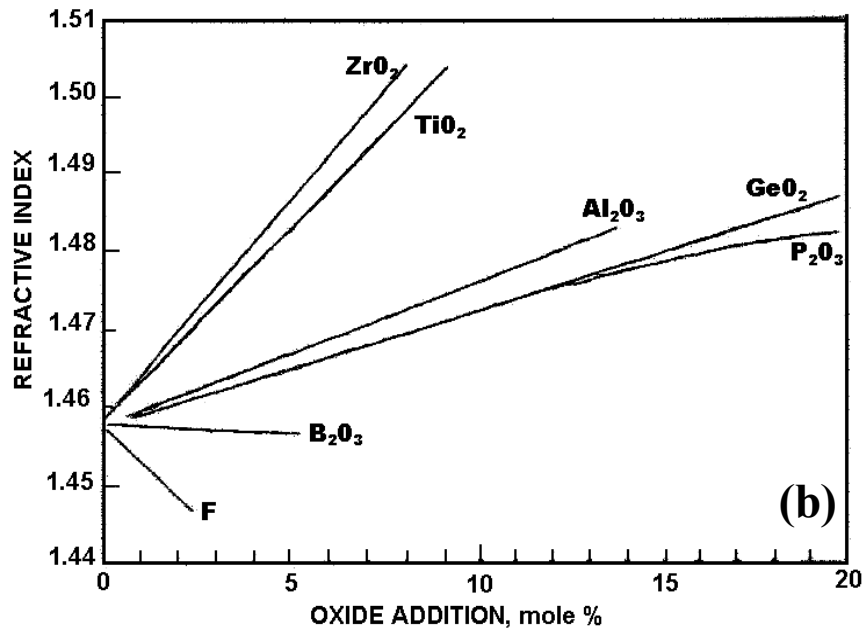
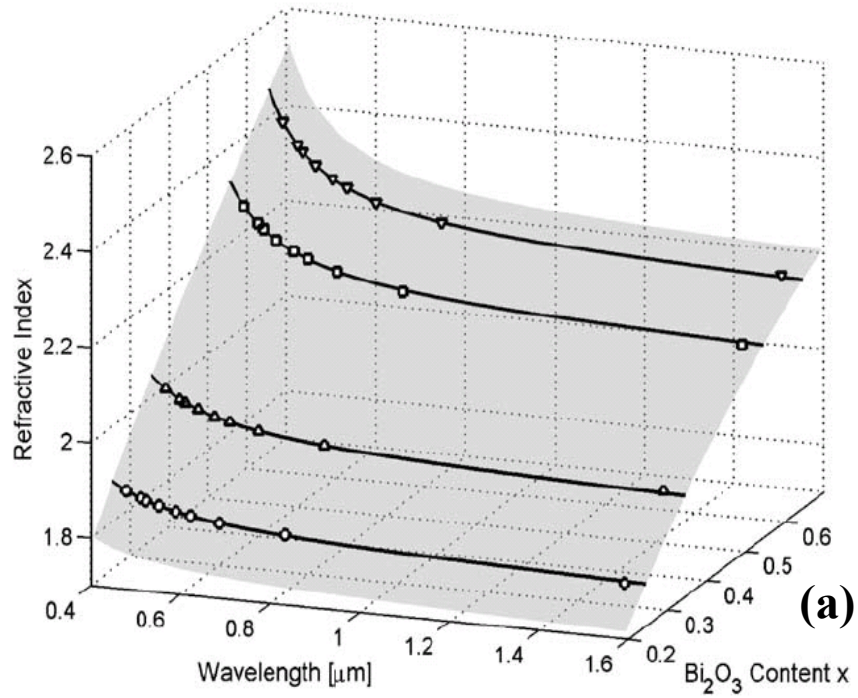


Figure 3.4 Refractive index of (a) bismuth borate glasses and (b) silica glasses with different dopant and oxide addition taken from Refs. [16] and [17]

local environment [12-15] as illustrated in Figure 3.4 (a) and (b). From the Judd-Ofelt theory, the fluorescence intensity of RE ions in glass host depends cubically on the glass host refractive index as stated in Eq. 2.16 and 2.17. Hence, whereas the refractive index increases with bismuth addition, more intense fluorescence emission are present. Besides that, fluorescence intensity also dependent on glass phonon energy.

Glass with low phonon energy requires more phonons to bridge the energy gap between the metastable state, $^4I_{13/2}$ and the next-lower ground state $^4I_{15/2}$. The energy gap between $^4I_{15/2}$ and $^4I_{13/2}$ level is 6500 cm^{-1} , while the phonon energy of Bi-O bonds is lower than that of Si-O bonds which are 500 cm^{-1} and 1150 cm^{-1} . As a result, bismuth-based glass requires almost twice the amount of phonon energy to bridge the energy gap. This consequently sink more pump photon energy and reduces the the nonradiative decay rate, in accordance to RE decay rates [20] as given by

$$\frac{1}{\tau_{\text{mea}}} = \frac{1}{\tau_{\text{rad}}} + \frac{1}{\tau_{\text{nr}}} \quad , \quad (3.1)$$

$$\frac{1}{\tau_{\text{nr}}} = W_0 \left(1 - \exp\left(-\frac{h\nu}{kT}\right) \right)^p \quad , \quad (3.2)$$

where the total lifetime τ_{mea} , radiative lifetime τ_{rad} , and nonradiative lifetime τ_{nr} , p is the number of phonons emitted, with energy $h\nu$, W_0 is the spontaneous rate for emission of p phonons of energy $h\nu$, k is the Boltzmann constant, T is the temperature.

Accordingly, the decrease of nonradiative decays was induced by the increasing measured lifetime with the higher number of phonons involved in the transition [12, 13, 20, 21]. However, the only drawback of adding a low phonon

energy composition is an increasing upconversion process [22] that can convert the infrared pump photon to a higher energy photon as discussed in Chapter 2.2.2. Visible upconversion processes have been recognised in the efficiency reduction of 1550 nm signal amplification thus, making the optical amplifier inapplicable.

In order to restrain the glass phonon energy to a medium level but still retain maximum optical amplification bandwidth, other elements have been introduced into the optical amplifier's glass host during fabrication. Alumina (Al_2O_3), germanium oxide (Ge_2O), phosphorus pentoxide (P_2O_5) and lanthanum oxide (La_2O_3) have been known for their ability to widen the Er^{3+} emission spectra [23, 24] and also the pump efficiency [25-27] without increasing the upconversion process. Co-doping a glass with alumina improves the Er^{3+} distribution to the centre of the core fibre because it is less volatile compared to other co-dopants such as germanium and boron [28]. Therefore, a fibre core with high and uniform Er^{3+} ion concentration without the ion clustering effect can be produced and thus, is also capable of eliminating the concentration quenching effect [25,29] and as the result, lowering the upconversion process. Other than aluminium, lanthanum co-doping is also capable of suppressing the Er^{3+} ion concentration quenching [30-32]. This is because in general, due to them having in the same group, the chemical properties and structure of La^{3+} ions and Er^{3+} ions are similar with the former having an ionic radius of 103.2 pm, while the latter has an ionic radius of 89.0 pm [27] as derived in Figure 3.5(a)). Accordingly, it is assumed with moderate concentration of La^{3+} ions compared to Er^{3+} ions, the La^{3+} ions can disperse the Er^{3+} ions evenly and uniformly in the glass host because the lanthanide ions have a tendency to form a cluster in the glass [27, 31, 32].

Glass co-doped with phosphorus can reduce Excited State Absorption (ESA) and also frequency upconversions [33] by creating an inhomogeneous ligand field. The inhomogeneities of the glass ligand field by the phosphorus co-dopant is supposed to be due to its pentavalent property that stoichiometrically bonds with oxygen atoms (see Figure 3.5(b)). This creates irregular Er^{3+} ions energy state manifolds that lower the overlap ratio δ between σ_{ESA} and σ_{GSA} , excited and ground state absorption cross sections, [34,35] respectively. This deficiency is defined as

$$\delta = \sigma_{\text{ESA}} / \sigma_{\text{GSA}} \quad (3.3)$$

The similar inhomogeneous ligand field effect is also expected to happen due to the potassium, K co-dopant addition. Potassium has high basicity that can attract more oxygen atom to form an oxide. With an increasing oxide bond, a larger oxygen electron density is produced and subsequently, increasing the strength of the local glass ligand field significantly [36].

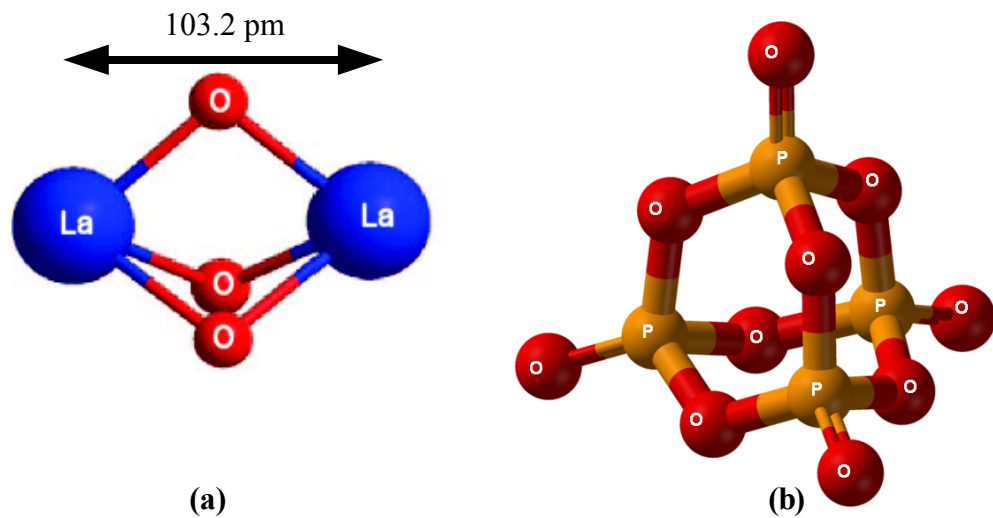
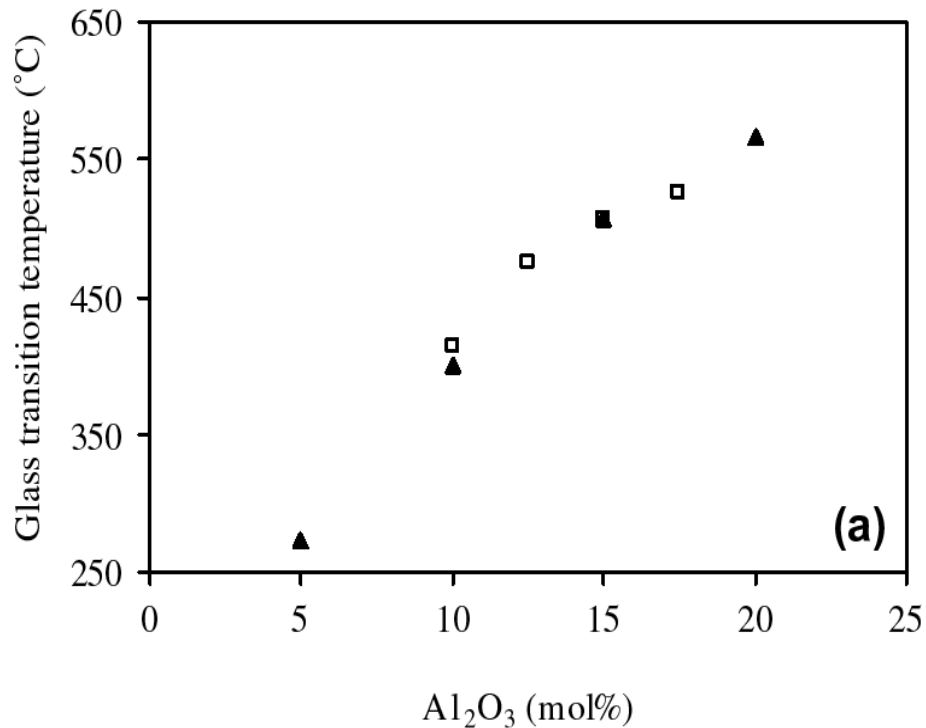


Figure 3.5 Lanthana cubical (a) and phosphorus pentavalent link with three singly- bonded and one doubly- bonded oxygen (b).

The final composition in the glass fabrication process depends on the elements itself and consolidation conditions. The volatility of elements used in the glass process is largely dependent on the glass transition temperature T_g . Glass transition temperature, T_g is the most important parameter in glass making and, it is defined as the temperature in which the amorphous phase of the glass is converted from a hard/stiff and glassy like state (which also known as Vitreous State) to a rubbery like state (in elastic and flexible conditions), with a viscosity of 10^{12} Pa·s [37]. On the other hand, dopants such as P_2O_5 , K_2O and La_2O_3 [17,18,19,35] are also added into the glass to decrease the transition temperature, T_g as illustrated in Figure 3.6. Glass with lower T_g are easier to fabricate and eliminates/reduces the volatility of the dopants during the densification process [38]. Some of the available data on refractive index and glass transition temperature of mixed glass formers compositions is presented in Figures 3.4 and 3.6.



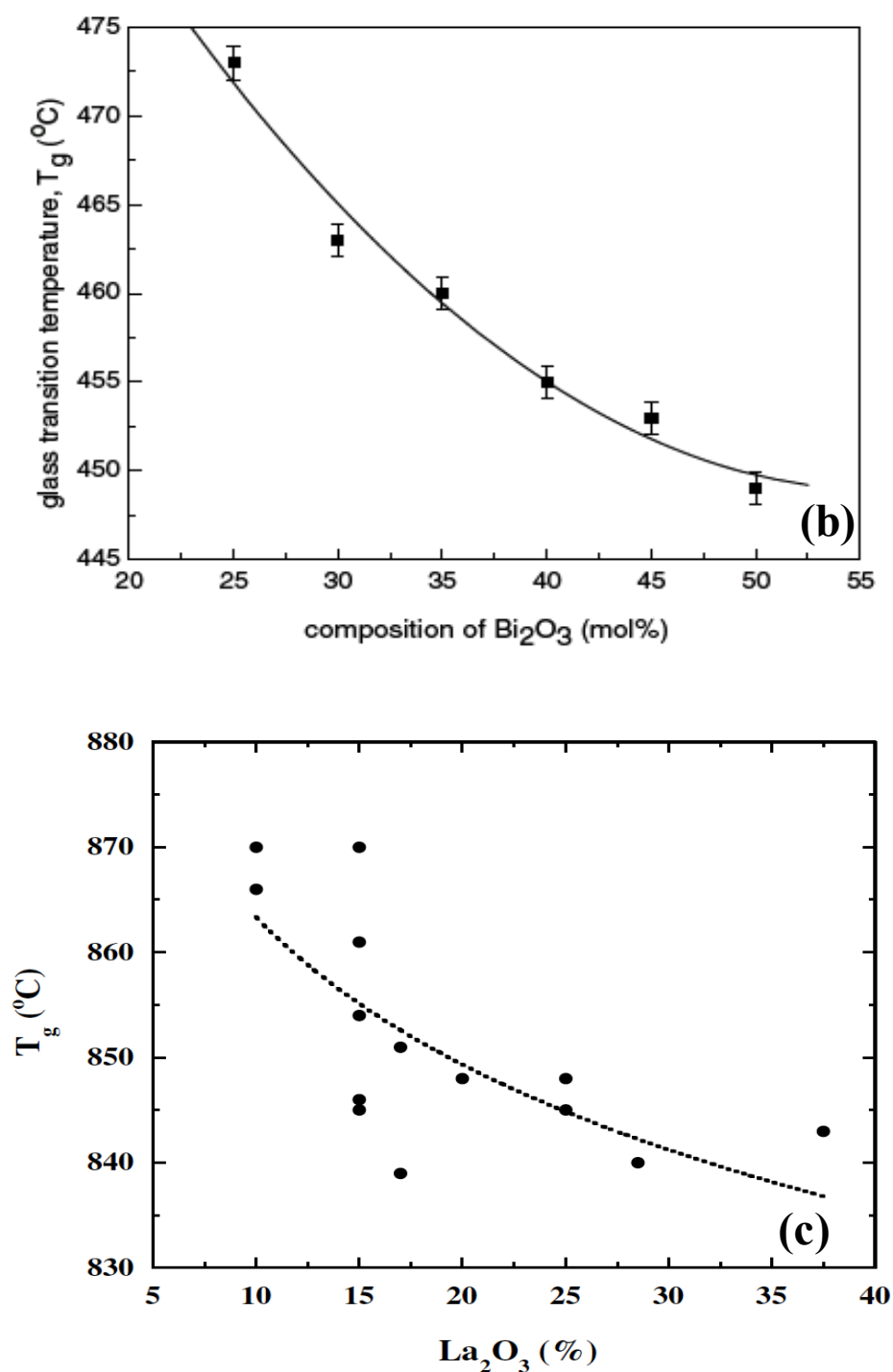


Figure 3.6 Variations of T_g (glass transition temperature) with (a) Al_2O_3 [17] (b) Bi_2O_3 [17,18] and (c) La_2O_3 [19].

Figure 3.7 indicates the element distribution in a Bi-EDF cross-section measured using the EDAX. The erbium composition represents the lowest distribution whereas the bismuth composition represent the highest distribution in comparison with other elements. From the data, almost all elements are distributed evenly along the measured area of 110 μm , clearly showing that there are no Er^{3+} ions clustering at the sample. The ion clustering has been reduced due to the fact that the Bi-EDF was fabricated using the mixed-former effect which then, lowers the upconversion effect.

The intensity of Al distribution on the fibre clearly reveals a peak line which is absent in other elements distributions. The high intensity at the edge of the fibre is supposed to be due to devitrification [17] and contamination from the fibre holder as the holder is also made from Aluminium.

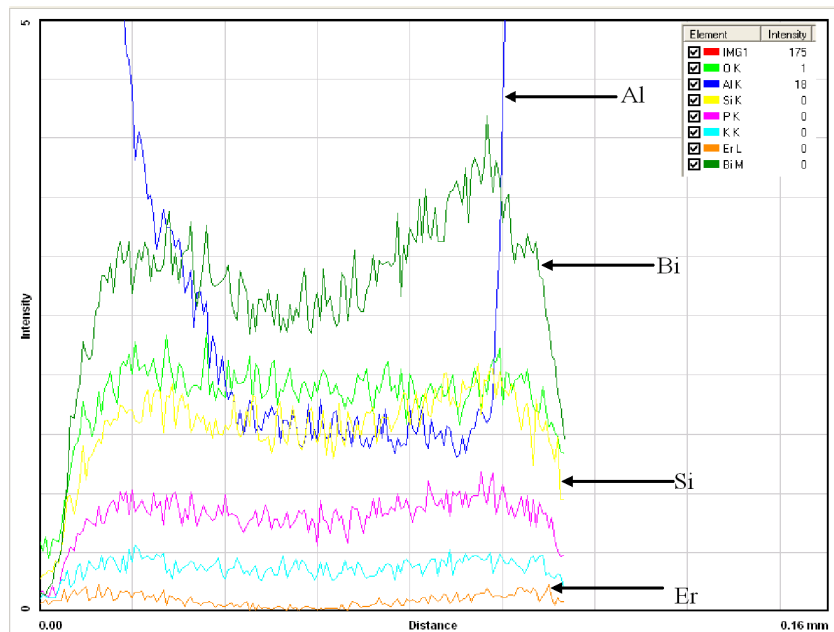


Figure 3.7 Element distribution on Bi-EDF sample from EDAX measurement.

3.3 Characteristics of Bi-EDF

The characteristics of the Bi-EDF was measured to comprehend the effect of glass composition in the performance of the Bi-EDFA. Table 3.2 lists the optical properties of T1L type bismuth fibre provided by Asahi Glass Co. Ltd.

Table 3.2 Bi-EDF Optical specification

Erbium concentration (wt. ppm)	3525
Numerical aperture (NA)	0.20
Cut-off Wavelength (nm)	<1300
Core diameter (μm)	5.4
Cladding diameter (μm)	124.5
Core/cladding refractive index	2.03/2.02

The Bi-EDF is coated with a plastic coating to protect the fibre from moisture and angle fusion spliced with silica fibre (Nufern 980-HP) as depicted in Figure 3.8. The mixed angle fusion splicing [40] is critical for Bi-EDF to reduce reflection and splicing loss due to large index differences between Bi-EDF and silica fibres. Without angled fusion splicing, the splice loss will be high and as a result, reducing the launched signal and pump light into the Bi-EDF and increasing the signal NF by

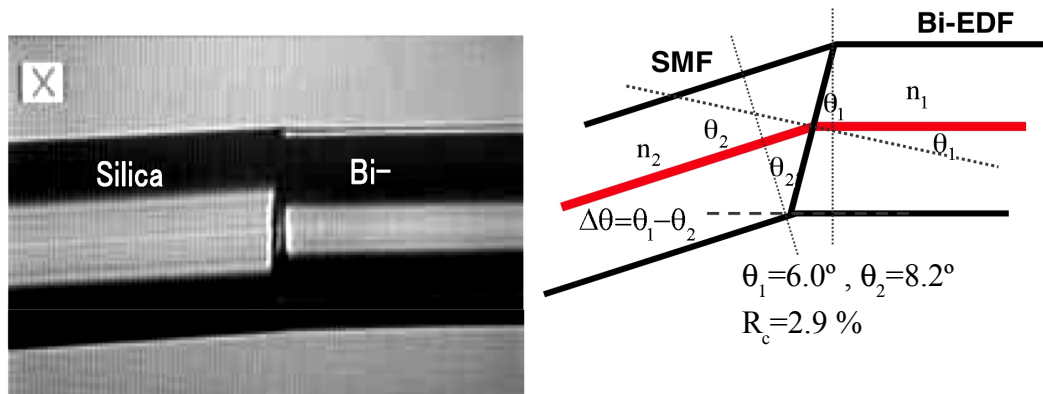


Figure 3.8 Mixed angle fusion splicing between Bi-EDF and Silica fibre.

the same amount [1].

$$\text{Loss}_{\text{MFD}}[\text{dB}] = -10 \log \frac{4}{\left[\frac{\text{MFD}_1}{\text{MFD}_2} + \frac{\text{MFD}_2}{\text{MFD}_1} \right]^2} \quad (3.4)$$

The total splice loss of the Bi-EDF is a sum of a loss due to mismatch in Mode-Field Diameters (MFD), reflections and also due to lateral misalignment between the fibres. However, only the MFD mismatch is considered because the splicing was done by Asahi Glass Co. and is undisclosed. Using the optical properties in Table 3.2, the MFD is calculated using the Marcuse empirical formula [39] for a 6.32 μm core diameter with 1550 nm input signal. From Eq. 3.4 [39], the splicing loss due to the MFD mismatch between Bi-EDF and silica (Nufern 980-HP) fibre is 0.023 dB per splice. The total estimated splice loss due to MFD mismatch is 0.047 dB. The reflection coefficient, R_c defined in Eq. 3.5 was calculated from the angle data of $\Delta\theta = -2.2^\circ$ provided by Asahi Glass Co. and was found to be 2.9 % which indicates effective reduction of optical reflection.

$$R_c = \frac{R_s + R_p}{2}, \quad (3.5)$$

$$\text{where } R_s = \left(\frac{n_1 \cos \theta_1 - n_2 \cos \theta_2}{n_1 \cos \theta_1 + n_2 \cos \theta_2} \right)^2$$

$$\text{and } R_p = \left(\frac{n_1 \cos \theta_2 - n_2 \cos \theta_1}{n_1 \cos \theta_2 + n_2 \cos \theta_1} \right)^2.$$

Room temperature absorption and fluorescence measurements were also performed on a Bi-EDF type T1L-049P/60704-05 with a fibre length of 49.1 cm. The absorption properties is decided from loss measurements using an Optical

Spectrum Analyser (OSA) by comparing the transmission spectra with and without the sample. The detailed experimental set-up is illustrated in Figure 3.9. The light source and OSA used in the illustration is ANDO AQ- 4303B White Light Source and AQ-6713C.

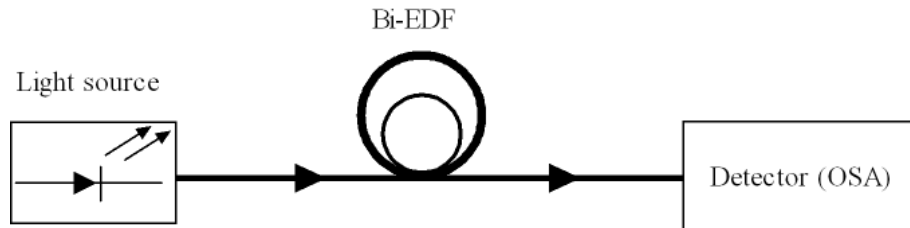


Figure 3.9 Transmission spectra measurement set-up, OSA: Optical Spectrum Analyser

The absorption spectrum from 700 to 1700 nm is demonstrated in Figure 3.10. From the absorption spectrum, the Bi-EDF insertion loss at 1550 nm is estimated by extrapolating the slope from 1200 nm and 1700 nm. It also can be seen that the Bi-EDF absorption is very high and due to the ANDO AQ- 4303B light source having limited light intensity, the detected absorption spectra was below the OSA sensitivity limit of -90 dBm that produces large errors in absorption measurements.

Due to the Er^{3+} ions having a zero absorption coefficient at 1310 nm, the insertion loss (including two splicing losses) was measured to be 2.479 dB while the estimated insertion loss at 1550 nm from the extrapolation is 2.12 dB. By subtracting the MFD loss, the Bi-EDF total splice loss is estimated to be 2.073 dB indicating a loss of 1.037 dB per splice. The extrapolation line also displays that the insertion loss of Bi-EDF is wavelength dependent with a slope of 0.0008. This dependence is expected to be due to the wavelength-dependent refractive index as specified in the Sellmeier equation by

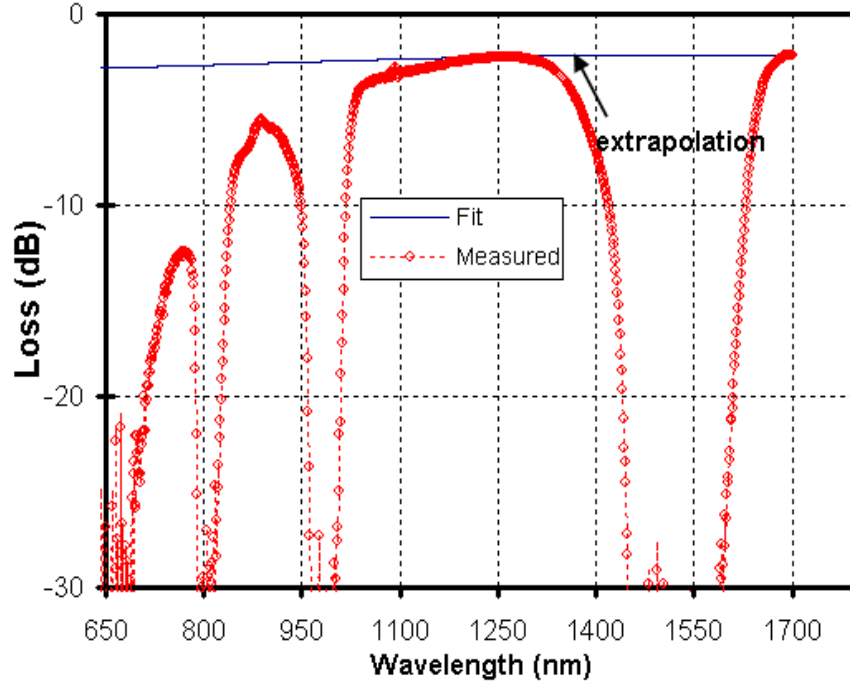


Figure 3.10 Absorption spectra of T1L bismuth fibre (Solid line indicate the data extrapolation).

$$n^2(\lambda) = 1 + \sum_i^3 \left[\frac{B_i \lambda^2}{\lambda^2 - C_i} \right] \quad (3.6)$$

where $B_{1,2,3}$ and $C_{1,2,3}$ are experimentally determined constants.

Figure 3.11 exhibit the relative absorption intensities for Bi-EDF compared with Si-EDF from Fibercore type 1500L. The absorption intensity at the 975 nm region exhibits the fact that Si-EDF has a larger absorption bandwidth than Bi-EDF. The absorption spectrum of Bi-EDF exhibits a wider cross-section with two distinguishable peaks at 1495 and 1530 nm. These two peaks actually represent the Er^{3+} ion metastable state of $^4\text{I}_{13/2}$ that has been split into two different energy states by the ligand field of the glass host. Besides that, at the 1530 nm peak Bi-EDF has a higher absorption cross-section of $7.58 \times 10^{-25} \text{ [m}^2\text{]}$ compared to $4.39 \times 10^{-26} \text{ [m}^2\text{]}$ of Si-EDF, and larger full-width half maximum (FWHM) value. Although the FWHM is

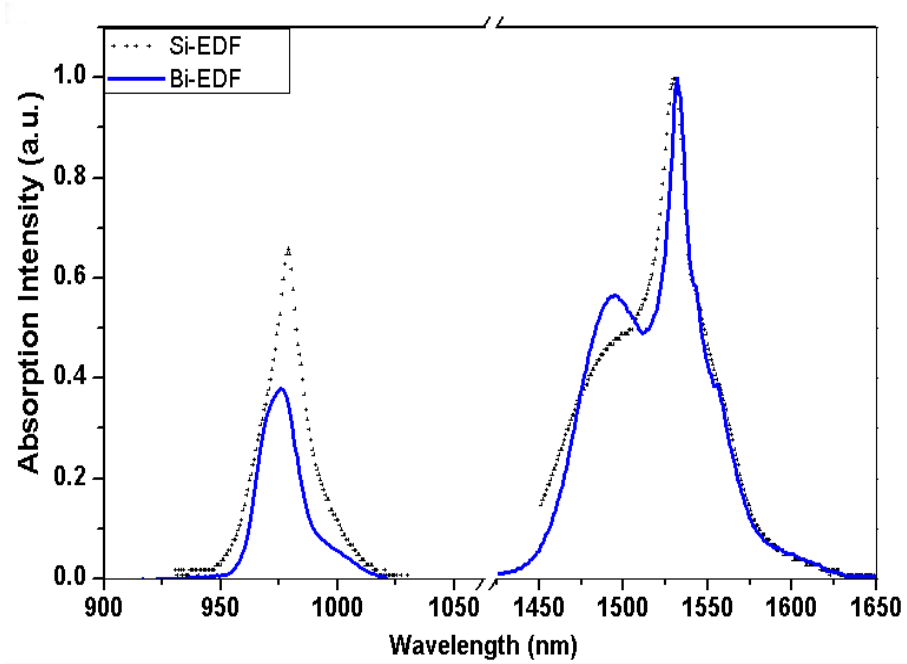


Figure 3.11 Normalised absorption intensity of Bi-EDF and Si-EDF (courtesy of Asahi Glass and Fibercore Ltd.)

often used as a semi-quantitative indication of optical bandwidth, in this case it indicates that the ligand field of the Bi-EDF induces a greater energy state degeneracy due to site-to-site variations, which is also known as the Stark effect [1,41] and widens the optical transitions.

The Stark effect can also be observed in the fluorescence spectrum; the spontaneous and stimulated emissions. The fluorescence spectrum was measured after the white light source in Figure. 3.9 was replaced with a high power 171 mW pump laser diode at 1480 nm wavelength. The fluorescence spectrum is shown in Figure 3.12.

The fluorescence spectrum of Bi-EDF has a broader spectra especially at longer wavelengths. The spectra FWHM is almost 2 times broader; about 80 nm compared with Si-EDF's FWHM of 40 nm when compared at similar fluorescence

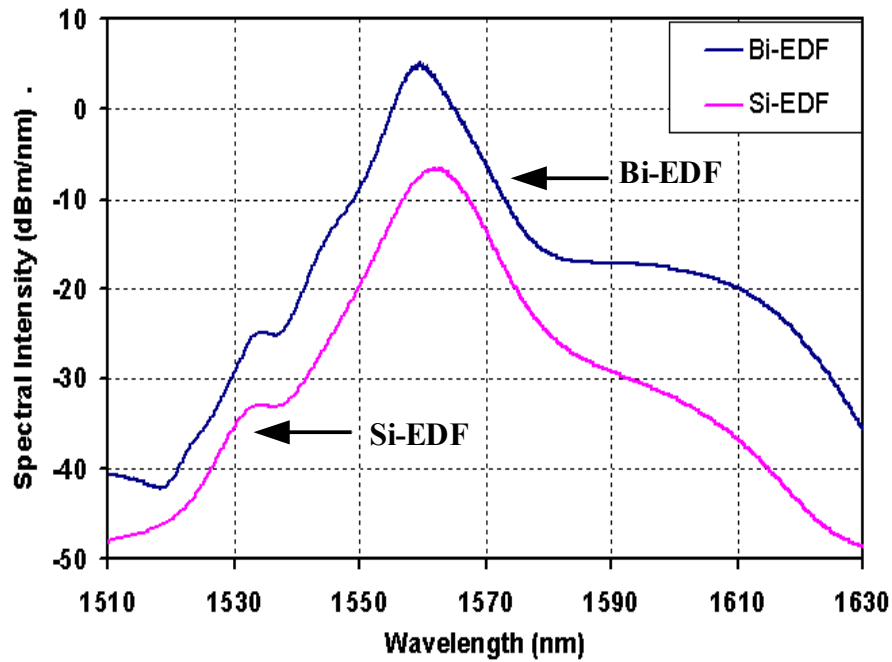


Figure 3.12 Fluorescence intensity of Bi-EDF and Si-EDF under 1480 nm pumping.

intensity. The output intensity is also higher compared to Si-EDF because the La^{3+} ions reduce the Er^{3+} ion clustering [32] and upconversion process, as a result, increasing the pump-to-signal conversion efficiency. The wider output spectra bandwidth and higher output power offers greater opportunity for an application in DWDM systems and long-haul telecommunication systems [42].

Figure 3.13 denoted the Er^{3+} ion fluorescence intensity under different glass host materials taken from Jianhu Yang *et al.* [13]. From the figure, it is obvious that Er^{3+} ion emissions in the bismuth glass have wider fluorescence spectra and higher peak emissions. The bandwidth of the fluorescence spectra is largely influenced by the variations and the ligand fields around RE ions from site-to-site, and the ligand fields depend mainly on the glass host [13]. Thus, the bismuth glass ligand field has a bigger influence on RE ions compared with other glass hosts. In the next section, the

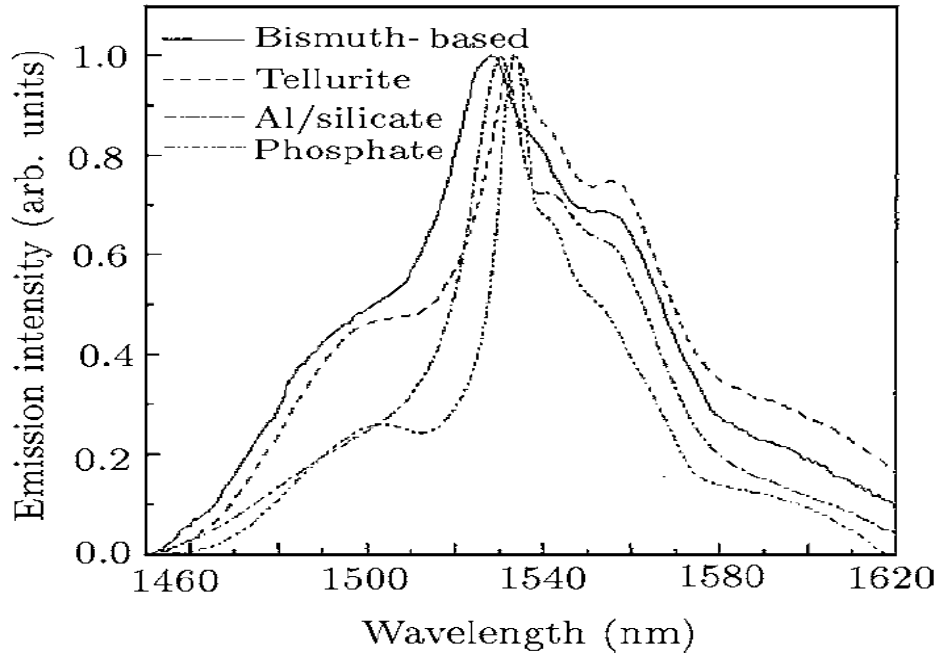


Figure 3.13 Normalised fluorescence spectra of Er^{3+} in various type of glasses under 979 nm pumping taken from Ref. [13]

ligand field strength of Bi-EDF is calculated and discussed using the Judd-Ofelt theory for a better understand effects of glass host in RE ion fluorescence.

3.3.1 Judd-Ofelt Intensity Analysis

The Judd-Ofelt theory [43, 44] is an optical intensity transition probability theory for RE elements (lanthanide and actinide) in an isotropic dielectric medium. The principles behind this theory are the static, free-ion and single ions approximations. This theory explains the strengths of the static electric field that is also known as the ligand field between RE ions with surrounding host ions. Ligand fields in the host medium arises from a perturbation of the free-ion Hamiltonian between initial and final states as stated in the last terms of Eq. 3.7 $\langle i || U_0 || j \rangle$, which

is referred to as the doubly reduced matrix elements of the tensor operator for the intermediate coupling [43-51].

$$P_{ij} = \frac{8\pi^2 m \nu}{3h(2i+1)n^2} \underbrace{\left(n \frac{(n^2+2)^2}{9} \right)}_{\chi_e} \overbrace{\sum_{t=2,4,6} \Omega_t \left| \langle i \| \hat{U}^{(t)} \| j \rangle \right|^2}^{\text{Oscillator}} \underbrace{\quad}_{\text{Tensor}}. \quad (3.7)$$

The matrix describes the optical transition from the admixture process of opposite parity states that are normally forbidden in $4f^N$ states of RE elements (the term forbidden here means an optical transition may occur in principle, but with a low probability). The tensors are virtually independent of the glass host [52, 53] and for Er^{3+} ions, the constant included in Table 3.3 was taken from M. J. Weber *et. al* [47]. Consequently, the oscillator terms that contains the information of the ligand field of the glass host with Judd-Ofelt coefficients, Ω_2 , Ω_4 , and Ω_6 can be written as the sum of three terms

$$\sum_{t=2,4,6} \Omega_t \left| \langle i \| U^{(t)} \| j \rangle \right|^2 = \Omega_2 |U^{(2)}|^2 + \Omega_4 |U^{(4)}|^2 + \Omega_6 |U^{(6)}|^2. \quad (3.8)$$

Table 3.3 Doubly reduced matrix element of $U^{(t)}$ for Er^{3+} taken from Ref. [47] and used in the Judd-Ofelt coefficient calculations

i	j	$[U^{(2)}]^2$	$[U^{(4)}]^2$	$[U^{(6)}]^2$
$^4I_{13/2}$	$^4I_{15/2}$	0.0188	0.1176	1.4617
$^4I_{11/2}$	$^4I_{15/2}$	0.0259	0.0001	0.3994
	$^4I_{13/2}$	0.021	0.11	1.04
$^4I_{9/2}$	$^4I_{15/2}$	0.0	0.1452	0.0064
	$^4I_{13/2}$	0.0003	0.0081	0.64

These coefficients reflect upon the strength of the ligand field and energy wave functions for energy state separation and it can be resolved by using a least-

square fitting method on the measured absorption spectra of RE and host glass.

The calculated Judd-Ofelt coefficients for Bi-EDF glass is presented in Table 3.4 along with comparison with other glass hosts.

Table 3.4 Judd-Ofelt coefficient for various glasses.

(I):LKBBG: $5\text{Li}_2\text{O} \cdot 5\text{K}_2\text{O} \cdot 10\text{BaO} \cdot 50\text{Bi}_2\text{O}_3 \cdot 30\text{Ga}_2\text{O}_3 \cdot 0.406\text{Er}_2\text{O}_3$; [54]

(II):Bismuth-Borate: $(\text{Er}_2\text{O}_3)_{0.0025}((\text{Bi}_2\text{O}_3)_{0.25}(\text{B}_2\text{O}_3)_{0.75})_{0.9975}$; [55]

(III):S25AlN: $25\text{SiO}_2 \cdot 25\text{AlO}_{3/2} \cdot 25\text{NaO}_{1/2} \cdot 0.5\text{ErO}_{3/2}$ [56]

Glass Composition	$\Omega_2 [10^{-20} \text{ cm}^2]$	$\Omega_4 [10^{-20} \text{ cm}^2]$	$\Omega_6 [10^{-20} \text{ cm}^2]$	$\sigma_{\text{RMS}} [10^{-8}]$
Bi-EDF	9.55	2.86	0.32	15.00
LKBBG ^(I)	5.66	1.39	0.74	6.13
Bismuth-borate ^(II)	4.58	1.44	1.53	-
S25AlN ^(III)	9.53	1.49	0.80	-

In the table, the σ_{RMS} coefficients is the root-mean-square deviation between measured (P_{exp}) and calculated (P_{calc}) oscillator strengths, which can be calculated using the following relationship:

$$\delta_{\text{RMS}} = \left[\sum \frac{(P_{\text{exp}} - P_{\text{calc}})^2}{N_{\text{tran}} - N_{\text{para}}} \right] . \quad (3.9)$$

Here N_{tran} and N_{para} are the number of transitions and the number of parameters, respectively.

Judd-Ofelt $\Omega_{2,4,6}$ Coefficient

The Ω_2 parameter from the Judd-Ofelt coefficients was found to be responsible for hypersensitive transitions in rare earth ions [57]. These transitions are highly dependent on the degree of the site symmetry (bonding) of Er^{3+} ions in the host glass

environment [58] and the covalent bonding coefficient between the glass host and the RE ions by controlling the effective nuclear charge of the ion [36]. The Ω_4 parameter represents the non-hypersensitive transition that is related to the change of local basicity and ionic packing ratio in the host glass environment while the Ω_6 coefficient also has a similar effect with Ω_4 and represents the rigidity of the solid host in which the dopant ions are situated [36, 57, 58].

The high value of the Ω_2 coefficient tells us that by using the mixed-former effect [13] technique to fabricate Bi-EDF glass, we have increased the Er^{3+} hypersensitive transitions. This combination creates large vacant spaces and allows large cations Er^{3+} ions to fill-in. For that reason, significantly increasing the number of Er^{3+} - O^{2-} ions bonding and reducing the ion clustering [32]. With low Er^{3+} ion clustering, the effect of concentration quenching [25, 29] is reduced significantly and this makes the pump-to-signal energy transfer more efficient [58].

At the same time, this mixed-former effect also increases the basicity of the glass host with a high Ω_4 value of $2.86 \times 10^{-20} [\text{cm}^2]$ due to the addition of potassium, K. With high local basicity, the ions-ligand bond distances of Bi-EDF increases and becomes asymmetrical. This affects the splitting of the Er^{3+} ion energy states and causes a broadening of the optical transition and enhances the absorption and fluorescence intensity significantly [59]. This effect conforms with the two absorption peaks as exposed in Figure. 3.10.

Although the Ω_6 coefficient of Bi-EDF is smallest compared with the others, this coefficient rules the radiative $^4\text{I}_{13/2} \rightarrow ^4\text{I}_{13/2}$ transition, since the reduced matrix elements, $\langle\|U^{(2)}\|\rangle$ and $\langle\|U^{(4)}\|\rangle$ of this transition are small [56]. The value exhibits

the fact that Bi-EDF has a rigid lattice matrix with both 6s and 5d shielding the 4f shell from external distortion. Tanabe *et. al.* and Weber *et. al* [56,60] found an opposite relationship between the Ω_2 and Ω_6 coefficients, where the high bonding ratio between Er^{3+} ions and the glass host (large Ω_2 values), will produce high rigidity glass (therefore low Ω_6 values) which explains the effect of large ion size of the glass modifier. This is expected as potassium has affected the Bi-EDF density as discussed earlier.

The σ_{RMS} from the calculation was found to be larger than 2×10^{-7} , indicating that the calculation process was unreliable and inaccurate [54]. This is because the Judd-Ofelt coefficient calculations required the assumptions that [59, 61, 62]

- the wave functions $|j\rangle$ are completely degenerate/separate in J (total degeneracy is equal to $2J+1$).
- the energy during the process is constant (energy conservation law)
- all energy states within the ground level manifolds are equally populated
- the host material is optically isotropic

From these assumptions, the discrepancies of the calculated Judd-Ofelt coefficient can originate from

- mixing in J states
- linear and non-linear shielding of the electron from the electrostatic crystalline electric field as a result of the distortion of the closed 5s and 5p shell outside the 4f shell by the lattice charges
- relativistic effects

- effects of electron correlation

Besides that, the large σ_{RMS} also originates from the absorption measurement and unaccounted magnetic dipole transitions of Bi-EDF because bismuth is well known as a diamagnetic element. It is also further supposed to originate from large error absorption measurements due to overlapping transitions of the ground level with the combination of the least-square fitting process making calculations of the coefficient inaccurate [56,61,62].

3.4 McCumber Cross Section Analysis

The McCumber theory [62] is a simple and straightforward yet accurate reciprocal method to designate the rare earth optical absorption or emission cross sections [62, 63, 64]. The fundamentals of this calculation are based on the generalization of the original Einstein's A and B coefficients that is applied to the broadband transitions between the Stark manifolds. The McCumber theory is temperature dependent and defines the absorption and emission cross-section as

$$\sigma_{\text{em}}(\nu) = \sigma_{\text{ab}}(\nu) \exp\left(-\frac{h(\nu - \epsilon)}{k_B T}\right), \quad (3.10)$$

where $\sigma_{(\text{em,ab})}$ is the emission and absorption cross section and $h\epsilon$ is the net thermodynamical free energy required to move one rare earth ion from the ground state to an excited state, while maintaining the lattice temperature T constant [1,62]. This expression was simplified by assuming an average energy separation δE_{ij} between Stark manifolds of ground state E_{1j} and excited state E_{2j} where

$$\exp\left(\frac{\varepsilon}{k_B T}\right) = \frac{\sum_{j=1}^j \exp\left(-\frac{E_{1j}}{k_B T}\right)}{\sum_{j=1}^j \exp\left(-\frac{E_{2j}}{k_B T}\right)} \exp\left(\frac{\delta E}{k_B T}\right) \quad (3.11)$$

$$= K \exp\left(\frac{\delta E}{k_B T}\right) \quad . \quad (3.12)$$

Here, the partial derivatives are the chemical potentials corresponding to the subgroups of ground state ions, population N_1 , and excited state ions, population N_2 [1] therefore, we can rewrite Eq. 3.10 to become

$$\sigma_{em}(\lambda) = \sigma_{ab}(\lambda) \exp\left[-\frac{hc}{k_B T} \left(\frac{1}{\lambda} - \frac{1}{\lambda^*}\right)\right] \quad , \quad (3.13)$$

where

$$\varepsilon = \frac{c}{\lambda^*} \quad , \quad (3.14)$$

here λ^* is the wavelength at which the absorption and emission cross sections are equal. In particular, the emission and absorption cross section ratio η is given by

$$\eta = \frac{\sigma_{em}(\lambda)}{\sigma_{ab}(\lambda)} \quad . \quad (3.15)$$

The calculated emission cross section from the measured absorption spectrum of Bi-EDF using the McCumber theory is given in Figure 3.14. It also shows the measured emission cross section of silica host for comparison purposes. From the fluorescence emission measurement, the peak cross-section was $7.58 \times 10^{-25} \text{ m}^2$ at a wavelength of 1533 nm. The calculated emission cross section reveals good agreement with the measured value at peak emission wavelength. The calculated shape of spectrum also fits well with the measured one. The calculated McCumber

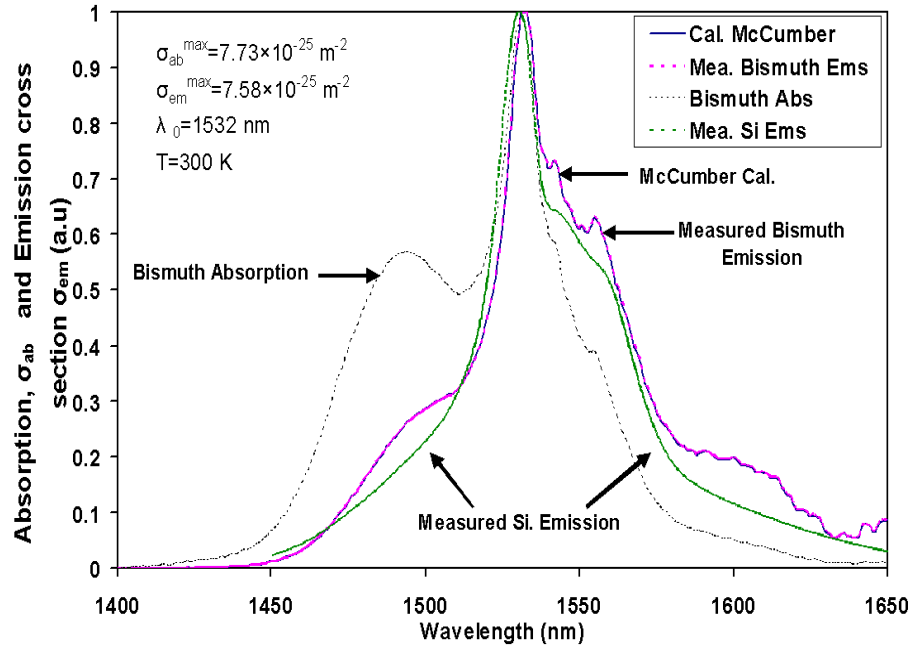


Figure 3.14 Experimental and calculated absorption and emission cross sections of Er^{3+} ions $^4\text{I}_{13/2}$ transition Bi-EDF.

emission cross-section indicates that under room temperature, the degeneracy of the excited $^4\text{I}_{13/2}$ and ground $^4\text{I}_{15/2}$ energy states due to the Stark effect are small therefore, producing a better populated energy state manifold according to Boltzmann temperature distribution.

Previously, the McCumber theory was well known with its limitation of overestimating the peak emission cross-section and distorted emission spectrum (especially in the S and L bands) due to underestimation of the Stark manifold of the excited $^4\text{I}_{15/2}$ and overestimation of the ground $^4\text{I}_{13/2}$ state [2]. The Stark manifold is very dependent on the glass host ligand field and composition, so it is difficult to measure accurately [65]. To further investigate the accuracy of the McCumber cross-section calculation, the difference between calculation and measured cross-section is elucidated in Figure 3.15. There are small differences between the calculated and

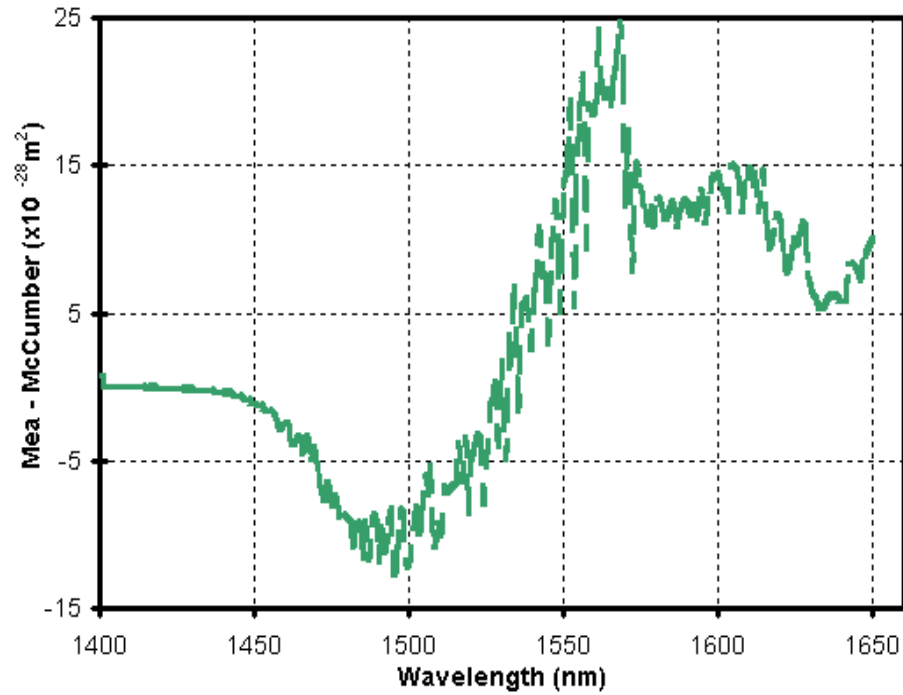


Figure 3.15 The difference between measured and calculated emission cross-section in Bi-EDF as a function of wavelength

measured emission cross-sections at shorter (1450 – 1530 nm) and longer (1530 – 1650 nm) region from the peak of the cross-section 1533 nm. The differences between both data is more centralised at the peak compared to at both the ends. The maximum deviation of the emission cross-section is found at 1568 nm of $+2.5 \times 10^{-29} \text{ m}^2$. At this region the emission spectra is more distorted compared to the short wavelength region as presented in Figure 3.15 and produces a larger difference to the calculated McCumber cross-section. This distortion is expected to originate from a lower ESA absorption cross-section effect that increases the long wavelength fluorescence intensity. Compared to silica-based glass, the bismuth-based glass has lower ESA absorption cross-section that is useful for new DWDM signal amplification.

The ratio of peak emission to the peak absorption cross-section (η^{peak}) is an important parameter for comparison of $\sigma_{\text{em,ab}}(\lambda)$ values. This comparison factor defines the absorption and emission cross-sections as a simple mathematical function that only relatively depends on the Stark manifold and the lattice temperature as stated in Eq. 3.15. From Figure 3.16, the η^{peak} of the calculated values (1533 nm) are found to vary by about -0.00018 from the measured cross-section of 1.0206. This small variation indicates that the measured and McCumber calculated absorption and emission cross-sections of Bi-EDF have good correlation. The uniformity of the spectral line shapes are mainly due to low Stark level degeneracy within the Boltzmann temperature distribution constant as the Er^{3+} ions are shielded by the 5d and 6s shell from the outside force.

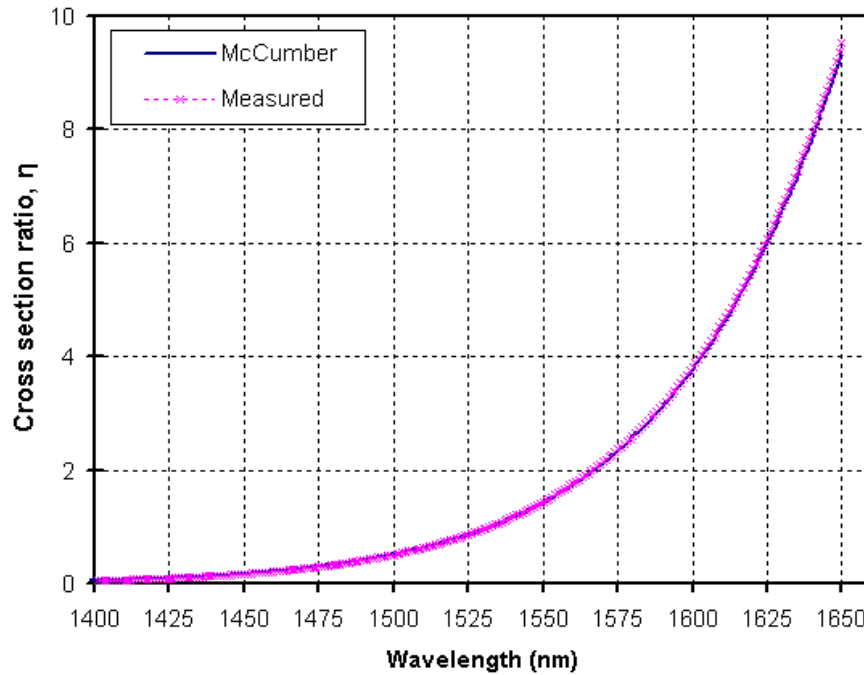


Figure 3.16 Measured and calculated McCumber cross-section ratio η of Bi-EDF

3.5 1550 nm Transition Lifetime

The lifetime of fluorescence emitted from the optical transition of Er^{3+} ions is an essential parameter to specify the efficiency of optical amplifiers and the characteristic of the glass host local environment [1-3]. For an efficient optical amplifier, the lifetime of the metastable state must be long enough in order to produce high population inversion. Lasers or optical amplifiers that have high population inversion are capable of maintaining a steady-state condition with moderate pump power [1,13]. By using rate equation of Eq. 2.8 to 2.10, and Eq. 3.1 again, the lifetime τ ($=1/W_2$) of an Er^{3+} ion is defined as

$$\tau = \frac{1}{W_2} = \frac{1}{{}^R W_{21}} + \frac{1}{{}^{\text{NR}} W_{21}} \quad , \quad (3.16)$$

where ${}^R W_{21}$ is the radiative decay rate and ${}^{\text{NR}} W_{21}$ is the nonradiative decay rate from the metastable state ${}^4\text{I}_{13/2}$ to the ground state ${}^4\text{I}_{15/2}$. Using the same Einstein relation between spontaneous and stimulated emission of Er^{3+} Stark level and the radiative transition oscillator strength in the glass, the lifetime can be calculated by [62,66]

$$\tau_0 = 1.51 \frac{g^2}{g^1} \frac{\lambda^2}{f_{\text{osc}} n^2 \chi} \quad , \quad (3.17)$$

where λ is the average transition wavelength, n the glass index of refraction, f_{osc} is the oscillator strength of transition, $g_{1,2}$ the statistical weights of the excited and ground state and χ is the ligand field correlation,

$$\chi = \frac{(n^2 + 2)^2}{9n} \quad (3.18)$$

These calculations requires an assumption [62] similar to section 3.3.1 to satisfy that can causes a discrepancy with measured lifetimes. From calculations, the Er^{3+} ion lifetime is found to be 5.45 ms.

Lifetime measurements are obtained using the time-resolved spectroscopy techniques, in which the optical amplifiers are pumped by a pulsed laser diode and the time decay of the fluorescence is measured. This technique requires that the excitation pulse width must be shorter than the lifetime, i.e. illustrated by Figure. 3.17.

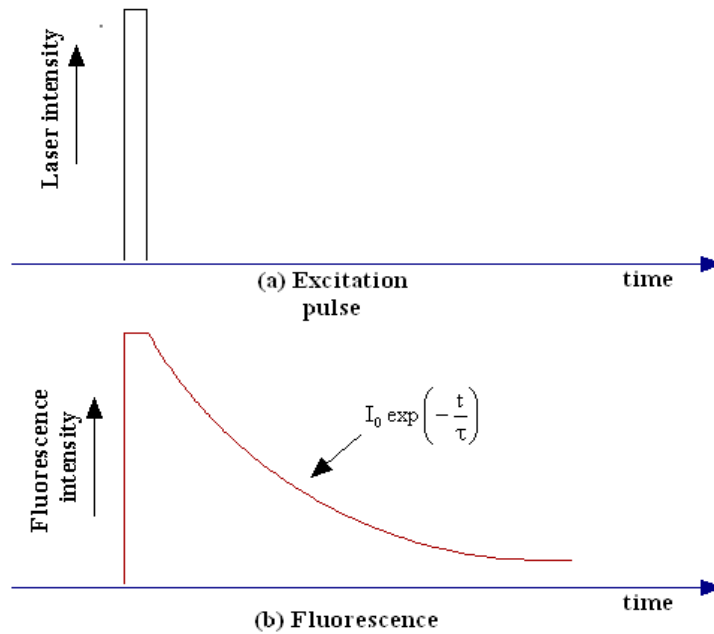


Figure 3.17 Determination of lifetime using a pulsed laser and time resolved measurements. (a) A narrow excitation pulse and (b) the time decay of the resulting fluorescence.

As specified in Figure. 3.17, the fluorescence decaying process is single-exponential function defined as,

$$I(t) = I_0 \exp\left(-\frac{t}{\tau}\right), \quad (3.19)$$

where I is the fluorescence intensity after a time t following the laser excitation. The

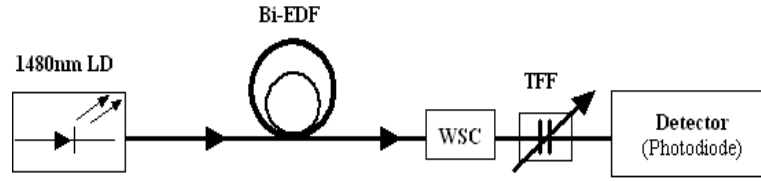


Figure 3.18 Experimental set-up for lifetime measurement. The Wavelength Selective Coupler (WSC) and the thin-film filter (TFF) is use to filter out the 1530 nm emission from the 1480 nm laser diode (LD).

lifetime is obtained by line fitting. The experimental set-up for lifetime measurement is depicted in Figure 3.18. The 1480 nm laser diode was pulse modulated by square wave at 70Hz with 7% duty cycle for pulse width of 1ms using Stanford Research System Inc, DG535 Pulse generator. This pulse width was fixed to be shorter compared to the total Er^{3+} ion decay time. The excitation power of the 1480 nm laser diode was set at 144 mW and the fibre is spliced with Bi-EDF.

The fluorescence decay spectra is detected by a HP DC-6 GHz 83440B photodiode that is connected to HP54510A 250 MHz digital oscilloscope. The decay curve is then transferred to a PC using a GPIB cable for further curve fitting analysis.

The decay curve of an Er^{3+} ion at 1530 nm of the Bi-EDF is demonstrated in Fig. 3.19. The decay curve is fitted with single-exponential decay function as outlined by the solid red line. From the fitting line, the lifetime was found to be about 2.84 ms, which is somewhat close to the result measured by Yang *et. al.* [13] and Hayashi *et. al.* [67] but much more shorter when compared to the lifetime of an Er^{3+} ion (from the calculation using Eq. 3.17) and also with conventional silica host glass [1]. The short lifetime is due to the high Bi_2O_3 content in the Bi-EDF that lowers the glass host phonon energy as explained by Oprea *et. al* [55]. Glass hosts with low phonon energy has an efficient pump photon energy transfer process that produces

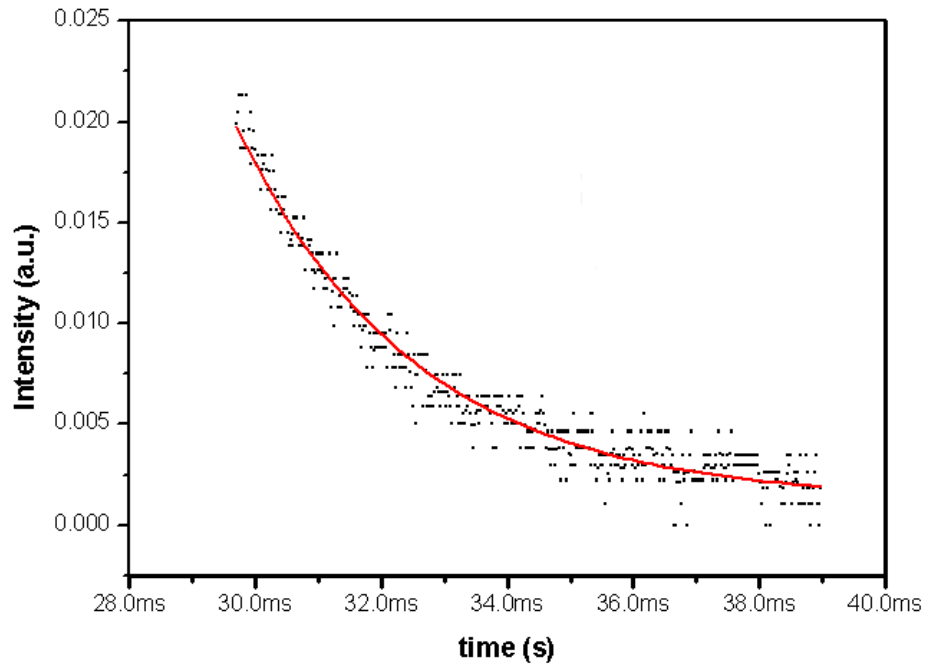


Figure 3.19 Measured 1550 nm lifetime of Bi-EDF. (Solid lines indicate fitting to the data)

the upconversion of visible fluorescence.

Besides that, glass host local environment irregularity by the high Er^{3+} ions concentration also reduces the lifetime of Er^{3+} ions as reported by Shinxun Dai *et. al.* and Auzel *et. al.* [68,69] due to radiation self-quenching that is also known as the radiation trapping effect. The radiation trapping effect is a cross-relaxation and cooperative frequency upconversion process [70,71] (mentioned in section. 2.2.2) that converts the pump photons to heat via phonon and multiphonon processes and visible light. This radiation trapping effect also depends on the glass host refractive index [72] where high refractive index glass hosts tend to increase the stimulated emission efficiency and as a result, reducing the lifetime of the $^4\text{I}_{13/2}$ metastable state.

The quantum efficiency (QE) and nonradiative decay ^{NR}W of the $^4I_{13/2} \rightarrow ^4I_{15/2}$ transition can be evaluated using emission probability from the Judd-Ofelt theory and Eq. 3.16 by

$$QE = \frac{\tau_{mea}}{\tau_{rad}} \quad . \quad (3.20)$$

The lifetime calculated using the Judd-Ofelt theory is found to be 4.51 ms, which is lower than the value calculated using Einstein's coefficients. From this calculation, the QE and ^{NR}W of Bi-EDF was found to be 63.0 % and 130.3 s⁻¹ respectively. for this reason, obviously the high Bi₂O₃ content increases the nonradiative lifetime and decreases both the radiative and measured lifetime and as a consequence reduces the quantum efficiency [12]. As explained by Oprea *et. al* [55], glass hosts with low phonon energy glass wastes more pump photons to vibrational energy subsequently, less pump energy can be transferred to the signal. This also indicates that a glass host with low phonon energy such as bismuth glass ($\approx 500 \text{ cm}^{-1}$) is a moderate signal efficiency optical amplifier with wider fluorescence bandwidth [4,16] by using the mixed former effect [13] fabrication technique.

3.6 Upconversion Fluorescence

The behaviour of Er³⁺ fluorescence from the energy transfer of dense and closely distributed ions in a glass host can simply be explained as upconversion fluorescence as discussed in section. 2.2.2. This upconversion have been identified as the major reason for low radiative emissions at the 1.5 μm region [1, 69] thus,

reducing the quantum efficiency of high Er^{3+} ion concentration optical amplifiers [1, 73-75]. The evaluation of upconversion characteristics was intensively studied by P. Blixt *et. al.* [73, 75] and E. Snoeks *et. al.* [76] using rate equations of a two level system (from Eq. 2.8, 2.9 and 2.10) for a 1.48 μm pumping system

$$\frac{dN_2}{dt} = S_{12}(1 - N_2) - S_{21}N_2 - W_{21}N_2 - C_{\text{CU}}N_2^2, \quad (3.21)$$

where, W_{21} is the radiative decay rate and C_{CU} is the cooperative upconversion coefficient, respectively. Using Eq. 3.16 and lifetime measurement, where in the case the laser diode is turned off, and then Eq. 3.21 can be simplified as

$$\frac{dN_2}{dt} = -\frac{N_2}{\tau} = -C_{\text{CU}}N_2^2. \quad (3.22)$$

The C_{CU} coefficient can be estimated by fitting of this function to the lifetime decay curve. Table 3.5 presents the calculated C_{CU} coefficient for bismuth host glass.

Table 3.5 Cooperative upconversion coefficients for bismuth host glass with comparison with other works

Er concentration (wt. ppm)	C_{CU} coefficient ($\times 10^{-24} \text{ m}^3/\text{s}$)
3250	4.63
3250 (La/B co-doped Bismuth-borate glass [77])	1.96

From the table, the C_{CU} coefficient was found to be higher when compared with bismuth-borate glass. From H. Hayashi *et. al.* [77], the 1550 nm lifetime largely depends on glass phonon energy, whereby as described in their work, by adding B_2O_3 (which has larger phonon energy (1400 cm^{-1})) reduces the energy loss to glass phonons and as a consequence, suppresses the C_{CU} coefficient of the Er^{3+} ions. Hence, the gain improvement at 1550 nm is expected with addition of high phonon

energy material during bismuth host glass fabrication.

The upconversion fluorescence measurement was performed by using a set-up as illustrated in Figure 3.9. The light source is replaced with two 1480 nm laser diodes with a total pump power of 288 mW and coupled bi-directionally using a 1480 nm wavelength-selective coupler (WSC). The fluorescence emitted by the Bi-EDF was detected transversely with a 25 cm Czerney-Turner monochromator which has a 2048-elements linear Photodiode Charge Coupled Device (PCCD) from Alton Instrument Corp that is connected to a computer. In order to increase the accuracy of the measurement, spectra resolution is fixed to 0.06 nm with maximum data points of 12,288 points.

The normalized emission spectra of Bi-EDF between 400 nm and 1100 nm under 1480 nm excitation is displayed in Figure. 3.20. The spectrum displays 7 peak

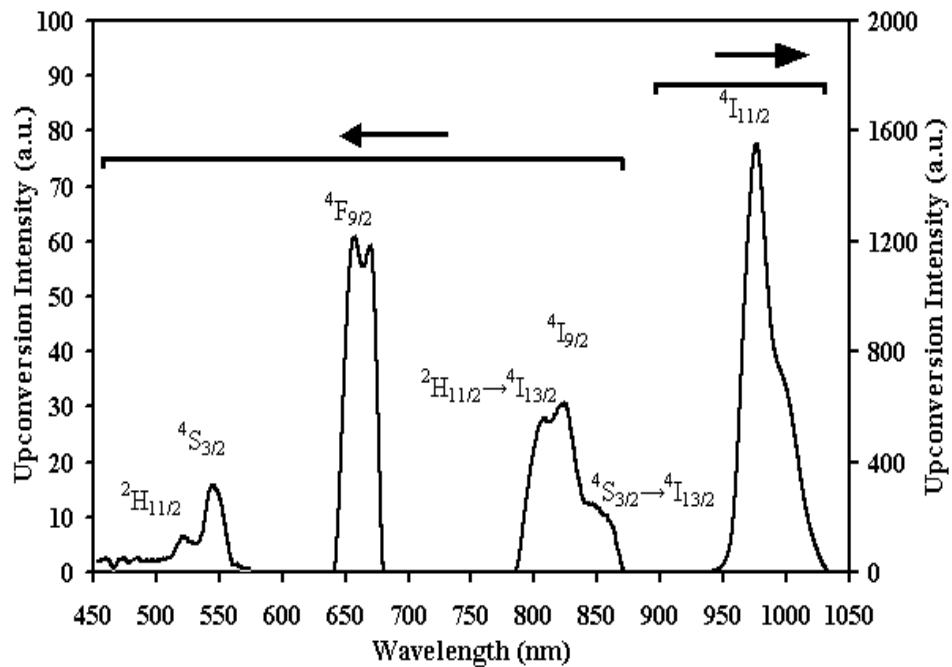


Figure 3.20 Measured upconversion fluorescence spectra of Bi-EDF under 1480 nm LD excitation

emissions centred at 521 nm, 544 nm, 658 nm, 807 nm, 825 nm, 847 nm and 976 nm. These corresponding peaks can be assigned to electronic transitions $^2H_{11/2}$, $^4S_{3/2}$, $^4F_{9/2}$ and $^4I_{11/2}$ of the Erbium ions. The most intense upconversion was detected at 975.481 nm with a FWHM of 27.1 nm which is 25 times higher compared with other upconversion emission. The intensity of the upconversion emission at 521 nm and 544 nm which is at the visible green range, are the highest energy states with a FWHM of 17.5 nm. Here, the emission originates from radiative transition of $^2H_{11/2}$ to $^4I_{15/2}$ states and $^4S_{3/2}$ to $^4I_{15/2}$.

In order to determine the responsible upconversion mechanisms, the upconversion intensity of 975 nm peaks was measured as a function of the 1480 nm pump power as shown in Fig. 3.21 (a). The intensity of the 975 nm fluorescence increases as the 1480 nm laser diode pump increases with an average slope of 2.18 ± 0.04 , approximately equalling the results obtained by P. Blixt *et. al.* [73] (slope = 2.2 ± 0.3) on normal Si_2O/Ge_2O fibre. From the figure, it is seen that the slope is higher; 2.50 at low pump power and reducing to 1.86 as the incident pump power is increased to 100 mW. Using this result and Eq. 3.21, the 975 nm upconversion mechanism can be explained using a combination of a two-particle upconversion model [73,75] and ESA [77]. It is also found that the efficiency of the upconversion process in Bi-EDF is lower compared to normal silica fibre because the Er^{3+} ion concentration of Bi-EDF was 3.8 times higher and more dispersed and as a result, yielding less concentration quenching effects.

From the result, it is believed that the upconversion process in Bi-EDF is due to the cross relaxation mechanism [77] between two Er^{3+} ions at the excited state

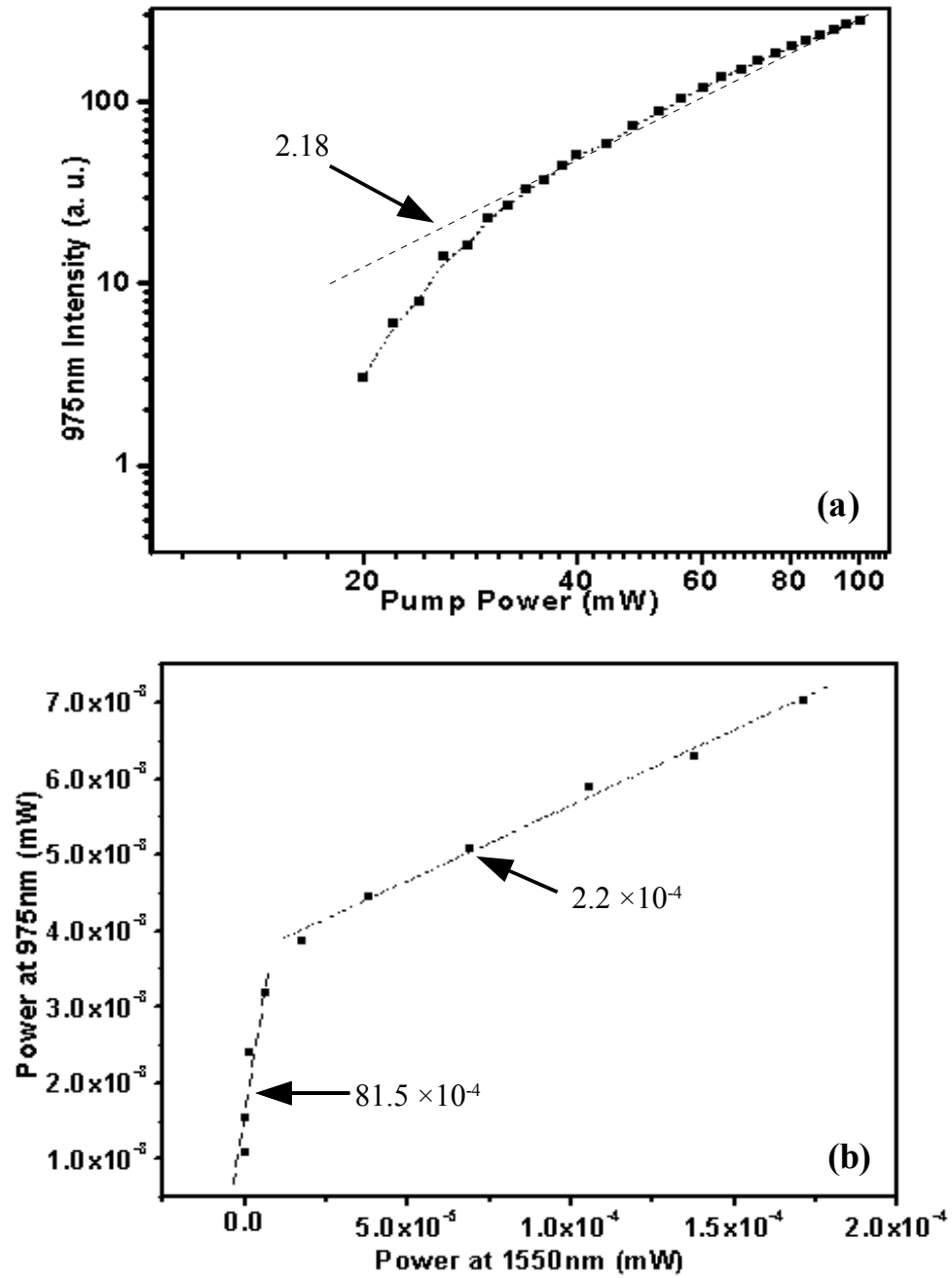


Figure 3.21 (a) The upconversion fluorescence at 975 nm versus 1480 nm pump power and (b) fluorescence power at 980 nm versus power at 1550 nm. The number in figure (a) and (b) denote the slope values at low and high pump power, respectively.

$^4I_{13/2}$ as the intensity at 975 nm is very dependent on the launched power of the 1480 nm laser diode. This is depicted in Fig. 3.21 (b). As the power of 1480 nm pump increases, the gradient of the graph also increases (≈ 4.0 , which is about twice the gradient at low pump power). This phenomenon can be explained as cross relaxation since the intensity of the 975 nm did not increase as observed at low pump power.

3.7 Optical Amplifier Figure-of-merit (FOM)

The figure of merit of optical amplifiers was introduced to characterise a standard parameter for amplification bandwidth and high output power / gain for optical telecommunication networks. The merit values are calculated using emission cross-section σ_{em} , lifetime τ and FWHM of the optical amplifiers [79-81]. The bandwidth FOM of optical amplifiers is calculated by the product of peak of stimulated emission cross-section and FWHM, while the gain FOM is a product of the peak of stimulated emission cross-section and emission lifetime.

$$\text{Bandwidth } FOM = \sigma_{em} \times FWHM , \quad (3.23)$$

$$\text{Gain } FOM = \sigma_{em} \times \tau_{1550} . \quad (3.24)$$

From the said calculation, the higher the FOM values, the better the bandwidth and gain properties of the optical amplifiers. Table 3.6 list the peak stimulated emission cross-section, FOM bandwidth and gain in various glass hosts for comparison. From the table, the tellurite and phosphate glass host has high peak emission compatible with bismuth glass host. However from the table it is clear that the FOM of bismuth host glass is better than other glass hosts. Consequently,

bismuth glass host is the most potential host material for developing broadband optical amplifiers for potential use in DWDM communication networks.

Table 3.6 FOM of various glass host for optical amplifiers

Host glass	Peak σ_{em} [10^{-25} m²)]	Bandwidth FOM [$\times 10^{-28}$ (s·m²)]	Gain FOM [$\times 10^{-25}$ (nm·m²)]
Bismuth	7.58	606.40	21.53
Silicate (Fibercore)	0.436	17.44	4.36
Tellurite [79]	7.50	487.5	15.0
Phosphate [82]	6.40	236.8	17.92

The important parameters of the physical and optical properties of Bi-EDF have been discussed in this chapter. The characterisation of the optical amplifier of the Bi-EDF that will be the most critical parameter in long-haul, high power optical system networks will be continued in the next chapter.

REFERENCES

- [1] E. Desurvire, “*Erbium-doped fiber amplifiers: Principle and Application*,” John Wiley & Son Inc., New York, 1994.
- [2] S. Tanabe, T. Hanada, “*Local structure and 1.5 μ m quantum efficiency of erbium doped glasses for optical amplifiers*”, J. Non-Cryst. Solids, Vol. 196, 1996, pp. 101
- [3] S. Tanabe, “*Optical transitions of rare earth ions for amplifiers: How the local structure works in glass*”, J. Non-Cryst. Solids, Vol. 259, 1999, pp. 1
- [4] D. R. Zimmerman, L. H. Spiekman, “*Amplifiers for the masses: EDFA, EDWA, SOA amplets for metro and access application*”, J. Lightwave Tech., Vol. 22, No. 1., 2004, pp. 63-70
- [5] J. N. Sandoe, P. H. Sarkies, S. Parke, “*Variation of Er^{3+} cross section for the stimulated emission with glass composition*”, J. Phys. D: Appl. Phys., Vol. 5, 1972, pp. 1788
- [6] D. Barbier, “*The present and future of EDWA technology*”, Optical Fiber Communication Conference and Exhibit, (OFC 2002), 2002, pp. 11
- [7] N. Antoniadis, N. Menon, N. Chbouki, “*Techno-economic value analysis of the role of banded amplification in evolving WDM metro network architectures*”, The 17th Annual Meeting of the IEEE Lasers and Electro-Optics Society, LEOS 2004, Vol 2, 2004, pp. 7
- [8] W. H. Zachariasen, “*The atomic arrangement in glass*”, J. Am. Chem. Soc., Vol. 54, pp. 3842-3851, 1932
- [9] Andreas Moller, Stephan Weinbruch, Frank J. Stadermann, Hugo M. Ortner,

- Klaus Neubeck, Adam G. Balogh, Horst Hahn, “*Accuracy of film thickness determination in electron probe microanalysis*”, Mikrochim. Acta, Vol. 119, 1995, pp. 41-47
- [10] S. Tanabe, N. Sugimoto, S. Ito, and T. Hanada, “*Broadband 1.5 μm emission of Er^{3+} ions in bismuth-based oxide glasses for a potential WDM amplifier*”, Jour. Lumin, Vol. 87-89, 2000, pp. 670
- [11] Y. Kuroiwa, N. Sugimoto, K. Ochiai, S. Ohara, Y. Fukasawa, S. Ito, S. Tanabe, T. Hanada, “*Fusion spliceable and high efficient Bi_2O_3 -based EDF for short-length and broad-band application pumped at 1480 nm*”, Optical Fiber Communication Conference (OFC 2001), 2001 OSA Technical Digest Series (Optical Society of America, 2001), pp. Tu15
- [12] Jianhu Yang, Shixun Dai, nengli Dai, Shiqing Xu, Lei Wen, Lili Hu, Zhonghong Jiang, “*Effect of Bi_2O_3 on the spectroscopic properties of erbium-doped bismuth silicate glasses*”, J. Opt. Soc. Am. B., Vol. 20, No. 5, 2003, pp. 810
- [13] Jianhu Yang, Dai Shi-Xun, Wen Lei, Liu Zhu-Ping, Hu Li-Li, Jiang Zhong-Hong, “*Mixed former effect: A kind of composition adjusting method of Er-doped glass for broadband amplification*”, Chi. Phys. Lett., Vol. 19, No. 10, 2002, pp. 1516
- [14] Zhou, Y.-X., Zhou, L., Chen, F., “*Compositional dependence of spectroscopic properties for a erbium-doped bismuth-based glass*”, Guangzi Xuebao/Acta Photonica Sinica, Vol. 36, 2007, pp. 177
- [15] Isabella-Ioana Oprea, Hartmut Hesse, Klaus Betzler, “*Luminescence of*

- erbium-doped bismuth-borate glasses*”, Jour. Opt. Mater., Vol 28, 2006, pp. 1136
- [16] Stewart E. Miller, Alan G. Chynoweth, “*Optical Fiber Telecommunication*”, Academic Press, Inc., 1979
- [17] Isabella-Ioana Oprea, Hartmut Hesse, Klaus Betzler, “*Optical properties of bismuth borate glasses*”, Jour. Opt. Mater., Vol. 26, 2004, pp. 235
- [18] E. T. Y. Lee, E.R. M. Taylor, “*Thermo-optic coefficients of potassium alumino-metaphosphate glasses*”, J. of Phy. And Chem. Of Solids, Vol. 65, pp. 1187-1192, 2004.
- [19] Jacqueline Johnson, Richard Weber, Marcos Grimsditch, “*Thermal and mechanical probabilities of rare earth aluminate and low-silica aluminosilicate optical glasses*”, Jour. Non-Cryst. Solid, Vol. 351, 2005, pp. 650-655
- [20] R. Reisfeld, Y. Eckstein, “*Dependence of spontaneous emission and nonradiative relaxations of Tm^{3+} and Er^{3+} on glass host and temperature*”, Jour. of Chem. Phys, Vol. 63, No. 9, 1975, pp. 4001
- [21] L. Petit, T. Cardinal, J.J. Videau, G. L. Flem, Y. Guyot, G. Boulon, M. Couzi, T. Buffeteau, “*Effect of the introduction of $Na_2B_4O_7$ on erbium luminescence in tellurite glasses*”, J. Non-Cryst. Solids, Vol. 298, 2002, pp. 76
- [22] S. Q. Man, R. S. F. Wong, E. Y. B. Pun, P. S. Chung, “*Frequency upconversion in Er^{3+} doped alkali bismuth gallate glasses*”, IEEE 12th annual Meeting of Lasers and Electro-optics Society 1999, (LEOS 1999), Vol. 2,

1999, pp. 812-813

- [23] Poole, S. B. “*Fabrication of Al_2O_3 co-doped optical fibres by a solution-doping technique*”, Fourteenth European Conference on optical Communication (ECOC 1988), Conf. Publ. No. 292, Vol. 1, 1988, pp. 433-436
- [24] B. J. Ainslie, J. R. Armitage, S. P. Craig, B. Wakefield, “*Fabrication and optimisation of the erbium distribution in silica based doped fibres*”, Fourteenth European Conference on Optical Communication, ECOC 1988, Conf. Publ. No. 292, Vol. 1, 1988, pp. 62-65
- [25] W. J. Miniscalco, “*Erbium-doped glasses for fiber amplifiers at 1500 nm*”, Jour. Lightwave Technol., Vol. 9, No. 2, 1991, pp. 234
- [26] Georges T., Delevaque E., Monerie M., Lamouler P. Bayon J. F. “*Pair induced quenching in erbium doped silicate fibers*,” IEEE Optical Amplifiers and their applications, Technical Digest, Vol. 17, 1992, pp. 71
- [27] H. Hayashi, S. Ohara, N. Sugimoto, S. Tanabe, “*Effects of lanthanum and boron addition on suppression of cooperative upconversion in bismuth oxide-based erbium-doped fibers*”, Japanese Journal of Applied Physics, Vol. 46, No. 6A, 2007, pp. 3452
- [28] B. J. Ainslie, “*A review of the fabrication and properties of erbium-doped fibers for optical amplifiers*”, Jour. Lightwave Technol., Vol. 9, No. 2, 1991, pp. 220
- [29] S. P. Craig-Ryan, J. F. Massicott, M. Wilson, B. J. Ainslie, R. Wyatt, “*Optical study of low concentration Er^{3+} fibres for efficient power amplifiers*”,

- European Conference on optical Communication (ECOC 1990), Vol. 1, 1990, pp. 571
- [30] Keiichi Aiso, Yoshio Tashiro, Tsuneo Suzuki, Takeshi Yagi, “*Erbium lanthanum co-doped fiber for L-band amplifier with high efficiency, low non-linearity and low NF*”, Optical Fiber Communication Conference and Exhibition, OFC 2001, Vol. 2, 2001, pp. TuA6-1
- [31] M. Nakazawa, Y. Kimura, “*Lanthanum co-doped erbium fibre amplifier*”, Electronics Lett., Vol. 27, No. 12, 1991, pp. 1065
- [32] H. Hayashi, S. Ohara, N. Sugimoto, S. Tanabe, “*Effects of Lanthanum and Boron Addition on suppression of cooperative upconversion in Bismuth Oxide-based erbium-doped fibers*”, Japanese Journal of Applied Physics, Vol 46, No. 6A, 2007, pp. 3452
- [33] T. M. Kwok, A. A. Pau, R. A. Betts, F. F. Ruhl, G. F. Zheng, “*Fabrication and characterisation of rare earth doped optical fibre*”, IEEE Region10 Conference on Computer and Communication Systems, 1990, pp. 104
- [34] G. R. Atkins, S. B. Poole, M. G. Sceats, H. W. Simmons, C. E. Nockolds, “*The influence of codopant and fabrication conditions on germanium defects in optical fiber preforms*”, IEEE. Photonics. Technol. Lett., Vol.4, No. 1.,1992, pp. 43
- [35] M. Monerie, T. Georges, P. L. Francois, J. Y. Allain, D. Neveux, “*Ground-state and excited-state absorption in rare-earth doped optical fibres*”, IEE Electro. Lett., Vol. 26, No. 5, 1990, pp. 320
- [36] S. Tanabe, T. Ohyagi, N. Soga, T. Hanada, “*Compositional dependence of*

- Judd-Ofelt parameters of Er^{3+} ions in alkali-metal borate glasses*", Phys. Rev. B., Vol. 46, No. 6, 1992, pp. 3305
- [37] A. D. McNaught, A. Wilkinson, "*The Gold Book, IUPAC Compendium of Chemical Terminology*", 2nd Edition, Blackwell Science, 1997
- [38] S. Sakaguchi, "*Consolidation of silica glass soot body prepared by flame hydrolysis reaction*", Jour. Non-Cryst. Solids, Vol. 171, 1994, pp. 249
- [39] D. Marcuse, "*Loss analysis of single-mode fiber splices*", The Bell System Technical Journal, Vol. 56, No. 5, 1977, pp. 703
- [40] S. Ohara, N. Sugimoto, K. Ochiai, H. Hayashi, Y. Fukasawa, T. Hirose, M. Reyes, "*Extra-broadband and highly efficient short length Bi_2O_3 -based EDF*", Optical Fiber Communication Conference and Exhibit, (OFC 2003), Vol. 2, 2003, pp. 635
- [41] K. Patek, "*Glass Lasers*", CRC Press, Butterworth, London, 1970
- [42] A. Mori, T. Sakamoto, K. Kobayashi, K. Shikano, K. Oikawa, K. Hoshino, T. Kanamori, Y. Ohishi, M. Shimizu, "*1.58 μm broad-band erbium-doped tellurite fiber amplifier*", J. Lightwave Technol., Vol. 20, No. 5, 2002, pp. 822
- [43] B. R. Judd, "*Optical absorption intensities of rare earth ions*" Phys. Rev., Vol. 127, 1962, pp. 750
- [44] G. S. Ofelt, "*Intensities of crystal spectra of rare earth ions*", J. Chem. Phys., Vol. 37, 1962, pp. 511
- [45] Guokui Liu, Bernard Jacquier, "*Spectroscopic properties of rare earths in optical material*", Springer Series in Material Science, 83, Tsinghua University Press and Springer -Verlag Berlin Heidelberg, 2005

- [46] M. J. Weber, "Spontaneous Emission Probabilities and Quantum efficiencies for Excited States of Pr^{3+} in LaF_3 ", J. Chem. Phys., Vol. 48, 1964, pp 4774
- [47] M. J. Weber, "Probabilities for radiative and nonradiative decay of Er^{3+} in LaF_3 ", Phys. Rev., Vol. 157, No. 2, 1967, pp. 262
- [48] W. T. Carnal, P. R. Fields, and K. Rajnak, "Electronic Energy Levels in the Trivalent Lanthanide Aquo Ions I. Pr^{3+} , Nd^{3+} , Pm^{3+} , Sm^{3+} , Dy^{3+} , Ho^{3+} , Er^{3+} and Tm^{3+} ", J. Chem. Phys., Vol. 49, No. 10, 1968, pp 4424
- [49] W. T. Carnall, Jan. P. Hessler, H. R. Hoekstra, C. W. Williams, "The absorption spectra and excited state relaxation properties of lanthanide and actinide halide vapor complexes. I. $\text{ErCl}_3(\text{AlCl}_3)_x$ ", J. Chem. Phys., Vol. 68, No. 9, 1978, pp. 4304
- [50] W. T. Carnall, G. L. Goodman, K. Rajnak, R. S. Rana, "A systematic analysis of the spectra of the lanthanides doped into single crystal LaF_3 ", J. Chem. Phys., Vol 90, No. 7, 1989, pp. 3443
- [51] C. Gorller-Walrand, L. Fluyt, A. Ceulemans, "Magnetic dipole transitions as standards for Judd-Ofelt parametrization lanthanide spectra", J. Chem Phys. Vol. 95, No. 5, 1991, pp. 3099
- [52] W. T. Carnall, G. L. Goodman, K. Rajnak and R. S. Rana, "A systematic analysis of the spectra of the lanthanides doped into single crystal LaF_3 ", J. Chem. Phys. Vol. 90, No. 8, 1989, pp. 3443
- [53] W. F. Krupke, "Radiative transition probabilities within the $4f^8$ ground configuration of Nd:YAG ", IEEE J. Quantum Electron, Vol. 7, No. 4, 1971,

pp.153

- [54] H. Lin, S. Tanabe, L. Lin, Y. Y. Hou, K. Liu, D. L. Yang, T. C. Ma, J. Y. Yu, E. Y. B. Pun, “*Near-infrared emissions with widely different widths in two kinds of Er^{3+} -doped oxide glasses with high refractive indices and low phonon energies*”, Jour. Lumin, Vol. 124, 2007, pp. 167
- [55] Isabella-Ioana Oprea, Hartmut Hesse, Klaus Betzler, “*Luminescence of erbium-doped bismuth-borate glasses*”, Jour. Opt. Mater., Vol. 28, 2005, pp. 1136
- [56] S. Tanabe, T. Ohyagi, S. Todoroki, T. Hanada, N. Soga, “*Relation between the Ω_6 intensity parameter of Er^{3+} ions and the ^{151}Eu isomer shift in oxide glasses*”, J. Appl. Phys., Vol. 73, No. 12, 1993, pp. 8451
- [57] W. T. Carnall, Jan P. Hessler, H. R. Hoekstra, C. W. Williams, “*The absorption spectra and excited state relaxation properties of lanthanide and actinide halide vapor*”, J. Chem. Phys. Vol. 68, No. 9, 1978, pp. 4303
- [58] K. Naito, Y. Benino, T. Fujiwara, T. Komatsu, “*Judd-Ofelt parameters of Er^{3+} in transparent TeO_2 -based nanocrystallized glasses*”, Jour. Solid State. Comm., Vol. 131, 2004, pp. 289
- [59] Gorller-Walrand C, Binnemans K, “*Spectral intensities of f-f transitions: Handbook on the Physics and Chemistry of rare earths*”, Elsevier Science B. V. Amsterdam: North-Holland), Vol. 25, Chap. 167, 1998, pp. 101
- [60] M. J. Weber, R. A. Saroyan, R. C. Ropp, “*Optical properties of Nd^{3+} in metaphosphate glasses*”, Jour. Non-Cryst. Solids, Vol. 44, Issue 1, 1981, pp. 137

- [61] Brian M. Walsh, “*Advance in spectroscopy for lasers and sensing; Judd-Ofelt theory: Principles and practices*”, Springer Netherlands, 2006
- [62] D. E. McCumber, “*Einstein relations connecting broadband emission and absorption spectra*”, Phys. Rev., Vol. 136, No. 4A, 1964, pp. A954
- [63] Robert C. Hilborn, “*Einstein coefficients, cross sections, f values, dipole moment, and all that*”, Am. Jour. Phys. Vol. 50, Issue 11, 1982, pp. 982
- [64] R. M. Martin, R. S. Quimby, “*Experimental evidence of the validity of the McCumber theory relating emission and absorption for rare-earth glasses*”, Jour. Opt. Soc. Am. B, Vol. 23, No. 9, 2006, pp. 1770
- [65] Michel J. F. Digonnet, Erik Murphy-Chutorian, Dario G. Falquier, “*Fundamental limitation of the McCumber relation applied to Er-doped silica and other amorphous-host lasers*”, IEEE Jour. Quant. Electro., Vol. 38, No. 12, 2002, pp. 1629
- [66] F. Auzel, D. Meichenin, A. Mendorioz, R. Balda, J. Fernandez, “*Determination of the quantum efficiency of Er^{3+} in glasses: indirect and direct methods*”, Jour. Lumin., Vol. 72-74, 1997, pp. 152
- [67] Hideaki Hayashi, Setsuhisa Tanabe, Naoki Sigimoto, “*Quantitative analysis of optical power budget of bismuth oxide-based erbium-doped fiber*”, Jour. Lumin., Vol. 128, 2008, pp. 333
- [68] Shinxun Dai, Weidong Xiang, Tiefeng Xu, Qiuhua Nie, Xiang Shen, “*Effect of radiation trapping on the emission properties of Er^{3+} : $^4I_{13/2} - ^4I_{15/2}$ transition in oxide glasses*”, Jour. Opt. Mater. , Vol. 30, 2008, pp. 1355
- [69] F. Auzel, P. Goldner, “*Towards rare-earth clustering control in doped*

- glasses*", Opt. Mater., Vol. 16, 2001, pp. 93
- [70] G. N. Van den Hoven, E. Snoeks, and A. Polman, "*Upconversion in Er-implanted Al_2O_3 waveguides*", Journal of Applied Physics, Vol. 79, No. 3, 1996, pp. 1258-1266
- [71] O. Lumholt, T. Rasmussen, A. Bjarklev, "*Modelling of extremely high concentration erbium-doped silica waveguides*", Electron. Lett., Vol. 29, No. 5, 1993, pp. 495
- [72] Shinxun Dai, Jianhu Yang, Lei Wen, Lili Hu, Zhonghong Jiang, "*Effect of radiative trapping on measurement of the spectroscopic properties of Yb^{3+} :phosphate glass*", Vol. 104, 2003, pp. 55.
- [73] P. Blixt, J. Nilsson, T. Carlness, and B. Jaskorzynska, "*Concentration dependent upconversion in Er^{3+} -doped fiber amplifiers: Experiments and Modeling*", IEEE Trans. Photonics. Technol. Lett. Vol. 3, No. 11, 1991, pp. 996-998
- [74] G. N. van den Hoven, E. Snoeks, A. Polman, C. van Dam, J. W. M. van Uffelen, M. K. Smit, "*Upconversion in Er-implanted Al_2O_3 waveguides*", Jour. Appl. Phys, Vol. 79, No. 3, 1996, pp. 1258
- [75] J. Nilsson, P. Blixt, B. Jaskorzynska, J. Babonas, "*Evaluation of parasitic upconversion mechanisms in Er^{3+} -doped silica-glass fibers by analysis of fluorescence at 980 nm*", Jour. Light. Technol. Vol. 13, No. 3, 1995, pp. 341
- [76] E. Snoeks, G. N. van den Hoven, A. Polman, B. Hendriksen, M. B. J. Diemeer, F. Priolo, "*Cooperative upconversion in erbium-implanted soda-lime silicate glass optical waveguides*", Jour. Opt. Soc. Am. B., Vol. 12,

Issue 8, pp. 1468, 1995

- [77] H. Hayashi, S. Ohara, N. Sugimoto, S. Tanabe, “*Effects of lanthanum and boron addition on suppression of cooperative upconversion in bismuth oxide-based erbium-doped fibers*”, Jap. Jour. Appl. Phys., Vol. 46, No. 6A, pp. 3452, 2007
- [78] M. Pollnau, D. R. Gamelin, S. R. Luthi, H. U. Gudel, “*Power dependence of upconversion luminescence in lanthanide and transition-metal-ion systems*”, Phys. Rev. B., Vol. 61, No. 5, 2000, pp. 3337
- [79] Jianhu Yang, Shixun Dai, Yuefen Zhou, Lei Wen, Lili Hu, Zhonghong Jiang, “*Spectroscopic properties and thermal stability of erbium-doped bismuth-based glass for optical amplifier*” Jour. Appl. Phys., Vol. 93, No. 2, 2003, pp. 977
- [80] Mingying Peng, Chen Wang, Danping Chen, Jianrong Qiu, Xiongwei Jiang, Congshan Zhu, “*Investigations on bismuth and aluminium co-doped germanium oxide glasses for ultra-broadband optical amplification*”, Jour. Non-Cryst. Solids, Vol. 351, 2005, pp. 2388
- [81] T. Suzuki, Y. Ohishi, “*Broadband 1400 nm emission from Ni^{2+} in zinc-alumino-silicate glass*”, Appl. Phys. Lett., Vol 84, No. 19, 2004, pp. 3804
- [82] Shibin Jiang, Tao Luo, Bor-Chyuan Hwang, Fred Smekatala, Karine Senechal, Jacques Lucas, Nasser Peyghambarian, “ *Er^{3+} -doped phosphate glasses for fiber amplifiers with high gain per unit length*”, Jour. Non-Cryst. Solids, Vol. 263&264, 2000, pp. 364

CHAPTER 4

CHARACTERISATION OF ERBIUM-DOPED BISMUTH FIBRE AMPLIFIER

4.1 Introduction

The explosive demand for data information fuelled by the Internet and cellular communications has prompted the rapid research and development of optical components and systems. In this regard, new specification of optical bandwidth has been plotted for long-haul optical telecommunication systems. This long-haul system induces much higher signal attenuation and relies on optical amplifiers to enhance the signal quality and distance. Optical amplifiers in current optical networks exploit the usage of erbium ions that have been doped into the silica glass material to do the signal amplification tasks. Although the development of optical amplifiers have reached full growth and maturity, new specifications have now demanded more detailed optical amplifier characterisation. The characterisation of EDFA in a glass host for optical telecommunication systems are important in order to design more efficient, higher quality optical amplifiers with lower production costs. Today, with the continuing demands and diversification into a wide variety of applications from long-haul broadband optical telecommunications to defence and military, medical, imaging, material study and so on, the new comprehensive characterisation and analysis of EDFAs will fulfil the criterion long sought after[1].

In an optical telecommunications network, the EDFA's type and parameter highly depends on its deployment in the network system. Generally, there are three

types of EDFAs in an optical network system [1]; the booster amplifier, the in-line amplifier and the pre-amplifier. These three types of EDFAs have different configurations and design but mostly demands similar requirements for optical telecommunications systems. For a booster type optical amplifier, which are placed right after the signal transmitter, the most important parameter is the capability to produce a high output signal for longer transmission lengths. The in-line type optical amplifier is placed between fibre links and is required to produce a broad amplification bandwidth to carry multiple WDM channel. The pre-amplifier, which is placed before the receiver ends, is required to be able to produce a low signal-to-noise output for low bit error detection. Hence, the common EDFA parameters for optical telecommunication networks are output power, amplification bandwidth and NF. In this chapter, these three parameters are measured and studied in detail for the EDFA evaluation in different configurations. The effects of a bi-directional pump configuration on the performance of the EDFA, the signal gain and the noise are also discussed. The efficiencies of the EDFA are calculated from the output signal power and discussed as well. Later, the effect of the fibre temperature on the signal gain, noise and efficiency is measured and further discussed.

4.2 EDFA Pumping Configurations

When light propagates in a dielectric medium such as glass, according to the Lambert-Beer Law,¹ the intensity of the light is absorbed by the medium itself and as a result, producing lower light intensity at the output ends. In an optical amplifier in

¹Lambert-Beer law, the input light intensity I_{in} is attenuated by the medium absorption of α and interaction length l giving the output intensity $I_{out} = I_{in} e^{-\alpha l}$

which the glass host is doped with RE ions such as erbium, the signal light is amplified at the signal wavelength in the presence of a strong additional light at a shorter wavelength known as the 'pump'. For that reason, the gain/loss experienced by the signal wavelength is a function of the absorbed pump light. For positive population inversion, the signal is amplified and for negative population inversion, the signal is absorbed. In the application of long-haul optical telecommunication systems, the amount of absorbed pump light must be high for the signal to experience a gain hence, making it an efficient optical amplifier [1-3].

The pumping configuration of an optical amplifier can be identified in three configuration types [1]. Forward pumping is defined as the situation whereby the pump light source is combined at the input ends of the erbium-doped fibre (EDF) and travels in same direction with the signal light. A backward pumping configuration is simply the reverse of this. Bi-directional pumping is a combination of both forward and backward pumping schemes and is the configuration in this study [3,4]. The schematic of the single pass bi-directional pumping bismuth erbium-doped fibre (Bi-EDF) configuration is illustrated in Figure 4.1.

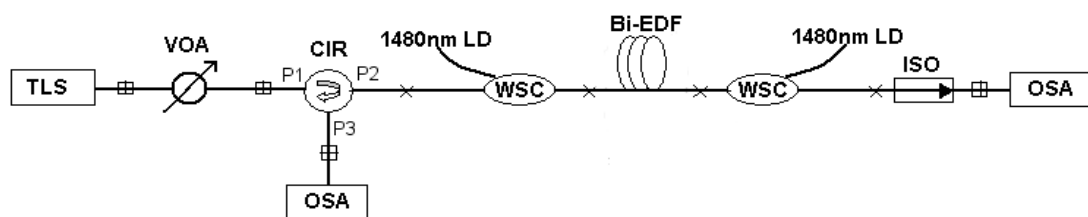


Figure 4.1 Basic single-pass bi-directional configuration set-up of Bi-EDF amplifier, TLS:Tunable Laser Source, VOA:Variable Optical Attenuator, CIR: Circulator, LD:Laser Diode, WSC: Wavelength Selective Coupler, ISO:Isolator, OSA:Optical Spectrum Analyser

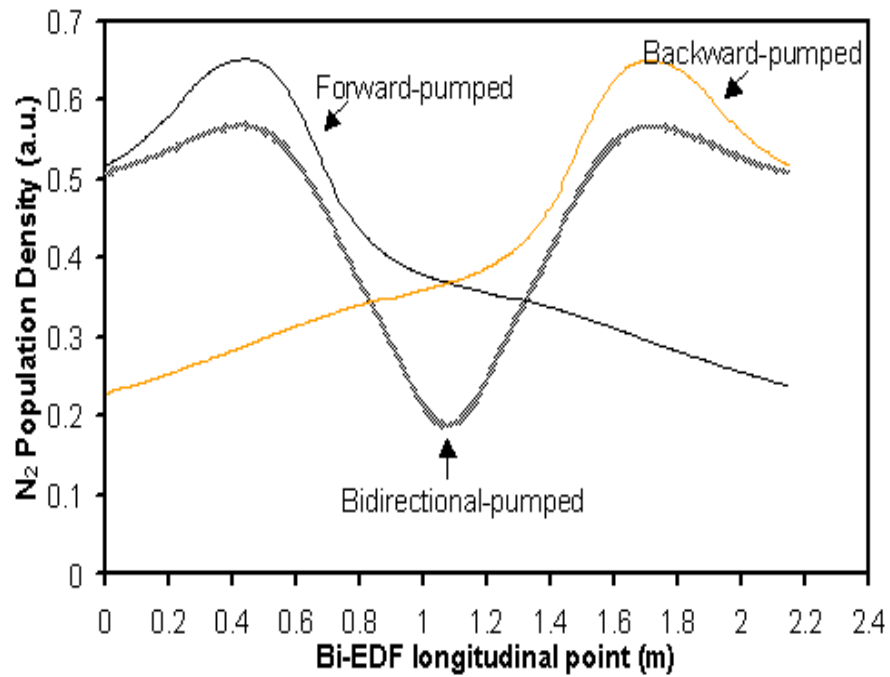
Single-pass in this configuration means that the signal is amplified only one time while a double-pass implies that the signal will be reflected by a reflector mirror and passed back to experience amplification for a second time [2]. The pump source wavelength of 1480 nm is combined with a thin-film filter (TTF) 1480/1550 nm WSC which has flat/constant wavelength transmission characteristics from 1512 nm to 1620 nm and is fusion spliced to the Bi-EDF. The input signal power from a Tunable Laser Source (TLS) ranging from 1520 nm to 1620 nm is controlled by a Variable Optical Attenuator (VOA) and connected to the Bi-EDF at the input end 'P1' of an Optical Circulator (CIR). The CIR is a non-reciprocal device based on principles similar to the optical isolator (ISO) that allows the routing of optical light from one end to the other end in an unique/specific manner. The CIR is used in order to measure the backward propagating Amplified Spontaneous Emission (ASE) simultaneously and also to eliminate any unexpected laser oscillation and Multipath Interference Noise (MPI) [2,4] at the input ends. The output signal gain, NF and output power of the optical amplifier are measured using an Optical Spectrum Analyser (OSA) at the output ends after the ISO.

4.3 EDFA Simulation

To comprehend the effect of the pump configuration in the EDFA, the population density of the excited state, N_2 (representing the amount of pump light being used for the amplification) was calculated from the amplifier rate equation (Eq. 2.9-2.11) using the software OptiAmplifier ver. 3.0.4 from Optiwave Corp. The parameters used in this calculation are listed in Table 4.1. The maximum available

Table 4.1 Bi-EDF parameters used for the theoretical calculation

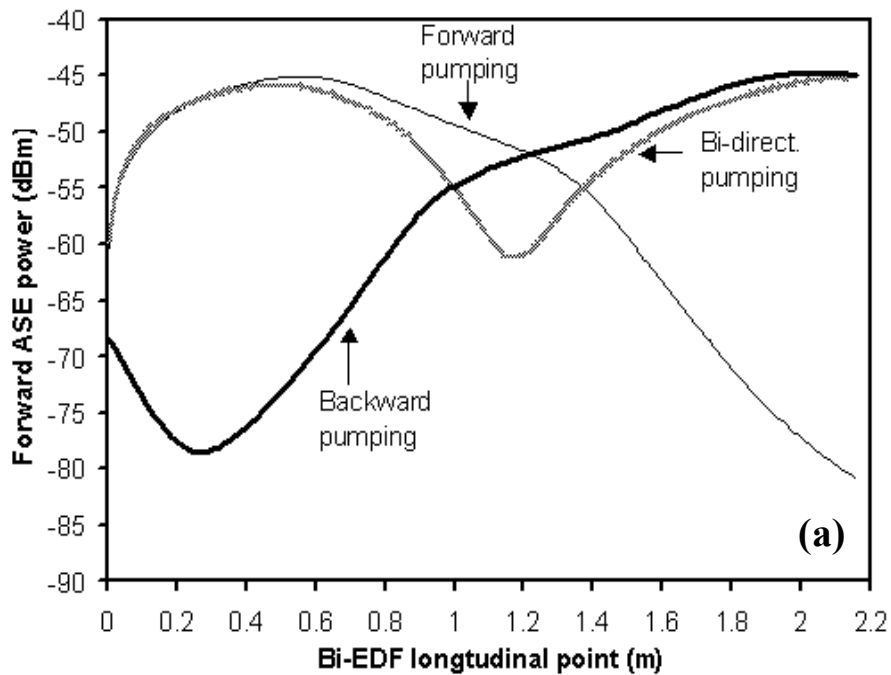
Bi-EDF parameters	
Fibre length	215.3 cm
Er ³⁺ concentration	7.6042 x10 ¹⁹ cm ⁻³
Core radius	2.7 μm
Peak absorption @1480nm	79.13 dB/m
@1560nm	44.11 dB/m
Peak emission @1480nm	31.32 dB/m
@1560nm	102.32 dB/m
MFD @1480nm	6.02 μm
@1560nm	6.28 μm
⁴ I _{13/2} lifetime	2.84 ms
Pump threshold	3.91 mW
Signal saturation power	2.97 mW
Cut-off wavelength	1300 nm


Figure 4.2 The excited state N₂ population density for Bi-EDF for different pumping configuration.

pump power was fixed at 160 mW and the length of the Bi-EDF fixed at 210 cm. The simulation result is simulated in Figure 4.2 and 4.3.

With limited pump power, under forward and backward configuration, only the beginning end of the Bi-EDF generates a higher N_2 population density compared with the bi-directional pumping scheme that is capable of generating a high population density at both ends. As the result from the simulation, splitting the pump power into a bi-directional pumping configuration, allows the pump source to be distributed more effectively and generate a longer N_2 population density length. Since the absorption efficiency of the pump source is increased, the generated fluorescence intensity also increases. On that account, a bi-directional pumping scheme is capable of producing a larger ASE and signal output. The calculated forward ASE and signal output power are shown in Figure 4.3 (a) and (b).

In Figure 4.3 (a) and (b) the forward ASE and output signal for the forward pumping configuration is attenuated as it propagates through the Bi-EDF. The limited



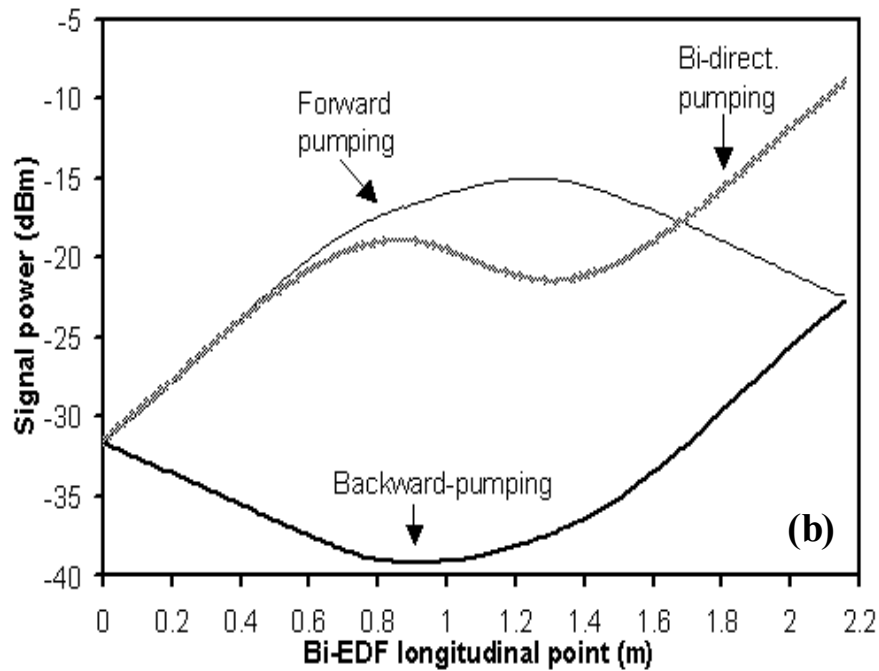


Figure 4.3 The simulation results of (a) forward ASE and signal power (b) for Bi-EDF for different pumping configuration.

available pump power of only 160 mW in the forward pumping scheme results in the optimal length of 120 cm of the Bi-EDF for maximum signal output power. The excess pump power calculated at this length is almost 40 fW revealing that the remaining Bi-EDF length acts as an absorbing media instead of a gain media. Although the signal obtained a net amplification at the input end, as the signal propagates further along the remaining length, the signal is absorbed. This is because there is no longer a pump source left to excite the Er^{3+} ions and as a consequence, producing lower population density. Whereas in bi-directional pumping, almost all the available length of the Bi-EDF is inverted by the pump source and acts as gain media as demonstrated in Figure 4.3 (b) thus, making it capable of generating a much higher forward ASE and signal output power. Therefore, the bi-directional pumping produces more N_2 population density as presented in Figure 4.2. The backward

pumping scheme on the other hand leaves the output signal suffering from greater attenuation as the signal has been absorbed at the Bi-EDF input end and only experiences amplification at the output end of the Bi-EDF. Consequently when the input signal power is reached at Bi-EDF output end, the power is very low, making the amplification process limited to a certain extent as that reason, producing lower output signal powers. Hence, this configuration is not suitable to excite high absorption cross-section EDFs such as the Bi-EDF efficiently.

4.4 Experimental Result

To fully understand the effect of the pump configuration, experimental verification was done using the Bi-EDF. The forward ASE spectrum of Bi-EDF (measured at the output end of the fibre) is presented in Figure 4.4 for different pump

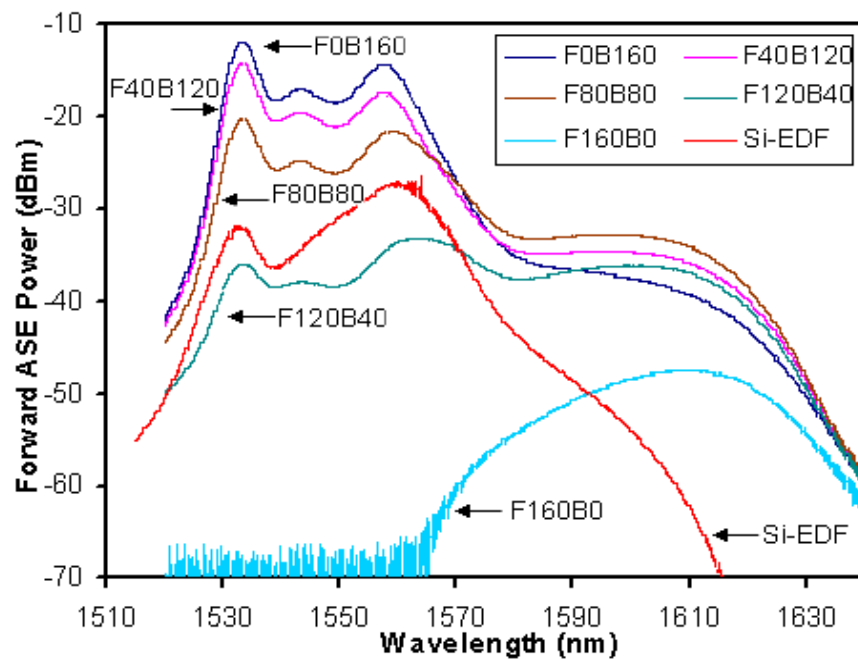


Figure 4.4 The Bi-EDF forward ASE spectrum for different pumping configuration

power ratios. The forward ASE of Si-EDF is also displayed in the figure for comparison purposes. The ASE power from the backward pumping (F0B160) generates the highest power while forward pumping (F160B0) is only capable of generating a low ASE power despite being pumped with the same amount of pump power. This is because the pump light is only capable of producing high population inversion at limited lengths of the input portion of the fibre. As a consequence, the ASE power from forward pumping suffered greater attenuation in reaching the end of the fibre as compared to the backward pumping configuration. From the figure, the ASE spectrum of bi-directional pumping is broader and more flatter due to effective pump light distribution. With a forward:backward pump power ratio of 120:40 mW, the ASE spectrum can be flattened from 1530 to 1610 nm without using any Gain-Flattening Filter (GFF) [5,6] or a modified core profile for wide-band 'white-light source' and optical amplifiers [7,8]. A flat ASE spectrum at the C- and L-band region demonstrates the ability of the Bi-EDF as a wide-band optical amplifier for DWDM optical telecommunications systems [3-5].

I. Gain and Noise Figure (NF)

EDFA gain and signal output power parameters are usually measured as a function of input signal wavelength and power. Basically, signal gain is defined as the positive signal power difference after propagating through the EDFA. When the signal is injected into the EDFA, it will be amplified by stimulated emission from the active medium (Er^{3+}) excited at its pump absorption spectrum. The gain medium will also emit spontaneous emission at the signal wavelength that manifests itself as

noise to the signal. The magnitude of the noise contribution to the amplification process is defined as the NF [1,9-10].

The NF in an EDFA is the combined contribution of Signal-Spontaneous Beat Noise, Spontaneous-Spontaneous (Sp-Sp) Beat Noise and Signal and ASE Shot Noise that originate from the active medium and distortion/noise from passive devices, (e.g. isolator, couple and circulator) while Multiple Path Interference Noise (MPI) is a result of the reflection in the system [1]. Usually, the NF is decided by Signal-Spontaneous Beat Noise and Shot Noise factor due to its larger contribution and is calculated by measuring the system gain and ASE power at signal wavelength [1,9]. This measurement is complicated and lacks accuracy because the ASE level at the signal wavelength is obscured by the signal itself and the spontaneous emission near the signal wavelength includes both ASE and Signal Spontaneous Emission (SSE) [9]. In order to solve this problem, three optical measurement techniques [1,9] have been developed that is capable of producing a precise and highly accurate method for ASE level and NF measurement. These techniques are

- ASE Interpolations
- Time Domain Extinctions
- Polarization Extinction

In this study, the optical amplifier performance on signal gain and noise figure (NF) were measured by an OSA using the ASE Interpolation Technique [10]. The ASE Interpolation technique relies on the determination of the ASE level at a specific offset (e.g. 1 nm) above and below the signal wavelength, and interpolating

between these two points to determine the average of the ASE level at the signal wavelength as illustrated in Figure 4.5. In this technique, the gain, G and NF are defined as

$$G(\lambda_s) = \frac{P_{\text{out}}(\lambda_s) - P_{\text{ASE}}}{P_{\text{in}}(\lambda_s)}, \quad (4.1)$$

and

$$NF_{\text{min}}(\lambda_s) = \underbrace{\frac{P_{\text{ASE}} \cdot \lambda_s}{hcB_w G(\lambda_s)}}_{\text{shot noise}} + \underbrace{\frac{1}{G(\lambda_s)}}_{\text{signal \& ASE mixing}}, \quad (4.2)$$

where $P_{\text{out,in}}$ is the signal output and input powers, P_{ASE} is the ASE power at signal wavelength λ_s , B_w is the measured signal spectral resolution and h is the Plank's constant. The gain of the EDFA is defined as the ratio of the output signal power to the input signal power.

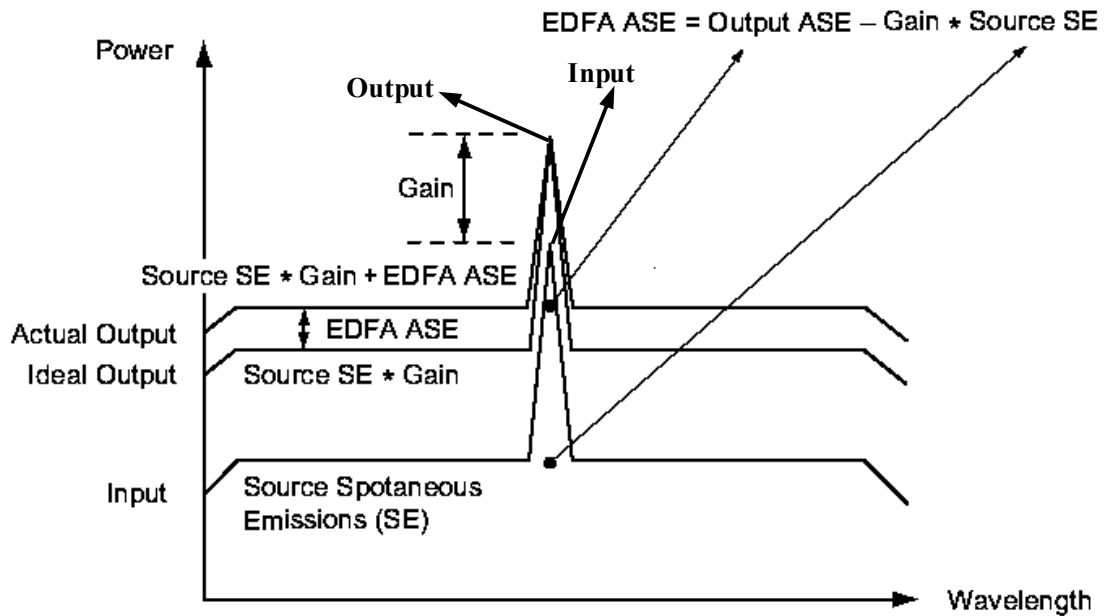


Figure 4.5 Determination of the ASE level using linear interpolation

From the figure, due to the input signal also containing Spontaneous Emission (SE) from the source, it also gets amplified when it propagates through the EDFA. For that reason, this extra gain produced by the SE must be removed to ensure the measurement gives the actual signal amplification. In order to remove/reduce the gain error, the TLS must have lower SE and good power stability.

The NF equation from Eq. (4.2) contains two important terms that contribute to noise of the EDFA that came from a) mixing of the signal and ASE; and b) shot noise of the active medium, (in which the first terms has a larger influence on the NF values). This calculation also requires that the output ASE power at the signal wavelength be resolved by using the interpolation technique because the ASE power at the signal wavelength was masked by the signal itself and cannot be directly measured.

The noise generated from the mixing of the signal and ASE is also known as the spontaneous emission factor, n_{sp} which sets the limit of minimum noise of an EDFA. The smallest n_{sp} is achieved when the gain becomes weakly dependent upon the launched pump power and approaches its maximum value $1/G \approx 0$, which corresponds to the regime of maximum inversion [1]. The NF_{min} and n_{sp}^{min} at signal wavelength, λ_s are given by

$$NF_{min}(\lambda_s) \approx \frac{P_{ASE} \cdot \lambda_s}{hcB_w G(\lambda_s)} = 2n_{sp}^{min}(\lambda_s) \quad (4.3)$$

$$= \frac{2}{1 - \frac{\sigma_e(\lambda_p)\sigma_a(\lambda_s)}{\sigma_e(\lambda_s)\sigma_a(\lambda_p)}} = \frac{2}{1 - \exp\left[\frac{hc(\lambda_p - \lambda_s)}{k_B T}\right]}, \quad (4.4)$$

where $\sigma_{e,a}(\lambda_{p,s})$ is the emission and absorption cross-sections at pump and signal wavelengths, k_B is the Boltzmann constant and T is the temperature. For the case of a two-level laser system (when using 1480 nm pump excitation), the Er^{3+} ions emission cross-section $\sigma_e(\lambda_p)$ is non-zero and causes the denominator in Eq. 4.4 to be smaller than 1, consequently producing the minimum achievable noise figure of higher than 2. As a result, 1480 nm pump excitation is less preferred compared with 980 nm pump excitation in a low noise EDFA design [1, 2].

Figure 4.6 (a) and (b) show the measurement of gain as a function of total pump power with different forward and backward power ratio at 1560 nm signal wavelength. In this measurement, the forward or backward LD pump power were fixed with power of 50, 100 and 150 mW while the opposite LD pump power are increased to maximum (e.g. F50 is defined as forward pump that was fixed at 50 mW while increasing the backward pump power to maximum). The figure also shows the gain for uni-directional pump for comparison purpose. All gain measurement was done with the input signal power fixed at 1 mW.

The Figure 4.6 (a) and (b) indicates the important gain region that reflect three possible gain regimes [1]

- the under-pumped regime where $G < 1$,
- the incomplete inversion regimes where the gain steeply increases with pump power and
- the near-complete inversion regime where the gain approaches the limiting values of $G(\infty)$.

Here, the limit gain $G(\infty)$ (using the principles of energy conservation) is defined as

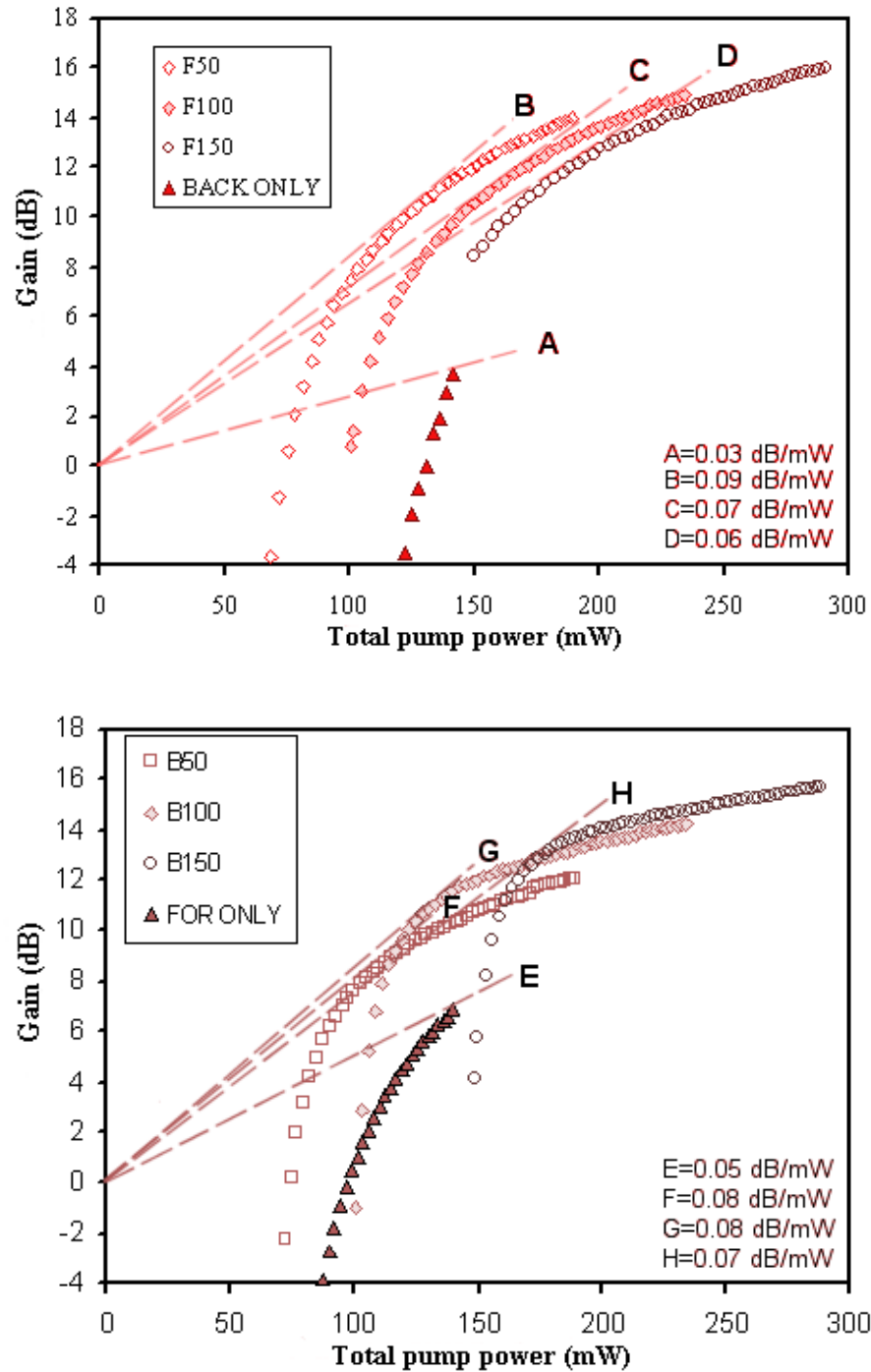


Figure 4.6 The gain of Bi-EDF for different forward (a) and backward (b) pump power ratio. The broken line correspond to gain coefficient of the Bi-EDFA. (A) = uni-directional backward pumping, (B,C,D) = bi-directional pumping with forward pump was fixed at 50, 100, 150 mW, (E) = uni-directional forward pumping, (F,G,H) = bi-directional pumping with backward pump power was fixed at 50, 100, 150 mW

[1,11]

$$G(\infty) = \exp\left(\frac{\eta_s - \eta_p}{1 + \eta_p} \alpha_s L\right), \quad (4.5)$$

where α_s is the Bi-EDF absorption coefficient at signal λ_s , L is the Bi-EDF length and $\eta(\lambda_{s,p}) = \sigma_e(\lambda_{s,p})/\sigma_a(\lambda_{s,p})$ as calculated from Eq. 3.14. Using the gain and signal output power relationships, the maximum possible Bi-EDF signal output power is given as [1, 11],

$$P_{out}^{max} = 1 + \frac{\lambda_p}{\lambda_s} \frac{P_p^{in}}{P_s^{in}}, \quad (4.6)$$

where $\lambda_{p,s}$ is the pump and signal wavelength and $P_{s,p}^{in}$ input signal and pump power.

From the Eq. 4.5 and 4.6, the calculated values of $G(\infty)$ and P_{out}^{max} of the Bi-EDF for $P_s^{in} = 1$ mW at 1560 nm signal wavelength and $P_p^{in} = 160$ mW pump power are 21.8 dB and 152.79 mW, respectively.

From the result obtained for the uni-directional forward or backward pumping configurations, when the available pump power is restricted to only 140 mW, the 1480 nm pump light is capable of carrying the Bi-EDF into an incomplete inversion regime. The maximum measured gain for forward and backward pump configurations were 6.84 and 3.67 dB, respectively. With additional pump power from the backward or forward direction 50, 100 and 150 mW, the Bi-EDF was able to operate in the near-complete inversion regime producing higher gain and signal output power at the same total pump power. The results reveal that pump light in a bi-directional pump configuration was distributed much better than a uni-directional pump configuration and produces more gain to the signal [1, 11, 12].

However, the signal gain variation with the uni-directional pump was found to vary by about 2.67 dB (= 6.84-3.67 dB) with the same pump power. This increment is almost 48% higher, which tells us that the uni-directional forward pumping configuration was more efficient and thus, produces more gain to the signal. Backward pumping suffers low signal gain because as the signal propagates from the input to the output end of the Bi-EDF, the signal power is attenuated by the Bi-EDF and hence limits the signal amplification. Although by utilising a high power pump source in a uni-directional pump configuration to pump the Bi-EDF can reduce the attenuation effects, this solution however proved to be largely inefficient and costly [12].

The gain for bi-directional pumping was found to greatly depend on forward or backward pump configuration. When the total pump power is fixed at 180 mW, the gain can vary from 1.37 to 2.24 dB for 50 mW to 150 mW additional pump power. The gain variations are listed in detail in Table 4.2.

Table 4.2 Gain variation in bi-directional pumping configuration with different pump power addition. Total pump power was fixed at 180 mW.

Adding (mW)	Gain generated by forward pump (dB)	Gain generated by backward pump (dB)
50	13.54	11.85
100	12.65	12.97
150	11.30	13.22
Gain difference ($G_{\max} - G_{\min}$)	-2.24	1.37

From the table, increasing the pump power from 50 to 150 mW at the input end causes the gain to decline to -2.24 dB whereas adding extra pump to the output

end leads to a gain growth of 1.37 dB. Hence, from the results, an extra pump light at the output end of the fibre is capable of generating a gain improvement whereas adding extra pump light to the Bi-EDF input end saturates the output signal light thus, reducing gain [1, 12]. This gain variation is expected due to the high power backward ASE that reflects back into the Bi-EDF and generates an effect of ASE self-saturation [1, 12, 13].

Self-saturation can cause a population inversion depletion and has been recognised as a limiting factor [13, 14] for high power optical amplifiers. If the effect is not minimised or controlled when designing an optical amplifier, it can worsen the efficiency of the system therefore, limiting the generated output signal power.

There are two kinds of saturation that affects optical amplifier performance, namely signal-induced saturation and ASE self-saturation. Signal-induced saturation occurs due to an insufficient number of pump photons to excite the RE ions in order to amplify a high power input signal, whereas ASE self-saturation is due to a high ASE power that 'dominates' and 'competes' with the signal photons [1]. The impact brought about on optical amplifiers is that these factors can reduce the actual signal inversion population, pump light absorption and worsen the actual signal gain and NF [13-16]. The signal-induced and ASE self-saturation effect can also affect in combination and incur more serious decline to the performance of the optical amplifiers.

In this regard, the gain reduction at the maximum forward pump addition is due to ASE self-saturation effect that limits the signal amplification at the input end of Bi-EDF. This result was found to match well with the signal power simulation as

depicted in Figure 4.3 (a) and (b) since the signal inversion varies with the EDF length [1, 12]. In the simulation, the pump power was equally divided subsequently, creating a fairly balanced ASE power. In the experiment, at high forward pump power, the backward ASE power increases and intensifies the ASE self-saturation effect at Bi-EDF input end. This effect however is less with the backward pump power as the ASE power distribution is more at EDF output end.

The transparency pump power P_p^{trans} where the gain, $G = 1$ is a practical parameter to explain the minimum pump power required for bleaching the input signal from the fibre background absorption. These pump power values allow optical amplifier designers to identify the threshold power to produce unity gain [1,10,11]. For better pump light distribution and output signal performance, the glass host background loss at the pump wavelength must be low to minimise the pump power attenuation.

In Figure 4.6 (a), the P_p^{trans} for uni-directional backward pumping configuration was about 131 mW but with an addition from 50 to 100 mW pump power at the input end brings out the transparency to be higher, rising from 74 mW to 101 mW. While in figure (b), the P_p^{trans} for uni-directional forward was found to be much lower; about 97 mW because of high signal amplification at the Bi-EDF input end, while addition from 50 to 100 mW pump power at output end produces almost similar P_p^{trans} values. So, in bi-directional pumping, the signal loss of Bi-EDFA can be easily overcome by adding extra pump power at the Bi-EDF input or output end

which subsequently, bring down the P_p^{trans} to the same value of 74 mW as characterised here. This result describes that the P_p^{trans} is very dependent on pump configuration rather than total pump power. By deploying bi-directional pumping configuration, low transparency pump power can be achieved. This enables the Bi-EDF to achieve a higher signal inversion and thus, produces an efficient optical amplifier. On that note, this configuration relatively offers an advantage in producing higher gain output due to the effective pump light distribution.

In order to understand the effects of input pump and gain, the gain coefficient was calculated and compared. The gain coefficient of an optical amplifier is defined as the tangent of the maximum gain to the maximum launched pump power² [1, 13]. Although the gain coefficient by definition [1, 13] does not indicate the inversion condition of the EDF, its can uncover the gain evolution from $G = 1$ or transparency to the maximum gain of the RE-doped fibre [1].

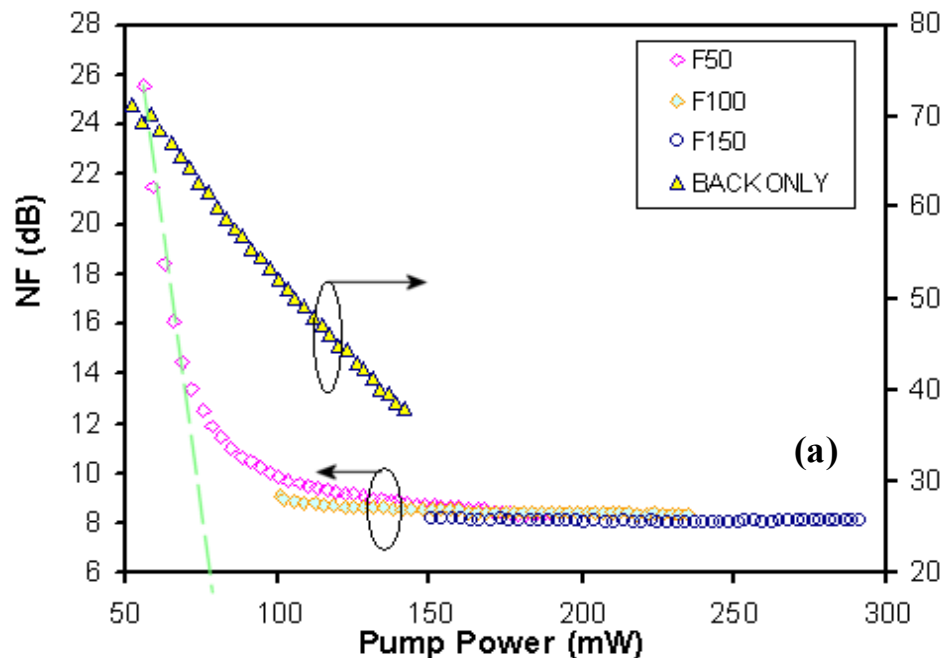
The gain coefficient for uni-directional forward and backward pumping configurations of the Bi-EDF were found to be 0.05 and 0.03 dB/mW, respectively with lower gain coefficient in the backward pumping scheme due to high signal absorption at the Bi-EDF input end. The highest coefficient was found to be about 0.09 dB/mW with a bi-directional pumping and 50 mW forward pump power. Other pump power combinations at 50 and 100 mW exhibit a gain coefficient at anywhere between 0.07 and 0.08 dB/mW. When the pump power accretion increases to 150 mW, the gain coefficient (either with bi-directional forward or backward pump configuration) deteriorates significantly. This reduction in coefficient is expected and

²As shown in Figure 4.6, the highest dB/mW ratio is not obtained at maximum launched pump power, where the gain curve levels off, but at the point defined by the tangent. This definition was defined in [1, 13] and adopted in this thesis

it originates from the effect of ASE self-saturation [1,12] as explained previously.

The bi-directional pumping NF of the Bi-EDF as a function of forward and backward pump powers are presented in Figure 4.7 (a) and (b). The uni-directional forward and backward pumping NF is also presented for comparison. From the result, the NF of the uni-directional backward pump configuration is very dependent on launched pump power compared with the forward pump scheme. At the same pump power of 140 mW, the NF of the backward pump configuration was 38.06 dB, that is almost 30 dB higher than the NF of the forward pump configuration which was only 8.13 dB. High signal absorption and limited pump power as consequence, produce low signal gain which leads to high NF penalty in this configuration.

When the amount of backward pump power is raise from 50 to 150 mW in the bi-directional pumping configuration, the NF was reduced exponentially and



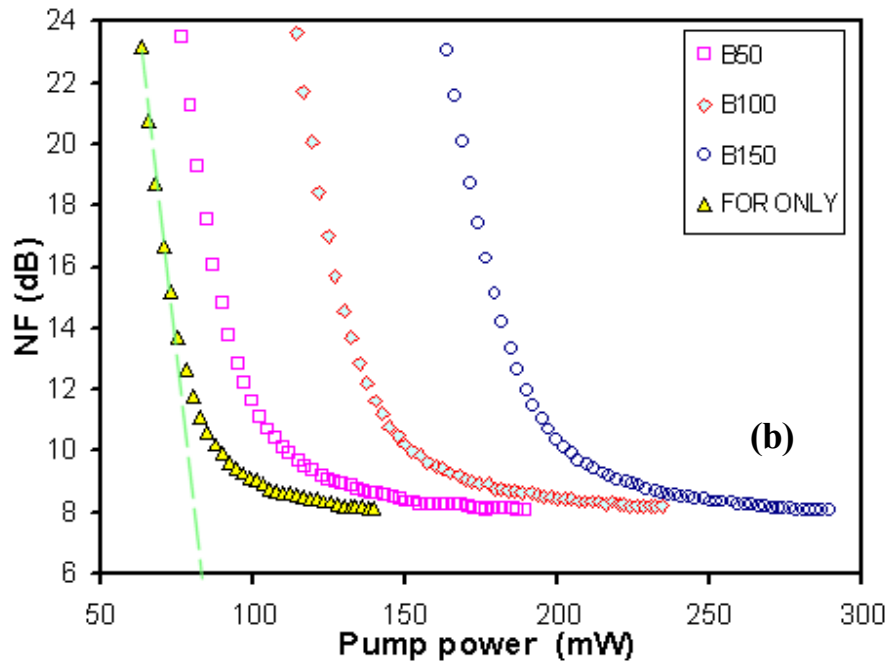


Figure 4.7 The NF of Bi-EDF for different forward (a) and backward (b) pump power increment. F: forward, B: backward (bi-directional), For/Back Only: Uni-directional forward/backward pump

settled down to a value of about 8 dB. However, the improvement rate with forward pump power add-on was much more faster, where only with 50 mW able to yield a similar NF reduction as presented in Figure 4.7 (a) compared to when adding extra pump power at the backward pump. At higher forward pump power addition, the minimum NF sank down to 9 dB. At this condition, putting an extra pump power will increase the gain but no further improvement of NF values was observed.

Using this minimum value and including the WSC loss and the Bi-EDF splice loss calculated from chapter 3.2, the actual NF of the Bi-EDF calculated using Eq. 4.2 was found to be 7.69 dB. This value is almost 3.78 dB higher than the calculated NF quantum limit n_{sp} (using Eq. 4.4) of 3.91 dB at a wavelength of 1560 nm. Hence, the reason for the higher NF value is assumed to be from other sources/effects such

as MPI, laser oscillation and saturation [1, 14-18]. These effects have the capability to deplete the optical amplifier inversion population specially at the input end and consequently produces a noisy output signal.

The NF results lead to an important finding for different pumping configurations of the Bi-EDF. Compared with the backward pump configuration, the forward pump configuration suffers lower NF penalty. As explained by E. Desurvire [12], forward pump configuration generates lesser signal-spontaneous beat noise [2, 17] due to high signal amplification at the Bi-EDF input end and also smaller ASE self-saturation effects [12-13]. Although this forward pumping configuration is the most desirable configuration for low noise optical amplifiers [14-16], low signal gain and general inefficiency forced optical amplifier designers to pick the bi-directional pumping configuration for high power applications since this pumping configuration has better pump power distribution [1]. In Figure. 4.7 (a), under pump deficiency (when the forward pump power is less than 78 mW), the saturation induced by signal-induced saturation will deteriorate the signal gain and NF. At the maximum pump power, the NF value was limited to 8.08 dB because the Bi-EDF was fully inverted by all available pump power. Accordingly, the NF values of this pumping configuration is very dependent on the amount of forward pump power launched into the Bi-EDF. A low NF value is achieved if the input end of EDF is fully inverted, therefore, producing maximum gain.

In the bi-directional pumping configuration, adding an extra pump power at the backward direction improved the pump light distribution along the fibre and as a result, yielding higher signal gain [17]. However, because the amplification is mostly

done at the output end of the Bi-EDF, this configuration causes higher NF penalties due to higher shot-noise from forward ASE at Bi-EDF output ends. While increasing an extra pump power at the fibre input end will improve the NF penalty of the optical amplifier, this however also generates a large amount of unwanted ASE that is capable of saturating the signal. Hence the signal gain and NF penalty of bi-directional pumping configuration is very dependent on the power ratio between the forward and backward pump. With an equal pump power ratio as indicated in Figure 4.8, the effect of the launched pump power on the signal gain and NF are more worse compared to the effects from non-equal pump power ratios. From the result, the optimum gain and NF can only be achieved at the maximum pump power of 290 mW, which in fact suffers from self-saturation [12-17].

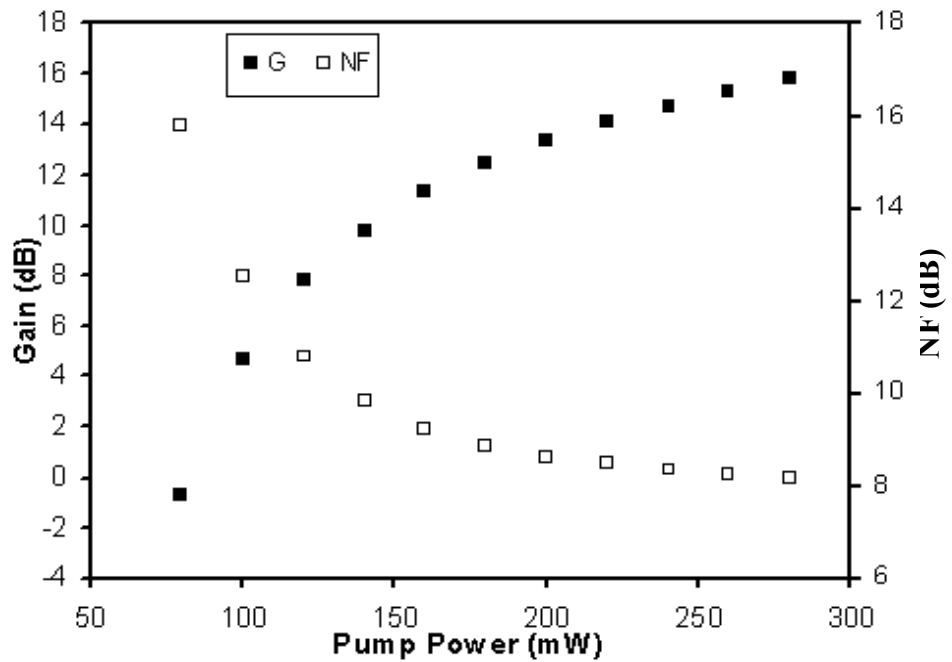


Figure 4.8 The gain and NF with bi-directional pumping with equal ratio (balanced)

For that reason, the pump power transparency obtained earlier has to be reconsidered. Since this pump power indicates the minimum pump power for the EDF to function as a lossless optical amplifier, the total pump power of 74 mW (ratio of 24 mW:50 mW) was found to be the lowest limit for the Bi-EDF to operate. At this pump power, the Bi-EDF is capable of offering an advantage of a more uniform pump power distribution for medium population inversion [15-17], thus generating better signal gain and pump efficiency. With other limiting factors such as signal-induced and ASE self-saturation, signal and pump background loss and splice joint loss are taken into consideration, this power is not a true indicator of the optimum pump power for low noise operation of the Bi-EDF optical amplifier. Only by complete optical amplifier characterisation, then the optimum pump power for low noise operation can be identified.

II. Quantum and power conversion efficiency (QCE, PCE)

The main intention of an optical amplifier is to amplify low power input signal to compensate the fibre link loss in an optical telecommunications system without adding extra noise to the signal. Long-haul transmission links require a high output power optical amplifier which is capable of giving good pump to signal conversion efficiency [18]. The conversion efficiency of pump photons into signal photons is known as Quantum Conversion Efficiency (QCE), and is defined as the ratio of the number of photons the amplifier adds to the signal divided by the number of photons due to the launched pump power, [1, 18], that is given by

$$\begin{aligned} \text{QCE} &= \frac{\Phi_s^{\text{out}} - \Phi_s^{\text{in}}}{\Phi_p^{\text{in}}} \\ &= \frac{\lambda_s}{\lambda_p} \left[\frac{P_s^{\text{out}} - P_s^{\text{in}}}{P_p^{\text{in}}} \right], \end{aligned} \quad (4.7)$$

where $\Phi_{s,p}^{\text{in,out}}$ are the input or output pump and signal photon fluxes, $\lambda_{s,p}$ are the signal and pump wavelength and $P_{s,p}^{\text{in,out}}$ are the input and output signal and pump powers. The maximum possible value for the QCE is unity, which corresponds to the case where all pump photons are effectively converted into signal photons. From the last term in Eq. 4.7, the Power Conversion Efficiency, PCE can be defined as,

$$\text{PCE} = \frac{P_s^{\text{out}} - P_s^{\text{in}}}{P_p^{\text{in}}}. \quad (4.8)$$

Figure 4.9 (a) describes the QCE as a function of pump power for different forward and backward pump ratios. The forward or backward pump power was fixed to 50, 100 and 150 mW while increasing the other pump power to its maximum value. For the uni-directional pump configuration (presented as FOR and BACK), the fibre background loss affected the pump efficiency of the optical amplifier. To achieve transparency, the forward pump configuration required less pump power of about 98 mW, while the backward pump required more than 130 mW of pump power, which consequently forced lower QCE in the backward pumping configuration. The maximum QCE obtained at the same pump power of 140 mW from backward pumping was only 1.0% compared to 2.9% from the forward pumping. This result however was found to disagree with the findings of R. I. Laming *et. al.* [13]. The large observed QCE difference was attributed to the Bi-EDF

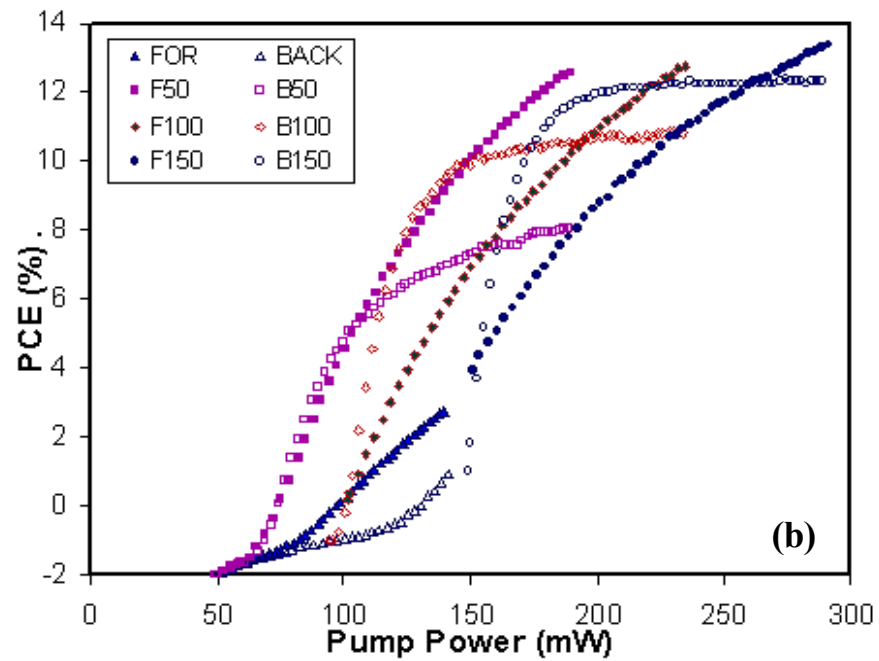
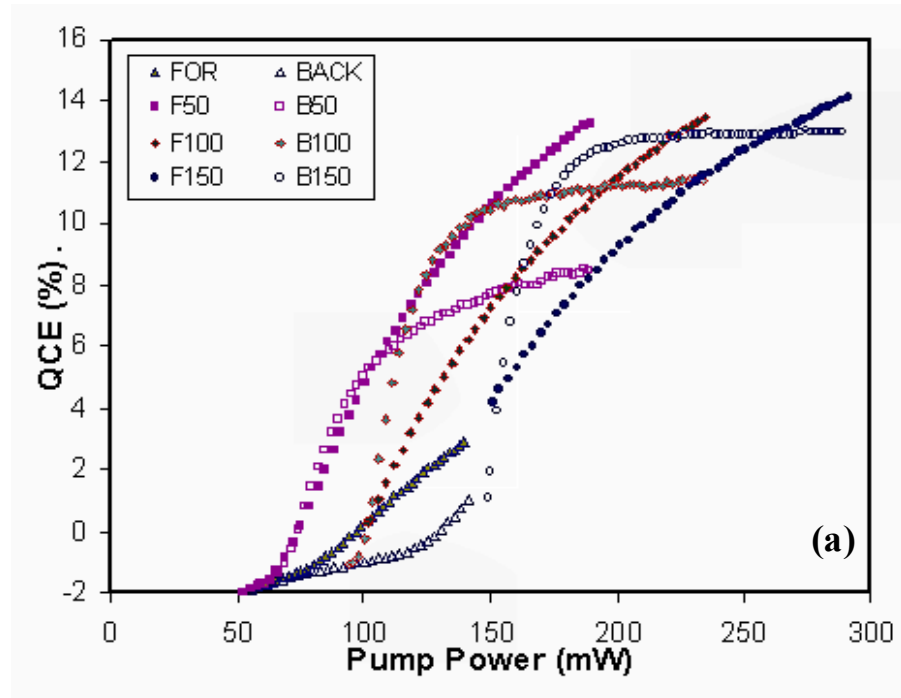


Figure 4.9 The (a) QCE and (b) PCE of Bi-EDF for different forward and backward pump ratio. F: forward, B: backward pumping (bi-directional); For/Back: Uni-directional forward/backward pump

high absorption loss and low signal gain due to limited available pump power at Bi-EDF input ends. As the pump power increases from 50 mW to 150 mW, the QCE of the Bi-EDF reveals a dependence on pump configuration rather than the amount of launched pump power as outlined by the slope tangents. The QCE with the forward pump incorporation increases almost linearly with total pump power but the QCE with the backward pump incorporation was found to be loosely non-linear and remains almost constant at higher pump power. With 150 mW backward pump addition, the QCE stayed at 12.95% when the launched total pump power was above 200 mW. Comparing this with forward pump addition, the QCE value was found to be increasing linearly with maximum pump power. From the figure (a), the maximum achieved QCE is 14.11 % with 150 mW forward pump addition. This corresponded to a total pump power of 290 mW.

The PCE of Bi-EDF shown in Fig. 4.9 (b) also displayed similar slope tangent as found in QCE result. Under heavy pumping conditions, (at 150 mW pump power addition) the output signal PCE of the forward pump add-on was 13.39 %, while the backward pump generates an output signal PCE of only about 12.29 % (generating about 1.10 % difference). Although the 1480 nm pump wavelength has been reported [2, 19, 20] as an optimum pump band for high conversion efficiency of conventional EDF, in a high Er^{3+} ion concentration Bi-EDF, the maximum achievable PCE is limited to only 13.39 % at total pump power of 290 mW. Optical amplifier with high RE doping concentration are prone to the concentration quenching effect [2, 21, 22] that is capable of reducing the efficiency of the 1.55 μm emission. Besides the effect of concentration quenching, the Bi-EDF signal gain is also affected by ASE

self-saturation from the high power backward propagating ASE that depleted the stimulated emission [12, 19, 20] as exhibited in Figure. 4.6 (a) and (b). Consequently, their inter-relationship, ultimately causes a low PCE value with backward pump addition from 50 to 150 mW.

From these efficiency results, the forward and backward pump ratio in the bi-directional pumping configuration have a large influence on the signal output power of the Bi-EDF optical amplifier. Consider the first condition when the backward pump power was fixed while the forward pump power is varied to maximum, the slope gradient of the QCE and PCE are steeper compared with the second condition when forward pump power was fixed instead. However above a certain pump power, the slope gradient declines to a constant for the remaining pump powers. This effect is actually caused by the ASE self-saturation as observed by E. Desurvire [1, 12] that reduces the population inversion of stimulated emission at the fibre input ends thus effecting the pump photon distribution along the fibre.

The forward and backward ASE power at the Bi-EDF ends as a function of pump power is illustrated in Figure 4.10. The launched pump power is fixed with equal ratios between forward and backward pump with input signal power of 0 dBm. From the figure, the backward ASE power P_{back} is five times higher than the forward ASE power P_{for} and begins to increase exponentially while the ratio between $P_{\text{for}}/P_{\text{back}}$ decreases towards unity as the pump power is increased. From the ratio, at low pump power where the generated backward ASE is low, the effect of signal-induced saturation is most significant. As the pump power increases, the inversion of the Bi-EDF is improved and generates a larger backward ASE power and overpowers the

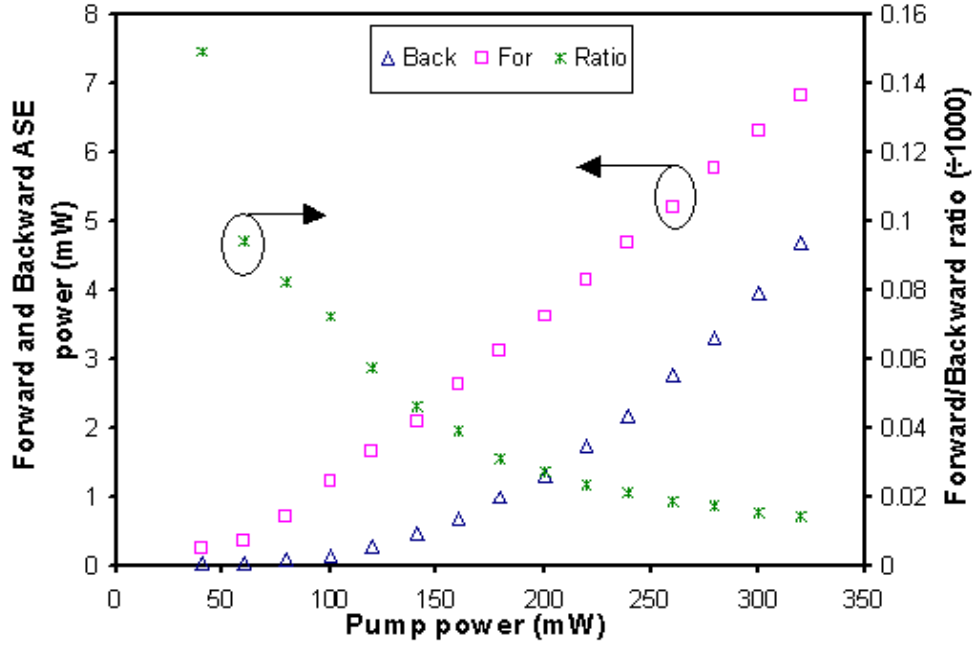


Figure 4.10 Forward and backward ASE spectrum power and power ratio $P_{\text{for}}/P_{\text{back}}$ as a function of total pump power with 0 dBm input signal (under bi-directional configuration with equal power ratio)

input signal. As a result, the backward ASE acts as broad-band saturating signal that is capable to saturate the input signal [2, 23]. By using an exponential growth function, the backward ASE power P_{ASE} was given as

$$P_{\text{ASE}}(P_{\text{pump}}) = 0.38 \exp\left(\frac{P_{\text{pump}}}{120.45}\right) - 0.66 \quad . \quad (4.9)$$

According to E. Desurvire *et. al.* [11], the onset of ASE self-saturation is when the power ratio between saturated signal power P_{sat} and ASE power P_{ASE} is $P_{\text{ASE}}/P_{\text{sat}} \approx 0.6$; and by using Eq. 4.9 with $P_{\text{sat}} = 1$ mW, the calculated minimum pump power is 143.9 mW. This corresponds to a forward pump power of 71.95 mW. Hence, in this bi-directional pumping configuration, the transition between signal induced saturation and ASE self-saturation is when the forward pump power is increased to above 71.95

mW.

III. Self-Saturation

The detailed analysis of self-saturation will be discussed under the effect of input signal with different forward and backward pump power ratios. Figure 4.11 (a) and (b) display the gain and NF of Bi-EDF as a function of input signal power from -40 dBm to 0 dBm (0.1 μ W to 1 mW). From (a), the gain values for bi-directional pumping configurations have similar slope pattern because the Bi-EDF was in a highly saturated condition. The signal gain difference between 250 mW and 300 mW at an input signal power of 0 dBm is 3.74 dB while at low input signal power the difference increases to about -11.99 dB. Due to low signal power and high backward ASE power at high forward pump power add-on, the effect of ASE self-saturation is induced and as a result, reduces the gain of the signal.

The input or output signal dynamic range which is defined as the input/output signal power where the maximum signal gain is reduced by -3 dB (that which is also known as the input/output saturation/compression power [1]) was found to decrease with increased pump power in the output signal dynamic range of -3.05 to 7.84 dBm. The details of the input and output signal dynamic range is presented in Table 4.3.

Table 4.3 Input and output signal dynamic range

Pump Configuration	P_{pump} (mW)	G_{max} (dB)	$P_{\text{sat}}^{\text{in}}$ (dBm)	$P_{\text{sat}}^{\text{out}}$ (dBm)
F50-B150	200	35.95	-36	-3.05
F150-B100	250	47.84	-37	7.84
F150-B150	300	39.67	-30	6.67
F100-B150	250	41.29	-33	5.29
F150-B50	200	44.27	-38	3.27

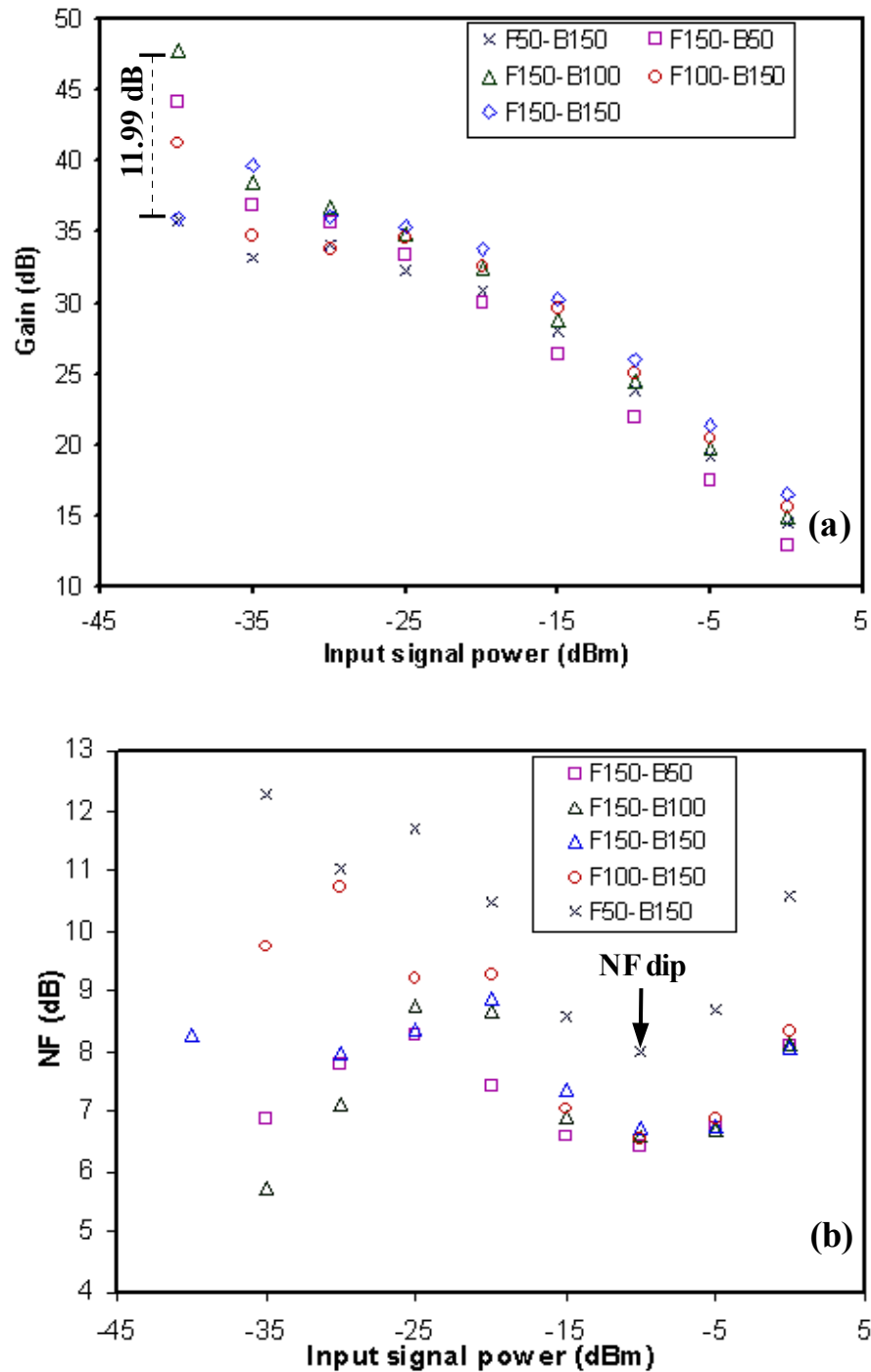


Figure 4.11 The gain (a) and NF (b) as a functions of input signal power at signal wavelength of 1560 nm with bi-directional pump configuration. F### - B\$\$\$: Forward pump = ### mW and backward pump = *** mW for a total pump power of ### + *** mW (bi-directional)

This input/output signal dynamic range is a useful experimental parameter to interpret the minimum input signal power for the optical amplifiers to operate near its peak performance. From the result obtained, Bi-EDF has a very limited dynamic range to operate under maximum output power performance. Consequentially, Bi-EDF is more suitable and effective to operate as a booster amplifier for high output power applications in optical telecommunication networks.

Since the Bi-EDF is fully inverted by the 1480 nm pump, the net effect is that the Bi-EDF falls under the effect of saturation (ASE self- and signal-induced) [2, 24]. This appears in a small signal NF dip at about -10 dBm input signal power, followed by a rapid increase at maximum input signal power as observed in Fig. 4.11 (b). Using the NF value at 0 dBm input signal power as a reference, the depth of the dip was found to be inversely proportional to total pump power and also has a higher dependence on forward pump addition. The depth values are listed in Table 4.4.

Table 4.4 The depths of the NF dip with total pump power

Configuration	Total pump power (mW)	NF at 0 dBm input signal (dB)	NF depth (dB)
F50-B150	200	10.59	2.60
F100-B150	250	8.36	1.82
F150-B150	300	8.05	1.31
F150-B100	250	8.14	1.53
F150-B50	200	8.10	1.67

The detailed characteristics of the NF dip effect [2,24] can be attributed to the influence of self-saturation by backward ASE generated by the forward pump and signal-induced saturation that changes the ASE and pump power distribution along

the fibre. When a sufficiently high input signal is injected into the Bi-EDF (in this case at about -10 dBm), the backward ASE power at the input ends is clamped therefore, suppressing the ASE self-saturation effect. This significantly produces a higher signal inversion at these regions. As the inversion at the input end is high, a lower spontaneous emission factor n_{sp} value is obtained thus lowering the overall NF values. However, with increasing input signal power, the signal-induced saturation become more powerful causing the NF value to degrade. The maximum excess spontaneous noise factor, X for a highly saturated EDFA [1, 2], which depend on G and P_s^{out} and is defined as

$$X = \frac{G \log G}{G - 1} \frac{P_s^{out}}{P_p^{in}} \frac{\lambda_s}{\lambda_p} \left(\frac{\omega_p}{\omega_s} \right)^2 \frac{\sigma_a(\lambda_s)}{\sigma_a(\lambda_p)} \quad (4.10)$$

where $\omega_{s,p}$ are the mode-field radii at signal and pump, respectively. So, the total minimum NF, NF_{min} is given by

$$NF_{min} = 2n_{sp}^{min} (1 + X). \quad (4.11)$$

Using Eq. 4.10 and 4.11, the signal-induced saturation affected the NF_{min} of the Bi-EDF by adding an extra 0.48 dB to a new value of 4.39 dB. For that reason, for low noise optical amplifiers, the signal-induced saturation can restrict the overall optical performance for low noise operation.

IV. Amplification bandwidth

The signal gain and NF as a function of input signal wavelength is shown in Figure. 4.12 (a) and (b). The input signal power is fixed at 0 dBm and signal wavelength is varied from 1532 nm to 1620 nm while the total pump power is varied

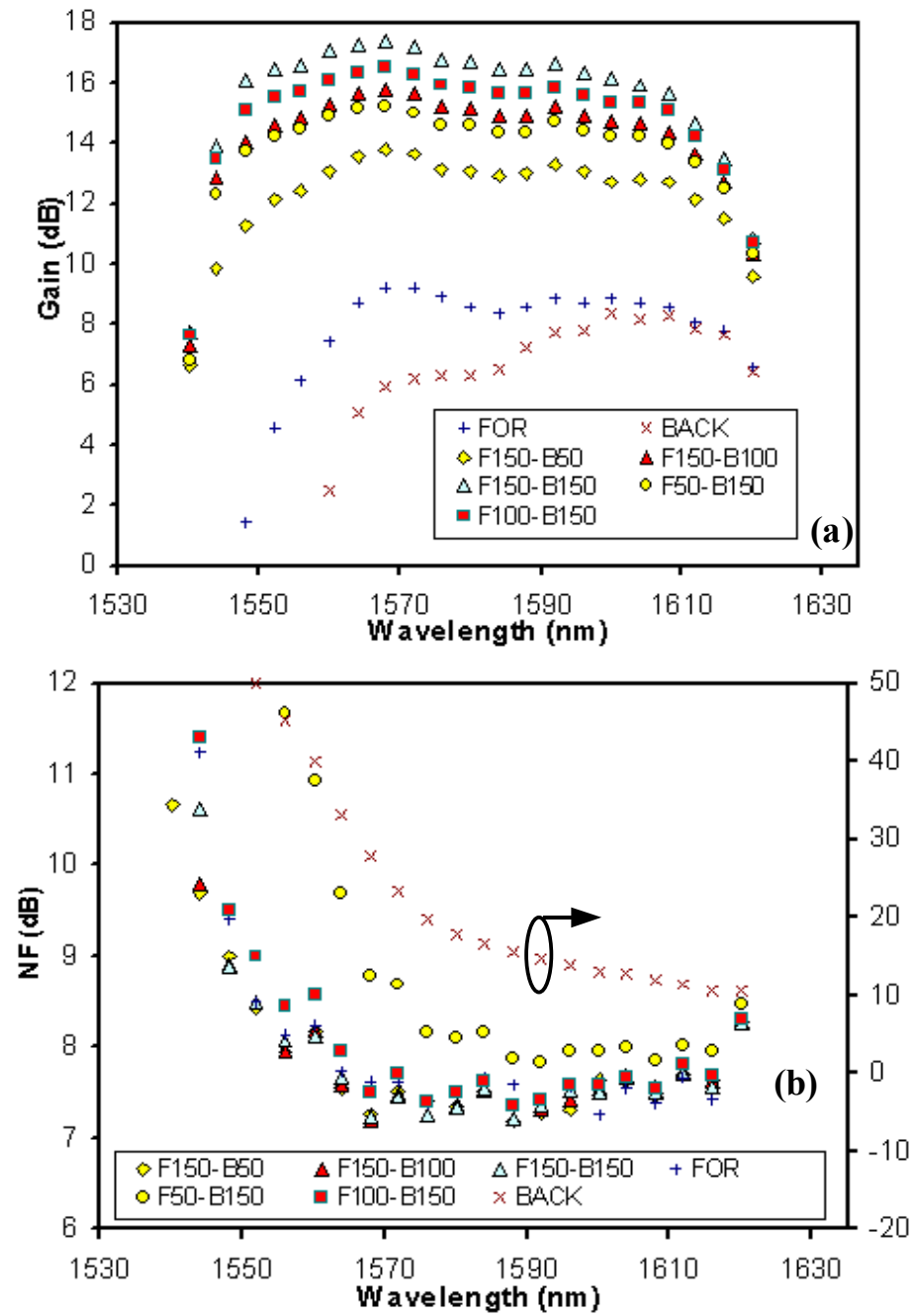


Figure 4.12 The gain (a) and NF (b) at 0 dBm input signal power as a functions of input signal wavelength at different bi-directional pump power configuration. FOR: forward, BACK: backward pumping (uni-directional), F### - B\$\$\$: Forward pump = %%% and backward pump = *** mW for a total pump power of %%% + *** mW (bi-directional)

from 200 to 300 mW under different bi-directional pump combination. The data from the unidirectional pumping is also presented for comparison purposes. From the gain result of the Bi-EDF, the 3 dB signal bandwidth is strongly dependent on pump configuration rather than total pump power. The signal gain and bandwidth when using high backward pump power was found to be higher and wider than the forward pump power at equivalent pump powers. At a maximum pump power of 300 mW, the 3 dB signal bandwidth is about 73 nm, ranging from 1545 to 1618 nm with a maximum signal gain of 17.39 dBm at 1568 nm. This is due to wider Er^{3+} ions emission cross section as characterised in section 3.4 and longer $^4\text{I}_{13/2}$ state (1550 nm) lifetime that enable an efficient longer wavelength stimulated emission [25, 26]. In addition to that, Bi-EDF optical amplifiers have a low effect on signal and pump ESA as reported by H. Hayashi *et. al.* [27] thus, improved the signal gain at longer wavelengths, around the 1600 nm region [1]. The other 3dB amplification bandwidth is listed in Table 4.5.

Table 4.5 3dB bandwidth of Bi-EDF bi-directional pumping

Pump Configuration	3dB bandwidth (nm)
F50-B150	67
F100-B150	71
F150-B150	67
F150-B100	72
F150-B50	72

From the gain profile, the effect of the signal re-absorption for longer signal amplification can be identified as the cause of signal bandwidth reduction when exposed at low total pump power configuration (e. g. at 200 mW). This configuration

produces a 3 dB signal bandwidth of 67 nm from 1547 to 1614 nm. An optimum configuration for maximum signal bandwidth with flat gain can be achieved by utilizing a higher forward pump power (with forward pump power ≥ 100 mW) as the signal gain at shorter wavelengths are more reliant on forward pump powers to boost the final output [28], whereas the backward pumping is used for longer signal amplification.

The NF as a function of input signal wavelength of the Bi-EDF is demonstrated in Figure 4.12 (b), which shows different results when compared to the gain results. At shorter wavelength (C-band) input signals, where the gain is high, the NF was found to be higher but slowly reduces to the lowest values as the input signal shifts to longer wavelengths. The lowest NF value (≈ 7 dB) was found at 1588 nm and a maximum pump power of 300 mW. The reason for this is because under highly saturated conditions, the excited state of the Er^{3+} ions is mostly populated producing high ion population density hence, generates more stimulated and also spontaneous emission [2, 28]. However, from the Bi-EDFA Er^{3+} ions emission cross section property, the shorter wavelength has larger emission coefficient than the longer wavelength. As a result, signals with shorter wavelengths will experience higher NF penalty due to larger shot noise effect from the spontaneous emission than input signals at longer wavelengths.

From the figure, the deviation of the NF values of Bi-EDF was small if the total pump power was above 250 mW where the Bi-EDF is fully inverted by the 1480 nm pump light. At pump powers below 200 mW, only the pumping configuration of F50-B150 has a higher NF penalty. This is because the input signal

experiences higher attenuation due to the Bi-EDF being in an under-pumped condition. Increasing the forward pump power to above 100 mW will increase the Bi-EDF input ends' population inversion therefore, lowering the overall NF penalty.

The QCE of Bi-EDF as a function of input signal wavelength at 0 dBm input signal power is displayed in Figure 4.13 . The QCE have similar line profile as the gain result with a maximum efficiency of 19.76% at 1568 nm input signal. The efficiency at both signal wavelength ends, at 1540 nm and 1620 nm is found to be rather restricted. At shorter input signal wavelengths, the signal-induced and ASE self-saturation [2, 28] are the sources of the restriction while at longer signal wavelength the signal absorption by the ESA effect is the main reason for the low quantum efficiency [28, 29].

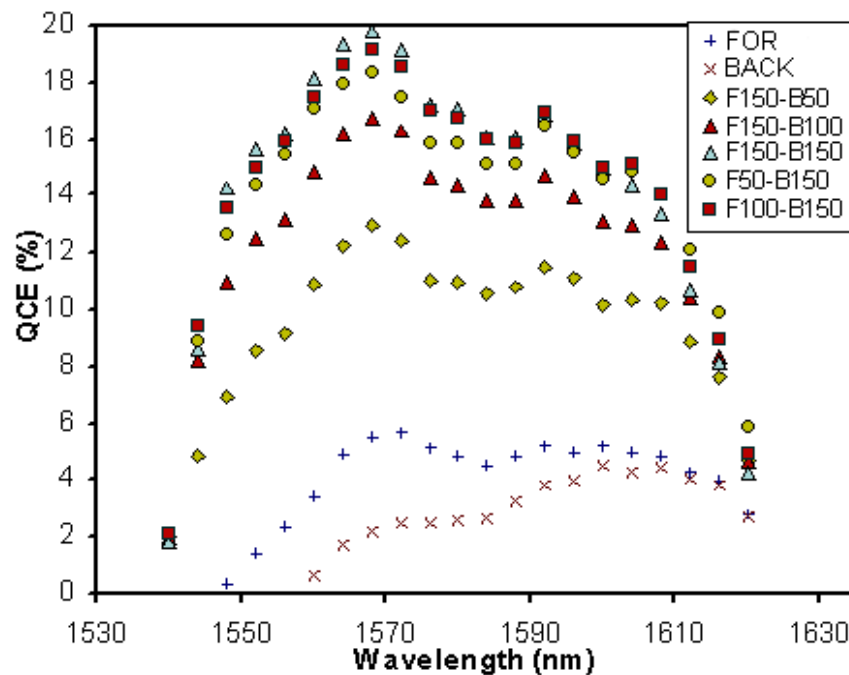


Figure 4.13 The QCE at 0 dBm input signal power as a functions of input signal wavelength at different bi-directional pump configuration. FOR: forward, BACK: backward pumping (uni-directional), F### - B\$\$\$: Forward pump = %%% and backward pump = *** mW for a total pump power of %%% + *** mW (bi-directional)

From the same Figure 4.13, in bi-directional pumping configuration, adding extra power at the Bi-EDF back end was found to be more effective than adding pump power at the input ends. When compared with a total pump of 200 mW (pump configuration of F50+B150 and F100+B50) and 250 mW (pump configuration of F100+B150 and F150+B100), the difference in the QCE was found to be much higher at low pump powers. For better analysis of this two pump power, the efficiency is varied with different forward and backward pump combination at same pump power as revealed in Figure 4.14. With high backward pump power, the QCE of the Bi-EDFA was found higher compared with high forward pump power and decreases with higher pump power. At 200 mW pump power, the maximum QCE difference was about 6.25 % and reduces to about 2.66% at an input signal of 1556

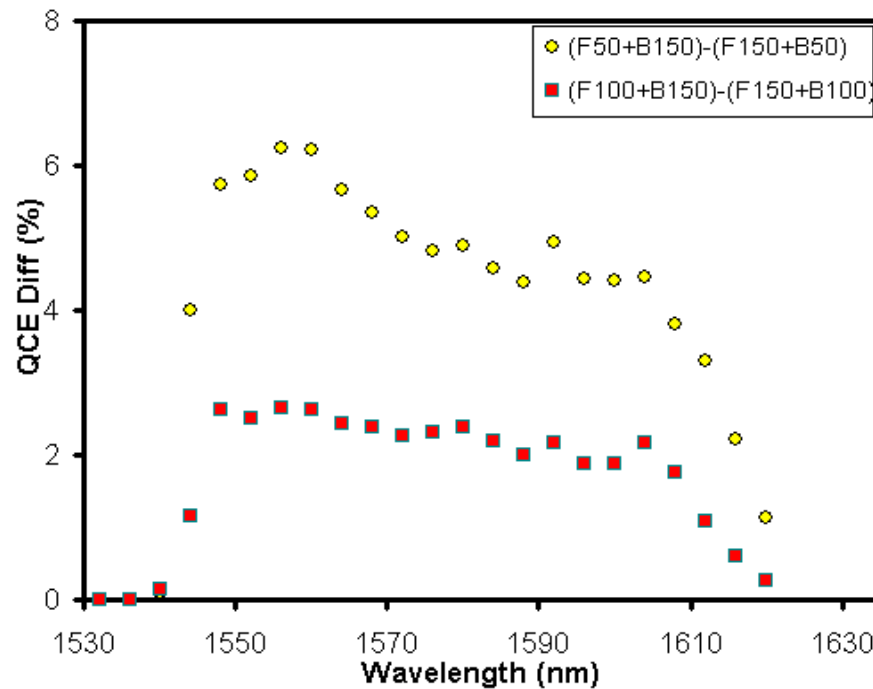


Figure 4.14 The QCE different as the function of input wavelength in bi-directional pump configuration at 200 and 250 mW pump power with different forward and backward pump power.

nm. With increasing total pump power, the population inversion of Er^{3+} ion in Bi-EDF is shifted from moderate to highly populated to its maximum, subsequently initiating a full signal amplification condition. Consequently, the difference in efficiency at highly saturated condition is less significant than in moderately saturated conditions. The most important point is the population inversion of Er^{3+} ion in bi-directional pumping configuration EDFA was maintained by backward pump power as observed by E. Desurvire *et. al.* [1, 12]. In this figure the minimum signal bandwidth for maximum efficiency was about 60 nm between 1548 to 1608 nm.

V. Temperature effect in Bi-EDF optical amplifier

The optical lasing action in a three level laser and optical amplifier system occurs when the excited RE ions in the metastable state decay to the ground state and release its energy in an optical form. The most efficient optical amplifier condition is such that all the decay process correspond to an optical radiative transition. However, for randomly aligned RE ions in glass material, there are other competing transitions that can also depopulate the metastable state and, as a result, reduce the number of stimulated photons emitted. These nonradiative transitions can effectively dissipate energy as heat or vibration (phonons) [1, 2, 27, 29] and there are also some other cases where the energy of pump photons or excited RE ions are re-absorbed to the higher energy level, which is also known as upconversion and ESA [1, 27, 29, 30].

$$\sigma_{\text{em}}(\nu) = \sigma_{\text{ab}}(\nu) \exp\left(-\frac{h(\nu - \varepsilon)}{k_B T}\right). \quad (4.12)$$

The glass host ligand field distributes Er^{3+} ions randomly and prompts multiple Stark level manifolds. From section 3.4, the transition between these Stark level manifolds is treated using the McCumber theory from the generalization of Einstein's A and B coefficients, which are temperature dependent as explicated in Eq. 3.9 (see Eq. 4.12). The pump absorption and signal emission cross section characteristics of an RE in the glass host shifts the spectral position, bandwidth and distribution with changing temperatures [2, 30, 31]. Therefore, when the EDF temperature increase / decrease, this makes a combined effect on pump and signal cross sections consequently produces a net change that influences the maximum signal output power and bandwidth.

In low phonon energy glass such as bismuth, phosphate and fluoride -based glass [28, 29, 30], multiphonon absorption can effectively reduce the radiative emission of Er^{3+} ion at the 1550 nm region. Using phonon and mutiphonon absorption coefficients, Eq. 3.1 and 3.2, the relationship between the nonradiative emission rate $^{\text{NR}}W$ and phonon absorption is [31]

$$\frac{1}{\tau_{\text{nr}}} = W_0 \left(1 - e^{-h\nu/kT}\right)^p. \quad (4.13)$$

Therefore any changes in fibre temperature will affect the Er^{3+} ions energy level nonradiative emission rates that produces net/combined changes in optical amplifier efficiency and performance.

The characterisation of the optical amplifier performance is examined between fibre temperatures of 0 °C to 63 °C to simulate the effect of temperature variations. The Bi-EDF was enclosed in an aluminium foil and placed in both a cool

and hot chamber to simulate these conditions. The casing temperature was monitored using a K-type thermocouple that is connected to a Fluke 53 II Digital thermometer. The temperature of the casing was controlled and maintained to enable the Bi-EDF to reach thermal equilibrium before and during the measurement of the optical gain and NF. The experimental set-up is illustrated in Figure 4.15. The input signal power was fixed at 0 dBm and its wavelength varied from 1520 nm to 1620 nm for a pump power of 300 mW.

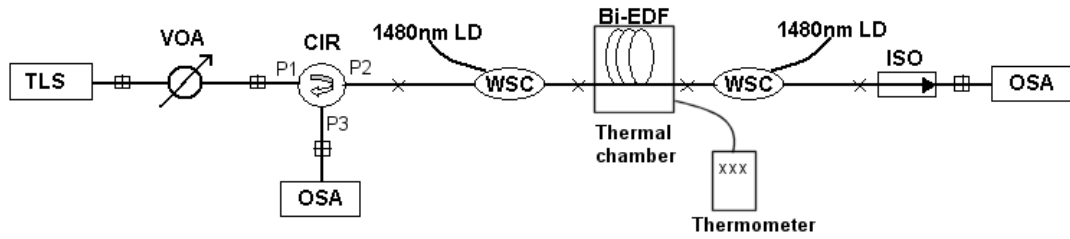


Figure 4.15 The experimental set-up to measure the effect of fibre temperature, TLS:Tunable Laser Source, VOA:Variable Optical Attenuator, CIR: Circulator, LD:Laser Diode, ISO:Isolator, OSA:Optical Spectrum Analyser

Figure 4.16 (a) and (b) describe the gain and NF behaviour of Bi-EDF with temperatures ranging from 0 °C to 63 °C for input wavelengths from 1520 nm to 1620 nm. From the emission cross sections calculated using the McCumber theory, the temperature effect is examined at the Er^{3+} ion emission peak. By using a Bi-EDF of length 215.3 cm, the gain peak is shifted from 1530 nm region to 1568 nm due to signal re-absorption for longer L-band signal amplification. As the temperature of the fibre increases, both the gain and NF values and profile were altered significantly especially at shorter input wavelengths [32, 33]. At low fibre temperatures, the signal gain of the Bi-EDF was found to be higher than the corresponding gain values at higher fibre temperatures.

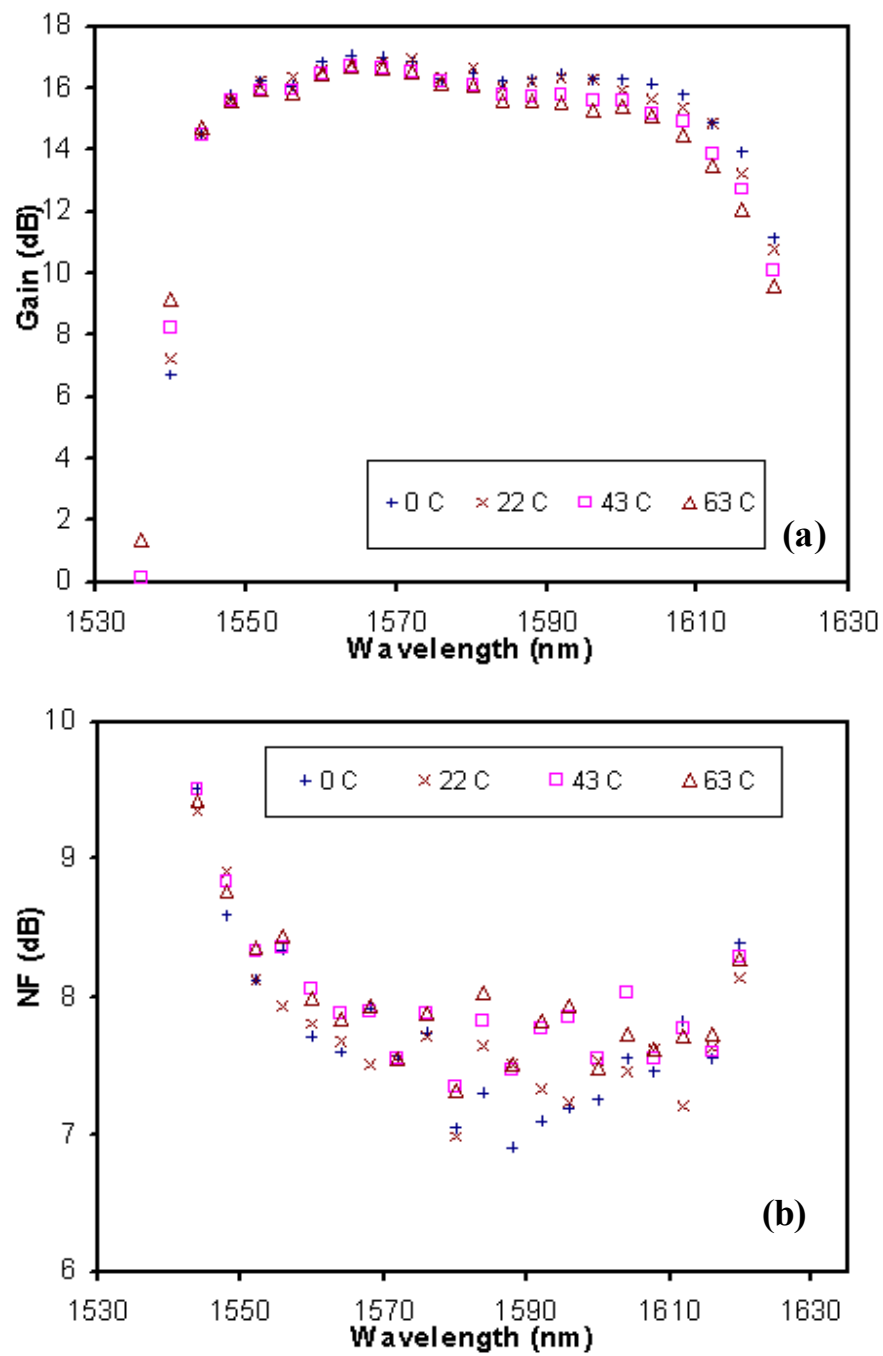


Figure 4.16 The gain (a) and the NF (b) at 0 dBm input signal power as a functions of input signal wavelength at different temperature.

A similar improvement was also found with the NF presenting a lower penalty at low fibre temperature. This result revealed that the population inversion of the Bi-EDF was higher and is able to run most efficiently at low temperatures. The details of the gain and NF differences for 0 °C ,22 °C , 43 °C and 63 °C are shown in Figure 4.17.

The maximum gain, ΔG and NF fluctuations, ΔNF were located at the cross section peak of Er^{3+} ions emission of 1532 nm, with $\Delta G = 11.06$ dB and $\Delta NF = 17.97$ dB at high temperature difference of 63 °C. The variations at a gain peak of 1568 nm is rather small, with $\Delta G = 0.40$ dB and $\Delta NF = 0.02$ dB for NF penalty. At low temperature difference of (0-22 °C) , the ΔG and ΔNF fluctuations are small, with maximum values of 5.07 dB for gain and 10.15 dB for NF.

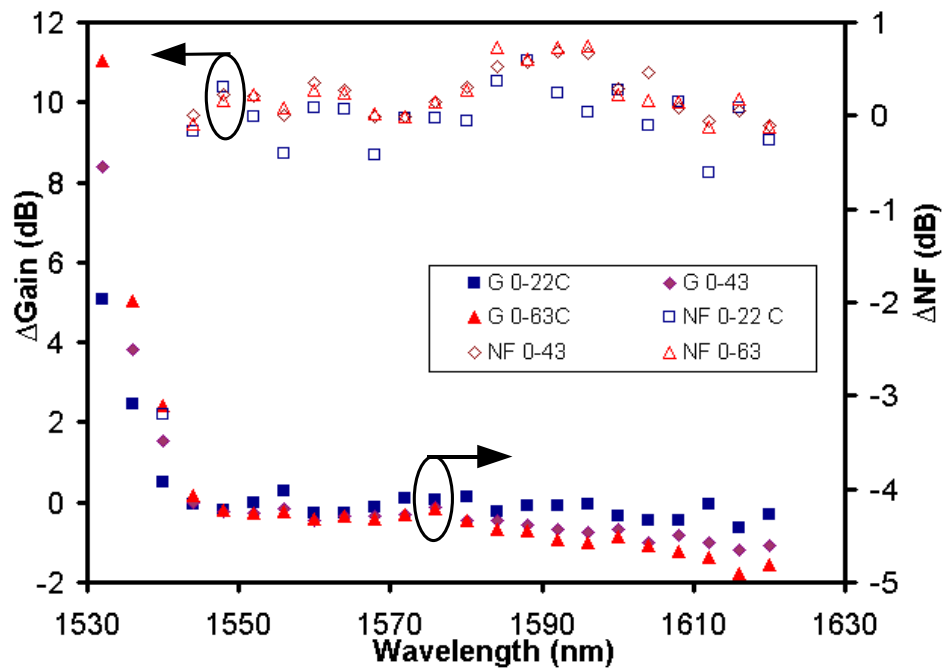


Figure 4.17 The gain and NF different at 0 °C and 63 °C as a functions of input signal wavelength.

At low temperatures, the Stark sublevels are more dense due to small Boltzmann thermal distribution [32], causing the upper Stark sublevels of the ground and metastable states to depopulate easier [33]. As a result, the pump absorption rate increases and produces intense fluorescence emissions at shorter input wavelength [32-34]. Besides that, the decreased number of thermally activated phonons causes low pump photon energy loss to glass host phonons and this subsequently, reduces the nonradiative emission of Er^{3+} ions. Therefore, these enhancements increase the input signal gain at shorter wavelengths.

To study the effect of the QCE with the fibre temperature, the slope coefficient of QCE and temperature was calculated as,

$$\text{QCE}_{\text{temp}} (\% / ^\circ\text{C}) = \frac{\Delta_{\text{QCE}}}{\Delta_{\text{temp}}} \quad (4.14)$$

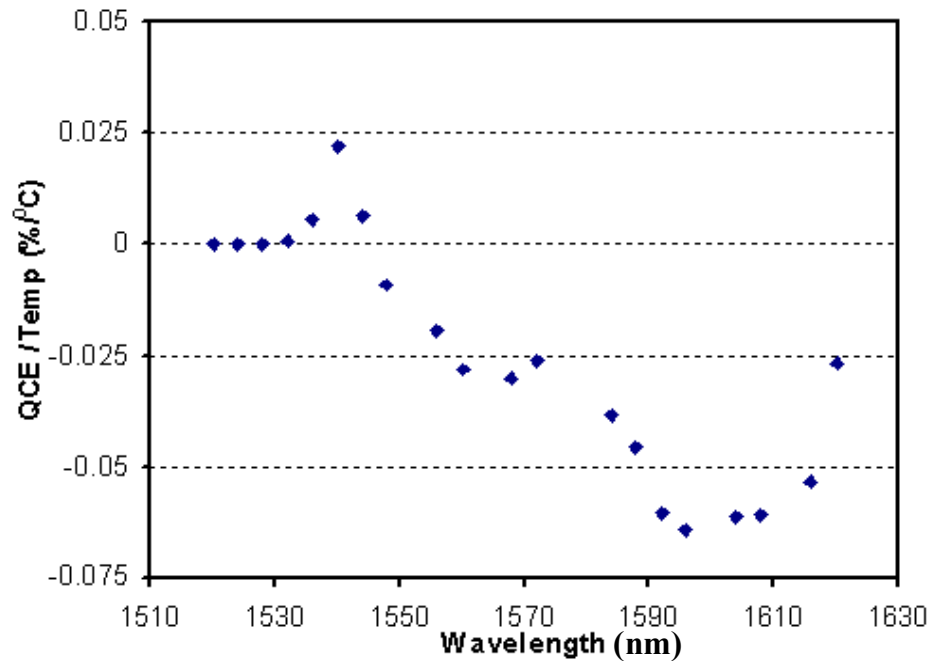


Figure 4.18 The QCE / temperature (slope coefficient) as a functions of input signal wavelength.

The results of Bi-EDF QCE/temperature versus wavelength is shown in Figure 4.17. At the Er^{3+} ions emission cross section peak, Bi-EDF exhibits a positive coefficient while longer input signals exhibits a negative coefficient. The reason for different coefficient polarities are the different signal amplification conditions whereby the longer band signal amplification is largely dependent on re-absorption of ASE at Er^{3+} ions emission peak [1]. The lowest coefficient (-0.06) was found at an input signal of 1596 nm. At longer input wavelengths at the 1610 nm region (where the ESA effect is most significant [28, 29]), higher fibre ambient temperature enhances the efficiency coefficient. When the fibre temperature is higher, the Er^{3+} ions thermal distribution increases causing the Stark sublevels to widen. As a result, the excited Er^{3+} ions at lower sublevel metastable states decay to the upper sublevel of the ground state with fast nonradiative and radiative processes. This causes the population density at metastable state to be lower and this reduces the ESA absorption significantly.

REFERENCES

- [1] E. Desurvire, "*Erbium-doped fiber amplifiers: Principle and Application*," John Wiley & Son Inc., New York, 1994.
- [2] Seo Yeon Park, Hyang Kyun Kim, "*Efficient and low-noise operation in gain-flattened 1580 nm band EDFA*", OFC/IOOC 1999 Technical Digest, Vol. 2, pp. 123, 1999
- [3] H. Ono, M. Yamada, Y. Ohishi, "*Signal output characteristics of 1.58 μ m band Er^{3+} -doped fibre amplifiers with cascaded configurations*", Electron. Lett. Vol. 34, No. 15, pp. 1513, 1998
- [4] K. Rottwitt, J. H. Povlsen, A. Bjarklev, O. Lumholt, B. Pedersen, T. Rasmussen, "*Optimum signal wavelength for a distributed erbium-doped fiber amplifier*", IEEE Photonics. Tech. Lett., Vol. 4, No. 7, 1992, pp. 714
- [5] R. Sommer, R. M. Fortenberry, B. Flintham, P. C. Johnson, "*Multiple filter functions integrated into multi-port GFF components*", Conference on Optical Fiber Communications and National Fiber Optic Engineers Conference, OFC/NFOEC 2007, 2007, pp.1
- [6] R. B. Sargent, "*Recent advances in thin films filters*", Optical Fiber Communication Conference, 2004, OFC 2004, Vol. 1, 2004, pp. 23
- [7] Y. B. Lu, P. L. Chu, A. Alphones, P. Shum, "*A 105-nm ultrawide-band gain-flattened amplifier combining C- and L- band Dual-core EDFAs in a parallel configuration*", IEEE Photonics. Tech. Lett., Vol 16, No. 7, 2004, pp. 1640
- [8] Y. B. Lu, P. L. Chu, "*Gain flattening by using dual-core fiber in erbium-*

- doped fiber amplifier*”, IEEE Photonics. Tech. Lett., Vol. 12, no. 12, 2000, pp. 1616
- [9] D. M. Baney, P. Gallion, R. S. Tucker, “*Theory and measurement techniques for the noise figure of optical amplifiers*,” Opt. Fib. Tech., Vol. 6, 2000, pp. 122
- [10] D. Baney, C. Hentschel, J. Dupre, “*Optical fiber amplifiers - measurement of gain and noise figure*”, HP Lightwave Symposium, 1993.
- [11] E. Desurvire, M. Zimgibl, H. M. Presby, D. DiGiovanni, “*Characterization and modelling of amplified spontaneous emission in unsaturated erbium-doped fiber amplifiers*”, IEEE Photonics. Tech. Lett., Vol. 3, No. 2, 1991, pp.127
- [12] E. Desurvire, “*Analysis of gain difference between forward- and backward-pumped erbium-doped fiber amplifiers in saturation regime*”, IEEE Photonics. Tech. Lett., Vol. 4, No. 7, 1993, pp.625
- [13] R. I. Laming, J. E. Townsend, D. N. Payne, F. Meli, G. Grasso, E. J. Tarbox, “*High-power erbium-doped-fiber amplifiers operating in the saturated regime*”, IEEE Photonics. Technol. Lett., Vol. 3, No. 3, pp. 253, 1991
- [14] J. F. Massicott, R. Wyatt, B. J. Ainslie, S. P. Craig-ryan, “*Efficient, high power, high gain, Er^{3+} doped silica fibre amplifier*”, Electron. Lett., Vol. 26, No. 14, 1990, pp. 1038
- [15] Piotr Myslinski, Dung Nguyen, Jacek Chrostowski, “*Effects of concentration on the performance of erbium-doped fiber amplifiers*”, Jour. Light. Technol., Vol. 15, No. 1, 1997, pp.112

- [16] F. W. Willems, J. C. van der Plaats, "*Experimental demonstration of noise figure reduction caused by nonlinear photon statistics of saturated EDFA's*", IEEE Photonics. Technol. Lett., Vol. 7, No.5, 1995, pp. 488
- [17] E. Desurvire, "*Analysis of distributed erbium-doped fiber amplifiers with fiber background loss*," IEEE Photonics. Tech. Lett., Vol. 3, No. 7, 1991, pp.625
- [18] E. Desurvire, "*Spectral noise figure of Er^{3+} -doped fiber amplifiers*", IEEE Photonics. Tech. Lett., vol. 2, No. 3, 1990, pp. 208
- [19] C. R. Giles, E. Desurvire, "*Modelling erbium-doped fiber amplifiers*", Lightwave Technol., Vol. 9, No. 2, 1991, pp. 271
- [20] Y. Kimura, K. Suzuki, M. Nakazawa, "*Noise figure characteristics of Er^{3+} -doped fibre amplifier pumped in 0.8 μm band*", Electron. Lett., Vol. 27, No. 2, 1991, pp. 146
- [21] R. G. Smart, J. L. Zyskind, J. W. Sulhoff, D. J. DiGiovanni, "*An investigations of the noise figure and conversion efficiency of 0.98 μm pumped erbium-doped fiber amplifiers under saturated conditions*", IEEE Photonics Technol. Lett., Vol. 4, No. 11, pp. 1291, 1992
- [22] B. Pedersen, M. L. Dakss, and W. J. Miniscalco, "*Conversion efficiency and noise in erbium-doped fiber power amplifiers*," in Optical Fiber Amplifiers and Their Applications, OSA Technical Digest Series, Vol. 13, 1991
- [23] F. A. Flood, "*Gain saturation behaviour in L-band*", IEEE Photonics. Technol. Lett. Vol. 12, No. 9, 2000, pp. 1156
- [24] J. F. Marcerou, H. Fevrier, J. Herve, J. Auge, "*Noise characteristics of the*

- EDFA in gain saturation regions*", Proc. Tropical Meeting of Optical Amplifiers and Applications, Optical Society of America (OSA), paper ThE1, p. 162, 1991
- [25] Jianhu Yang, Shixun Dai, Nengli Dai, Shiqing Xu, Lei Wen, Lili Hu, Zhonghong Jiang, "*Effect of Bi_2O_3 on the spectroscopic properties of erbium-doped bismuth silicate glasses*", J. Opt. Soc. Am. B., Vol 20, No. 5, 2003, pp. 810
- [26] Yongzheng Fang, Lili Hu, Meisong Liao, Lei Wen, "*Effect of bismuth oxide introduction on spectroscopic properties of $\text{Er}^{3+}/\text{Yb}^{3+}$ co-doped aluminophosphate glasses*", Jour. Alloys and Compd, Vol. 457, 2008, pp. 19-23
- [27] Hideaki Hayashi, Setsuhisa Tanabe, Naoki Sugimoto, "*Quantitative analysis of optical power budget of bismuth oxide-based erbium-doped fiber*", Jour. Lumin., Vol. 128, 2008, pp. 333
- [28] Tsair-Chun Liang, Yung-Kuang Chen, Jing-Hong Su, Weng-Hung Tzeng, Chiek Hu, Ying-Tso Lin, Yin-Chieh Lai, "*Optimum configuration and design of 1480 nm pumped L-band gain-flattened EDFA using conventional erbium-doped fiber*", Opt. Comm., Vol. 183, 2000, pp. 51
- [29] James A. Harrington, "*Infrared fibers and their application*", SPIE Press, 2004
- [30] M. Poonau, D. R. Gamelin, S. R. Luthi, H. U. Gudel, "*Power dependence of upconversion luminescence in lanthanide and transition-metal-ion system*", Phys. Rev. B, Vol. 61, No. 5, 2000, pp.3337

- [31] R. Reisfeld, Y. Eckstein, “*Dependence of spontaneous emission and nonradiative relaxations of Tm^{3+} and Er^{3+} on glass host and temperature*”, Jour. of Chem. Phys, Vol. 63, No. 9, 1975, pp. 4001
- [32] E. Desurvire, J. R. Simpson, P. C. Becker, “*High-gain erbium-doped traveling wave fiber amplifier*”, Optics Lett., Vol 12, No. 11, 1987, pp. 888
- [33] Felton A. Flood, “*Comparison of temperature dependence in C-band and L-band EDFAs*”, Jour. Light. Technol., Vol. 19, No. 4, 2001, pp. 527
- [34] C. A. Miller, T. J. Whitley, S. C. Fleming, “*Thermal properties of an erbium-doped fibre amplifier*”, IEE Proceeding, Vol. 137, Pt. J, No. 3, 1990, pp. 155

CHAPTER 5

BISMUTH-BASED EDFA IN WDM OPTICAL NETWORK

5.1 Introduction

Transmission of multiple data in WDM optical network simultaneously has many advantages for higher data capacity telecommunication system. The data capacity of WDM can be increased by employing optical filter (e.g. Interference filters, diffraction grating filters, or prism filter [1]) in single optical fibre link to combine multiple data channels that correspond to different signal wavelengths. It is capable to support higher data rate at lower cost and allow for more efficient data load and distribution [1]. Also with the aids of optical amplifiers to boost the signal strength, signal transmission is expanded to maximum distance.

In this chapter, optical performance characterisation of bismuth-based EDFA for WDM optical networks is discussed. The measurement of gain flatness, gain slope, gain clamping effect and channel spacing were done by using 4 signal wavelengths. From the results, the overall performance of bismuth-based EDFA for WDM optical networks is evaluated and discussed.

5.2 Gain Equalisation in WDM Optical Systems

The WDM optical network implements a multiple signal channel that span across the amplification bandwidths. The signal channel is equally separated and contains as many as 1021 signal channels [1] that cover from C-band to L-band

region. Some of the new WDM optical systems that are combined with Raman optical amplifier have very close signal channel spacing, which is about 50 GHz (≈ 0.4 nm) to support the demands of higher data capacity [2]. In order for the EDFA to be used as an amplification device, it must have equal signal gain at every signal channel to balance the output signal at transmitter ends. As the EDFA gain profile is not spectrally uniform, the investigation of this signal equalisation (flatness) in WDM optical network is crucial. This parameter is important for WDM optical network systems to achieve error free detections (low bit-error rate) and low Composite Second Order (CSO) distortion in analog systems [3]. There are several techniques that have been used for gain equalisation in WDM optical networks such as gain clamping method, incorporating passive or active filter to flatten the gain profile, cascading EDFAs with different gain profile, spatial hole burning method and adjustment of input signal powers [3].

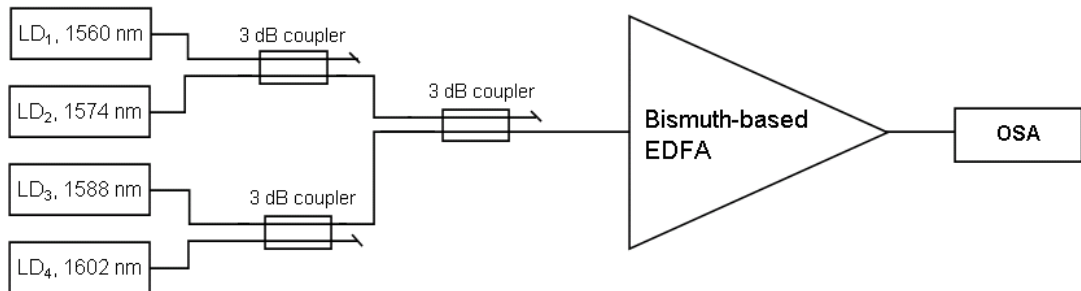


Figure 5.1 Schematic for 4 channel WDM optical system, LD: Laser diode, OSA: Optical Spectrum Analyser

The gain equalisation measurement was done in an experimental set-up depicted in Figure 5.1. In this figure, the configuration of bismuth-based EDFA is similar to bi-directional configuration that was shown in previous Figure 4.1. The

pump power of the bismuth-based EDFA was set to 150 mW in both forward and backward direction, giving a total pump power of 300 mW. The signal wavelengths of the WDM channel were 1560 nm, 1574 nm, 1588 nm and 1602 nm covering both C- and L-band regions with wavelength spacing between channels of 14 nm combined by using 3 units of 3-dB couplers. The WDM signals were limited to only 4 channels due to the limitation of our equipment in the laboratory. Each input signal power was arranged at -5 dBm, producing a total input power of 1 dBm (1.26 mW) to the bismuth-based EDFA. The measurement of output signal gain, NF and Signal-to-Noise (SNR) was performed by OSA built-in functions.

The results obtained for the 4 channel WDM testing system are demonstrated in Figure 5.2. From the figure, the highest signal gain of about 16.85 dB was obtained at wavelength of 1602 nm and it corresponds to an output power of 11.48 dBm. However, the lowest signal gain detected was about 13.65 dB for the input wavelength of 1560 nm that corresponds to 3.2 dB gain fluctuation. When comparing the results of the 4 channel WDM signal with a single signal gain profile in Figure 4.12 (a), the input signal at shorter wavelength (1560 nm) experienced higher gain than input signal at longer wavelength (1602 nm) although the shorter signal wavelength has higher signal gain than longer signal wavelength. These results indicate that when Bi-EDFA was incorporated into WDM optical networks, shorter input signal wavelength experiences greater signal-induced saturation effect. This effect is also known as signal cross-saturation where the saturation effect was produced by other signal wavelengths [1]. Cross-saturation occurs as the signal amplification in the EDFA was done with the same excited Er^{3+} ions and since most

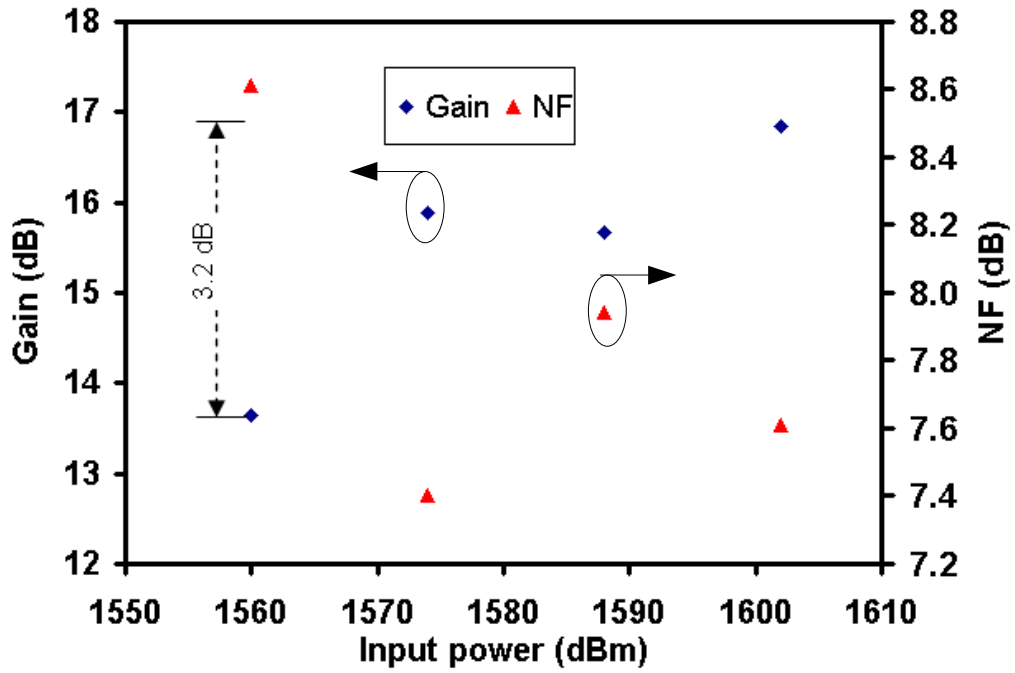


Figure 5.2 Signal gain and NF for the 4 channel WDM testing system.

of its energy was dominated by the high power saturating signal, the other signal could be stimulating lesser Er^{3+} ions in the excited state and thus yields lower gain [1]. At shorter wavelength in multichannel EDFA, the excited ions population density is lower thus making the signal suffer greater gain fluctuation and vice-versa with population density at longer wavelength. The low ion population density at shorter wavelength is due to signal re-absorption for longer signal amplification (L-band region). Consequently, these cause the shorter input signal wavelength to experience higher NF value of about 8.6 dB as shown in the result. As the signal shifts to longer wavelength, the gain and NF were improved as the effect of gain saturation slowly diminishes.

The output signal SNR and the signal noise level are illustrated in Figure 5.3. The SNR of an optical amplifier is defined as the ratio between signal peak power and noise power level. It was measured directly by an Ando AQ6317C OSA by using ASE level linear interpolation method [4] (see section 4.2.2 (Gain and NF)). SNR measurements characterised the electrical current noise levels generated by the optical amplifier at the receiver photodiode. It is given as [3, 5]

$$\text{SNR} = \frac{G^2 S_{\text{out}}}{N + N'} \quad , \quad (5.1)$$

where G is the gain of the system, S_{out} is the electrical signal output power, N is the electrical noise power level of the photodiode and N' is the optical noise (shot-noise and ASE beat noise) generated from the optical amplifier that was converted by the photodiode into an additional noise background.

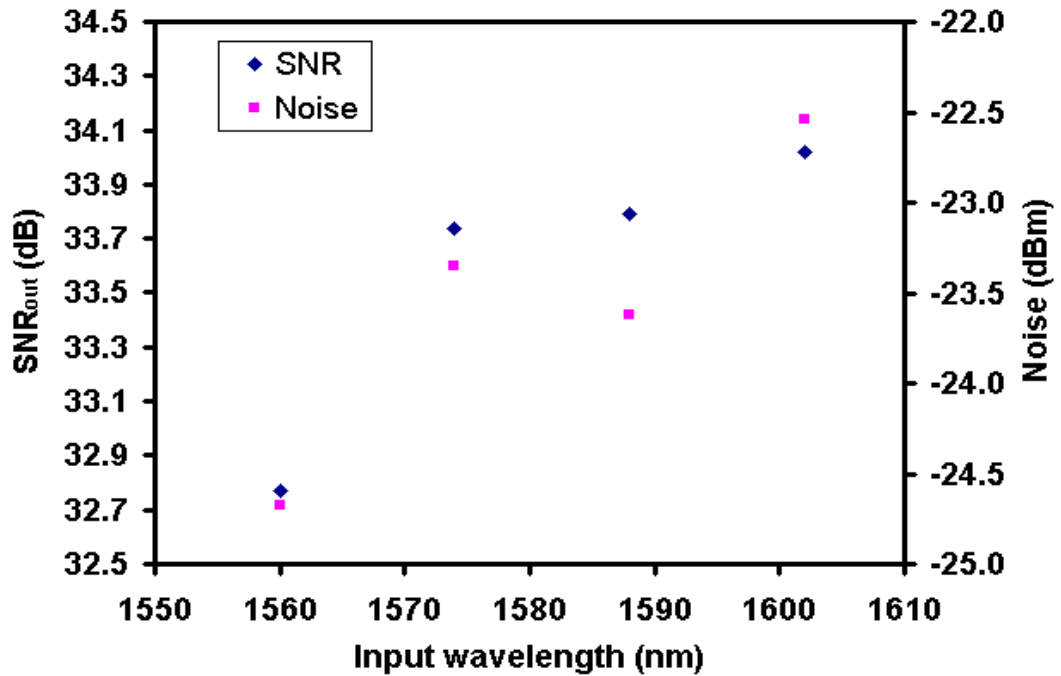
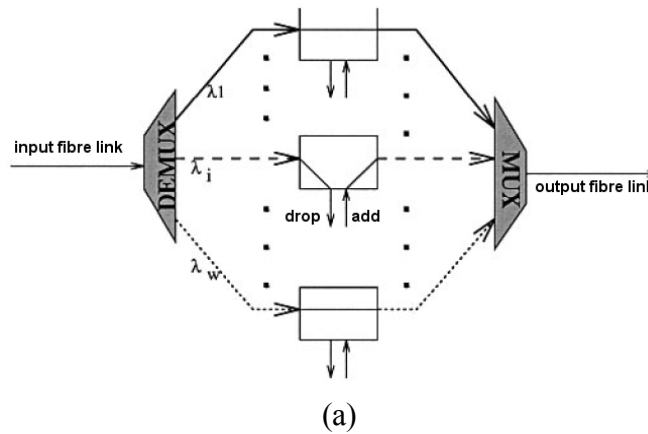


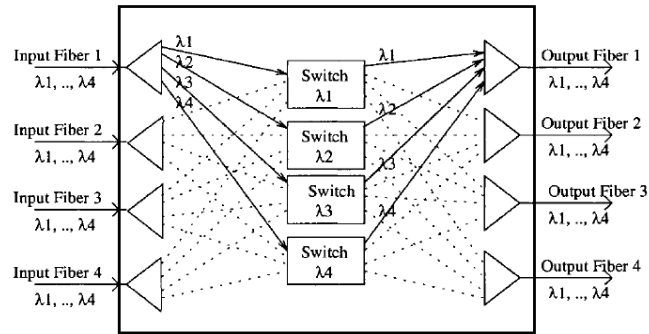
Figure 5.3 The signal SNR and noise level for the 4 channel WDM testing system.

From the result, the output SNR of Bi-EDF has a similar slope with signal gain due to its dependence on the signal gain as represented by Eq. (5.1). The highest SNR_{out} was found to be 34.02 dB at wavelength of 1602 nm. Input signals at longer wavelengths have better SNR_{out} because the ASE power level at this region was lower than that at shorter wavelengths. However, the noise level of the Bi-EDF optical amplifier was found to be higher at longer signal wavelength. This was because at a longer wavelength, the noise level of the Bi-EDF which originated from the shot-noise and ASE beat noise was largely affected by the signal ESA process [3, 6] that came from transition of Er^{3+} ion energy level $^4I_{13/2}$ to the $^4I_{9/2}$.

The gain equalisation of an optical amplifier also depends on total signal input power. In the case of second generation WDM optical systems that utilise channel add-drop or cross-connect scheme [3, 7], the signal number and direction are reconfigurable depending on data load and demands. The diagram of wavelength Add/Drop Multiplexer and 4x4 Active Cross-connect Switch is illustrated in Figure 5.4.

In order to study the signal channel add/drop effect in Bi-EDFA, optical gain and NF were measured in two experiments. In the first assessment, the input signal





(b)

Figure 5.4 Wavelength Add/Drop Multiplexer (WADM) (a) and 4x4 Active Cross-connects Switch (b)

channel was turned off one after the other while maintaining the total input signal to 0.95 mW to simulate a channel drop. In the second assessment, the input signal power at a wavelength of 1560 nm was varied from -30 to -5 dBm to simulate channel add. The results obtained are demonstrated in Figure 5.5.

Figure 5.5 (a) indicates the signal gain at an input signal of 1560 nm when one of the other three signal channels was turned off. The signal gain at -5 dBm input power was fluctuated to a maximum of +3.14 dB to a single channel drop. The gain fluctuation was found to be higher when the signal channel at 1602 nm is turned off because of long signal wavelength re-absorption property [3]. While other signal channels at 1574 nm and 1588 nm exhibit lower gain fluctuation that originates from the gain saturation effect [3, 8]. As a result, the signal channel at 1560 nm experiences an extra gain when the signal at 1602 nm is turned off.

In the second evaluation, when the signal channel was added into Bi-EDF by adjusting the input signal power at 1560 nm from -30 dBm to -5 dBm, the gain decreases slowly from 15.47 dB to 13.56 dB thereby producing a gain fluctuation of

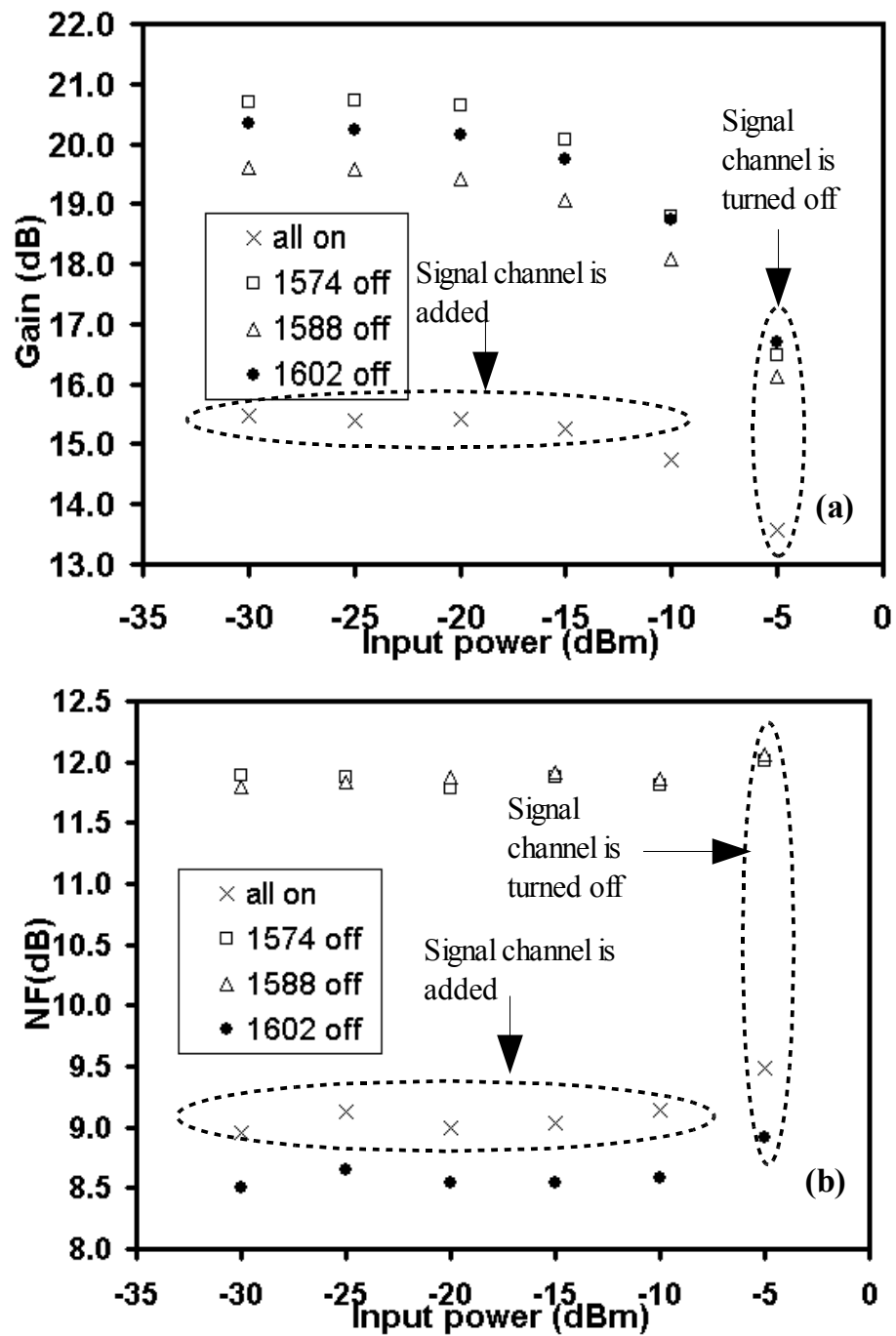


Figure 5.5 Gain and NF at 1560 nm when another signal channel is dropped and added into the Bi-EDFA

1.91 dB. The addition of an extra signal channel into the EDFA has modified its steady-state population inversion to a new level. This reduced the signal gain and increased the overall NF as elucidated by M. Zirngibl *et. al.* [9, 10]. This effect that is known as gain saturation has large influences on EDFA signal gain under the signal channel addition. The impact of gain saturation on Bi-EDFA is presented in Figure 5.5 (b). From the results, the NF at 1560 nm was found to increase to a maximum of 2.88 dB when the signal channel at 1574 nm and 1588 nm were turned off. However, when the signal channel at 1602 nm is turned off, the NF was improved to 8.92 dB. The improvement was expected from the reduction of ESA effect in Bi-EDFA. This result indicates that Bi-EDFA in 4 channels WDM optical system were affected by the ESA and gain saturation effect that conforms the Er^{3+} ions homogeneity property.

The gain variation across the signal channel is defined by the gain slope. The

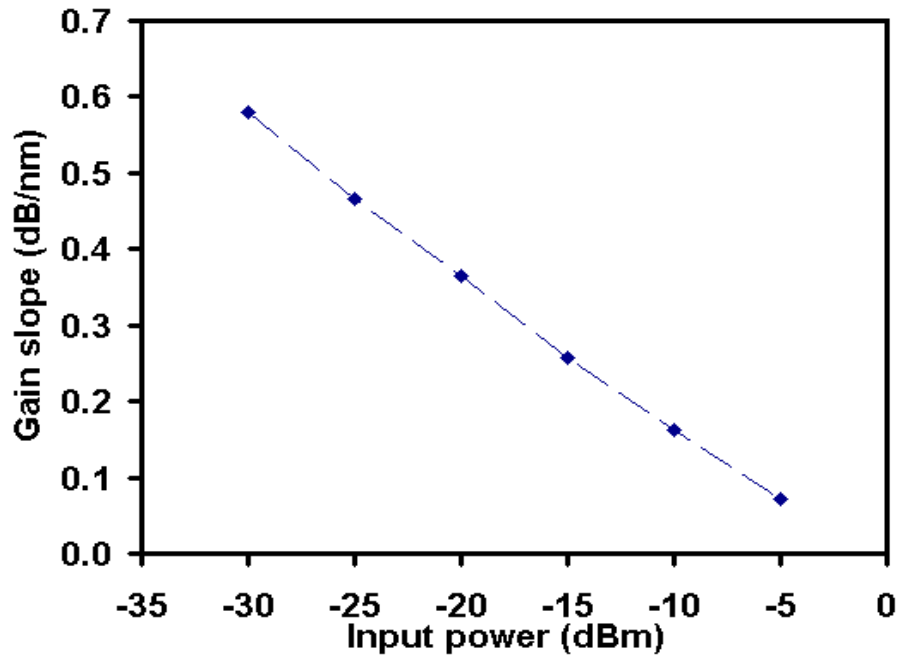


Figure 5.6 Gain slope between 4 signal channels when the input power at 1560 nm was varied from -5 to -30 dBm.

gain slope for 4 channels Bi-EDFA is depicted in Figure 5.6. For a gain bandwidth of 42 nm (from 1560 to 1602 nm), and an input signal channel of 1560 nm, the slope fell from 0.58 dB/nm to 0.07 dB/nm with the signal power increment from -30 to -5 dBm. This variation was originated from different gain saturation condition and signal re-absorption when adding a signal [3] thus, modifying the gain slope between signal channel.

I. Gain Saturation

The effect of saturation to the signal output power in Bi-EDFA discussed in section 4.2.2 was only limited to ASE influence. In reality, the saturation effect was initiated by other factors that reduce the population inversion of the EDF, thereby limiting the scaling of high output power. In a highly saturated condition, the output signal of an EDFA can be saturated when the stimulated emission that is induced by the high power signal (laser or ASE) becomes comparable (or competing) to the pumping rate [3]. The saturating signal in the case of multi-wavelength WDM optical system can originate from the signal itself or laser oscillation [9, 11, 12]. Laser oscillation occurs when the EDFA gain is high enough to compensate for the return loss of any reflecting element in the path of the ASE signal. This ASE signal is then reflected back and forth into the EDF, which operates as a laser oscillation.

Gain saturation in Bi-EDFA was characterised by monitoring the gain variation at signal channel with different saturating signal wavelengths and output powers. Signal gain and NF at each signal channel that were measured with signal input power at wavelength of 1560 nm was varied from -30 to -5 dBm. The input

signal power for other signal channels were arranged to -5 dBm. The result of the measurement is given in Figure 5.7.

The gain variation of Bi-EDFA was limited to a maximum value of 0.92 dB at 1574 nm (shorter wavelength region) as indicated in Figure 5.7 (a). At longer wavelength, the gain variation was as low as 0.54 nm. This result conformed the previous one where the shorter signal channel experienced a higher gain saturation effect in Bi-EDFA. The NF of Bi-EDFA in Figure 5.7 (b) also show good performance, producing reduction values where the input signal channel at 1588 nm experienced an improvement at almost 0.68 dB. As discussed in the previous result, the NF improvement at shorter signal channel was due to low gain compression by reduction of gain saturation effect. In contrast, at longer signal channel, the improvement was due to low ESA effect that transfer the energy of excited Er^{3+} ions to a still higher excited state.

The signal gain at -5dBm input channel of 1560 nm with different saturating signal powers from -25 to 9.9 dBm is presented in Figure 5.8. The saturating signal wavelength were adjusted to 1581, 1582, 1584 and 1587 nm. Due to the fact that Bi-EDFA was operating in a fully saturated condition, the signal gain fluctuation was smaller when adjusting the saturating signal wavelength compared to the signal power of the saturating signal itself. This result indicated that the gain saturation effect was largely dependant on signal power rather than the signal wavelength. A small signal gain fluctuation was produced because at room temperature (that have fast intra-manifold thermalization effect [3, 13]) the EDFA gain profile was dominated by homogeneous broadening effect [3, 13, 14] where in this case the

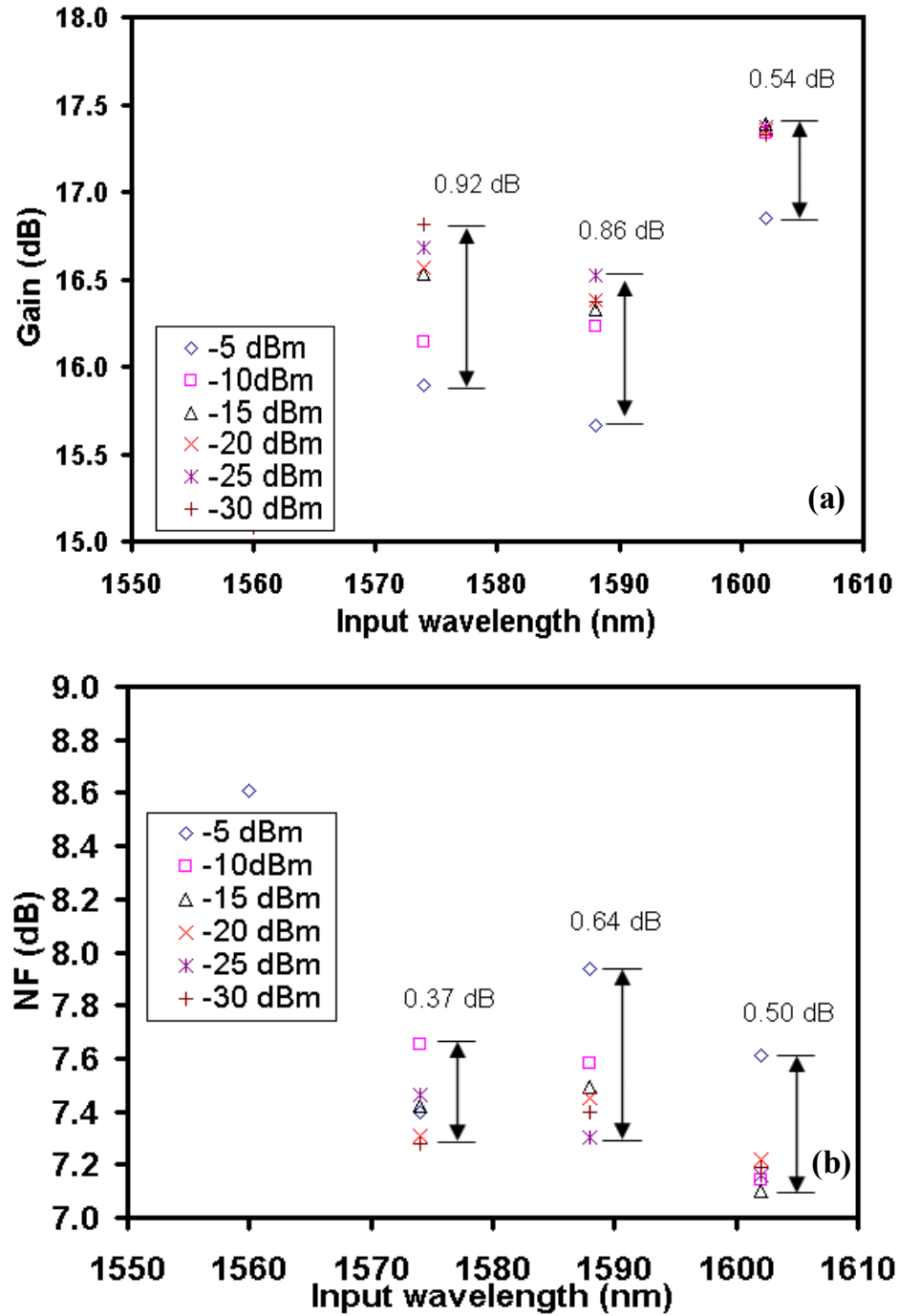


Figure 5.7 The signal gain (a) and NF (b) at 1560 nm when a other signal channel is dropped and added into the Bi-EDFA

stimulated emission from excited Er^{3+} ion was uniformly saturated by the high power saturating signal. Therefore, the saturating signal and signal channel were capable to access the energy stored in the Er^{3+} ions that was coupled to $^4\text{I}_{13/2}$ metastable state. This result implies that Bi-EDFA is a completely homogeneous gain medium compared to normal silica-based EDFA as reported by K. Inoue *et.al.* [15].

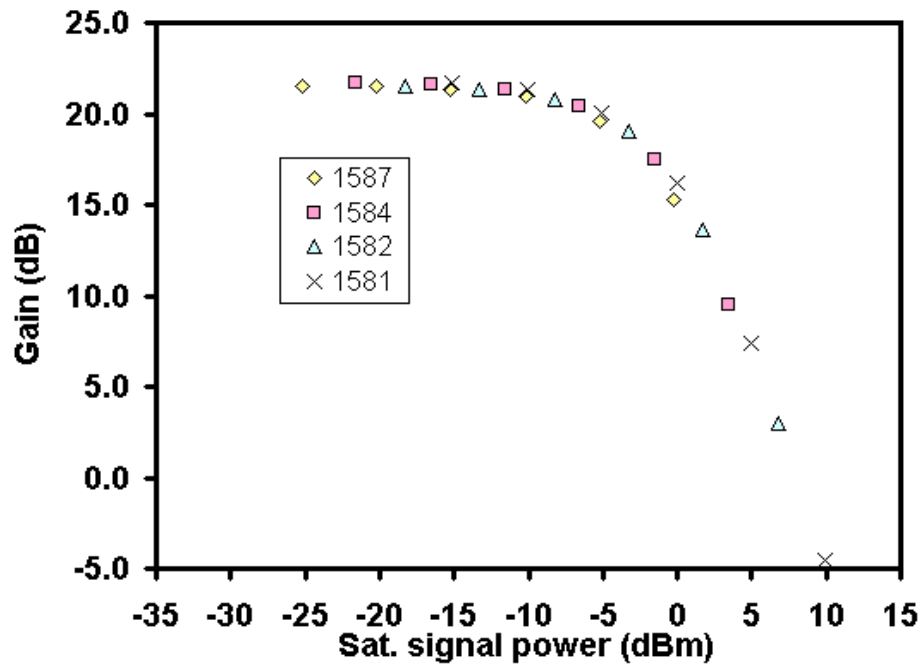


Figure 5.8 Signal gain at 1560 nm with different saturating signal wavelengths

II. Gain Compression

The gain saturation dynamic range that is also knowns as gain compression has similar definition with input signal dynamic range but it is measured in the presence of saturating signal [3, 16]. In order to measure the gain compression of Bi-EDFA, the saturating signal power wavelength of 1586.7 nm was varied from 0 to -15.23 dBm. This saturating signal wavelength was calculated based on the input signal wavelength that was arranged at 1560 nm with signal power from -5 to -30 dBm.

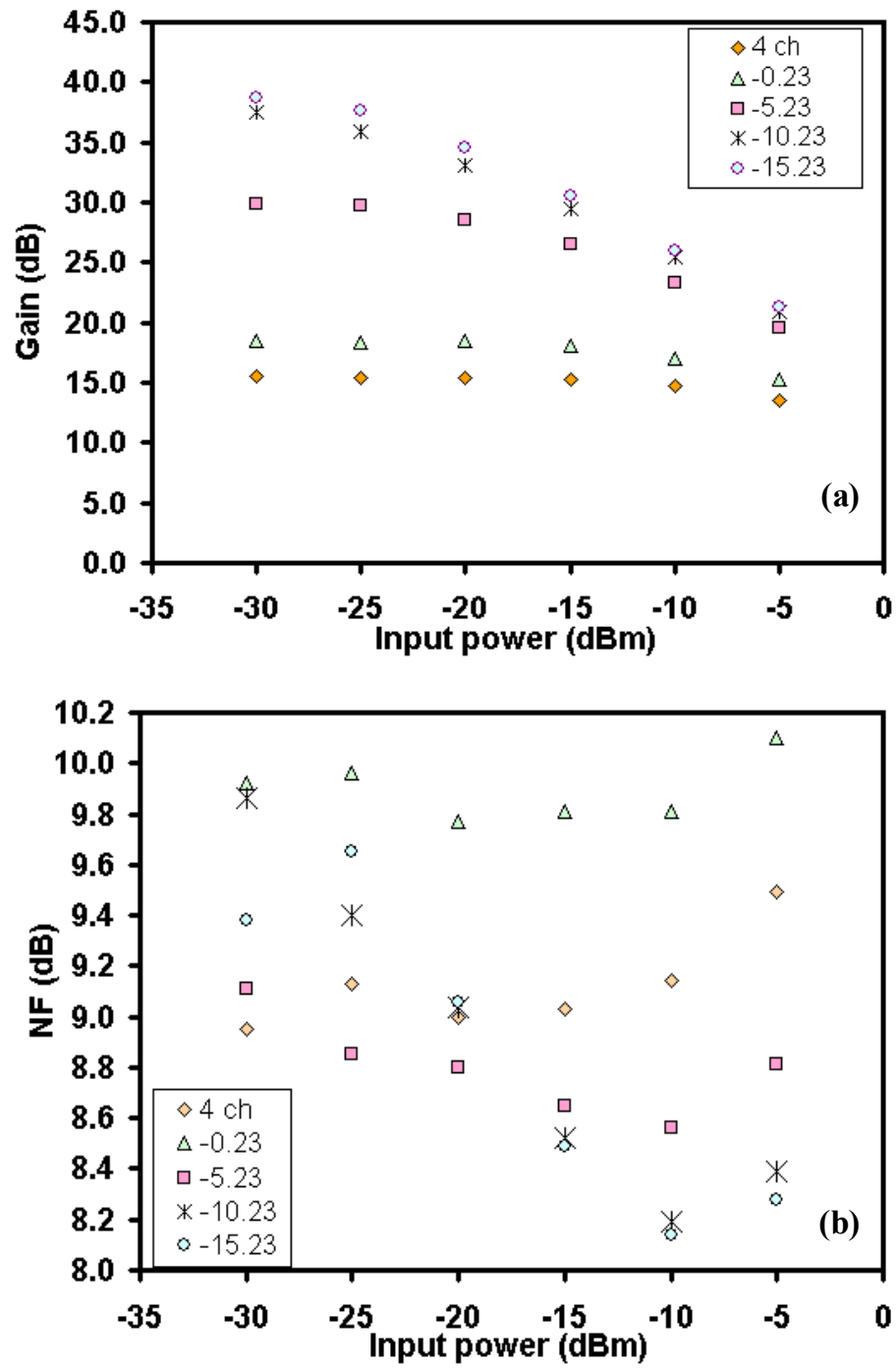


Figure 5.9 Signal gain (a) and NF (b) at 1560 nm with different saturating signal powers.

Figure 5.9 (a) illustrates the signal gain at 1560 nm with different saturating signal powers. The results for the 4 channel systems are also included in the figure for comparison. From the figure, the gain compression had improved with high saturating signal power. At high saturating signal power of -0.23 dBm, the gain compression of Bi-EDFA was 24.7 dB extending the input signal power to -5.3 dBm. With higher gain compression, Bi-EDFA was capable to sustain high input power signal that increased the output signal power over much longer transmission distances. However, as the Bi-EDFA is operated in high saturating signal power, the NF penalty increased to a maximum of 9.96 dB. Although the total output signal gain was clamped to higher input signal, this technique has a drawback due to high NF penalty. By reducing the saturating signal power to -5 dBm, led to a reduction in the gain compression to 14 dB for the maximum input power of -16 dBm. Then the NF penalty then dropped to 9.11 dB, showing only 0.85 dB improvement. Lowering the saturating signal power further down resulted in little gain compression and NF penalty enhancement as the Bi-EDFA was still under heavy saturation.

III. Gain Flatness

The inherent signal wavelength dependence of the gain and NF characteristic and performance of EDFA corresponds to the distribution of Er^{3+} ion Stark manifolds in the glass fibre. Under normal amplification operation, this lead to the suffering of WDM optical networks from an imbalance in the output power and SNR of the channels [17]. In this case, the channel that experiences the least gain is degraded more by the ASE noise [18]. Silica-based EDFA has narrow gain flatness in C- and

L-band regions, thus forcing large gain difference between channels and restricting the usable amplification bandwidths of the EDFA. Therefore, a minimal gain ripples in WDM optical networks are critical in order to minimize the distortion and amplification bandwidths.

For application in WDM optical networks that require larger amplification bandwidth, the gain flatness can be improved by operating the EDFA in deep saturation conditions [3, 17], thus minimising the gain difference between C- and L-band signals.

The Bi-EDFA gain flatness was measured by probing a signal gain and NF at input power of -20 dBm from wavelength of 1540 to 1620 nm that were combined with high saturating signal at 1586.7 nm. The saturating signal power was changed from 0 and -10 dBm to simulate the gain saturation effect. The gain and NF of Bi-EDFA gain flatness are plotted in Figure 5.10.

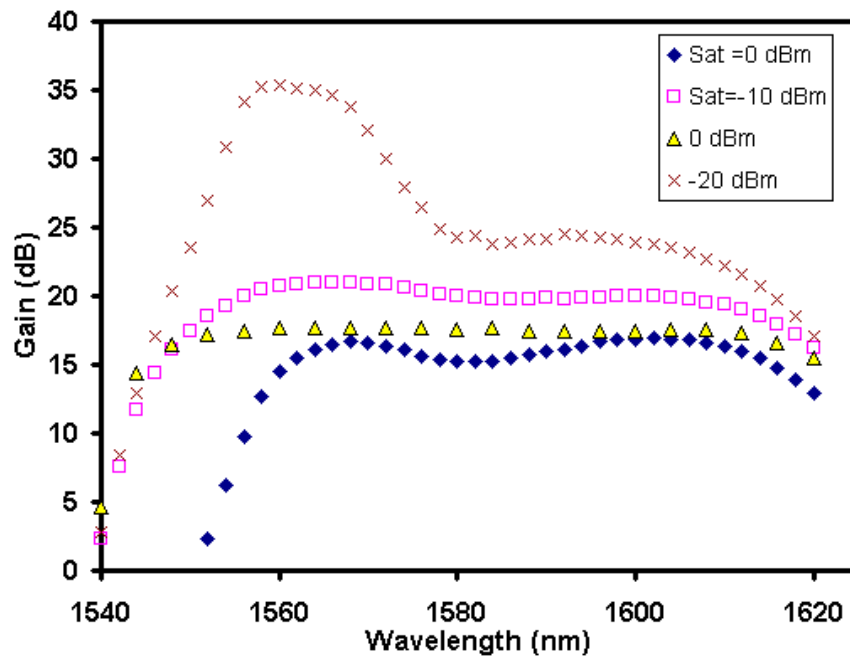


Figure 5.10 Gain flatness of Bi-EDFA. Gains for input signal power of 0 and -20 dBm are given for comparison, Sat: saturating laser power

At a maximum saturating signal power of 0 dBm in Figure 5.10, the gain flatness for an input signal wavelength of 1560 to 1612 nm was about 2.49 dB before a slight improvement to 1.97 dB at a lower saturating signal power of -10 dBm. When the Bi-EDFA was operated without saturating signal at similar input signal power, the gain flatness worsened to a maximum 13.88 dB. However at a higher input signal power of 0 dBm, the gain flatness was enhanced to less than 0.4 dB. In this case, the gain profile of the Bi-EDFA was saturated by the input signal itself [3, 17-18].

Although the gain flatness was improved with high power input signal, the NF performance of the Bi-EDFA was seriously affected. In the Figure 5.11, at an input signal of 0 dBm, the most minimum NF was limited to only 6.26 dB. However, with saturating signal powers of 0 dBm and -10 dBm, the most minimum NF was

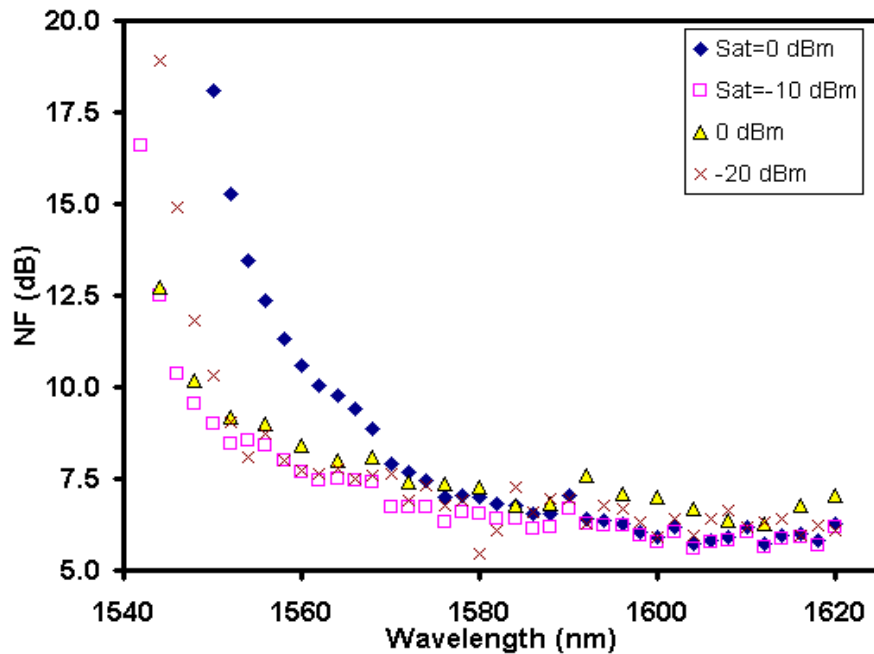


Figure 5.11 NF of the signal input for gain flatness measurement of Bi-EDFA. The NF for input signal power of 0 and -20 dBm is presented for comparison

found to be 5.72 dB and 5.60 dB respectively. The gain saturation has caused a small NF penalty of 0.66 dB which can be considered for maximum gain flatness. The gain flatness from saturating signal has shown more advantages especially with lower NF penalty that was suitable for WDM optical networks.

Saturating signal power effect on peak powers of Bi-EDFA also demonstrated in Figure 5.12. The peak power of more than 17 dBm was attained when implementing high input signal of 0 dB. From the observation, the signal peak power is dependent on the saturating signal power. When the saturating signal power was reduced from 0 dBm to -10 dBm, the corresponding signal peak power increased from 10 dBm to 14.6 dBm (exhibiting a discrepancy of around 4.6 dB). As the peak power of the signal depends on saturating signal power, the accessible amplification bandwidths have also been affected. To utilise these, the saturating

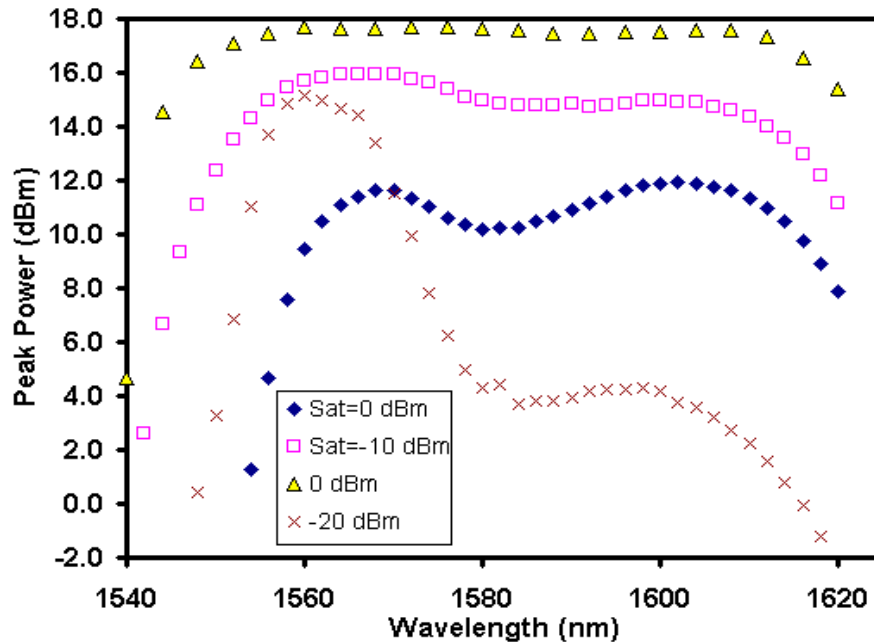


Figure 5.12 Peak power of Bi-EDFA in gain flatness measurement. The peak power for input signal power of 0 and -20 dBm is shown for comparison

signal power has to be reduced which consequently worsen the gain flatness quality. Therefore, this will limit the overall performance of Bi-EDFA in WDM optical network systems.

IV. Gain Spectral Hole Burning

Gain Spectral Hole Burning (GSHB) is a phenomenon that causes the gain deviation or a hole in the spectral region when a strong signal is added into the EDFA. At room temperature, the gain profile comprises of contributions from a number of transitions between different sublevels in the Stark split manifolds of the ground and excited states due to the site-to-site variation from ligand field [3]. Because of the rapid thermal relaxation occurring between the different sublevels, the saturation behaviour of the gain profile will tend to be homogeneously broadened across its full width [3,15].

The homogeneous property in the glass laser (in this case the EDFA) arise from the lifetime and dephasing time of the transition state and depends on the both radiative and nonradiative process [19, 20]. The faster the lifetime or dephasing time, the broader the transition. While the inhomogeneous broadening is the measure of the various different glass sites in which an ensemble of Er^{3+} ion can be situated. As the result of the variations of the glass local environment, there will be shifts in the Stark manifolds and the fluorescence or absorption observed [19]. Thus, the inhomogeneous line is a superposition of a set of homogeneous lines.

Consequently, if the homogeneous width of each transition is less than the inhomogeneous width and also less than the wavelength separation (in multichannel

WDM system) to neighbouring transition, the inhomogeneous effect should play a role near such transaction. This causes the Er^{3+} ions population inversion to be a function of input wavelength [3,15].

When an EDFA operates in the presence of a high input signal, population inversion at that wavelength will be reduced and this subsequently leads to reduction in the signal gain. If an input signal wavelength is within the width of the inhomogeneous spectral broadening, a gain fluctuation (hole) will occur due to spectral hole burning.

Siegman [21] has shown that the difference between homogeneous and inhomogeneous spectral broadening can be measured for RE doped glass medium with saturation hole-burning technique [3,22].

The GSHB measurement was investigated by using an experimental set-up that was proposed by A. K. Srivastava *et. al.* [3, 22] by evaluation of the gain profile in the presence of a saturating signal at 1560 nm with different saturating power. The gain profile was probed by -20 dBm input signal from 1550 nm to 1620 nm. In order to maintain the population inversion of the Bi-EDFA, a gain locking signal of 1580 nm was used with input power of -20 dBm.

Figure 5.13 depicts the gain spectrum under different saturating powers for GSHB measurement. From the result, at a saturating signal power of 0 dBm, that comprises of 5 dB gain compression, the dip in the gain spectrum was about 0.342 dB. However by comparing with the normal silica-based EDFA, the gain spectral hole-burning dip reported by A. K. Srivastava *et. al.* [22] was almost a half (≈ 0.14 dB) lower than in Bi-EDFA. As the gain spectral hole burning is resulted by multiple

population densities within Stark manifold of ground and excited states, the dip

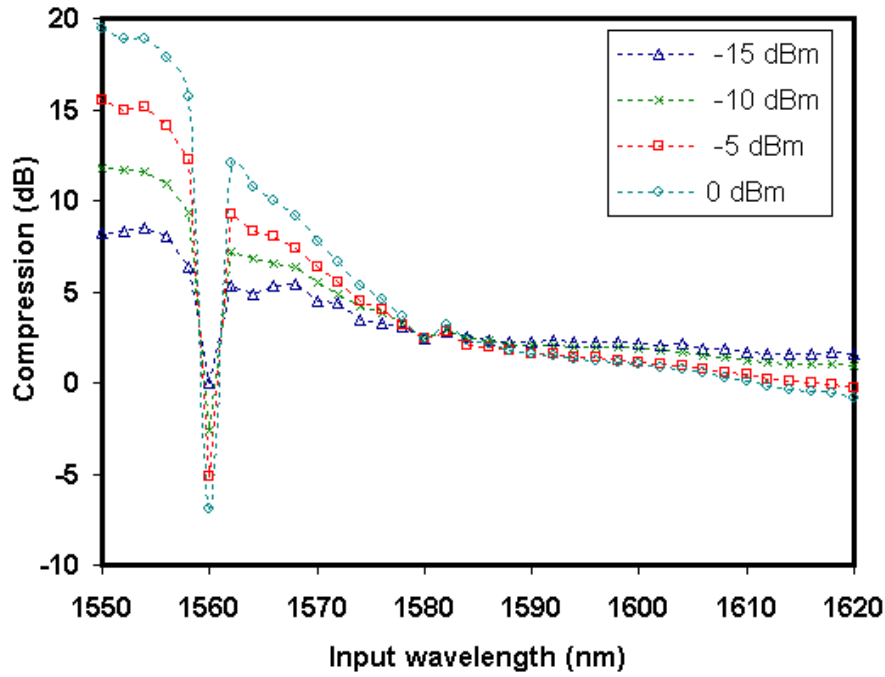


Figure 5.13 The spectral hole-burning effect with different saturating signal power at 1560 nm

represents the stimulated emission rate of the Er^{3+} ions at that manifold. High saturating signal power will fasten the stimulated emission rate at that wavelength and hence, reduce population density at the Stark manifold [3, 23]. Although S. Ono *et. al.* [24, 25] have reported that the dip of gain spectral hole-burning effect in highly doped silica-based EDFA was not affected by high power saturating signal due to the fast energy migration process between Er^{3+} ions, Bi-EDFA has different type of concentration quenching process as discussed previously in section 3.3.5. As the main energy transfer in Bi-EDFA was contributed by cross-relaxation process, the number of Er^{3+} ions at excited state is exhausted at much faster rate, thus producing deeper gain spectral hole burning dip in Bi-EDFA [15].

As presented by the results, the hole depends on the saturating signal input

power and also the wavelength as observed by F. A. Flood [26]. The gain difference was found less as the input signal shifts from shorter wavelengths to longer wavelength due to the smaller inhomogeneous broadening effect at this region [2, 26]. Consequently, when puts in multichannel WDM optical networks, Bi-EDFA was able to support more channel loading at L-band compared to that at C-band since the gain difference is lesser and flatter.

The characteristic and performance of Bi-EDFA in WDM optical networks have been experimentally demonstrated. The gain variation and NF penalty for a 4 channel WDM system at an input signal of -5 dBm shows a slightly worse performance, but capable to produce much higher signal output power. The Bi-EDFA also exhibits greater gain saturation and compression at higher input signal compared to normal silica-based EDFA due to the higher Er^{3+} ion concentration in the Bi-EDFA. However, the optical performance of the 4 channel WDM system indicates that Bi-EDFAs have the potential of being optical amplifiers for WDM optical networks.

REFERENCES

- [1] Brandom C. Collings, Matthew L. Mitchell, Luc Boivin, Wayne H. Knox, “*A 1021 channel WDM system*”, IEEE Photonics. Technol. Lett., Vol. 12, No. 7, 2000, pp. 906
- [2] Michel W. Chbat, Herve A. Fevrier, “*Low-cot, high capacity ultra-long-haul WDM systems based on wide-band raman amplification*”, 28th European Confer. on Optical Communication 2002, (ECOC 2002), Vol. 3, 2002, pp. 1
- [3] E. Desurvire, “*Erbium-doped fiber amplifiers: Principle and Application,*” John Wiley & Son Inc., New York, 1994.
- [4] D. Baney, C. Hentschel, J. Dupre, “*Optical fiber amplifiers - measurement of gain and noise figure*”, HP Lightwave Symposium, 1993.
- [5] Farbert, A. Elbers J. P., Bock H. Neuhauser R. Glingener C., “*Practical method to measure optical SNR in multi terabit systems*”, The 14th Annual Meeting of the IEEE Lasers and Electro-Optics Society, 2001, (LEOS 2001), Vol. 1, 2001, pp. 26
- [6] Maxim Bolshtyansky, Idan Mandelbaum, Fred Pan, “*Signal Excited-state absorption in L-band EDFA: Simulation and measurement*”, Jour. Light. Technol., Vol. 23, Iss. 9, 2005, pp. 2796
- [7] Biswanath Mukherjee, “*Optical Networks Series*”, Springer Science+Business Media, Inc, 2006
- [8] E. Desurvire, M. Zirngibl, H. M. Presby, D. DiGiovanni, “*Dynamic gain*

- compensation in saturated erbium-doped fiber amplifiers*", IEEE Photonics Technol. Lett., Vol. 3, No. 5, 1991, pp. 453
- [9] M. Zirngibl, "*Gain control in erbium-doped fibre amplifiers by an all-optical feedback loop*", Electron. Lett., Vol. 27, No. 7, 1991, pp. 560
- [10] M. Zirngibl, P. B. Hansen, G. Raybon, B. Glance, E. Desurvire, "*Passive gain control by all-optical feedback loop in erbium-doped fiber amplifiers*", Proc. Conference on optical Fiber Communication 1991(OFC 1991), 1991, p100
- [11] Zannin M., Taccheo S., Ennsner K., Careglio D., Sole-Pareta J., "*Effective amplification of real WDM burst traffic using optical gain clamping*", Conference on Quantum Electronics and Laser Science 2008 (CLEO/QELS 2008), 2008, pp. 1
- [12] G. Sacchi, S. Sugliani, A. Bogoni, F. Di Pasquale. R. Di Muro, R. Magri, G. Bruno, F. Cavaliere, "*Design and experimental characterization of EDFA-based WDM ring networks with free ASE light recirculation and link control for network survivability*", Jour. Lightwave Technol., Vol. 23, No. 3, 2005, pp. 1170
- [13] A. A. Kaminskii, "*Laser Crystals*", Springer series in optical sciences, Springer-Verlag, New York, 1990
- [14] D. M. Baney, J. Stimple, "*WDM EDFA gain saturation characterisation with reduced set of saturating channels*", IEEE Photonics Technol. Lett., Vol 8, No. 12, 1996, pp. 1615

- [15] K. Inoue, H. Toba, N. Shibata, K. Iwatsuki, A. Takada, M. Shimizu, “*Mutual signal gain saturation in Er^{3+} -doped fibre amplifier around 1.54 μm wavelength*”, Electronics Lett., Vol. 25, Iss. 9, 1989, pp. 594
- [16] E. Desurvire, C. R. Giles, Jay R. Simpson, “*Gain saturation effects in high-speed multichannel erbium-doped fiber amplifiers at $\lambda=1.53 \mu m$* ”, Jour. Lightwave Technol., Vol. 7, No. 12, 1989, pp. 2095
- [17] S. Yoshida, S. Kuwano, K. Iwashita, “*Gain-flattened EDFA with high Al concentration for multistage repeatered WDM transmission systems*”, Electronics Lett., Vol. 31, No. 20, 1995, pp. 1765
- [18] Ozan K. Tonguz, Felton A. Flood, “*EDFA-based DWDM Lightwave transmission systems with end-to-end power and SNR equalization*”, IEEE Transaction on Communications, Vol. 50, No. 8, 2002, pp. 1282
- [19] P. C. Becker, N. A. Olsson, J. R. Simpson, “*Erbium-doped fiber amplifiers, Fundamentals and technology*”, Academic Press, San Diego, 1997
- [20] P. W. Milonni, J. H. Eberly, “*Laser*”, Wiley, New York, 1988
- [21] A. E. Siegman, “*Lasers*”, University Science Books, Mill Valley, CA, 1986
- [22] A. K. Srivastava, J. L. Zyskind, J. W. Sulhoff, J. D. Jr. Evankow. M. A. Mills, “*Room temperature spectral hole-burning in erbium-doped fiber amplifier*”, Optical Fiber Communication Conference, 1996, (OFC 1996), 1996, pp. 33
- [23] M. Bolshtyansky, “*Theory, simulation and measurement for new model of spectral hole burning in EDFA*”, Optical Fiber Communication Conference,

2003, (OFC 2003), 2003, Vol. 2., pp. 604

- [24] S. Ono, S. Tanabe, M. Nishihara, E. Ishikawa, “*Effect of erbium ion concentration on gain spectral hole burning in silica-based erbium-doped fiber*”, Optical Fiber Communication Conference 2005 (OFC 2005), Vol. 4, 2005, pp 3
- [25] S. Ono, S. Tanabe, M. Nishihara, E. Ishikawa, “*Study on the dynamics of a gain spectral hole in silica erbium-doped fiber at 77 K*”, Jour, Opt. Soc. Am. B., Vol 22, No. 8, 2005, pp. 1594
- [26] F. A. Flood, “*Gain saturation behaviour in L-band*”, IEEE Photonics. Technol. Lett. Vol. 12, No. 9, 2000, pp. 1156

CHAPTER 6

DISCUSSION and CONCLUSION

6.1 Introduction

In this thesis, an optical amplifier for Dense Wavelength Division Multiplexing (DWDM) networks that was fabricated by Asahi Glass Co. Ltd by utilising bismuth glass host has been characterised. The fabrication process was based on a mixed-former fabrication technique [1, 2] to produce a multicomponent glass that involves doping with a high concentration of Er^{3+} ions of 3250 wt. ppm. This method has successfully produced a glass host that has high Er^{3+} ions concentration with minimal ion clustering as reported by Jianhu Yang *et. al.* [1, 2]. Therefore, this new bismuth-based erbium-doped optical amplifiers require shorter fibre lengths to achieve higher signal output powers compared to that of conventional silica-based erbium-doped optical amplifiers. With shorter fibre length, the signal propagation length is also reduced, thus significantly reducing non-linear effects such as FWM, XPM, SPM and stimulated Brillouin scattering. For optical amplifier manufacturers, shorter active fibre length indicates that the final product will have a smaller spatial dimension and reduced costs. In addition, this fabrication method also widens the radiative fluorescence spectrum of the Er^{3+} ion. This increases the signal amplification bandwidth [1, 2] that is beneficial for long-haul DWDM optical networks.

6.2 Erbium-doped Bismuth Optical Fibre Spectroscopic Properties

The bismuth oxide fibre was fabricated by using three glass former elements, bismuth oxide Bi_2O_3 , silica SiO_2 and alumina Al_2O_3 . This optical fibre has a high core/cladding refractive index at 1550 nm of 2.03/2.02. By implementing Marcuse equation, the calculated mode-field diameter (MFD) was determined to be about 6.1 μm with a core radius of 2.55 μm . The smaller core radius causes the doped Er^{3+} ions to confine in the centre of the fibre core for better pump and signal absorption and amplification. The utilisation of multiple glass former elements causes the bismuth glass to possess multiple advantages such as higher RE ion concentration; lower glass devitrification, wider gain bandwidth, high refractive index and lower nonradiative energy transfer that significantly enhances the efficiency of the 1.55 μm radiative emission for DWDM signal amplifications [1,2]. From the Judd-Ofelt theory, the effect of the glass composition is explained by the $\Omega_{2,4,6}$ coefficients [4-6]. A high Ω_2 coefficient value indicates that the Er^{3+} ions in the bismuth-based erbium-doped fibre are very well placed and have a high site symmetry at the vicinity of the network former and non-bridging oxygen bonds. This reduces the ion clustering effect efficiently. The Ω_4 and Ω_6 coefficients, which are related to the glass covalency, glass basicity and fraction of the non-bridging oxygen ions are found to be comparable and/or lower compared to conventional silica-based glass. From the calculated Ω_6 coefficient, the addition of Bi_2O_3 leads to an increase in the number of non-bridging ions and covalent bonds, respectively as reported by Shiqing Xu *et. al.* [4] and T. V. Bocharova *et. al* [7]. These result in higher peak emission cross-section

and broader emission bandwidth. The calculated emission cross-section that relies on the McCumber theory also exhibits a similar result of spectral broadening at the longer wavelength region as well as a low ESA absorption cross-section coefficient.

In spite of these advantages, a higher content of Bi_2O_3 and Er_2O_3 ultimately affects the glass host local environment by resulting in a shorter Er^{3+} ion metastable level lifetime of 2.84 ms. This consequently reduces the efficiency of the optical amplifier. Optical amplifiers with longer metastable lifetimes are capable of maintaining its excited state population inversion longer, and as a result, producing a higher energy conversion efficiency. The reasons for the lower lifetime value are due to the effect of the Er^{3+} ions radiation quenching and the addition of Bi_2O_3 that reduce the overall glass phonon energy. Bi_2O_3 has a low phonon energy of about $\approx 500 \text{ cm}^{-1}$ compared to that of silica glass of $\approx 1000 \text{ cm}^{-1}$. With lower phonon energy, the non-radiative decay rate of the Er^{3+} ion at the $^4\text{I}_{13/2}$ level in the bismuth-based glass was found to be shorter by about 130.3 s^{-1} thus, leading to a significant increase in the multiphonon relaxation rates. This consequently increases the emission upconversion process to the higher energy level. The upconversion process wastes the pump photon energy that leads to reduction in the important $1.55 \text{ }\mu\text{m}$ radiative emission for WDM optical communications. The upconversion measurement from 400 nm to 1100 nm that implements a 1480 nm laser diode excitation detects a high 975 nm emission from the bismuth-based fibre. This upconversion process has a quadratic dependence on 1480 nm excitation at low powers due to the fact that it is a two-photon absorption scheme but it increases to a 4x dependence at higher excitation powers. The explanation for the latter situation is given as follows. At low pump

power, most Er^{3+} ions are quenched by the cooperative energy transfer (CET) but as the pump power increases, other higher rate quenching mechanisms such as 532 nm upconversion process, energy transfer to glass impurities and defects and ESA occur.

From the optical absorption and fluorescence emission measurements, a bismuth-based optical amplifier has a higher peak coefficient of $7.58 \times 10^{-25} \text{ m}^2$ and wider full-width half-maximum (FWHM) value of about 80 nm (especially at longer wavelengths) as compared to silica-based optical amplifiers. At this region, silica-based optical amplifiers have a low signal gain coefficient due to a higher ESA as reported by E. Desurvire *et. al.* [5]. Therefore, by utilising a new bismuth-based optical amplifier, this longer wavelength region can be employed for signal amplification that is needed for DWDM optical communication networks.

The glass performance defined by the figure of merits (FOM) of bismuth-based optical amplifier is the highest compared to other glass hosts such as tellurite and phosphate where the bandwidth FOM is $606.40 \times 10^{-28} (\text{s} \cdot \text{m}^2)$ and gain FOM is $21.53 \times 10^{-25} (\text{nm} \cdot \text{m}^2)$. The major reason for this high optical performance is because of the careful consideration in the material chosen and the fabrication method used in designing the Bi-EDFA. Therefore, this merits potential application of bismuth-based optical amplifiers for DWDM communication networks.

6.3 C+L band Bismuth-based EDFA

The Bismuth-based optical amplifier properties were evaluated by incorporating a single-pass bi-directional pumping scheme of a pump wavelength of 1480 nm. This pumping configuration was employed [5] because it is the most effective and efficient technique to demonstrate the Bi-EDFA's full potential. Another benefit is that the 1480 nm pump light was evenly distributed throughout the entire Bi-EDF length. This significantly increases the overall Er^{3+} ion population inversion density along the active Bi-EDF, and for this reason, pushing the Bi-EDFA to regions of near-complete inversion. From the measured forward ASE spectrum, the bi-directional pumping arrangement has the widest and flattest output spectrum. This was done without using any Gain-Flattening Filter (GFF) that makes it suitable for DWDM signal amplifications.

This pumping technique also improved the output signal gain and noise of the optical amplifier. The input signal experienced less attenuation because the amplification was done at both Bi-EDF ends with significantly smaller noise contribution. From the result obtained, the signal gain from the bi-directional pumping was almost 34 % higher than the uni-directional pumping when comparing at the same pump power. The gain to pump power coefficient also improved from 0.03 dB/mW to a maximum of 0.09 dB/mW, and thus, bringing down the pump power transparency of Bi-EDF to only 74 mW. Meanwhile, the signal NF was reduced to 8.58 dB at similar conditions. The pump to signal QCE of the Bi-EDFA also improved to about 8.58 %, indicating better and lower energy transfer loss

between pump and signal.

The advantage of implementing two laser diode pumps is to allow indirect control of self-saturation effect in Bi-EDFA by adjusting the pump ratio between forward and backward pumps. This self-saturation effect has been known as a limiting factor in high power optical amplifiers that deteriorates the amplified signal quality and overall performance.

When the power of forward pump at Bi-EDF is increased, the backward ASE power was intensified and competes with the actual input signal. This ASE behaved as such a high power pseudo-signal which competed for gain with the input signal and as a result, reduced the available gain for the signal.

From the result obtained in chapter 4, by adjusting the forward and backward pump ratio to be 1:3 out of the total pump power, the Bi-EDF input end's population inversion was maintained low and as a result, producing less self-saturation effect to the incoming signal. In addition, the signal gain was also improved up to 4% while the NF was enhanced up to 3 % at maximum pump power. Although the enhancements are small in near-complete inversion, the pump ratio is much larger under moderate inversion where it is preferable and more suitable for low-noise application. The QCE also improved to 6.25 %, signifying better pump light distribution due to the reduction of the ASE self-saturation effect. Modified bi-directional pump ratios also enhanced the Bi-EDFA amplification bandwidth to 72 nm especially at longer input signal wavelengths.

The Bi-EDFA has lower phonon energy due to its high Bismuth contents. Low phonon energy glasses are influenced greatly by ambient temperature as

indicated by reduction of the $^4I_{13/2}$ nonradiative emission rate and McCumber theory [5]. These are because absorption and emission cross section are temperature dependent [5]. From the result, the signal gain and NF of Bi-EDFA were varied to a maximum of $\Delta G = 11.06$ dB while the $\Delta NF = 17.97$ dB at a signal wavelength of 1536 nm. The temperature coefficient of the Bi-EDFA was found to depend on the input signal wavelength with input signals beyond the Er^{3+} ion peak emission of 1530 nm that have a negative coefficient. This is due to the amplification property of long input signal wavelengths that is largely dependent on the Stark levels of the Er^{3+} ions.

6.4 Bi-EDFA in WDM optical network system

In this chapter, the performance of Bismuth-based EDFA was investigated with a 4 channel WDM optical system. The signal channel gain, NF and SNR were found to be effected moderately by the signal-induced saturation and gain profile flatness. These were because the gain profile of Bi-EDFA was a combination of two gain regions, C- and L-bands. C-band signal amplification was initiated directly by excitation from a LD pump at 1480 nm that depends on the pump intensity. While L-Band signal amplification was originated from C-band signal and ASE re-absorption which depend on the photon wavelength. This amplification was possible when the primary pump sources were not sufficient to create population inversions at the region that was far away from the pump. The EDFA acted as a quasi-two level laser system [5] which eventually resulted in the amplification depending on the Stark

levels splitting by Boltzman distribution [8].

At shorter wavelengths, the gain and NF between signal channels were found to produce larger variations than those at longer wavelength. The gain variation at shorter wavelengths was about 0.92 dB before reducing to 0.54 dB at longer wavelengths. In addition, the NF penalty was found about 0.37 dB at shorter wavelengths, before increasing to 0.50 dB at longer wavelengths. These results were related to L-band signal saturation induced by high power backward ASE that created a broad-band gain depression as explained by Flood F. A. *et. al.* [9]. The SNR of the signal also enhanced to a maximum 1.25 dB at longer wavelengths due to a higher signal gain at this region. From signal channel add/drop experiment to investigate gain saturation effect, the Bi-EDFA gain profile was influenced largely by addition of signal at longer wavelengths.

Although Bi-EDFA is capable of both shifting the ESA $^4I_{13/2} \rightarrow ^4I_{9/2}$ transition to longer wavelengths as well as producing larger gain coefficient, in highly saturated condition, the output signal still suffers ESA which leads to reduction in the total output signal power. Therefore, the usable amplification bandwidth of Bi-EDFA was only limited to 1612 nm before the ESA effect dominates the signal gain. In addition to that, the GSHB in the Bi-EDFA was found to be much higher compared to silica-based EDFAs. This effect has been known to produce gain fluctuation in closely spaced signal channels found in dense WDM optical system [10].

Generally, the Bi-EDFA has demonstrated that it has sufficient gain with less ripples to produce large gain dynamic range or compression with an acceptable gain flatness from C-band to extended L-Band (1530 nm to 1620 nm) for applications in

WDM optical networks. The amplification bandwidths were expanded to a maximum of 73 nm, hence increasing the channel number and spacing to enhance signal crosstalk, Composite Second Order (CSO) distortion and bit error rate.

6.5 Issues and Suggestion for Future Work

The Bi-EDFA is a high-potential broadband optical amplifier for optical telecommunication networks. The mixed-former fabrication method has successfully yielded an advanced host material for optical amplifiers. This technique can enhance the RE doping concentration and therefore, improving the output signal gain, NF and efficiency. The Bi-EDFA has been doped to a maximum of 26000 ppm with negligible concentration quenching effect [11] that results in a significant reduction in EDF length to a minimum of 63 cm for L-band amplification [12].

However high splice losses, complicated fabrication methods and low phonon energies generally limit Bi-EDFA optical efficiency and performance. These limitations must be decreased before introducing the Bi-EDFA to real world optical systems. Splice losses of this device can be minimised by using multiple dummy fibres with higher refractive index and spliced using angle splicing method in order to lessen its Fresnel reflection (thus, increasing the signal gain and NF). The efficiencies of the Bi-EDFA can be improved by suppressing the upconversion process through lanthanum (La) and boron (B) addition into the glass host [13].

Full understanding of gain, noise and efficiency of optical performance in highly doped optical amplifiers should be revisited because optical fibres are more

prone to undesirable effects such as self-saturation (ASE and signal-induced) and concentration quenching. In WDM optical systems, where the high total input power is combined with the cascade EDFA configuration, the gain, NF and SNR of the output signal will degrade and hence increase the signal crosstalk and bit-error rates of the system. With this knowledge, future work on ultrawide band optical amplifiers that includes multiple RE ions namely thulium (Tm^{3+}) and praseodymium (Pr^{3+}) in a bismuth host glass or other host glasses could be done to expand and improve the accessible amplification bandwidth for future DWDM telecommunication networks.

REFERENCES

- [1] Jianhu Yang, Shixun Dai, Nengli Dai, Shiqing Xu, Lei Wen, Lili Hu, Zhonghong Jiang, “*Effect of Bi_2O_3 on the spectroscopic properties of erbium-doped bismuth silicate glasses*”, J. Opt. Soc. Am. B., Vol. 20, No. 5, 2003, pp. 810
- [2] Jianhu Yang, Dai Shi-Xun, Wen Lei, Liu Zhu-Ping, Hu Li-Li, Jiang Zhong-Hong, “*Mixed former effect: A kind of composition adjusting method of Er-doped glass for broadband amplification*”, Chi. Phys. Lett., Vol. 19, No. 10, 2002, pp. 1516
- [3] F. Auzel, P. Goldner, “*Toward rare-earth clustering control in doped glasses*”, Optical Material, Vol. 16, 2001, pp. 93
- [4] Shiqing Xu, Zhongmin Yang, Shixun Dai, Guonian Wang, Lili Hu, Zhonghong Jiang, “*Effect of Bi_2O_3 on spectroscopic properties of Er^{3+} -doped lead oxyfluorosilicate glasses for broadband optical amplifiers*”, Jour. Non-Cryst. Solids, Vol. 347, 2004, pp. 197
- [5] E. Desurvire, “*Erbium-doped fiber amplifiers: Principle and Application,*” John Wiley & Son Inc., New York, 1994.
- [6] K. Binnemans, C Gorller-Walrand, “*Letter to the editor: Are the Judd-Ofelt intensity parameters sensitive enough to reflect small compositional changes in lanthanide-doped glasses?*”, Jour. Of Phys: Condens. Matt., Vol. 10, no. 10, 1998, L167
- [7] T. V. Bocharova, J. L. Adam, G. O. Karapetyan, F. Smektala, A. M. Mironov,

- N. O. Tagil'tseva, "*Analysis of rare-earth ion spatial distribution in fluorophosphate glasses in terms of segregation phenomenon*", Jour. Of Phys. and Chem. Of Solids, Vol. 68, 2007, pp. 978
- [8] A. E. Siegman, "*Lasers*", Mill Valley, CA, University Science Books, 1986
- [9] Felton A. Flood, "*Gain saturation behaviour in L-band EDFAs*", IEEE Photonics. Technol. Lett., Vol. 12, No. 9, 2000, pp. 1156
- [10] A. K. Srivastava, J. L. Zyskind, J. W. Sulhoff, J. D. Jr. Evankow. M. A. Mills, "*Room temperature spectral hole-burning in erbium-doped fiber amplifier*", Optical Fiber Communication Conference, 1996, (OFC 1996), 1996, pp. 33
- [11] Y. Kuroiwa, N. Sugimoto, K. Ochiai, S. Ohara, Y. Fukusawa, S. Ito, S. Tanabe, T. Hanada, "*Bi₂O₃ based erbium doped fiber (Bi-EDF) for candidates of the broadband and compact amplifiers*", Reports of the Research Laboratory, Asahi Glass Co. Ltd, Vol. 21, 2001, paper 2
- [12] N. Sugimoto, Y. Kuroiwa, K. Ochiai, S. Ohara, Y. Fukusawa, S. Ito, "*Novel short-length EDF for C+L band Amplification*", Optical Amplifiers and Their Application 2000 (OAA 2000), PDP3, pp. 1
- [13] H. Hayashi, S. Ohara, N. Sugimoto, S. Tanabe, "*Effects of lanthanum and boron addition on suppression of cooperative upconversion in bismuth oxide-based erbium-doped fibers*", Japanese Jour.. Of. Appl. Physics, Vol. 46, No. 6A, pp. 3452

APPENDIX

Reprint of Selected Papers

1. S. W. Harun, N. Tamchek, S. Shahi, and H. Ahmad, “*L-band Amplification and Multi-wavelength Lasing with Bismuth-based Erbium Doped Fiber*”, Progress in Electromagnetics Research Symposium (PIERS), Vol. 6, 1-12, 2009.
2. S. W. Harun, S. N. Aziz, N. Tamchek, N. S. Shahabuddin, H. Ahmad, “*Brillouin fibre laser with 20 m long photonic crystal fibre*”, IET Electron. Lett, Vol. 44, Issue 18, 2008
3. H. Ahmad, N. Tamchek, W. Y. Chong, K. Thambiratnam, S. W. Harun, “*Erbium-doped Fibre Amplifier-Influence of Host Material*”, 2nd International Conference on Functional Materials and Devices 2008, (ICFMD 2008), Kuala Lumpur.
4. N. Tamchek, W. Y. Chong, S. W. Harun, H. Ahmad, “*C- and L-band Erbium-doped Fibre Amplifiers Based on Bismuthate Glass*”, National Physics Conference 2007 (PERFIK 2007), Kuala Terengganu (Malaysia) 26-28 December 2007
5. N. Tamchek, W.Y Chong, P. Poopalan, S. W. Harun, H. Ahmad, “*Green Upconversion of Erbium-doped Bismuth-based fibre*”, TS3E-1,MMU International Symposium on Information and Communication Technologies (M2USIC) 2007, Kuala Lumpur

L-BAND AMPLIFICATION AND MULTI-WAVELENGTH LASING WITH BISMUTH-BASED ERBIUM DOPED FIBER

S. W. Harun, N. Tamchek, S. Shahi, and H. Ahmad [†]

Photonics Research Center
University of Malaya
Kuala Lumpur 50603, Malaysia

Abstract—Bismuth-based EDF (Bi-EDF) is comprehensively studied as an alternative medium for optical amplification. The bismuth glass host provides the opportunity to be doped heavily with erbium ions to allow a compact optical amplifier design. The gain spectrum of the Bi-EDF amplifier has a measured amplification bandwidth of 80 nm with a quantum conversion efficiency of 20% obtained using 1480 nm pumping and 215 cm long of doped fiber. A multi-wavelength laser comb is also demonstrated using a four-wave mixing effect in a backward pumped Bi-EDF. The laser generates more than 10 lines of optical comb with a line spacing of approximately 0.41 nm at 1615.5 nm region using 146 mW of 1480 nm pump power.

1. INTRODUCTION

Recently, Bismuth-based erbium-doped fibers (Bi-EDFs) have been extensively studied for use in compact amplifiers with short gain medium lengths. This fiber incorporates lanthanum (La) ions to decrease the concentration quenching of the erbium ions in the fiber [1], which allows the erbium ion concentration to be increased to more than 1000 ppm. A fiber with such a high erbium dopant concentration is expected to have enormous potential in realizing a compact erbium-doped fiber amplifiers (EDFAs) and EDFA based devices. The Bi-EDF also exhibits a very high fiber nonlinearity, which can be used for realizing new nonlinear devices such as wavelength converter and laser source [2, 3]. Multi-wavelength lasers are required for dense wavelength

Corresponding author: S. W. Harun (swharun@um.edu.my).

[†] The first author is also with Department of Electrical Engineering, University of Malaya, Kuala Lumpur 50603, Malaysia.

division multiplexing (DWDM) optical system, which is an enabling technology to fulfill a demand of bandwidth in the modern information age.

In this paper, the optical performance of the Bi-EDF amplifier (Bi-EDFA) is characterized and compared with that of Si-EDFA. Then, a multi-wavelength laser is demonstrated using the Bi-EDF assisted by FWM process.

2. CHARACTERIZATION OF THE Bi-EDF

The Bi-EDFA is characterised for its luminescence and lifetime properties and its gain and noise figure performance. In this Bi-EDFA, the Bi-EDF is bi-directionally pumped by a 1480 nm laser with total power of 288 mW. The Bi-EDF used in this experiment is commercially available from Asahi Glass Co and has an Er^{3+} ion concentration of 7.6×10^{25} ions/ m^3 with a Lanthanum ion co-dopant concentration of approximately 4.4 wt%. The fibre used has a length of 181.9 cm, a core/cladding refractive index of 2.03/2.02 and a NA of 0.20. It is angle spliced to a single-mode fiber in order to reduce splice point reflections.

For the luminescence experiment, the two 1480 nm pump laser diodes are operated in CW mode while for the lifetime experiment the 1480 nm pumps are pulse modulated using a square-wave function generator at 70 Hz. The 1550 nm fluorescence spectra is measured using an optical spectrum analyser (OSA) and the lifetime of the erbium ion in the Bi-EDF is measured using the decay, which is detected using HP 83440B photodiodes with a digital oscilloscope. The decay oscillogram is transferred to a computer via General Purpose Interface Bus (GPIB) hardware, and the decay lifetime is obtained by fitting the single-exponential function to the experimental fluorescence decay curves. The gain and noise figure of the Bi-EDFA are also investigated. The experiment is then repeated using a 30 m commercially available Si-EDF from Fibercore Ltd. with an Er^{3+} doping concentration of 2.0×10^{25} ions/ m^3 for comparison purposes.

Figure 1 shows the measured and calculated emission cross-section using the McCumber theory and also the Si-EDF emission cross-section as a comparison. The McCumber emission cross-section was calculated using absorption cross-sections provided by Asahi Glass Co, and it can be seen in the figure that the calculated emission cross-section agrees well with the experimental data. This optical emission peaks at the $1.53 \mu\text{m}$, which is obtained due to the population inversion between energy level $^4\text{I}_{13/2}$ and $^4\text{I}_{15/2}$. Also from Fig. 1, it can be seen that the Bi-EDF has wider emission spectra as compared to Si-EDF, especially

at the longer wavelengths at 1620 nm because of its larger emission cross-section. The Si-EDF has a bandwidth of only 40 nm while the Bi-EDF bandwidth is almost double at 80 nm for the same emission intensity. The widening of the emission spectra is believed to be a result of the Stark level of the Er^{3+} ions in the Bi-EDF, which is separated to a larger degree due to the larger ligand field as shown by the absorption cross-section. As shown in Fig. 1, despite the Bi-EDF having a higher absorption cross-section of $7.58 \times 10^{-25} \text{ m}^2$ at the 1530 nm peak as compared to the Si-EDF absorption cross-section (which is only $4.39 \times 10^{-26} \text{ m}^2$), the peak full-width half maximum (FWHM) of the Bi-EDF is narrower than the FWHM of the Si-EDF. This is due to the larger inhomogeneous energy level degeneracy that the ligand field of the Bismuth host glass induced as a result of site-to-site variations, also known as the Stark effect [4], causing the widened optical transitions. Other elements such as potassium oxide also have similar glass basicity expander effects [5] and are used in the fabrication of Bi-EDF to obtain a broader amplification region.

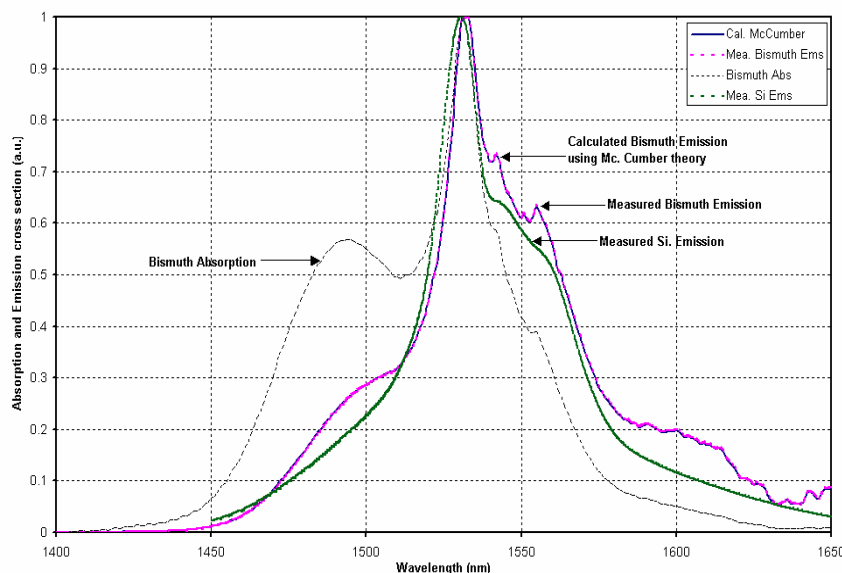


Figure 1. Absorption and emission cross-section of Bi-EDF and Si-EDF. (The Bismuth absorption cross-section is obtained from Asahi Glass Co.). The calculated Bismuth emission curve coincides very well with the measured curve.

Figure 2 shows the lifetime decay curve of Er^{3+} ions of Bi-EDF, which was measured at wavelength of 1530 nm. The decay curve is

fitted with the single exponential decay function using the least square method as shown by the solid line. From the fitting curve, the lifetime of the erbium ion was measured to be approximately 2.84 ± 0.08 ms, which is shorter than that measured by Yang et al. [6] and much more lower than the compared lifetime of Er^{3+} ions in a silica host glass [4]. The quantum efficiency η and non-radiative transition rate W^{NR} at the 1550 nm emission are calculated to be 63.0% and 130.3 s^{-1} , respectively. This shows that the Bi-EDF is capable of generating the sought-after high population inversions with only a modest pump power [7]. Furthermore, this indicates that glass hosts with low phonon energies such as bismuth glass (500 cm^{-1}) can be used to design an efficient optical amplifier with a wider fluorescence bandwidth [6, 7]. The wider fluorescence bandwidth is also attributed to the effect of the alumina and Lanthanum co-dopants towards the Er^{3+} ions distribution in the Bi-EDF which reduces the concentration quenching effect of the Er^{3+} ions, thus increasing the quantum efficiency [8, 9].

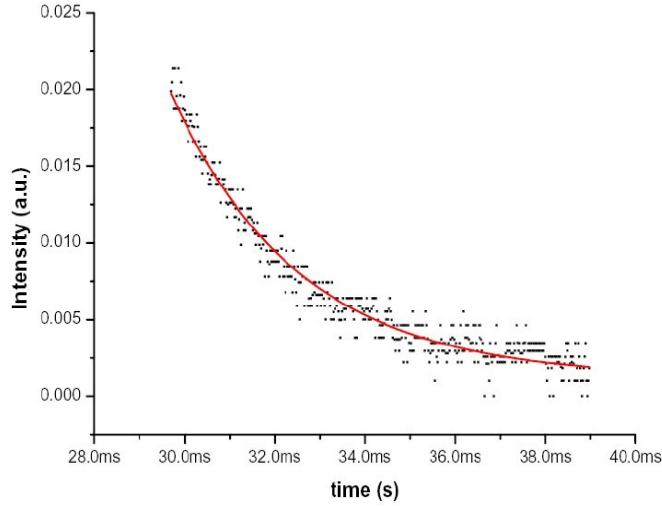


Figure 2. The measured lifetime of the erbium ion in Bi-EDF at 1530 nm. The fitting curve to the data is represented by the solid line.

The complete compositional analysis of the Bi-EDF glass is also investigated and measured using Energy Dispersive X-Ray Microanalysis (EDX) techniques. In this measurement, the sample is bombarded with electron energy accelerate at 20 kV and the emitted X-Rays from the sample are captured and analysed with the system software. Fig. 3 shows the measured energy spectrum of the Bi-

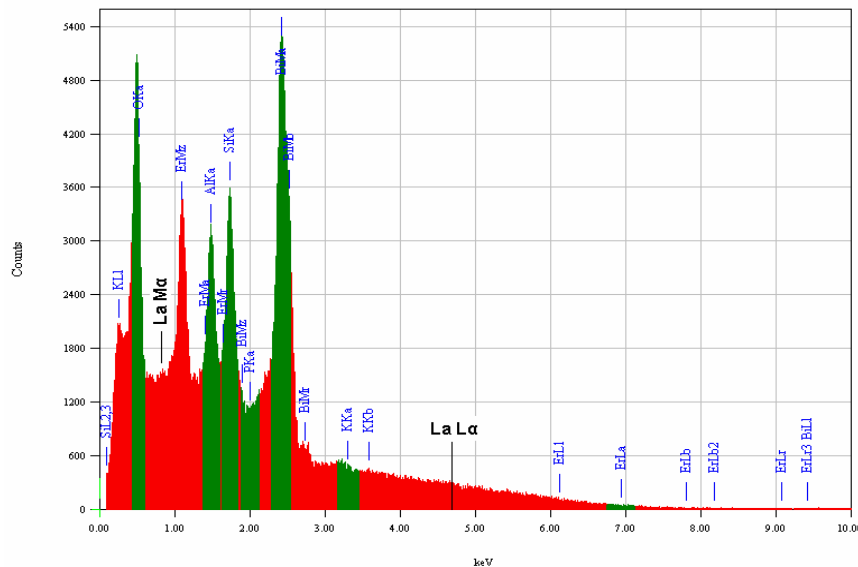


Figure 3. The measured energy spectra of the Bi-EDF using EDX.

EDF glass. In the experiment, an elemental analysis is performed using the bundled in software build-in with the ZAF method to calculate the errors. The complete compositional analysis of the Bi-EDF glass using EDX is summarized in Table 1. From the analysis, the glass network formers for the Bi-EDF are determined to be bismuth oxide, silica and alumina while the other markers are determined to be the glass network modifiers. The glass former is more prevalent elements in the glass structure than the glass modifier. By utilizing bismuth oxide and alumina as the main glass network former, the local glass basicity near the Er^{3+} ions sites is expanded as reported by Yang et al. [10] and Ainslie et al. [8], effectively increasing the crystal field (ligand field) of the glass. This has the result of enhancing the 1530 nm fluorescence full-width-half-maximum (FWHM) spectrum [8,10] making it comparably broader than that obtainable with a silica glass host.

3. AMPLIFICATION CHARACTERISTICS

In order to gauge the behaviour of the Bi-EDF in optical amplification, then Bi-EDF optical amplifier characteristics and performance is evaluated by measuring the signal gain and noise figure. In this

experiment, the Bi-EDF is bi-directionally pumped by a 1480 nm laser with total power of 288 mW. The gain (G) and noise figure (NF) are measured by an optical spectrum analyzer (OSA) using the following equations;

$$G(dB) = 10 \log_{10} \left(\frac{P_{out} - P_{ASE}}{P_{in}} \right) \quad (1)$$

$$NF(dB) = 10 \log_{10} \left(\frac{1}{G} + \frac{P_{ASE}}{h\nu\Delta\nu G} \right) \quad (2)$$

where P_{in} , P_{out} , and P_{ASE} are the input power, the output power and the amplified spontaneous emission power (ASE) power, respectively. h is the photon energy and $\Delta\nu$ is the OSA's resolution. Fig. 4 compares the gain and noise figure of the Bi-EDFA with the Si-EDFA at input signal of 0 dBm. The gain of the Bi-EDFA is approximately 3 dB or 50% higher than that of the Si-EDFA with a flat gain profile. The Bi-EDFA gain bandwidth is also wider by 15 nm than that of the Si-EDFA, to give the Bi-EDF gain bandwidth of approximately 80 nm spanning from 1540 nm up to 1620 nm. This 15 nm increase in the gain bandwidth represents the potential addition of 18 signal channels of a 100 GHz transmission system with the implementation of Bi-EDF optical amplifiers [11]. However, the high Er^{3+} ions doping concentration and high insertion loss of the Bi-EDF incur a higher noise figure penalty of approximately 2.6 dB than the noise figure penalty of a Si-EDF when spliced to a conventional SMF. This increased noise figure is attributed to the effect of multiple reflections from both the fibre splice points whereby the signal is reflected back into the Bi-EDF due to the large refractive index difference, causing multi-path interference (MPI) noise [4].

Figure 5 shows the quantum conversion efficiency (QCE) and

Table 1. The Bi-EDF glass composition analysis using EDX.

Element	Mass (%)	Error (%)
Bi_2O_3	67.80	1.88
SiO_2	14.24	0.81
Al_2O_3	16.96	0.87
K_2O	0.05	0.29
P_2O_5	0.53	0.64
Er_2O_3	0.42	1.67
Total	100.00	6.17

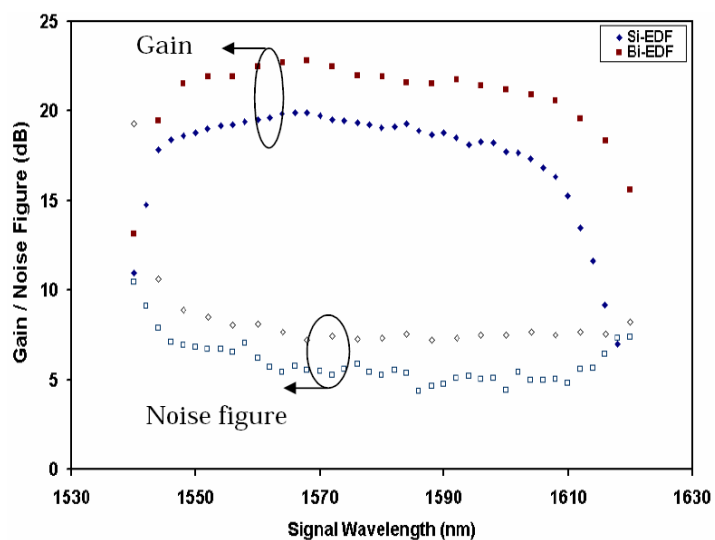


Figure 4. Comparison of the measured signal gain and noise figure at input signal power of 0 dBm between Si-EDFA and Bi-EDFA.

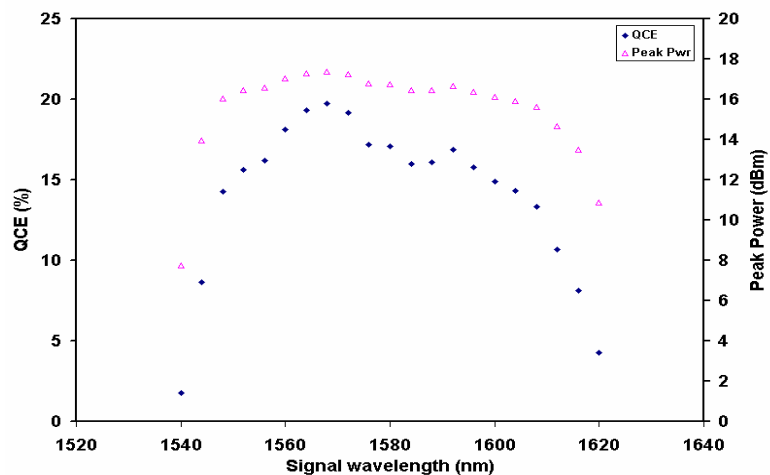


Figure 5. Measured QCE of 0 dBm input signal power from 1540 nm to 1620 nm for Si-EDF and Bi-EDF.

output power of the Bi-EDFA against signal wavelength. The QCE is pump wavelength independent and defined as [4]:

$$\text{QCE} = \left(\frac{\lambda_s}{\lambda_p} \right) \frac{P_s^{\text{out}} - P_s^{\text{in}}}{P_p^{\text{in}}} \quad (3)$$

where $\lambda_{p,s}$ are the pump and signal wavelengths, $P_s^{\text{out},\text{in}}$ are the signal output and input powers and P_p^{in} is the pump power. From energy conservation principles, the maximum value for the QCE is unity when:

$$\frac{P_s^{\text{out}} - P_s^{\text{in}}}{P_p^{\text{in}}} = \frac{\lambda_p}{\lambda_s} \quad (4)$$

The highest QCE is determined by Eq. (4) to be approximately 19.7% at 1568 nm while the lowest QCE is calculated to be 1.7% at 1540 nm. The higher QCE in the Bi-EDF amplifier is due to the phonon energy of the glass host is much lower than the Er^{3+} ions energy gaps and this significantly reduces the pump photon energy loss to non-radiative emission [12]. Therefore, almost all the pump photons are converted to signal photons in the amplification process. With its high pump to signal conversion efficiency, the Bi-EDF is an efficient optical amplifier with shorter fibre length as compared to Si-EDF.

4. NONLINEAR CHARACTERISTICS

Beside a broadband amplification, the Bi-EDF also exhibits a very high fiber nonlinearity, which can be used for realizing new nonlinear devices such as multi-wavelength laser [13,14]. A multi-wavelength laser is demonstrated using the Bi-EDF assisted by FWM process in a ring cavity resonator as shown in Fig. 6. The multi-wavelength laser resonator consists of the 215 cm long of Bismuth-based EDF (Bi-EDF), which is backward pumped using a 1480 nm laser diode, isolators, polarization controller (PC) and 10 dB output coupler. Wavelength division multiplexer (WDM) is used to combine the pump and laser wavelengths. Polarisation controller (PC) is used to control the birefringence in the ring cavity so that the output laser generated can be controlled and optimized. Two optical isolators are used to ensure unidirectional operation of the laser. A 10 dB coupler is used to tap the output of the laser via 10% port as shown in Fig. 1, which is then characterized by an optical spectrum analyzer (OSA) with a resolution of 0.015 nm. The operating wavelength of the multi-wavelength laser is determined by the backward pumped Bi-EDF gain spectrum which covers the long-wavelength band (L-band) region from 1570 to 1620 nm

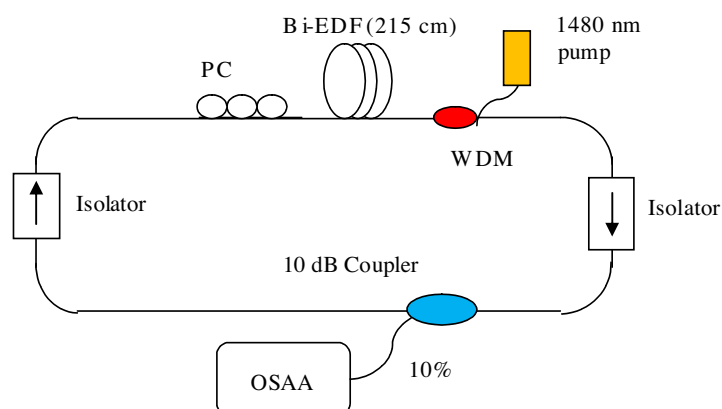


Figure 6. Experimental set-up for the proposed a Bi-EDF based multi-wavelength ring laser.

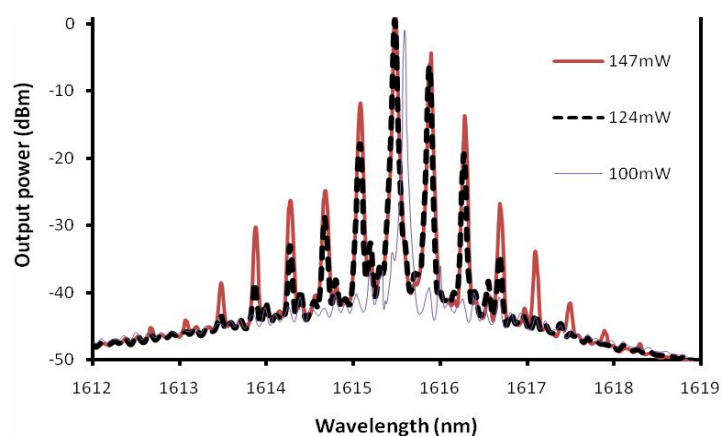


Figure 7. Output spectrum of the proposed Bi-EDF based multi-wavelength ring laser at different 1480 nm pump powers.

as well as the cavity loss. The Bi-EDF amplifier has small signal gain of approximately 30 dB at the L-band region with a pump power of 150 mW.

Figure 7 shows the output spectrum of the multi-wavelength laser for different 1480 nm pump power. As shown in the figure, the oscillating laser lines are observed in the 1615.5 nm region, which is fall within an extended L-band region. The amplification bandwidth of the Bi-EDF is extended to this region due to the suppression of excited-state absorption (ESA). The laser operates at this region due

to the cavity loss which is lower at the longer wavelength. The backward pumped Bi-EDF generates amplified spontaneous emission at this region which oscillates in the ring cavity to generate at least two oscillating lines with a constant spacing due to the longitudinal modes interference. The strong forward oscillating laser generates a backward propagating reflected light in the gain medium (due to scattering and Fresnel reflection) to form a standing wave which interferes each other to form a multiple modes. The multi-wavelength laser generation with a constant spacing is assisted by the four-wave mixing process, which annihilates photons from these waves to create new photons at different frequencies. A PC has been used to control the polarisation and the birefringence inside the cavity, which in turn control the number of line generated, channel spacing and the peak power.

As shown in Fig. 7, more than 10 lines are obtained at the maximum pump power of 147 mW. At the minimum pump power of 100 mW, the erbium gain is lower and only one strong oscillating laser is generated. Since another oscillating laser line is below the threshold of the FWM process and thus no additional frequencies lines were observed. The number of generated line as well as the peak power is observed to increase as the pump power for the 1480 nm laser diode increases which is attributed to the increment of the erbium gain with pump power. This situation provides sufficient signal power for the FWM process to generate additional lines. In this experiment, the strongest line has a peak power of approximately -2 dBm and the line spacing is measured to be around 0.41 nm, which is determined by the cavity length and the birefringence in the ring cavity. The number of lines is limited by the availability of the 1480 nm pump power or erbium gain, fiber nonlinearity and polarisation filtering effect in the linear cavity resonator. The multi-wavelength output is observed to be stable at room temperature with only minor fluctuations observed coinciding with large temperature variances.

5. CONCLUSION

The composition and characteristic of the Bi-EDF and its optical performance with 1480 nm excitation have been comprehensively studied. Compared to the current Si-EDF, the Bi-EDFA only requires a shorter length of active fibre to achieve amplification and can significantly reduce the complexity and cost of optical amplifier. The Bi-EDF is also capable of producing high quantum efficiency amplifiers that significantly benefits optical amplifier designers. The Bi-EDF also has a shorter 1530 nm emission lifetime due to the high refractive index and Er^{3+} doping concentration. In the proposed Bi-EDFA, the

efficiency of 17.9% can be achieved with an amplification bandwidth of 80nm after being pumped at wavelength of 1480nm. We have also demonstrated a multi-wavelength laser comb using a Bi-EDF fiber as both linear and nonlinear gain media. The multi-wavelength generation is due to oscillating Bi-EDF laser lines which interacts each other to create new photons at other frequency via four-wave mixing process. The generated laser comb has more than 10 lines at the maximum 1480nm pump power of 147mW with a constant spacing of approximately 0.41 nm.

REFERENCES

1. Guan, B. O., H. Y. Tam, S. Y. Liu, P. K. A. Wai, and N. Sugimoto, "Ultrawide-band La-codoped Bi_2O_3 -based EDFA for L-band DWDM systems," *IEEE Photon. Technol. Lett.*, Vol. 15, 1525–1527, 2003.
2. Inoue, K. and H. Toba, "Wavelength conversion experiment using fiber four-wave mixing," *IEEE Photon. Technol. Lett.*, Vol. 4, 69–72, 1992.
3. Ohara, S. and N. Sugimoto, " Bi_2O_3 -based erbium-doped fiber laser with a tunable range over 130 nm," *Opt. Letts.*, Vol. 33, 1201–1203, 2008.
4. Desurvire, E., *Erbium-doped Fibre Amplifiers: Principle and Application*, John Wiley & Son Inc., New York, 1994.
5. Tanabe, S., T. Ohyagi, N. Soga, and T. Hanada, "Compositional dependence of Judd-Ofelt parameters of Er^{3+} ions in alkali-metal borate glasses," *Phys. Rev. B*, Vol. 46, No. 6, 3305, 1992.
6. Yang, J. H., S. X. Dai, L. Wen, Z. P. Liu, L. L. Hu, and Z. H. Jiang, "Mixed former effect: A kind of composition adjusting method of Er-doped glass for broadband amplification," *Chin. Phys. Lett.*, Vol. 19, 1516, 2002.
7. Reisfeld, R., L. Boehm, Y. Eckstein, and N. Lieblich, "Multiphonon relaxation of rare earth ions in borate, phosphate, germanate and tellurite glasses," *J. Luminescence*, Vol. 10, No. 3, 193–204, 1975.
8. Ainslie, B. J., J. R. Armitage, S. P. Craig, and B. Wakefield, "Fabrication and optimisation of the erbium distribution in silica based doped fibres," *Fourteenth European Conference on Optical Communication, ECOC 1988*, Conf. Publ. Vol. 1, No. 292, 62–65, 1988.
9. Aiso, K., Y. Tashiro, T. Suzuki, and T. Yagi, "Erbium lanthanum Co-doped fiber for L-band amplifier with high efficiency, low non-

- linearity and low NF,” *Optical Fibre Communication Conference and Exhibition, OFC 2001*, Vol. 2, TuA6-1, 2001.
10. Yang, J., S. Dai, N. Dai, S. Xu, L. Wen, L. Hu, and Z. Jiang, “Effect of Bi_2O_3 on the spectroscopic properties of erbium-doped bismuth silicate glasses,” *J. Opt. Soc. Am. B*, Vol. 20, No. 5, 810, 2003.
 11. Takeda, S. and Y. Shigeoka, “An optical thin film bessel filter for 40 Gbit/sec-100 GHz spacing D-WDM system,” *28th European Conference on Optical Communication*, Vol. 5, 1–2, 2002.
 12. Desurvire, E., J. L. Zyskind, and C. R. Giles, “Design optimization for efficient erbium-doped fibre amplifiers,” *IEEE Journal Lightwave Technol.*, Vol. 8, 1730, 1990.
 13. Singh, S. P., R. Gangwar, and N. Singh, “Nonlinear scattering effects in optical fibers,” *Progress In Electromagnetics Research*, PIER 74, 379–405, 2007.
 14. Shen, G. F., X. M. Zhang, H. Chi, and X. F. Jin, “Microwave/millimeter-wave generation using multi-wavelength photonic crystal fiber Brillouin laser,” *Progress In Electromagnetics Research*, PIER 80, 307–320, 2008.

Brillouin fibre laser with 20 m-long photonic crystal fibre

S.W. Harun, S.N. Aziz, N. Tamchek, N.S. Shahabuddin and H. Ahmad

Brillouin fibre laser is demonstrated using a very short length of photonic crystal fibre (PCF). A simple ring resonator is used in the experiment which consists of a 20 m long highly nonlinear PCF and 49 cm long Bismuth-based erbium-doped fibre (Bi-EDF). The proposed Brillouin laser is able to generate up to 3 Stokes and 3 anti-Stokes lines in the 1560 nm region at a channel spacing of 0.09 nm.

Introduction: The area of photonic crystal fibre (PCF) technology has progressed rapidly in recent years and has been successfully applied to the development of a variety of photonics devices and applications [1, 2]. PCFs are a class of micro-structured fibre which possesses a solid core surrounded by a cladding region that is defined by a fine array of air holes that extend along the full fibre length. PCFs are typically made of a single material, usually pure silica, and guide light through a modified form of total internal reflection since the volume average index in the core region of the fibre is greater than that of the surrounding micro-structured cladding [3].

One of the most promising applications of PCFs is in the development of nonlinear optical devices for fibre-optic communication systems. PCFs can have much higher nonlinearity per unit length than conventional fibres, and devices based on such fibres can thus be much shorter in length, and/or operate at lower power levels. One of the nonlinear devices is the Brillouin fibre laser (BFL), which uses a nonlinear gain from the Brillouin effect in optical fibre. BFLs have been realised in previous reports, using about more than 70 m-long PCF as a gain medium [4, 5]. In this Letter, a new configuration of BFL is proposed using only 20 m of PCF, which we believe to be the first experimental demonstration using such a very short length of PCF. The BFL utilises a bismuth-based erbium-doped fibre (Bi-EDF) in the cavity to minimise the total fibre length.

Experiment and results: The experimental setup for the PCF-based BFL is shown in Fig. 1. The ring resonator consists of a circulator, a 20 m-long polarisation-maintaining PCF, a 49 cm-long Bi-EDF, two 1480 nm pump diodes, two wavelength selective couplers (WSCs), two isolators, a 95/5 coupler and a polarisation controller (PC). The PCF used as a nonlinear gain medium is a polarisation-maintaining fibre which has a cutoff wavelength of 1000 nm, zero dispersion wavelength of 1040 nm, nonlinear coefficient of $11 \text{ (W} \cdot \text{km)}^{-1}$ and a mode-field diameter of $4.0 \text{ } \mu\text{m}$. The Bi-EDF used as a linear gain medium has an erbium concentration of 3200 ppm with a cutoff wavelength of 1440 nm and a pump absorption rate of 130 dB/m at 1480 nm. The EDF is pumped bidirectionally using two 1480 nm lasers. Optical isolators are used to ensure a unidirectional operation of the BFL. Circulator and optical isolators used in this experiment are a polarisation insensitive type. An external cavity tunable laser source (TLS) with a linewidth of approximately 20 MHz and a maximum power of 6 dBm is used as the Brillouin pump (BP).

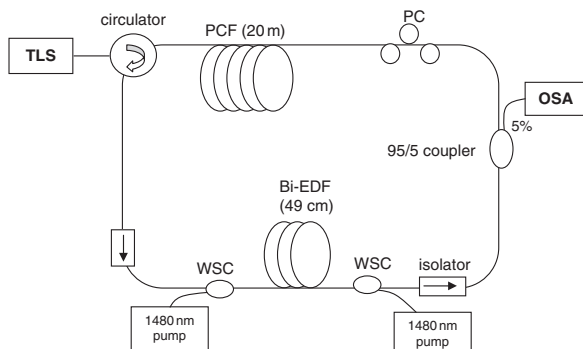


Fig. 1 Configuration of Brillouin fibre laser

The BP is injected into the ring cavity and then the PCF via the circulator to generate the first Stokes at the opposite direction. However, since the PCF length is not sufficient, the back-scattered light due to

Rayleigh scattering is relatively higher than the first Stokes. Both the back-scattered pump and the first Stokes lights are amplified by the bidirectionally pumped Bi-EDF and oscillate in the ring cavity to generate the dual-wavelength laser. The line spacing between them is obtained at approximately 11 GHz, which is equivalent to the Stokes shift in the SMF. The interaction between these two lines in both the PCF and the Bi-EDF generates another additional Stokes and anti-Stokes. The output of the linear cavity BEFL is tapped from the 95/5 coupler and characterised by an optical spectrum analyser (OSA) with a resolution of 0.015 nm.

The operating wavelength of the BFL is determined by the bidirectionally pumped Bi-EDF gain spectrum which covers the C-band region from 1525 to 1565 nm as well as the cavity loss. The free-running spectrum of the BFL (without BP) is shown in Fig. 2 in which many peak wavelengths are generated within the 1559–1562 nm region. The multiwavelength generation is attributed to the comb filter which is formed due to interference inside the polarisation-maintaining PCF. The comb filter slices the amplified spontaneous emission spectrum from the Bi-EDF amplifier and then oscillates in the ring cavity to generate a multi-line spectrum, as shown in Fig. 2. The wavelength lines are generated in the region where the difference between the Bi-EDF's gain and cavity loss is largest. The free-running BFL also exhibits a peak power of approximately –10 dBm with bandwidth of approximately 3 nm. The chosen BFL operating wavelength must be within or close to the bandwidth of the free-running BFL. Therefore, the BP is set within this region in this experiment.

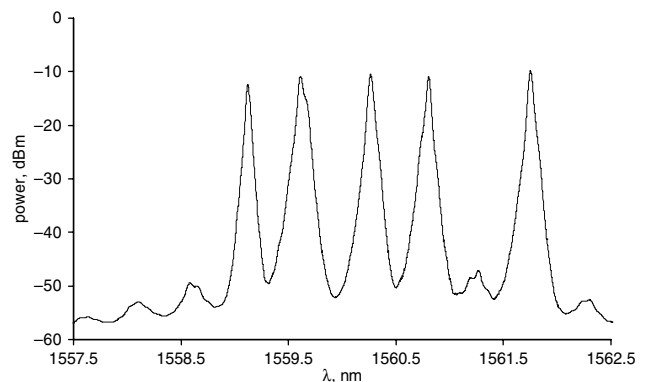


Fig. 2 Free-running spectrum of BFL (without Brillouin pump)

Fig. 3 shows the output spectrum of the proposed BFL configuration at different 1480 nm pump power. The BP wavelength is set at 1560 nm, which is within the lasing bandwidth of the free-running BFL, and the BP power is fixed at 6 dBm. In the experiment, the combined pump powers of both 1480 nm laser diodes was varied from 144 to 220 mW. Below pump powers of 140 mW, the erbium gain is very low and cannot sufficiently compensate for the loss inside the laser cavity and thus no Stokes are observed. The generated wavelength as well as the peak power is observed to increase as the combined pump power for the 1480 nm laser diodes increases, which is attributed to the increment of the erbium gain with pump power. This situation provides sufficient signal power for stimulated Brillouin scattering as well as the four-wave mixing to generate Stokes and anti-Stokes. In this experiment, three Stokes and three anti-Stokes are obtained at the maximum 1480 nm pump power of 220 mW. The first Stokes has a peak power of –12.6 dBm with a 3 dB bandwidth of about 0.02 nm, limited by the OSA resolution of 0.015 nm. The multiple peaks have a spectral spacing of 0.09 nm within a bandwidth of approximately 0.5 nm, which is limited by the availability of the Brillouin pump power, fibre nonlinearity and polarisation filtering effect. The number of lines can be largely increased by adjusting the effective cavity length so that the spacing of the polarisation comb filter matches with the Brillouin spacing. The multiwavelength output of the BFL is observed to be stable at room temperature with only minor fluctuations observed coinciding with large temperature variances. Since bismuth fibres typically have a reasonably higher nonlinear coefficient compared to PCF, an even shorter BFL could be realised by replacing the PCF with undoped bismuth fibre. This would alleviate potential limitations caused by the birefringent nature of the PCF.

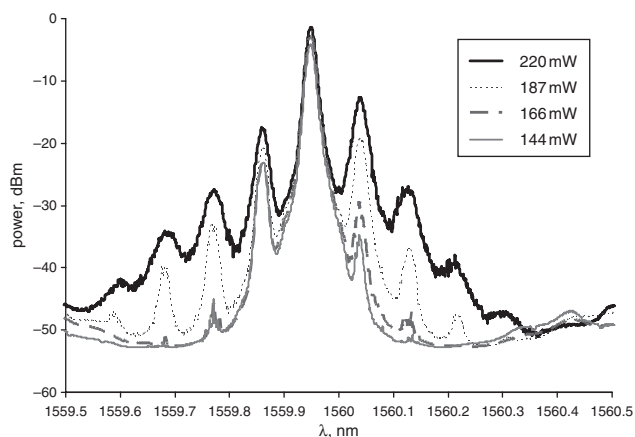


Fig. 3 BFL output spectra at different 1480 nm pump powers

Conclusion: A new configuration of BFL is proposed and demonstrated using just 20 m-long PCF. The BFL uses a ring cavity structure with a Bi-EDF amplifier to generate Stokes and anti-Stokes via stimulated Brillouin scattering and four-wave mixing processes. The proposed BFL is able to generate up to three Stokes and three anti-Stokes lines with a channel spacing of 0.09 nm at the 1560 nm region at a BP power of 6 dBm and 1480 nm pump power of 220 mW. The multiwavelength BFL is stable at room temperature and also compact owing to the use of only 20 m-long PCF and 49 cm-long Bi-EDF.

© The Institution of Engineering and Technology 2008

11 May 2008

Electronics Letters online no: 20081310

doi: 10.1049/el:20081310

S.W. Harun (*Department of Electrical Engineering, University of Malaya, Kuala Lumpur, 50603, Malaysia*)

E-mail: swharun@um.edu.my

S.N. Aziz, N. Tamchek, N.S. Shahabuddin and H. Ahmad (*Photonics Research Center, University of Malaya, Kuala Lumpur, 50603, Malaysia*)

References

- 1 Petropoulos, P., Monro, T.M., Belardi, W., Furusawa, K., Lee, J.H., and Richardson, D.J.: 'A 2R-regenerative all-optical switch based on a highly nonlinear holey fibre', *Opt. Lett.*, 2001, **26**, pp. 1233–1235
- 2 Lee, J.H., Yusoff, Z., Belardi, W., Monro, T.M., Teh, P.C., and Richardson, D.J.: 'A holey fibre Raman amplifier and all-optical modulator'. Proc. 27th European Conf. on Optical Communication (ECOC2001), PD.A.1.1, pp. 46–47
- 3 Bjarklev, A., Broeng, J., and Bjarklev, A.S.: 'Photonics crystal fibres' (Kluwer Academic, Amsterdam, The Netherlands, 2003)
- 4 Lee, J.H., Yusoff, Z., Belardi, W., Ibsen, M., Monro, T.M., and Richardson, D.J.: 'Investigation of Brillouin effects in small-core holey optical fibre: lasing and scattering', *Opt. Lett.*, 2002, **27**, pp. 927–929
- 5 Yang, X., Dong, X., Zhang, S., Lu, F., Zhou, X., and Lu, C.: 'Multiwavelength erbium-doped fibre laser with 0.8-nm spacing using sampled Bragg grating and photonic crystal fibre', *IEEE Photonics Technol. Lett.*, 2005, **17**, pp. 2538–2540

Erbium-Doped Fibre Amplifiers – Influence of Host Material

H. Ahmad¹, N. Tamchek¹, W. Y. Chong¹, K. Thambiratnam¹ and S. W. Harun²,

¹ *Photonics Research Centre, University of Malaya,
50603 Kuala Lumpur, Malaysia*

² *Dept. of Electrical Engineering, Faculty of Engineering, University of Malaya,
50603 Kuala Lumpur, Malaysia*

Email: harith@um.edu.my

PACS: 42.81.-i

Abstract: Erbium-doped optical fibre amplifiers (EDFAs) have boosted the Wavelength-Division-Multiplexed (WDM) transmission system with the popularization of Internet usage worldwide. However, present silica-based EDFAs have limitations that restrict the full utilization of optical fibre transmission. In order to design wide-band optical amplifiers, it is important to understand the characteristics of host glass in erbium-doped fibre amplifiers. In this paper, a bismuthate glass material is proposed as a new glass host erbium-doped fibre amplifiers. A Judd-Ofelt analysis of erbium absorption spectra reveals that bismuthate-host has high Ω_6 Judd-Ofelt coefficient, and the comparison of the emission cross-section using McCumber theory with measured data also shows very good agreement. The gain spectrum of the erbium-doped bismuthate-host glass has a wider amplification bandwidth of 80 nm and a high quantum conversion efficiency of 70% obtained using 1480 nm pumping.

Keywords: Wavelength-Division-Multiplexed (WDM), erbium-doped fibre amplifier, bismuthate glass

Introduction

A key enabling technologies of long-haul optical communications networks is the erbium doped fibre amplifier (EDFA). EDFAs have allowed for the deployment of Dense Wavelength Division Multiplexed (DWDM) optical network technologies due to their ability to amplify multiple signals simultaneously. This has made the EDFA a much cheaper and efficient method of amplifying optical communication systems compared to previously used electronic regenerators.

EDFAs are critical in determining the usable bandwidth of a network. Typically, optical communication systems are confined to two side-by-side transmission regions. The first region is known as the Conventional (C-Band) and ranges from 1530 to 1560 nm, while the second region is the Long-Wavelength (L-Band), which falls between 1560 nm to 1610 nm. Conventionally, C- and L-Band optical amplification is done using EDFAs consisting of Erbium as the active gain medium in a silica-glass host. Silica-glass was the chosen host for the EDFA as it is easy to splice to conventional silica-glass transmission fibres. It was also a significantly easier optical transmission medium to be fabricated, compared to other host glass materials such as phosphorous [1] and telluride [2]. The use of the silica-glass host thus reduced the complexity and cost of the EDFA and increased its commercial viability. However, the silica-glass host does bring about certain limitations in the performance of the EDFA. The primary limitation of the Si-

EDFA is the dopant concentration that the host can sustain, with the maximum reported dopant concentration of 2.0×10^{25} ions/m³ in the silica-glass host [3]. The host's ability for a high dopant concentration is important in order to produce a higher single gain per pump power without requiring an increase in the Erbium Doped Fibre (EDF) length. The Er³⁺ ion distribution should ideally be confined as a delta function in the centre of the fibre core [3,4] to obtain the maximum signal gain, but as the rare earth concentration is increased the ion distribution and distance is reduced due to residual interactions such as ion clustering [3] and local charge compensation [4]. This in turn leads to detrimental effects such as the reduction of fluorescence bandwidth and lifetime as well as concentration quenching [3,4,5] and is especially profound in Si-EDFAs.

As the concentration limit is an inherent characteristic of the silica-glass host, other methods must be found to increase the doping concentration of the erbium ions so as to be able to produce shorter EDFAs. Co-doping erbium ions with ytterbium ions have been able to increase the gain of the Si-EDFA [6], while other hosts such as phosphate, fluorophosphates, fluoride, tellurite and germanate [1,2,3] glasses have also been considered. Recently, Bismuth glass-based hosts have shown increasing potential for use as EDFA applications, due to their good broadband properties [7] (i.e. broader flat gain amplification region) as well as relatively easy splicing to currently used silica and bismuth glass transmission fibres. They are also easier to fabricate as compared to other glass-hosts, thus making them a more commercially viable option.

In this paper we report a new oxide glass composition based on a bismuthate glass host, in which Er³⁺ ions show a very broad emission as compared to silica glass. The optical performance of the new bismuth-based amplifier is characterized and compared with that of silica-based amplifiers. The efficiency of the amplifier is measured under 1480nm pumping configuration to investigate the efficiency of the pump to signal photon conversion.

Optical Amplifier Concepts

Optical fibre amplifiers work on the principle of light amplification by stimulated emission of radiation, similar to that of a laser as shown in Figure 1. It requires pump photons with energy equivalent to the dopant (Er³⁺) absorption wavelength to generate a population inversion in the amplifier medium. When an incoming signal photon stimulates an excited electron, the electron relaxes back to the lower energy state, in the process emitting a second signal photon with the same energy and phase as the incoming photon. This process continues as long as there is a significant population inversion, which is largely dependent on the glass host material [8,9,10]. To realize broadband and high signal gain with high pump-to-signal efficiency, the emission spectra and Er³⁺ ions lifetime are vital properties to the evaluation of optical amplifiers [8,11]. The emission spectra of Er³⁺ ions in glass largely depend on the glass former and modifiers materials [8,10]. Therefore with specific host material, a broad and flat gain spectra optical amplifier can be fabricated.

The most common glass network former is silica tetrahedron (SiO₄)₂ linked with broad-bond angled oxygen atoms link to form a tetrahedral structural. This material capable to form a glass structure which forming a three-dimensional matrix with oxygen atoms. Other compounds, such as oxides of alkali-metals or alkali-earth metals, (i.e Sodium, Lithium, Aluminum, Germanium, etc) can be added to the glass as network modifiers. These modifiers cause the former bridging ions to become non-bridging, thus breaking the lattice and resulting in a looser network structure. These modifiers facilitate the incorporation of trivalent rare earth ions such as Er³⁺ ions and also to lower the glass fusion temperature and viscosity. However, the glass composition has a significant effect on the performance of the amplifier. Each element used in the fabrication has distinct properties depending on glass host and there have been many

attempts to identify and understand these characteristics [12,13]. This can be done by performing a spectroscopic analysis on glass host itself, and requires the researcher to fabricate the glass host

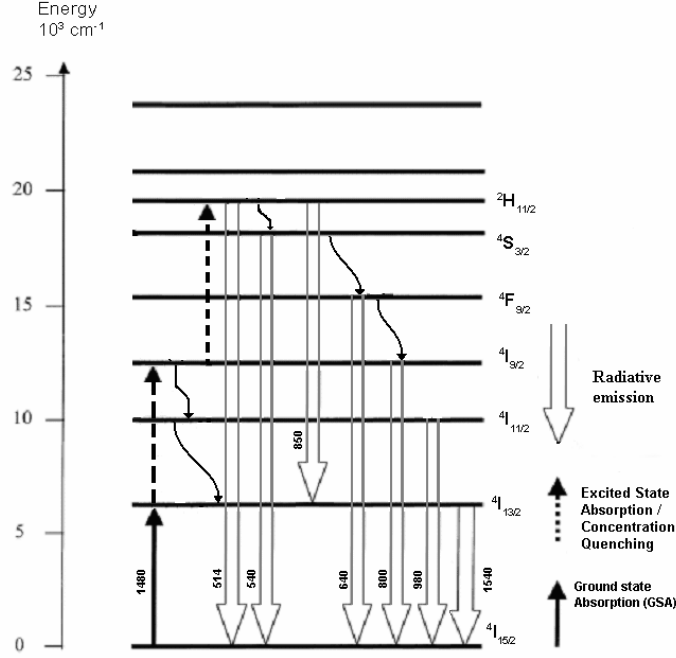


Figure 1: Energy state diagram of Er³⁺ ions showing Ground State Absorption (GSA), radiative transitions, Excited State Absorption (ESA) transition and concentration quenching (cooperative upconversion and pair induced quenching (PIQ))

and carry out the details spectroscopy analysis of the glass. This is however very complicated, due to the number of parameters involved and can often lead to erroneous conclusions. Alternatively, the characteristics of the host glass can be understood by relating the transmission loss or absorption spectrum to the amplified emission spectrum as demonstrated by B. R. Judd [14], G. S. Ofelt [15] and McCumber [16].

Judd and Ofelt independently developed the theoretical background for the calculation of rare earth optical transitions induced by the crystalline field (also known as ligand field) in a glass host. According to the Judd-Ofelt theories, the transition between an initial J manifold |(SL)J⟩ and final J' manifold |(S'L')J'⟩, S_{JJ'} for the oscillator strength of an electric dipole is defined as,

where the three $\langle\langle U^{(t)} \rangle\rangle$ terms are the reduced matrix elements of the unit tensor operators calculated in the intermediate-coupling approximation [17] while the coefficient Ω_t (t=2,4,6) is

$$S_{JJ'} = \sum_{t=2,4,6} \Omega_t \langle\langle (SL)J \| U^{(t)} \| (S'L')J' \rangle\rangle^2 \quad (1)$$

the intensity parameter that contains the information [18, 19 and 20] of the effect of the glass host on rare-earth doping. The values of Ω_t are calculated using least-square method [17, 21 and 22] of:

$$\int_{\text{band}} k(\lambda) d\lambda = \rho \frac{8\pi^3 e^2 \bar{\lambda}}{3ch(2J+1)} \left[\frac{(n^2+2)^2}{9n} \right] \sum_{t=2,4,6} \Omega_t \langle\langle (SL)J \| U^{(t)} \| (S'L')J' \rangle\rangle^2 \quad (2)$$

$$\int_{\text{band}} k(\lambda) d\lambda = \rho \frac{8\pi^3 e^2 \bar{\lambda}}{3h(2J+1)} \left[\frac{(n^2 + 2)^2}{9n} \right] S_{JJ'} \quad (3)$$

where $k(\lambda)$ is the absorption coefficient at λ , $\bar{\lambda}$ is the mean wavelength of the absorption band, ρ is the Er^{3+} concentration, h is the Plank constant, c is the velocity of light, e is the elementary electric charge and n is the refractive index.

Using these coefficient, the spontaneous emission probability $A_{JJ'}$ [17, 22] can be computed as

$$A_{JJ'} = \frac{64\pi^4 e^2 n}{3h(2J+1)\bar{\lambda}} \left[\frac{(n^2 + 2)^2}{9} \right] S_{JJ'} \quad (3)$$

The probabilities for magnetic-dipole transitions were not considered since they are generally small. τ , the lifetime of an excited state i to ground state j is determined by a combination of probabilities for all possible radiative W_{ij}^R and non-radiative W_{ij}^{NR} decay rates and is given as:

$$\frac{1}{\tau_i} = \sum_j W_{ij}^R + \sum_j W_{ij}^{NR} \quad (4)$$

According to R. Reisfeld et. al. [23], W_{ij}^{NR} is related to multi-phonon relaxation of the Er^{3+} ions in the glass material. Therefore with the measured lifetime and $A_{JJ'}$ probabilities from Eq. (3), the non-radiative decay rate W^{NR} and radiative quantum efficiency, η can be calculated using Eq. (4), to give;

$$W^{NR} = \frac{1}{\tau_{J'}} - A_{JJ'} \quad (5)$$

$$\eta_{JJ'} = \tau_{J'} \cdot A_{JJ'} \quad (6)$$

As an optical amplifier requires a long metastable state lifetime to maintain high population inversion [4] under steady-state conditions, a high rate W_{ij}^{NR} will result in the loss of the pump photon energy to phonon energy, producing a concentration quenching effect [24] and subsequently reducing the efficiency of the optical amplifier. The concentration quenching effect acts as pump photon energy sink and can be observed from the fluorescence spectra at high frequencies. To minimize energy losses, optical amplifiers is fabricated with a glass host that has a low phonon energy and capable of high quantum efficiencies. However, the low phonon energy glass host reduces the decay rate of the excited state of $^4I_{11/2}$ to the metastable state of $^4I_{13/2}$, limiting the pumping efficiency [10].

Experimental Setup

The Bi-EDF glass composition is measured by Scanning Electron Microscopy (SEM) and Energy Dispersive X-Ray Microanalysis (EDX) techniques using a JEOL JSM 6460LA with the capability to detect light elements from Boron up to Uranium for the composition element analysis. For the EDX measurement, the sample is bombarded with electron energy accelerate at 20 kV and the emitted X-Rays from the sample are captured and analysed with the system software.

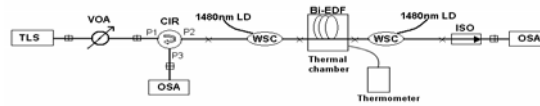


Figure 2: Experimental setup for Bi-EDF and Si-EDF Characterisation

The experimental setup is shown in Figure 2. The EDF is bidirectionally pumped by two 1480 nm laser diodes with total power of 288mW and coupled via a wavelength selective coupler (WSC). For the luminescence experiment, the two 1480 nm pump laser diode operate in a CW mode while for the lifetime experiment, the 1480 nm pumps are pulse modulated using a square-wave function generator at 70 Hz for 1530 nm and 200 Hz for 545 nm lifetime measurement. The luminescence spectrum is detected transversely from the fiber using a monochromator and a 2048-elements linear Photodiode Charge Coupled Device (PCCD) from Alton Instrument Corp.

The Bismuth-based erbium-doped fibre (Bi-EDF) used in this experiment is commercially available from Asahi Glass Co and has an Er^{3+} ion concentration of 7.6×10^{25} ions/ m^3 with a Lanthanum ion co-dopant concentration of approximately 4.4 wt%. The core/cladding refractive index is 2.03/2.02 with a NA of 0.20. The Bi-EDF length used is 181.9 cm and the fibre is angle spliced to a single-mode fibre in order to reduce splice point reflections. Both splice point ends have a total insertion loss of about 1.4 dB measured at 1310 nm. The 30m silica-based erbium-doped fibre (Si-EDF) used for the purpose of comparison is commercially available from Fibercore Limited with a Er^{3+} doping concentration of 2.0×10^{25} ions/ m^3 . The 1530 nm fluorescence spectra and decay is monitored at the WSC 1530nm input port, with the spectra detected using an optical spectrum analyzer (OSA) and the decay detected using BPX66 and HP 83440B photodiodes with a HP54510A 250 MHz digital oscilloscope. The decay oscillogram is transferred to a computer via General Purpose Interface Bus (GPIB) hardware. The decay lifetime is obtained by fitting the single-exponential function to the experimental fluorescence decay curves. For optical amplifier characteristic measurements, the input signal is tuned from 1540 nm to 1620 nm at an input signal power of 0 dBm. All measurements are performed at room temperature.

Result and Discussion

The energy spectrum of the sample from the EDX measurement and an elemental analysis is performed using the bundled-in software for JEOL with quantitative setting of standardless and ZAF for oxide calculations and the results are shown in Table 1. From the data, the glass network formers of Bi-EDF are determined to be bismuth oxide, silica and alumina while the other markers are determined to be the glass network modifiers, as the glass formers will be the more prevalent elements in the glass structure than the glass modifiers. The error percentage is computed by the bundled-in software.

Table 1: Bi-EDF glass composition analysis from EDAX

Element	Mass (%)	Error (%)
Bi ₂ O ₃	67.80	1.88
SiO ₂	14.24	0.81
Al ₂ O ₃	16.96	0.87
K ₂ O	0.05	0.29
P ₂ O ₅	0.53	0.64
Er ₂ O ₃	0.42	1.67
Total	100.00	6.17

By utilizing bismuth oxide and alumina as the main glass network former, the local glass basicity near the Er³⁺ ions sites is expanded as reported by Jianhu Yang et. al. [25] and Ainslie et. al. [26], effectively increasing the crystal field (ligand field) of the glass. This has the result of enhancing the 1530 nm fluorescence full-width-half-maximum (FWHM) spectrum [25,26] making it comparably broader than that obtainable with silica glass host. Figure 3 shows the relative absorption intensity of the Bi-EDF compared with that of the Si-EDF. Despite the Bi-EDF having a higher absorption cross-section of $7.58 \times 10^{-25} \text{ m}^2$ at the 1530 nm peak as compared to the Si-EDF absorption cross-section which is only $4.39 \times 10^{-26} \text{ m}^2$ on, the peak full-width half maximum (FWHM) of the Bi-EDF narrower than the FWHM of the Si-EDF. This can be attributed to larger inhomogeneous energy level degeneracy that the ligand field of the Bismuth host glass had induced as a result of site-to-site variations, also known as the Stark effect [10] and widens the optical transitions. Other elements such as potassium oxide also have similar glass basicity expender effects [27] and are used in the fabrication of Bi-EDF to obtain a broad amplification region.

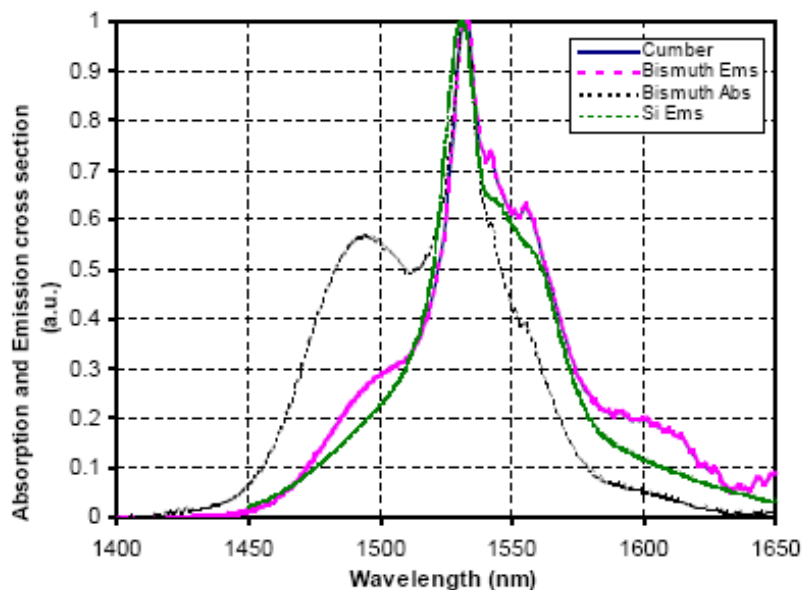
**Figure 3:** Emission cross-section of Bi-EDF and Si-EDF

Figure 3 also shows the calculated emission cross-section using the McCumber Theory. The McCumber Theory estimates agree well with the measured emission cross-section of the Bi-EDF. The optical emission at the 1.53 μm band from the energy levels $^4\text{I}_{13/2}$ to $^4\text{I}_{15/2}$ is the most important characteristic for optical communication systems and this is clearly shown in Figure 3. The Bi-EDF has a wider emission spectra, especially at the longer wavelengths at 1620 nm because of its larger emission cross-section as compared to Si-EDF [24] which has a bandwidth of only 40 nm while the Bi-EDF bandwidth is almost double at 80 nm at a similar emission intensity. It is believed that the Stark level of the Er^{3+} ions in the Bi-EDF is separated to a larger degree due to the larger ligand field, causing the emission spectrum to widen. The Judd-Ofelt coefficient Ω_t ($t=2,4,6$) calculated for the Bi-EDF are $9.55 \times 10^{-20} \text{ cm}^2$, $2.86 \times 10^{-20} \text{ cm}^2$ and $0.32 \times 10^{-20} \text{ cm}^2$ respectively and it is determined that the value of Ω_6 in the Bi-EDF is very small compared to other glasses [28]. According to Tanabe et. al. [28], the Ω_6 value relates to the nature of the chemical bonding and is a major factor in determining the transition probability of the Er^{3+} ions ^4F orbitals. Currently, the smaller value is attributed to the small Erbium atom ^6S electron density but without more detailed measurements on the glass chemical structure and ligand field strength this claim cannot be confirmed. The lifetime decay curve was measured to be approximately 2.84 ms, which is shorter than that measured by Yang et. al. [8] and much more lower than the compared lifetime of Er^{3+} ions in a silica host glass [10]. The quantum efficiency η and non-radiative transition rate W^{NR} at the 1550 nm emission is calculated using Eqs. (4) and (5) to be 63.0 % and 130.3 s^{-1} respectively. This shows that the Bi-EDF is capable of generating the sought after high population inversions with only a modest pump power [23] due to the higher quantum efficiency. Furthermore, this indicates that glass hosts with low phonon energies such as bismuthate glass (500 cm^{-1}) can be used to design an efficient optical amplifier with a wider fluorescence bandwidth [8, 23]. The wider fluorescence bandwidth is also attributed to the effect of the alumina and Lanthanum co-dopants towards the Er^{3+} ions distribution in the Bi-EDF which reduces the concentration quenching effect of the Er^{3+} ions, thus increasing the quantum efficiency [26, 29].

The normalized emission spectra of the Bi-EDF between 400 nm to 1100 nm under 1480 nm pump excitation is shown in Figure 5. The Bi-EDF shows 7 peak emissions centered at 521, 544, 658, 807, 825, 847 and 976 nm which correspond to the electronic transitions of the $^2\text{H}_{11/2}$, $^4\text{S}_{3/2}$, $^4\text{F}_{9/2}$ and $^4\text{I}_{11/2}$ levels of the Er^{3+} ions. The intensity of the upconversion emission at 521 and 545 nm which is can be seen as visible green light is for the highest energy states with a full-width at half-maximum (FWHM) of 17.5 nm. Here, the emission originates from radiative transition of the $^2\text{H}_{11/2}$ to $^4\text{I}_{15/2}$ states and the $^4\text{S}_{3/2}$ to $^4\text{I}_{15/2}$ states while the fluorescence is due to the effects of concentration quenching. In order to determine the responsible upconversion mechanisms, the upconversion intensity of different peaks are measured as a function of the 1480 nm pump power.

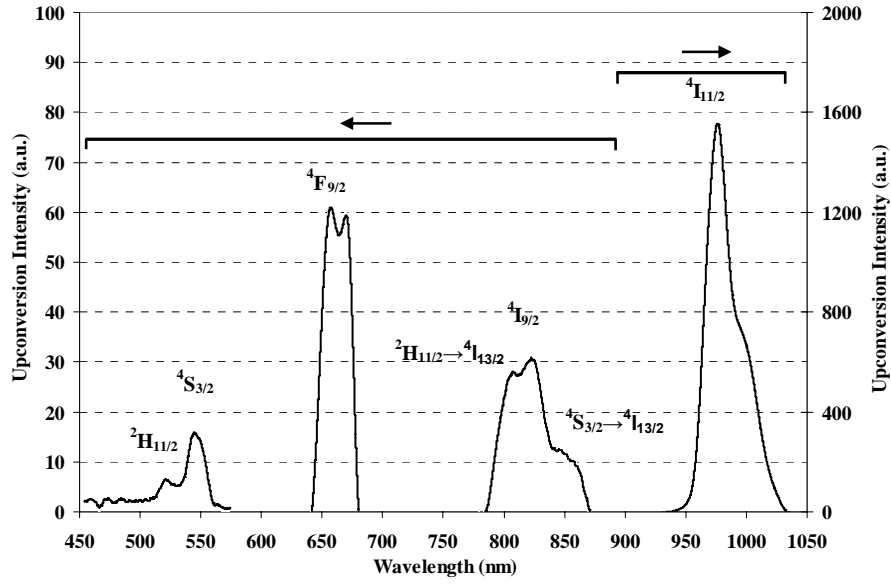


Figure 4: Upconversion fluorescence spectra under 1480 nm excitation. The radiative transitions are indicated from their initial state and terminated at the ground state of $^4I_{15/2}$ except as indicated by its final state

The most important characteristic of the Bi-EDF is its ability to amplify optical signals. As such, the Bi-EDF optical amplifier characteristics and performance is evaluated by measuring the signal gain and noise figure for a 0 dBm input signal as shown in Figure 5 (a). The gain of Bi-EDF is approximately 3 dB or 50% higher than that of the Si-EDF optical amplifier with a flat gain profile. The Bi-EDF gain bandwidth is also wider than the Si-EDF gain by 15 nm to be approximately 80 nm, spanning from 1540 nm up to 1620 nm. This 15 nm increase in gain bandwidth represents the potential addition of 18 signal channels of a 100GHz transmission system with the implementation of Bi-EDF optical amplifiers [30]. However, the high Er^{3+} ions doping concentration and high insertion loss when spliced to conventional SMF results in the Bi-EDF having a higher noise figure penalty. A higher noise figure penalty of approximately 2.6 dB is observed for the Bi-EDF when compared to the Si-EDF. This increased noise figure is suspected to be the effect of multiple reflections from both the fiber splice points whereby the signal is reflected back into the Bi-EDF due to the large refractive index difference or multi-path interference noise [10, 31].

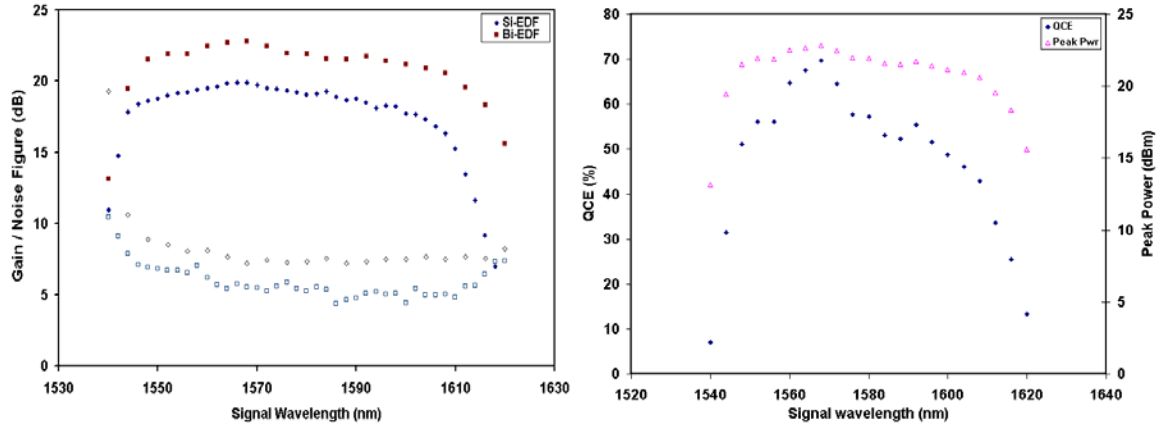


Figure 5: Measured signal gain and noise figure (a) and QCE (b) of 0 dBm input signal power from 1540 nm to 1620 nm for Si-EDF and Bi-EDF.

Figure 5 (b) shows the quantum conversion efficiency (QCE) and output power of the Bi-EDF. The QCE is pump wavelength independent and defined by B. Pederson et al. [9] as,

$$QCE = \left(\frac{\lambda_s}{\lambda_p} \right) \frac{P_s^{out} - P_s^{in}}{P_p^{in}} \quad (7)$$

where $\lambda_{p,s}$ is pump and signal wavelength, $P_s^{out,in}$ is signal output and input power and P_p^{in} is pump power. The highest QCE is determined to be approximately 69.7 % at 1568 nm while the lowest QCE is calculated to be 7 % at 1540 nm. The higher QCE is due to the higher phonon energy of the glass host than the Er^{3+} ions energy gaps and this significantly reduces the pump photon energy loss to non-radiative emission [4, 7 and 17]. Therefore, almost all the pump photons are converted to signal photons in the amplification process. With its high pump to signal conversion efficiency, the Bi-EDF is an efficient optical amplifier with shorter fibre length as compared to Si-EDF.

Conclusion

The bismuthate host glass with a high Er^{3+} ions doping is a potential candidate to replace current Si-EDF optical amplifiers due to its better performance and characteristics. The Bi-EDFA only requires a shorter length of active fibre to achieve amplification and can significantly reduce the complexity and cost of optical amplifier manufactures and will bring down the total cost of operations. The Bi-EDF is also capable of producing high quantum efficiency amplifiers that significantly benefits optical amplifier designers. The Bi-EDF has a shorter 1550 nm emission lifetime due to the high refractive index and Er^{3+} doping concentration, and has a wider amplification bandwidth of 80 nm and high QCE of 70% using 1480 nm pumping. However, high insertion losses and multipath reflections between splice points arising from splicing joints to SMFs must be improved before the Bi-EDF can be implemented in optical communication networks.

Acknowledgements

We would like to thank Seiki Ohara of Asahi Glass Company for his kind cooperation and support with Bi-EDF data. This work was supported by UM PJP Grant (F0255).

References

- [1] Chung Jiang, Weisheng Hu, Qingji Zeng, "Improved gain characteristics of high concentration erbium-doped phosphate fiber amplifier", IEEE Photon. Tech. Lett., Vol. 16, No. 3, 2004, pp. 774
- [2] Lihui Huang, Shaoxiong Shen, Xiaobo Liu, Animesh Jha, "Broadband emissions in Er^{3+} - Tm^{3+} codoped tellurite glass fibre", Conference on Laser and Electro-optics (CLEO 2004), Vol. 1, 2004, pp. 1
- [3] P. Myslinski, C. Szubert, A. J. Bruce D. J. DiGiovanni, B. Palsdottir, "Performance of high-concentration erbium-doped fiber amplifier", IEEE Photon. Tech. Lett., Vol. 11, No. 8, 1999, pp. 973
- [4] E. Desurvire, J. L. Zyskind, C. R. Giles, "Design optimization for efficient erbium-doped fiber amplifiers", IEEE Journal Light. Tech. Vol. 8, pp. 1730, 1990
- [5] Nikonorov, N.; Przhevuskii, A. "Concentration dependence of upconversion quenching rate in Er-doped glass fiber", Lasers and Electro- Optics Society Annual Meeting, (LEOS '97) Conference Proceedings., IEEE, Vol. 2, 1997, pp. 306 – 307
- [6] Y. Jeong, S. Yoo, C. A. Codemard, J. Nilsson, J. K. Sahu, D. N. Payne, R. Horley, P. W. Turner, L. Hickey, A. Harker, M. Lovelady, A. Piper, "Erbium:Ytterbium codoped large-core fiber laser with 297-W continuouswave output power", IEEE J. of Selected Topics in Quantum Electronics, Vol. 13, 2007, pp. 573-579
- [7] S. Ohara, N. Sugimoto, K. Ochiai, H. Hayashi, Y. Fukasawa, T. Hirose, M. Reyes, "Extra-broadband and highly efficient short length Bi_2O_3 -based EDF", Optical Fiber Communication Conference and Exhibition, OFC 2003, Vol. 2, 2003, pp. 635
- [8] Yang. J. H., Dai. S. X. Wen. L., Liu. Z. P. Hu. L. L. Jiang. Z. H., "Mixed Former Effect: A kind of composition adjusting methos of Er-Doped Glass for Broadband Amplification", Chin. Phys. Lett., Vol 19, 2002, pp. 1516
- [9] Anthony E. Siegman, "Lasers", University Science Books, U.S., 1986
- [10] E. Desurvire, "Erbium-doped fiber amplifiers: Principle and Application," John Wiley & Son Inc., New York, 1994.
- [11] A. Mori, Y. Ohishi, S. Sudo, "Erbium-doped tellurite glass fibre laser and amplifier", Electron. Lett., No. 10, Vol. 33, 1997, pp. 863
- [12] V. V. Dvoyrin, V. M. Mashinsky, E. M. Dianov, A. A. Umnikov, M. V. Yashkov, A. N. Guryanov, "Absorption, fluorescence and optical amplification in MCVD Bismuth-doped silica glass optical fibres", European Conference on Optical Communications (ECOC) 2005, Vol. 4, Th. 3.3.5, 2005
- [13] Y. Fujimoto, M. Nakatsuka, "Optical amplification in bismuth-doped silica glass", Appl. Phys. Lett., Vol. 82, No. 19, pp. 3325, 2003
- [14] B. R. Judd, "Optical absorption intensities of rare-earth ions", Phys. Rev., Issues 3, Vol. 127, 1962, pp. 750
- [15] G. S. Ofelt, "Intensities of crystal spectra of rare-earth ions", J. Chem. Phys., Issue. 3, Vol. 37, 1962, pp. 511
- [16] D. E. McCumber, "Einstein relations connecting broadband emission and absorption spectra", Phys. Rev., Vol. 136, No. 4A, 1964, pp. A954
- [17] M. J. Weber, "Probabilities of radiative and non-radiative decay of Er^{3+} in LaF_3 ", Phys. Rev., Vol. 157, 1967, pp. 262
- [18] R. D. Peacock, "The intensities of lanthanide f-f transition", in Structure and Bonding (Springer-Verlag, Berlin), Vol. 22, 1975, 83

- [19] S. Tanabe, T. Ohyagi, S. Todoroki, T. Hanada, N. Soga, "Relation between the Ω_6 intensity parameter of Er^{3+} ions and the ^{151}Eu isomer shift in oxide glasses", J. Appl. Phys., No. 12, Vol. 73, 1993, pp. 8451
- [20] S. Tanabe, T. Ohyagi, N. Soga, T. Hanada, "Compositional dependence of Judd-Ofelt parameters of Er^{3+} ions in alkali-metal borate glasses", Phys. Rev. B., No. 6, Vol. 46, 1992, pp. 3305
- [21] W. T. Carnall, P. R. Fields, K. Rajnak, "Electronic energy levels in the Trivalent Lanthanide Aquo Ions. I. Pr^{3+} , Nd^{3+} , Pm^{3+} , Sm^{3+} , Dy^{3+} , Ho^{3+} , Er^{3+} and Tm^{3+} ", J. Chem Phys. No. 10, Vol. 49, 1968, pp. 4424
- [22] W. F. Krupke, "Optical absorption and fluorescence intensities in several rare-earth-doped Y_2O_3 and LaF_3 single crystals", Phys. Rev., No. 1, Vol. 145, 1966, pp. 321
- [23] Rolli, Raffaella, Chiasera, Alessandro, Montagna, Maurizio, Moser, Enrico, Ronchin, Sabina, Pelli, Stefano, Righini, Giancarlo C., Jha, Animesh, Tikhomirov, Victor K., Tikhomirova, Svetlana A., Duverger, Claire, Galinetto, Pietro, Ferrari, Maurizio, "Rare-earth-activated fluoride and tellurite glasses: optical and spectroscopic properties", Vol. 4282, 2001, 109
- [24] D. L. Dexter, James H. Schulman, "Theory of concentration quenching in organic phosphors", Jour. Chem. Phys. Vol. 22, No. 6, 1954, pp. 1063
- [25] Jian Yang, Shixun Dai, Nengli Dai, Shiqing Xu, Lei Wen, Lili Hu, Zhonghong Jiang, "Effect of Bi_2O_3 on the spectroscopic properties of erbium-doped bismuth silicate glasses", J. Opt. Soc. Am. B, Vol. 20, No. 5, 2003, pp. 810
- [26] B. J. Ainslie, J. R. Armitage, S. P. Craig, B. Wakefield, "Fabrication and optimisation of the erbium distribution in silica based doped fibres", Fourteenth European Conference on Optical Communication, ECOC 1988, Conf. Publ. No. 292, Vol. 1, 1988, pp. 62-65
- [27] S. Tanabe, T. Ohyagi, N. Soga, T. Hanada, "Compositional dependence of Judd-Ofelt parameters of Er^{3+} ions in alkali-metal borate glasses", Phys. Rev. B., Vol. 46, No. 6, 1992, pp. 3305
- [28] S. Tanabe, N. Sugimoto, S. Ito, T. Hanada, "Broad-band 1.5 μm emission of Er^{3+} ions in bismuth-based oxide glasses for potential WDM amplifier", J. of Lumin, Vol. 87, 2000, pp. 670
- [29] Keiichi Aiso, Yoshio Tashiro, Tsuneo Suzuki, Takeshi Yagi, "Erbium lanthanum co-doped fiber for L-band amplifier with high efficiency, low non-linearity and low NF", Optical Fiber Communication Conference and Exhibition, OFC 2001, Vol. 2, 2001, pp. TuA6-1
- [30] Takeda, S.; Shigeoka, Y., "An optical thin film Bessel filter for 40Gbit/sec -100GHz spacing D-WDM system", 28th European Conference on Optical Communication, 2002, Vol. 5, 2002, pp.1 – 2
- [31] D. M. Baney, P. Gallion, R. S. Tucker, "Theory and measurement techniques for the noise figure of optical amplifiers," Opt. Fib. Tech., Vol. 6, 2000, pp. 122

C- AND L-BAND ERBIUM-DOPED FIBRE AMPLIFIERS BASED ON BISMUTHATE GLASS

N. Tamchek¹, W. Y. Chong¹, S. W. Harun², H. Ahmad¹

¹ Physics Department, Faculty of Science,

² Faculty of Engineering,

University of Malaya, 50603 Kuala Lumpur, Malaysia. Email: nizamtm@um.edu.my

ABSTRACT. Erbium-doped optical fibre amplifier have boost the Wavelength-Division-Multiplexed (WDM) transmission system with the popularization of Internet usage worldwide. Present silica-based erbium-doped fibre amplifier have a few limitations that restrict the full utilization of optical fibre transmission. In order to design a wide-band optical amplifiers, it is important to understand the characteristics of host glass in erbium-doped fibre amplifiers. In this paper, bismuthate glass material is proposed as a new glass host for C- and L-band erbium-doped fibre amplifiers. Judd-Ofelt analysis of erbium absorption spectra reveals that bismuthate-host have high Judd-Ofelt coefficient. The gain spectra of Erbium-doped bismuthate-host glass have a wider amplification bandwidth of 80nm and a high quantum conversion efficiency of 70% was obtained using 1480nm pumping. This shows that Bi-EDF is a promising candidate of WDM transmission system optical amplifier.

Keywords: Wavelength-Division-Multiplexed (WDM), erbium-doped fibre amplifier, bismuthate glass

PACS: 42.81.-i

1.0 INTRODUCTION

The increasing demand in capacity for Wavelength-Division-Multiplexed (WDM) transmission system has rendered the silica-based fibre amplifier a bottle neck in optical transmission systems due to its limitation such as useful amplification bandwidth, low power conversion efficiency, high unit cost and bulkiness. Today's WDM transmission system designers only consider the full utilization of C- and L- band amplification [1,2,3] region when designing an optical amplifiers. Although optical fibre amplifier have been playing a crucial role in optical transmission systems both at 1.55 μ m and 1.3 μ m, there exist further requirement for better performance [1,2,4]. Therefore, as the optical transmission technology evolved, these limitations will become the bottleneck for bandwidth expansion.

Optical fibre amplifier works by the basic principle of light amplification by stimulated emission of radiation, similar to laser operation as shown in Fig 1. It requires pump photons with energy equivalent to the rare-earth (Er^{3+} ions) absorption wavelength to generate a population inversion in the amplifier medium. When an incoming signals photon stimulates an excited electron, the electron relaxes back to the lower energy state and emits a second signal photon with the same energy and phase as the incoming photon. This process will continue as long as the population inversion in the glass medium is high and produces more signal photons. The population inversion of the amplifiers largely depends on the glass host material (phonon energy, optical absorption, refractive index), rare-earth doping concentration, and the pump and signal photon energy [4,5,6].

To realize broadband and high signal gain with high pump-to-signal efficiency, the emission spectra and Er^{3+} ions lifetime are vital properties to the evaluation of optical amplifiers [4,7]. The emission spectra of Er^{3+} ions in glass largely depend on the glass former and modifiers materials [4,6]. Therefore with specific host material, a broad and flat gain spectra optical amplifier can be fabricated. According to Judd-Ofelt theories [8,9] by using the oscillator strength of an electric dipole, the transition between an initial J manifold $|(SL)J\rangle$ and final J' manifold $|(S'L')J'\rangle$, $S_{JJ'}$ is define as,

$$S_{JJ'} = \sum_{t=2,4,6} \Omega_t \left| \langle (SL)J \| U^{(t)} \| (S'L')J' \rangle \right|^2 \quad (1)$$

where three $\langle U^{(t)} \rangle$ terms are the reduced matrix elements of the unit tensor operators calculated in the intermediate-coupling approximation [10] and the coefficient Ω_t ($t=2,4,6$) are the intensity parameters that contains information

[11,12,13] of the effect of the glass host with rare-earth doping. The values of the Ω_i is calculated using least-square method from [10,14,15],

$$\int_{\text{band}} k(\lambda) d\lambda = \rho \frac{8\pi^3 e^2 \bar{\lambda}}{3ch(2J+1)} \left[\frac{(n^2+2)^2}{9n} \right] \sum_{t=2,4,6} \Omega_t \left| \langle (SL)J \| U^{(t)} \| (S'L')J' \rangle \right|$$

$$\int_{\text{band}} k(\lambda) d\lambda = \rho \frac{8\pi^3 e^2 \bar{\lambda}}{3ch(2J+1)} \left[\frac{(n^2+2)^2}{9n} \right] S_{JJ'} \quad (2)$$

where $k(\lambda)$ is the absorption coefficient at λ , $\bar{\lambda}$ is the mean wavelength of the absorption band, ρ is the Er^{3+} concentration, h is Plank's constant, c is the light velocity, e is the elementary electric charge, and n is the refractive index. By using these coefficient, the spontaneous emission probabilities, $A_{JJ'}$ is [10,15],

$$A_{JJ'} = \frac{64\pi^4 e^2 n}{3h(2J+1)\bar{\lambda}} \left[\frac{(n^2+2)^2}{9} \right] S_{JJ'} \quad (3)$$

Here, the probabilities for magnetic-dipole transitions were not considered since they are generally small.

The τ lifetime of an excited state i to ground state j is determined by a combination of probabilities for all possible radiative W_{ij}^R and non-radiative W_{ij}^{NR} decay rates,

According to R. Reisfeld *et. al.* [16], the W_{ij}^{NR} is related to multiphonon relaxation of the Er^{3+} ions in the glass

$$\frac{1}{\tau_i} = \sum_j W_{ij}^R + \sum_j W_{ij}^{NR} \quad (4)$$

material. Therefore with the measured lifetime and $A_{JJ'}$ probabilities from Eq. (3), the non-radiative decay rate W^{NR} and radiative quantum efficiency, η can be calculated using Eq (4),

$$W^{NR} = \frac{1}{\tau_j} - A_{JJ'} \quad (5)$$

$$\eta_{JJ'} = \tau_j \cdot A_{JJ'} \quad (6)$$

An optical amplifier requires a long metastable state lifetime to maintain high population inversion [4] under steady-state conditions. Here, when W_{ij}^{NR} rate is high, the pump photon energy is lost to phonon energy, thus reducing the efficiency of the optical amplifier. Optical amplifiers fabricated with a glass host that has low phonon energy minimizes energy losses and are capable of high quantum efficiencies. However, glass host with low phonon energy slows the decay from excited states (pump absorption level) to the metastable state, thus limiting the pumping efficiency [6]. Therefore, optical fibre amplifier hosts should have medium phonon energy and a wider emission spectrum for broadband amplification.

In this study, we report a new oxide glass composition based on bismuthate glass as a host, in which erbium ions show very broad emission compared to silica glass. The optical performance of the new bismuth-based amplifier was characterized and compared with silica-based amplifiers. The efficiency of the amplifier is measured under 1480nm pumping configuration to investigate the efficiency of pump to signal photon conversion.

2.0 EXPERIMENTAL

The experimental setup is shown in Fig. 2. The Bismuth-based erbium-doped fibre (Bi-EDF) used in this experiment is commercially available from Asahi Glass Co. It has an Er^{3+} ions concentration of 3250 wt. ppm and Lanthanum co-dopant of approximately 4.4 wt%. The core/cladding refractive index is 2.03/2.02 with NA=0.20. The fibre length is 181.9 cm. The Bi-EDF is angle spliced with single-mode fibre to reduce splice point reflection. Both splice point ends have a total insertion loss of about 1.4 dB measured at 1310nm. The silica-based erbium-doped fibre (Si-EDF) used for comparison is commercially available from Fibercore Limited with 960 wt. ppm of Er^{3+} doping. The length of the Si-EDF is 30m.

The EDF was bidirectionally pumped by 1480nm laser diode with total power of 288mW, coupled via a wavelength selective coupler (WSC). In the optical amplifier characterization, the 1480nm laser diode is operated in CW mode while for the lifetime measurement, the 1480nm laser diode was square wave modulated at 70Hz with 7% duty cycle using a signal generator which produces an off-time of about 13ms. The 1530nm fluorescence decay is monitored at the WSC 1530nm input port. The decay is detected with a silicon PIN photodiode and captured by a

HP54510A 250 MHz bandwidth digital oscilloscope. The decay oscillogram is transferred to a computer via GPIB connection. Decay lifetime is obtained by fitting the single-exponential function to the experimental fluorescence decay curves. For optical amplifier characteristic measurement, the input signal was tuned from 1540nm to 1620nm with input signal power of 0dBm. All measurement was performed at room temperature.

3.0 RESULT and DISCUSSIONS

The optical emission at 1.53um band is the most important characteristic for optical communication system. This fluorescence emission from energy levels $^4I_{13/2}$ to $^4I_{15/2}$ is shown in the Fig. 3. The Bi-EDF has a wider emission spectra especially at longer wavelength around 1620nm because it has a larger emission cross section than Si-EDF [17]. The emission spectrum of Si-EDF has a bandwidth of about 40nm while Bi-EDF bandwidth is almost doubled at 80nm when compared at similar emission intensity. It is believe that Stark level of Er^{3+} in Bi-EDF is more separated due to crystal field (ligand field) that widen the emission spectrum. The Judd-Ofelt coefficient Ω_i ($i=2,4,6$) calculated for Bi-EDF are $9.55 \times 10^{-20} \text{ cm}^2$, $2.86 \times 10^{-20} \text{ cm}^2$ and $0.32 \times 10^{-20} \text{ cm}^2$, respectively. It was found that the value of Ω_6 in this Bi-EDF is very small compared with other glasses [17]. According to Tanabe *et. al.* [17], the Ω_6 value is related to the nature of chemical bonding and it is a major factor in determining the transition probability of Er^{3+} ions 4f orbitals. The smaller value is suspected due to small Erbium atom 6s electron density. However without further details measurement on the glass chemical structures and ligand field strength, this claims cannot be conform by now.

The lifetime decay curve of Er^{3+} ions at 1530nm in Bi-EDF is shown in Fig. 4. The decay curve is fitted with single exponential decay as shown by the solid red line. The lifetime was found to be about 2.84ms, which is shorter than that measured by Yang *et. al.* [4] and much more lower when compared the lifetime of Er^{3+} ions in silica host glass [6]. The quantum efficiency η and non-radiative transition rate W^{NR} at 1550nm emission is calculated using Eq. (4) and (5), to be 63.0% and $130.3s^{-1}$, respectively. Therefore Bi-EDF is capable of generating high population inversions with modest pump power [16] due to the higher quantum efficiency. This also indicates that glass with low phonon energy such as bismuthate glass (500cm^{-1}) is capable of producing an efficient optical amplifier with wider fluorescence bandwidth [4,16]. It is suspected that the effect of Lanthanum co-doping affects the Er^{3+} ions distribution in Bi-EDF and reduces the upconversion, thus increasing the quantum efficiency. Optical amplifiers characteristic and performance is evaluated by measuring signal gain and noise figure at 0 dBm input signal as shown in Fig. 5 and 6. The gain of Bi-EDF is about 3 dB or 50% higher than Si-EDF optical amplifier. The gain bandwidth is also wider at approximately 80nm, spanning from 1540nm up to 1620nm. The 15nm increase in gain bandwidth represents a potential addition of 18 signal channels at 100GHz transmission system with the implementation of Bi-EDF optical amplifiers [18].

However, with the high Er^{3+} ions doping and high insertion loss when spliced to SMF, Bi-EDF have higher noise figure penalty. The maximum noise figure penalty is approximately 2.6 dB when comparing to Si-EDF. This is suspected to be the effect of multiple reflections from both fibre splice points where the signal is reflected back into the Bi-EDF due to large refractive index difference or multipath interference noise [6,19].

Fig. 7 shows the quantum conversion efficiency (QCE) and output power of the Bi-EDF. QCE is pump wavelength independent and defined by B. Pederson *et al.* [9] as,

The highest QCE is about 69.7 % at 1568nm and the lowest is 7 % at 1540nm. The higher QCE is due to higher

$$QCE = \left(\frac{\lambda_s}{\lambda_p} \right) \frac{P_s^{out} - P_s^{in}}{P_p^{in}} \quad (7)$$

phonon energy of the glass host than Er^{3+} ions energy gaps that significantly reduces the pump photon energy loss to non-radiative emission [4, 7, 16]. Therefore, almost all the pump photon is converted to signal photon in the amplification process. With its high pump to signal conversion efficiency, BI-EDF is an efficient optical amplifier with shorter fibre length compared to Si-EDF.

4.0 CONCLUSION

Bismuthate host glass with high Er^{3+} ions doping is a potential candidate to replace current Si-EDF optical amplifiers due to its better performance and characteristics. Bi-EDFA only requires a shorter length of active fibre to achieve amplification. This advantage can significantly reduce the complexity and cost of optical amplifier manufactures and will bring down the total cost of operations. Bi-EDF is also capable of producing high quantum efficiency amplifiers that significantly benefits optical amplifier manufacturer. However Bi-EDF have shorter 1550nm emission lifetime due to the high refractive index and Er^{3+} doping concentration. Other problems such as

high insertion loss and multipath reflections between splice points when spliced to SMF must be improved before the Bi-EDF can be implemented in optical communication networks.

ACKNOWLEDGEMENTS

We would like to thank Seiki Ohara of Asahi Glass Company for his kind cooperation and support with Bi-EDF data. This work was supported by UM PJP Grant (F0255).

REFERENCES

- [1] Atkins, C.G.; Massicott, J.F.; Armitage, J.R.; Wyatt, R.; Ainslie, B.J.; Craig-Ryan, S.P., "High-gain broad spectral bandwidth erbium-doped fibre amplifier pumped near 1.5 μm ", *Electronics Lett*, Vol. 25, 1989, pp. 910 – 911
- [2] Ainslie, B.J.; Craig-Ryan, S.P.; Davey, S.T.; Armitage, J.R.; Atkins, C.G.; Massicott, J.F.; Wyatt, R., "Erbium doped fibres for efficient optical amplifiers", *IEE Proceedings-Optoelectronics*, Vol. 137, 1990, pp. 205 - 208
- [3] Kinoshita S., "Broadband fiber optic amplifiers", *Optical Fiber Communication Conference*, 2001, TuA1
- [4] Yang. J. H., Dai. S. X. Wen. L., Liu. Z. P. Hu. L. L. Jiang. Z. H., "Mixed Former Effect: A kind of composition adjusting methos of Er-Doped Glass for Broadband Amplification", *Chin. Phys. Lett.*, Vol 19, 2002, pp. 1516
- [5] Anthony E. Siegman, "Lasers", University Science Books, U.S., 1986
- [6] E. Desurvire, "Erbium-doped fiber amplifiers: Principle and Application," John Wiley & Son Inc., New York, 1994.
- [7] A. Mori, Y. Ohishi, S. Sudo, "Erbium-doped tellurite glass fibre laser and amplifier", *Electron. Lett.*, No. 10, Vol. 33, 1997, pp. 863
- [8] B. R. Judd, "Optical absorption intensities of rare-earth ions", *Phys. Rev.*, Issues 3, Vol. 127, 1962, pp. 750
- [9] G. S. Ofelt, "Intensities of crystal spectra of rare-earth ions", *J. Chem. Phys.*, Issue. 3, Vol. 37, 1962, pp. 511
- [10] M. J. Weber, "Probabilities of radiative and non-radiative decay of Er^{3+} in LaF_3 ", *Phys. Rev.*, Vol. 157, 1967, pp. 262
- [11] R. D. Peacock, "The intensities of lanthanide f-f transition", in *Structure and Bonding* (Springer-Verlag, Berlin), Vol. 22, 1975, 83
- [12] S. Tanabe, T. Ohyagi, S. Todoroki, T. Hanada, N. Soga, "Relation between the Ω_6 intensity parameter of Er^{3+} ions and the ^{151}Eu isomer shift in oxide glasses", *J. Appl. Phys.*, No. 12, Vol. 73, 1993, pp. 8451
- [13] S. Tanabe, T. Ohyagi, N. Soga, T. Hanada, "Compositional dependence of Judd-Ofelt parameters of Er^{3+} ions in alkali-metal borate glasses", *Phys. Rev. B*, No. 6, Vol. 46, 1992, pp. 3305
- [14] W. T. Carnall, P. R. Fields, K. Rajnak, "Electronic energy levels in the Trivalent Lanthanide Aquo Ions. I. Pr^{3+} , Nd^{3+} , Pm^{3+} , Sm^{3+} , Dy^{3+} , Ho^{3+} , Er^{3+} and Tm^{3+} ", *J. Chem Phys.* No. 10, Vol. 49, 1968, pp. 4424
- [15] W. F. Krupke, "Optical absorption and fluorescence intensities in several rare-earth-doped Y_2O_3 and LaF_3 single crystals", *Phys. Rev.*, No. 1, Vol. 145, 1966, pp. 321
- [16] Rolli, Raffaella, Chiasera, Alessandro, Montagna, Maurizio, Moser, Enrico, Ronchin, Sabina, Pelli, Stefano, Righini, Giancarlo C., Jha, Animesh, Tikhomirov, Victor K., Tikhomirova, Svetlana A., Duverger, Claire, Galinetto, Pietro, Ferrari, Maurizio, "Rare-earth-activated fluoride and tellurite glasses: optical and spectroscopic properties", Vol. 4282, 2001, 109
- [17] S. Tanabe, N. Sugimoto, S. Ito, T. Hanada, "Broad-band 1.5 μm emission of Er^{3+} ions in bismuth-based oxide glasses for potential WDM amplifier", *J. of Lumin.*, Vol. 87, 2000, pp. 670
- [18] Takeda, S.; Shigeoka, Y., "An optical thin film Bessel filter for 40Gbit/sec -100GHz spacing D-WDM system", 28th European Conference on Optical Communication, 2002, Vol. 5, 2002, pp. 1 – 2
- [19] D. M. Baney, P. Gallion, R. S. Tucker, "Theory and measurement techniques for the noise figure of optical amplifiers," *Opt. Fib. Tech.*, Vol. 6, 2000, pp. 122

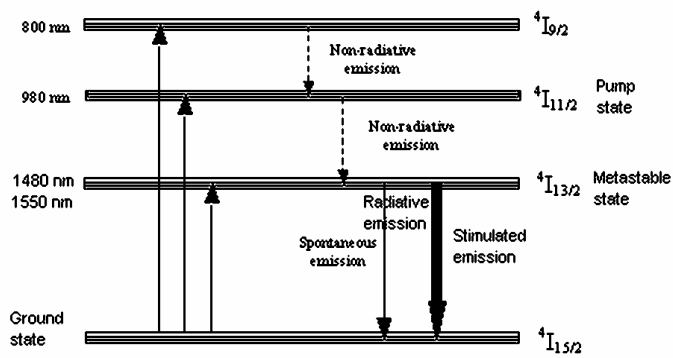


Figure 1. Energy level diagram of Er^{3+} in glass host showing absorption and emission transitions.

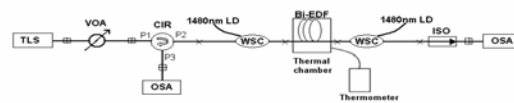


Figure 2. Experimental setup

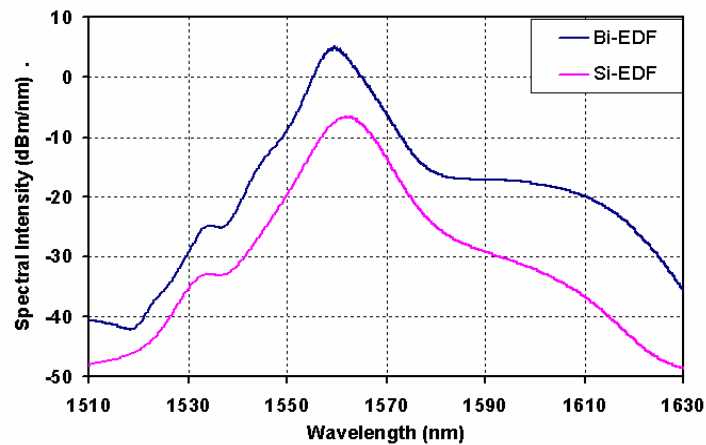


Figure 3. Emission cross section of Bi-EDF and Si-EDF.

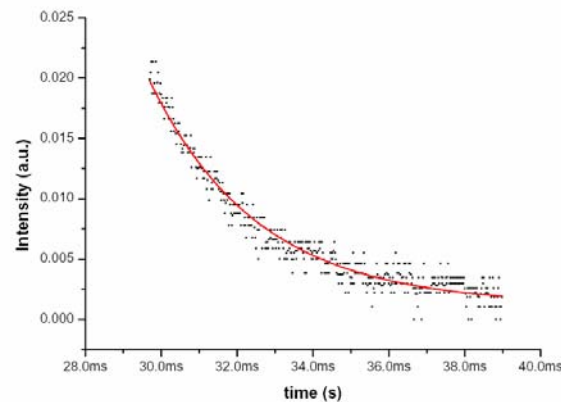


Figure 4. Measured 1550nm lifetime of Bi-EDF. (Solid lines indicate fitting to the data)

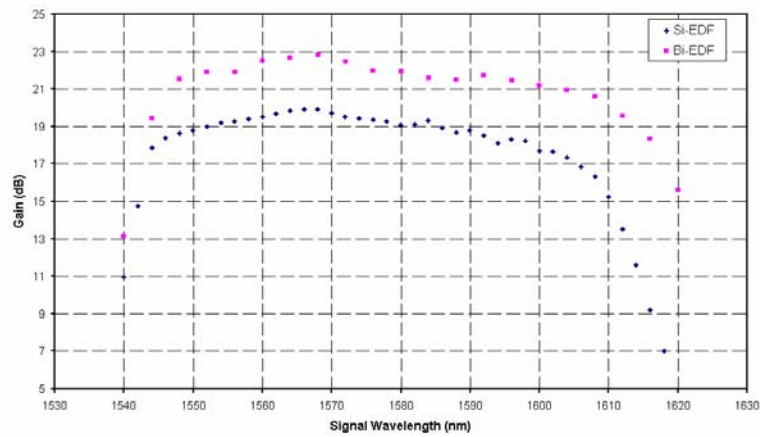


Figure 5. Measured signal gain with 0dBm input signal power from 1540nm to 1620nm wavelength for Si-EDF and Bi-EDF.

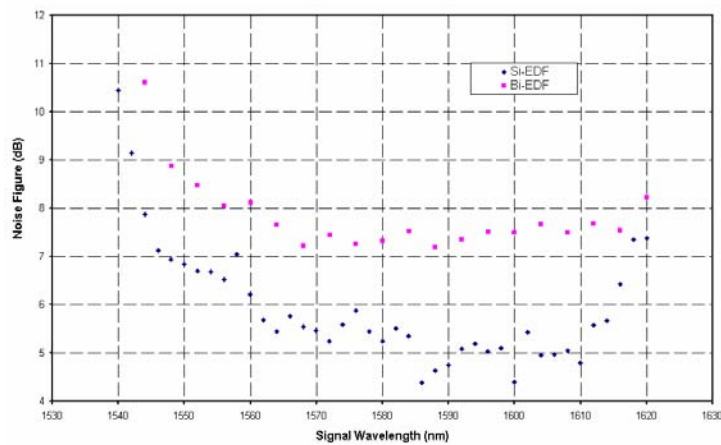


Figure 6. Measured signal noise figure with 0dBm input signal power from 1540nm to 1620nm of Si-EDF and Bi-EDF.

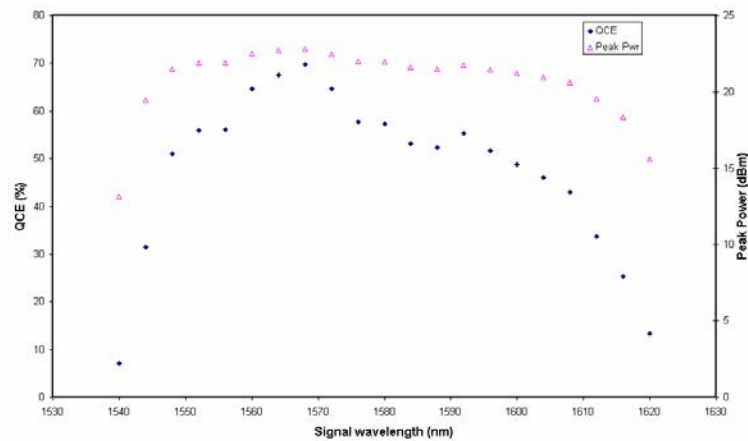


Figure. 7 Quantum conversion efficiency (QCE) and output power of the Bi-EDF.

Green upconversion of Erbium-doped Bismuth-based fibre

N. Tamchek, W. Y. Chong, P. Poopalan, S. W. Harun, H. Ahmad
 Photonic Laboratory, University of Malaya, Malaysia.
 nizamtm@um.edu.my

Abstract

Green upconversion emission characteristics of Erbium-doped Bismuth-based fibres when pumped with 1480nm laser diode have been investigated. Broad green emission peaking at 521nm and 544nm was observed when pumped by 1480nm with a half maximum (FWHM) at 544nm peak of 17.5nm. It is found that the upconversion emission process is dominated by concentration quenching effect at low 1480nm pump power and replaced by Excited State Absorption at high 1480nm pump power.

Key words: green upconversion, Bismuth-based fibre, life-time, concentration quenching

1. Introduction

Erbium-doped glasses especially silica glass have attracted much attention following the success of erbium-doped fibre amplifier [1]. The choices of practical host material for erbium doping have been known to be limited to silica-based due to its low splice loss to transmission fibre. However, with increased demand in data transmission and new optical fibre fabrication technology, the ability to fabricate new host material for fibre amplifier is crucial. Fluoride, ZBLAN, Bismuth and Telluride glass have been potentials to become host material due to their respective advantages. The main reason for their selection and effectiveness is due to the ability for high Erbium doping concentration with relatively low concentration quenching effect to generate higher signal gain and wider gain bandwidth capability [2, 3, 4, 5, 6]. Other host glass such as Telluride has low signal gain due to high up-conversion emission rates [2] and difficulty to splice with single-mode fibre (SMF), while high material cost is an obstruction to use fluoride glass [3].

Bismuth-based glasses are very attractive hosts for rare-earth ions doping and have significant advantages in optical fibre field. The low phonon energy, high refractive index and capability for high concentration rare-earth doping yield low non-radiative decay rates of rare-earth energy states, high radiative emission rates and generates better quantum efficiency in shorter length of doped fibre [7, 8, 9]. These characteristics of Bismuth-based glass give rise to a new type of optical fibre for

optical amplification that cannot be observed in other host glasses.

The efficiency of the optical amplifier is calculated from the output power generated per pump power at optical transmission region which spanned from 1520nm to 1620nm, the transmission window mainly utilised today. The selection of pump laser diode wavelength is a critical factor due to Excited State Absorption (ESA) and concentration quenching (cooperative upconversion and pair induced quenching (PIQ)) that reduces the efficiency of optical amplifier significantly. These effects have caused degradation of pump to signal power efficiency as reported by [9,10,11] due to cooperative upconversion which also referred to as cross relaxation. The energy state diagram of Er^{3+} ions and its radiative transitions in Figure 1 shows Excited-state Absorption (ESA) and concentration quenching effects. The concentration quenching effects depend on Er^{3+} ions concentration. It's occur when two (or a cluster of) Er^{3+} ions interact and energy is being transferred from one Er^{3+} ions to another Er^{3+} ions, promoting it to a higher energy states while the ion itself drop to ground states. ESA, on the other hand, is independent of Er^{3+} ions concentration but depends on pump intensity and occurs through absorption of photon by excited Er^{3+} ions, promoting it to a higher energy state [12].

In this work, we report the characteristics and mechanism of upconversion emission of Er^{3+} ions in Bismuth-based glass to evaluate its optical performance. The measurement of upconversion intensity shows that both ESA and concentration quenching effect are taking place and also has fast upconversion decay rates.

2. Experiment

The Bismuth-based Erbium-doped fiber (Bi-EDF) used is commercially available from Asahi Glass Co. with Er^{3+} concentration of 3250 wt. ppm, Lanthanum (La) co-doping of approximately 4.4 wt%. and Numerical Aperture (NA) of 0.20 with core/cladding refractive index of 2.03/2.02. The Bi-EDF length is 51.5 cm. The fibre output end was put in index matching gel to reduce Fresnel reflection.

The fibre was pumped by 1480nm pump laser diode and coupled to the Bi-EDF using wavelength selective coupler (WSC). For luminescence experiment, the 1480nm pump laser

diode is operated in CW mode while in lifetime experiment, the 1480nm pump was pulse modulated

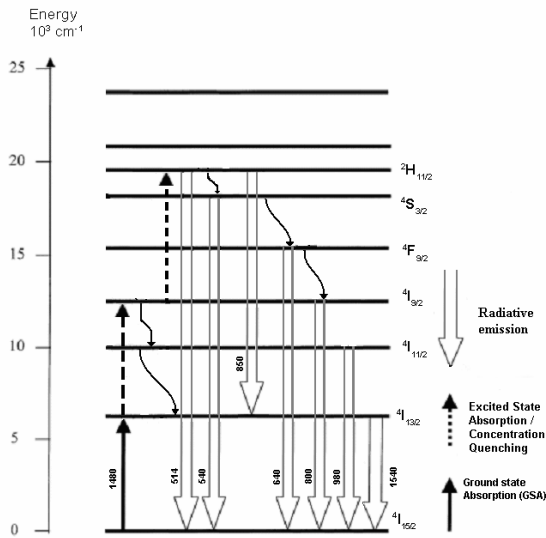


Figure 1: Energy state diagram of Er³⁺ ions showing Ground State Absorption (GSA), radiative transitions, Exited State Absorption (ESA) transition and concentration quenching (cooperative upconversion and pair induced quenching (PIQ)).

using a function generator at 200Hz with 12.94% duty cycle output. The pulse off-time is fixed to 4.3ms to enable the measurement of emission decay time of Er^{3+} ions. The luminescence spectra were detected transversely from the fibre using a monochromator and 2048-elements linear Photodiode Charge Coupled Device (PCCD) from Alton Instrument Corp.

For lifetime measurement, the fluorescence decay is monitored by silicon PIN photodiode and captured using HP54510A 250 MHz digital oscilloscope. The decay oscillogram is transferred to a computer using GPIB cable. The lifetime was obtained by fitting the single-exponential function to the experimental fluorescence decay curves. The specific upconversion wavelength power was detected using Optical Spectrum Analyzer (OSA) set at 0nm scan setting. All the measurement was performed at room temperature.

3. Result

The normalized emission spectra of Bi-EDF between 400 nm to 1100nm under 1480nm pump excitation are shown in Figure 2. The Bi-EDF shows 7 peak emissions centred at 521nm, 544nm, 658nm, 807nm, 825nm, 847nm and 976nm. The corresponding peak can be assigned to the electronic transition ${}^2\text{H}_{11/2}$, ${}^4\text{S}_{3/2}$, ${}^4\text{F}_{9/2}$ and ${}^4\text{I}_{11/2}$ of Er^{3+} ions. The intensity of upconversion emission at 521nm and

545nm, which is visible green are the highest energy states with a full-width at half-maximum (FWHM) of 17.5nm. Here, the emission is originated from radiative transition of $^2\text{H}_{11/2}$ to $^4\text{I}_{15/2}$ states and $^4\text{S}_{3/2}$ to $^4\text{I}_{15/2}$ state.

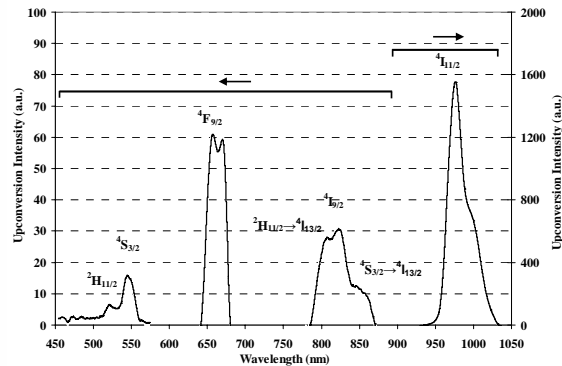


Figure 2: Upconversion fluorescence spectra under 1480nm excitation. The radiative transitions are indicated from their initial state and terminated at ground state $^4I_{15/2}$ excepts indicated by its final state.

In order to determine the responsible upconversion mechanisms, the upconversion intensity of different peaks was measured as a function of 1480nm pump power.

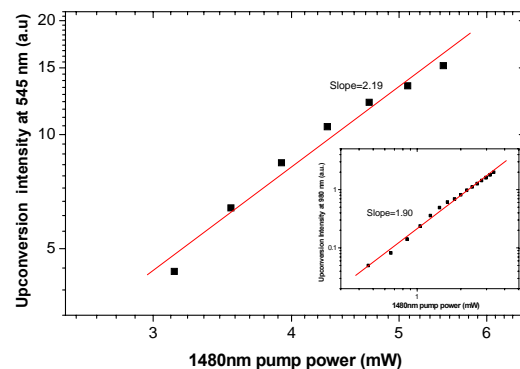


Figure 3: Upconversion fluorescence intensity at 545nm relative to 1480nm pump power. The inset is upconversion fluorescence at 980nm versus 1480nm pump power. (The solid lines is fit to the data)

Figure 3 shows the upconversion intensity at 545nm with 1480nm pump power on log/log scale and the inset shows the upconversion intensity at 980nm with 1480nm pump power for comparison. The slope for upconversion at 545nm is 2.19 while upconversion slope at 980nm is 1.90, confirming that the upconversion emission at 545nm is a two photon process which are cooperative upconversion and PIQ mechanism. The upconversion emission at 980nm exhibits a slope of less than 2 due to additional effect from ESA which is single ions process. At higher

pump power, the slope of 980nm upconversion emission reduced even further, showing a more dominant ESA effect.

Figure 4 shows decay curves of Bi-EDF at 545nm when pumped with 1480nm pump laser diode. The Bi-EDF lifetime of 306us shows good agreement with the predicted value of 300us from [8]. The lifetime of Er^{3+} ions in glass host is dependent on the host phonon energy from the energy transfer rate equation,

$$\frac{1}{\tau_{\text{exp}}} = \sum_j (A_{ij}^R + A_{ij}^{\text{NR}})$$

where τ is the total lifetime observed experimentally, A_{ij}^R is the radiative decay rate of level i and the A_{ij}^{NR} is the non-radiative decay rate between energy levels i and j . Here the non-radiative decay rate is largely depended on glass host vibration phonon energy and if it's larger than total radiative decay rate, $\sum A_{ij}^{\text{NR}} > A_{ij}^R$, fluorescence will not be observed. Bismuth-based glass has a low phonon energy of 500 cm^{-1} and longer total lifetime at 1530nm of 3~4ms [7,8], the infrared fluorescence at 1530nm is more efficient compared to visible fluorescence at 545nm.

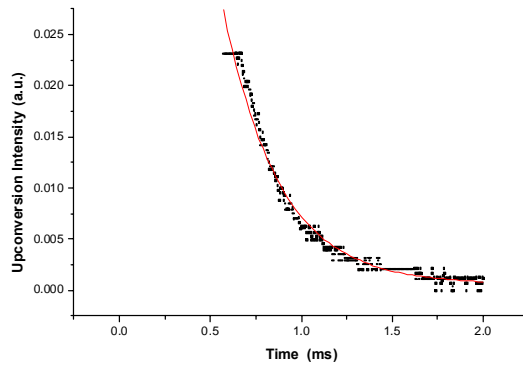


Figure 4: 545nm upconversion decay curves. The solid red line is a fit to the data.

4. Discussion and Conclusion

The upconversion characteristics and mechanism of Bi-EDF is investigated in this study. From our results, Bi-EDF shows broad upconversion emission with multiple peaks corresponding to Er^{3+} ion energy state under 1480nm pump excitation. The highest upconversion energy of Bi-EF is observed at 521nm and 545nm. The upconversion emission mechanisms involved are concentration quenching and ESA process. The 1480nm pump energy excites the Er^{3+} ions to $^4\text{I}_{13/2}$ state and populates the excited state. When the excited state population became higher, cooperative upconversion mechanism causes the ions to populate the higher $^4\text{I}_{9/2}$ state, which then quickly decayed to $^4\text{I}_{11/2}$ state due to phonon nonradiative decay. From this state, the Er^{3+} ions

excited to the $^2\text{H}_{11/2}$ by also cooperative upconversion. The green emission peak at 521nm arise from radiative transition from this $^2\text{H}_{11/2}$ state to ground state $^4\text{I}_{15/2}$. The other emission peak at 545nm and also 658nm is caused by phonon nonradiative decay from $^2\text{H}_{11/2}$ state to the $^4\text{S}_{3/2}$ and $^4\text{F}_{9/2}$ states, and radiatively decay to ground state $^4\text{I}_{15/2}$. However, this 2 photon upconversion process of Bi-EDF is slowly taken over by 1 ions process as the pump power increases due to effect of ESA as the effect is dependent to pump power. The lifetime of 521nm 545nm emission is 306us which is small compared with the lifetime of 1530nm emission [7,8].

Bismuth-based Erbium-doped fibre (Bi-EDF) with low upconversion inversion, low phonon energy, high reflective index and capable of high Er^{3+} ion doping without clustering, is a suitable material for broadband optical fibre amplification in WDM communications systems. The upconversion fluorescence measured from 400nm to 1100nm shows 7 emission peaks corresponding to Er^{3+} ion energy states. The green emissions at 512nm and 544nm have a full-width at half maximum of 17.5nm. The lifetime of these two peaks is 306us which is comparatively shorter than the lifetime of 1530nm emission. Therefore Bi-EDF is a suitable material in future broadband optical amplifier for replacing current silica-based erbium-doped optical amplifier.

5. References

- [1] R. J. Mears, L. Reekie, I. M. Jauncey and D. N. Payne, "Low-noise erbium doped fibre amplifier operating at 1.54 μm ," *Electron. Lett.*, 1987, Vol.23, No. 19, pp. 1026-1028
- [2] A. Mori Y. Ohishi, M. Yamada, H. Ono, S. Sudo, "Broadband amplification characteristics of telluride-based EDFAs," *Integrated Optics and Optical Fibre Communications*, 11th International Conference on, and 23rd European Conference on Optical Communication (Conf. Publ. No. 448), 1997, Vol. 3, 22-25
- [3] Yamada, M.; Ohishi, Y.; Kanamori, T.; Ono, H.; Sudo, S.; Shimizu, M., "Low-noise and gain-flattened fluoride-based Er^{3+} -doped fibre amplifier pumped by 0.97 μm laser diode", *Electronics Lett.*, 1997 Vol 33, Issue 9, 809 – 810
- [4] Sugimoto, N.; Kuroiwa, Y.; Ito, S.; Tanabe, S.; Hanada, T., "Broadband 1.5 μm emission of Er^{3+} ions in bismuth-based oxide glasses for WDM amplifier", *Lasers and Electro-Optics Society 1999 12th Annual Meeting. LEOS '99*, 1999, Vol 2, 814 - 815

- [5] Millar, C.A.; Brierley, M.C.; France, P.W., "Optical amplification in an erbium-doped fluorozirconate fibre between 1480 nm and 1600 nm", Optical Communication, 1988. ECOC 88. Fourteenth European Conference on (Conf. Publ. No.292), 1988, Vol 1, 66 – 69
- [6] S. Tanabe, N. Sugimoto, S. Ito, T. Hanada, "Broad-band 1.5 μm emission of Er^{3+} ions in bismuth-based oxide glasses for potential WDM amplifier", J. Lumin, 2000, Vol. 87-89, 670
- [7] S. Q. Man, E. Y. B. Pun, P. S. Chung, "Upconversion luminescence of Er^{3+} in alkali bismuth gallate glasses", Appl. Phys. Lett. B, 2000, Vol 77, 483
- [8] H. Lin, S. Tanabe, L. Lin, Y.Y. Hou, K. Liu, D.L. Yang, T.C. Ma, J.Y. Yu and E.Y.B. Pun, "Near-infrared emissions with widely different widths in two kinds of Er^{3+} -doped oxide glasses with high refractive indices and low phonon energies", J. Lumin, 2007, Vol 124, 167-172
- [9] Delevaque, E.; Georges, T.; Monerie, M.; Lamouler, P.; Bayon, J.-F., "Modeling of pair-induced quenching in erbium-doped silicate fibers", PTL, IEEE, 1993, Vol 5, 73 – 75
- [10] Shixun Dai, Tiefeng Xu, Qiuhua Nie, Xiang Shen and Xunsi Wang, "Investigation of concentration quenching in $\text{Er}^{3+}:\text{Bi}_2\text{O}_3\text{-B}_2\text{O}_3\text{-SiO}_2$ glasses", Physics Letters A, 2006, Vol 359, 330-333
- [11] Atkins, C.G.; Massicott, J.F.; Armitage, J.R.; Wyatt, R.; Ainslie, B.J.; Craig-Ryan, S.P., "High-gain broad spectral bandwidth erbium-doped fibre amplifier pumped near 1.5 μm ", Electronics Letters, Vol 25, 1989, 910 – 911
- [12] E. Desurvire, "Erbium-doped fiber amplifiers: Principle and Application", John Wiley & Son Inc., New York, 1994.